FOI-R--1636--SE
April 2005
ISSN 1650-1942
Scientific report

Potential of Reducing the Environmental Impact of Civil Subsonic Aviation by Using Liquid Hydrogen

Fredrik Svensson

Systems Technology
SE-164 90 Stockholm

CRANFIELD UNIVERSITY

SCHOOL OF ENGINEERING

Ph.D. THESIS

Academic Year: 2001-2004

FREDRIK SVENSSON

Potential of Reducing the Environmental Impact of Civil Subsonic Aviation by Using Liquid Hydrogen

Supervisor: Professor Riti Singh

April 2005

This thesis is submitted in partial fulfilment of the requirements for the degree of Doctor of Philosophy

ABSTRACT

Mainly owing to the dwindling fossil oil resources and the environmental concerns of discharging greenhouse gases into the atmosphere, it is essential to find an alternative to kerosene for civil aviation.

The overall objective of this thesis is to evaluate the potential of reducing the environmental impact of civil subsonic aviation by using hydrogen fuel. Mainly due to the complex interactions among a number of different fields affected by the introduction of hydrogen in aviation and due to the nature of the research question, the chosen scientific approach for this thesis is to carry out a broad study covering a number of selected fields. Engine and combustion chamber design are studied in detail, along with the cruise altitude for minimum environmental impact. Airport implications, and available and envisioned methods for hydrogen production are discussed.

From a technical point of view, it seems to be feasible to use hydrogen for aero gas turbines. In terms of pollutant emissions, hydrogen use offers the possibility of a significantly reduced number of emission species, resulting in only H_2O and small quantities of NO_x emissions.

For minimum environmental impact, the results suggest that cryoplanes should cruise at an altitude of about 2-3 km below where conventional aircraft cruise today. If the priority is to lower the mission fuel consumption, the results indicate that an engine employing increased combustor outlet temperature, overall pressure ratio and by-pass ratio, seems to be the most attractive choice. The mission NO_x emissions, on the other hand, seem to be reduced by using engines with a weak core and lowered by-pass ratio.

Ignoring the cost implications, from an airport infrastructure point of view, it seems feasible to change to hydrogen use. With respect to the availability of energy, it would be reasonable to change from kerosene to liquid hydrogen as fuel for all civil aviation refuelling in Sweden.

ACKNOWLEDGEMENTS

The work accomplished in the thesis was financially sponsored by the Swedish Energy Agency, the Swedish Defence Research Agency and the European Commission.

I would like to thank Professor Riti Singh, my supervisor, for giving me the valuable support and advice which have enabled me to carry out this project. His technical knowledge and kindness for support in both technical and practical matters are gratefully acknowledged.

The work has greatly benefited from contacts and discussions with Anders Hasselrot and Anette Näs at FOI, Matthew Whellens at Rolls-Royce plc, Anthony Jackson consultant at Cranfield University, Professor Friedemann Suttrop at Fachhochschule Aachen, Germany, and Stefano Boggia at MTU Aero Engines. I thank you all. Special thanks go to Anders Hasselrot for providing advice on aircraft aerodynamics, and to Anette Näs, Sven-Erik Thor (FOI) and Susan Raia Canali for help in the proof reading of the thesis.

Rachel Smith and Sue Gow are greatly acknowledged for solving all the administrative issues. I would also like to thank Jan Westerberg formerly at FOI who contributed to the initiation of this Ph.D. project.

Last, but not least, I would like to thank my fiancée Jenny for always supporting me.

TABLE OF CONTENTS

LIST OF FIGURES

LIST OF TABLES

NOMENCLATURE

Abbreviations and Chemical Formulae

A/C	Aircraft
AMA	Aircraft Mission Analysis (modelling tool, see section 4.3)
APU	Auxiliary power unit
CEA	Chemical equilibrium applications
CFC	Chlorofluorocarbons
CH	Hydrocarbon radical
CH_4	Methane
CIAM	Central Institute of Aviation Motors
CL	Class
CMR	Cryoplane, medium-range
CO	Carbon monoxide
CO_2	Carbon dioxide
DLR	Deutsches Zentrum für Luft- und Raumfahrt
DOE	Department of Energy
EEFAE	Efficient and Environmentally Friendly Aero Engine
EQHHPP	Euro-Québec Hydro-Hydrogen Pilot Project
ESDU	Engineering Sciences Data Unit
FH	Fachhochschule
FL	Flight level
FOI	Swedish Defence Research Agency
GSP	Gas turbine simulation program
GWP	Global warming potential
H	Hydrogen atom
H_2	Hydrogen (gaseous)
HCN	Hydrogen cyanide
HE	Heat exchanger
H_2O	Water vapour
HO_2	Hydroperoxyl radical
HP	High-pressure
HPC	High-pressure compressor
IAE	International Aero-Engines AG
ICAO	International Civil Aviation Organisation
IEA	International Energy Agency
IPCC	Intergovernmental Panel on Climate Change
ISA	International standard atmosphere
JAEC	Japanese Aero Engines Corporation
KE	Kerosene equivalent
KSPA	Kuibyshev Scientific-Production Association
LCA	Life cycle assessment
LH_2	Liquid hydrogen
LNG	Liquid natural gas
LP	Low-pressure
LPP	Lean pre-mixed pre-vaporized (combustor)

LPT	Low-pressure turbine
LTO	Landing and take-off
MAP	Model of Aircraft Plume
MR	Medium-range
N	Nitrogen atom
N_2	Nitrogen (gaseous)
NASA	National Aeronautics and Space Administration
NGL	Natural gas liquid
NGV	Nozzle guide vane
NLR	National Aerospace Laboratory
nm	Nautical mile
N_2O	Nitrous oxide
NO	Nitrogen oxide
NO_x	Nitrogen oxides (NO + NO_2)
NO_2	Nitrogen dioxide
O	Oxygen atom
O_2	Oxygen (gaseous)
O_3	Ozone
ODAC	Oil Depletion Analysis Centre
OH	Hydroxyl radical
OPEC	Organisation of the Petroleum Exporting Countries
PC	Personal computer
Piano	Project Interactive Analysis and Optimisation (software)
ppb	Part per billion
ppb(V)	Part per billion, related to volume
ppm	Part per million
ppm(V)	Part per million, related to volume
PZ	Primary zone
RK	Reference kerosene-fuelled aircraft
RQL	Rich-burn, Quick-quench, Lean-burn (combustor)
RR	Rolls-Royce
SAS	Scandinavian Airlines
SCAA	Swedish Civil Aviation Administration
SCB	Statistics Sweden
SMR	Steam methane reforming
SO_x	Sulphur oxides
T/O	Take-off
UHC	Unburned hydrocarbons
VIGV	Variable inlet guide vane
VSV	Variable stator vane
USGS	United States Geological Survey

Notations

Symbol	*Definition*	*Unit*
A	Area	m^2
	Constant	-

a	Acceleration	m/s^2
	Speed of sound	m/s
AM	Aircraft mass	kg
AW	Aircraft weight	N
B	Constant	K/m
b	Wall thickness	m
BFL	Balanced field length	m
BPR	By-pass ratio	-
C	Constant	Pa, K/Pa s or DU/kg
C_D	Drag coefficient	-
C_{D0}	Drag coefficient at zero lift	-
C_L	Lift coefficient	-
C_{Lmax}	Maximum lift coefficient with extended flaps and slats	-
C_{L2}	Lift coefficient at the take-off safety speed, V_2	-
C_p	Specific heat at constant pressure	J/kg K
C_v	Specific heat at constant volume	J/kg K
C_1	Constant	s
C_2	Constant	s^2/m
c	Mixing ratio of CO_2 (after addition)	ppm(V)
c_0	Mixing ratio of CO_2 (before addition)	ppm(V)
CDS	Drag coefficient times reference area	m^2
COT	Combustor outlet temperature	K
D	Constant	Pa/m
	Diameter	m
	Drag	N
DOC	Direct operating cost	Any currency
E	Constant	-
	Work output (or input)	W
E_i	Warming effect of trace gas i	W/m^2
EI	Emission index of pollutant emission	g/kg
ESFC	Energy specific fuel consumption	J/N s
EW	Dry engine weight	kg
F	Constant	Pa
	Thrust	N
FAR	Fuel-air ratio	-
FPR	Fan pressure ratio	-
FW	Fuel weight	kg
G	Constant	1/m
h	Altitude	m
	Enthalpy	kJ/kg
	Pressure height	m
I	Constant	kg/m^3
IAS	Indicated air speed	m/s
J	Constant	kg/m^4
k	Constant	- or kg/m^3
	Rate factor	cm^3/mole s

L	Length	m
	Constant	-
	Lift	N
L/D	Aerodynamic efficiency	-
$(L/D)_2$	Aerodynamic efficiency at V_2	-
LHV	Lower heating value	MJ/kg
LSF	Linear scale factor	-
M	Constant	kg/m^3
	Mass	kg
m	Constant	-
	Mixing ratio of CH_4 (after addition)	ppm(V)
m_0	Mixing ratio of CH_4 (before addition)	ppm(V)
Ma	Mach number	-
MTOM	Maximum take-off mass	kg
MTOW	Maximum take-off weight	kg
MW	Molecular weight	g/mol
N	Constant	1/m
n	Constant	-
	Mixing ratio of N_2O (after addition)	ppm(V)
	Number	-
n_0	Mixing ratio of N_2O (before addition)	ppm(V)
Nu	Nusselt number	-
OFPR	Outer fan pressure ratio	-
OME	Operating mass empty	kg
OPR	Overall pressure ratio	-
P	Pressure	Pa
	Production rate	$g(species)/g(NO_x)$
Pr	Prandtl number	-
Q	Emission	kg
	Heat transfer	W
q_{ref}	Reference dynamic pressure ($=\rho_3 * U_{ref}^2/2$)	kg/m s
R	Gas constant	J/kg K
R_u	Universal gas constant	J/mole K
Re	Reynolds number	-
RF	Radiative forcing	W/m^2
RoC	Rate of climb	m/s
S	Distance	m
	Sensitivity function	W/m^2 DU
	Wing area	m^2
SFC	Specific fuel consumption	g/kN s
SOT	Stator outlet temperature	K
SPT	Specific thrust	N s/kg or m/s
SSLT	Static sea-level thrust	N
T	Temperature	K
	Time horizon	yr
T_0	Surface temperature of the Earth	K
t	Time	yr, d or s
TAS	True air speed	m/s

TET	Turbine entry temperature	K
TEM	Total engine mass	kg
TOM	Take-off mass	kg
TOP	Take-off parameter	N/m^2
U	Overall heat transfer coefficient	W/m^2 K
U_{ref}	Mean velocity across the plane of maximum of cross-sectional area of the casing in the absence of a liner (refers to a combustor)	m/s
UFL	Unfactored field length	m
V	Velocity	m/s
V_{mol}	Volume of a mol (273.15 K, 101325 Pa)	m^3
V_2	Take-off safety speed	m/s
W	Mass flow	kg/s
X	Species	DU
	Volume fraction	-
Y	Mass fraction	-
	Species	DU
α	Convection heat transfer coefficient	W/m^2 K
γ	Climb angle	°
	Ratio of specific heats (C_p/C_v)	-
Δ	Change	Any unit
ε	Thermal effectiveness of a heat exchanger	-
η	Efficiency	-
λ	Climate sensitivity parameter	K m^2/W
	Thermal conductivity	W/m K
μ	Rolling friction coefficient	-
ρ	Density	kg/m^3
σ	Relative atmospheric density	-
τ	Residence time	yr or d
ϕ	Equivalence ratio	-
ψ	Mole fraction	-

Subscripts and Superscripts

1	Engine intake front flange
2	Compressor inlet
3	Compressor outlet, combustor inlet
4	Combustor outlet, turbine inlet
5	Turbine outlet
6	Engine outlet
A	Air
	Area
a	Ambient
c	Carnot
	Cold
CO2	Carbon dioxide

corenoz	Nozzle of the core
cseg2	Second segment of take-off climb
dat	Datum
eng	Engine
F	Fuel
f	Fluid
fan	Fan of turbofan engine
g	Combustion gases
	Gas generator (compressor(s), high-pressure turbine and combustor)
gin	Combustion gases at inlet
gout	Combustion gases at outlet
h	Highest
	Horizontal
	Hot
HE	Heat exchanger
H2	Hydrogen
H2in	Hydrogen at inlet
H2O	Water vapour
H2out	Hydrogen at outlet
i	Generic number
	Inner
ic	Initial cruise
ISA	International standard atmosphere
j	Jet
KE	Kerosene equivalent
l	Lowest
lm	Log mean
m	Exponent in equation (4-5)
	Maximum
	Mean
N	Nacelle
	Net
n	Exponent in equation (4-5)
NOx	Nitrogen oxides ($NO + NO_2$)
N07	Net at 0.7 times the take-off safety speed, V_2
N2	Net at the take-off safety speed, V_2
o	Outer
	Overall
O3	Ozone
OH	Overhead
outcore	Exhaust of the core
v	Vertical
p	Propulsive
pz	Primary zone
R	Reaction zone
rf	Rolling friction
s	Static

st	Stoichiometric
sto	Total take-off static
t	Total
tf	Energy transformation from the low-pressure turbine to the fan
th	Thermal
v	Vertical
vol	Volume
X	Species X
*	Nominal measured quantities
∞	Rated output (refers to certification according to ICAO's standard)

1 INTRODUCTION

Since commercial aviation started in 1920 it has undergone spectacular growth, and today it has become a fundamental part of business and commerce. Mainly for business purposes, engine and aircraft manufacturers, and airlines compile forecasts for the future traffic growth. As the global gross domestic product growth and aviation traffic are closely linked, most air traffic growth forecasts are based upon assessments of global economic trends. Over the next 20 years global passenger aviation traffic is expected to grow, averaging around 5.3% annually over the next 20 years [Rogers et al., 2002], implying an almost threefold traffic volume at the end of this period. It is expected that capacity growth, i.e. number of seats offered, will expand at a slower rate, provided that passenger load factors maintain their improving trend over the long term.

In addition to the anticipated air traffic growth, the greenhouse effect generated by emissions produced by human activity, particularly carbon dioxide, has become an increased concern. The majority of scientists today are in agreement that discharging greenhouse gases into the atmosphere has an impact on the global climate. Furthermore, the dwindling fossil oil resources raise concerns. It is, therefore, essential to find an alternative to kerosene for civil aviation. In the context of this thesis, hydrogen, in the longer term produced from renewable energy sources, is addressed as a suitable future fuel in order to cope with these concerns.

In this introductory chapter, first the scientific approach for the thesis is given (section 1.1), followed by an overview of the environmental concerns in general of conventional aviation, i.e. not cryoplanes (section 1.2). As one of the two main reasons for looking at hydrogen for aviation is the existing and foreseen climate change due to the combustion of fossil fuels, a fairly detailed explanation (in the context of this thesis) of the greenhouse effect and its potential consequences is given. This section also provides a brief insight on which are the pollutant emissions of conventional aviation, how they are formed and their effects on the environment, with emphasis on global warming. The second main reason for wanting to find an alternative to kerosene is that oil is a limited resource that is expected to be depleted within the next few decades. Therefore, an overview of the availability of fuel resources and effects on fuel costs is given in section 1.3. In section 1.4 the subject of using an alternative fuel for aviation is introduced, and previous work on hydrogen is outlined in section 1.5. The objectives and scope of the thesis are included in section 1.6, and finally this chapter is finished by an outline of the thesis structure (section 1.7).

1.1 Scientific Approach for the Thesis

Introducing a novel fuel for civil aviation will affect various fields, e.g. the fuel distribution systems, the engines, the airframe and the environmental impact, particularly if the fuel is cryogenic in contrast to kerosene. All of these issues are important to know in order to judge the potential of this technology as a measure to conform to future constrains on civil aviation, especially related to environmental issues and limited oil resources. Because the introduction of hydrogen will influence the complex interactions with a number of different fields affected by the introduction of

hydrogen and because hydrogen is not considered a practical alternative at present but a number of years ahead, the most appropriate approach is to carry out a broad study. A broad study results in making it possible to define those fields of which more research and development are necessary in order to move towards liquid hydrogen-fuelled aircraft in civil aviation. A broad approach will provide knowledge on the technical feasibility of this fuel change, taking practical aspects into account.

Moreover, in order to address properly the overall research question of the thesis, i.e. the potential of reducing the environmental impact of civil subsonic aviation by using hydrogen, conducting a broader study is the more suitable approach to take. For these reasons, the chosen scientific approach for this thesis is to carry out a broad study covering a number of selected fields, rather than one in-depth study limited to one subject.

The research presented in this thesis was partly performed in collaboration with the EC-sponsored project CRYOPLANE, in which both Cranfield University and FOI were involved. Being involved in the CRYOPLANE project offered access to the results and the comprehensive knowledge obtained within the project, and contacts with other experienced researchers within the field were established. The connections to the CRYOPLANE project and to Cranfield University's extensive experience in gas turbine technology, formed the basis for this Ph.D. project.

1.2 Environmental Concerns of Aviation

In recent years the environmental effects of emission from civil aviation have been under discussion, and there is a growing body of evidence that future growth in air traffic might result in significant impacts on local air quality and the global climate [Rogers et al., 2002]. While the concerns of local air quality usually arise from the potential impact on human health of high concentrations of gaseous or particulate species over a relatively small area (tens of square kilometres), the global concerns relate to the potential impacts of the emissions on climate change.

This section is introduced with an overview of the physical mechanisms behind the greenhouse effect (section 1.2.1). The influence of man-made emissions on the climate system, both up until the present point in time and projected influences for the future, are discussed. Section 1.2.2 provides a brief overview of the formation principles, mitigation strategies, and the effects on the environment and human health of the exhaust emissions of aircraft. Assessments of the climate impact of aviation today and in the future are given.

1.2.1 The Greenhouse Effect and Its Potential Consequences

In trying to understand the greenhouse effect one should be aware that the Earth's climate system is an extremely complex interactive system. Following the definition in IPCC (2001), the climate system consists of five major components: the atmosphere, the hydrosphere (all liquid surface and subterranean water), the cryosphere (sea ice, ice sheets and glaciers), the land surface and the biosphere, which are forced or influenced by various external forcing mechanisms, of which the sun is the most important one.

Although the components of the climate system are very different, they are linked by fluxes of mass, heat and momentum. Whilst most of these interactions are understood, some are poorly known or perhaps even unknown. Describing the interactions among all these components and attempting to provide a thorough description of the climate system is beyond the ambitions of this section. The interested reader is referred to IPCC (2001).

For a stable climate on Earth, a balance is required between the incoming solar radiation and the outgoing radiation emitted by the climate system. Following the explanation given in IPCC (2001) on the sun and the global energy balance, about 31% of the incoming solar radiation of 342 W/m^2 is immediately reflected back into space by clouds, the atmosphere and the Earth's surface. The remaining radiation (235 W/m^2) is partly absorbed by the atmosphere, but most of it (168 W/m^2) warms the Earth's surface, i.e. the land and oceans. In turn, the Earth's surface emits heat as infrared radiation, sensible heat (thermals) and water vapour which releases its heat at altitude when it condenses. A schematic description of the energy balance is shown in Figure 1-1. The left-hand side of the figure shows what happens with the incoming solar radiation, while an explanation of what happens with the heat released from the Earth is given on the right-hand side of the figure.

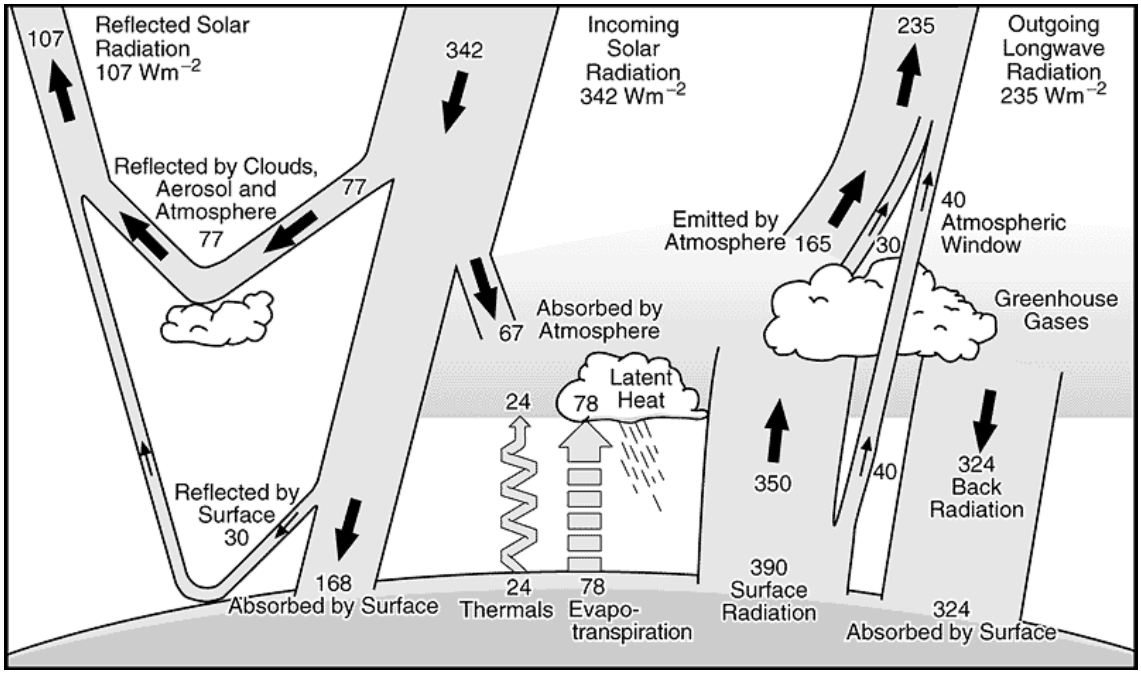

Figure 1-1. The Earth's annual and global mean energy balance [IPCC, 2001].

In order to achieve a balance between the incoming solar radiation and the outgoing radiation, the climate system itself should radiate on average 235 W/m^2 back into space. As any physical object radiates energy of an amount and at wavelengths typical for the temperature of the object (e.g. at a higher temperature more energy is radiated at shorter wavelengths), there is a certain effective emission temperature that corresponds to the average radiation back into space, i.e. 235 W/m^2. With typical wavelengths in the infrared part of the spectrum this temperature is equal to -19 °C, which is 33 °C lower

than the average temperature of 14 °C at the Earth's surface [IPCC, 2001]. The effective emission temperature of -19 °C corresponds in mid-latitude to a height of approximately five kilometres. This deviation in temperature is explained by the radiative properties of the atmosphere in the infrared part of the spectrum.

Within the atmosphere a number of trace gases, so-called greenhouse gases, which own the features of being partly transparent for shortwave radiation (from the sun), while a significant part of the longwave heat radiation (from the Earth's surface) are absorbed and emitted. The most important greenhouse gases are carbon dioxide, methane (CH_4), nitrous oxide (N_2O) and ozone (O_3). These gases have only a total volume mixing ratio of less than 0.1%, but play an essential role in the Earth's energy budget. Furthermore, the atmosphere contains the natural greenhouse gas water vapour (volume mixing ratio in the order of 1%).

That is to say that the main part of the radiation from the sun is absorbed by the Earth's surface without being absorbed or reflected in the atmosphere. However, a substantial part of the infrared radiation from the Earth's surface is absorbed by the greenhouse gases in the atmosphere. In turn, these gases emit infrared radiation in all directions including downward to the Earth's surface. Hence, the greenhouse gases trap heat within the atmosphere, giving an average temperature on the surface of the Earth 33 °C lower than the temperature corresponding to the average radiation back into space. This mechanism is called the natural greenhouse effect [IPCC, 2001].

Human beings, like other living organisms, have always influenced their environment. However, since the beginning of the Industrial Revolution in the mid-18th century, the impact of human activities has become significant and extends to a much larger scale (continental or even global). In particular the combustion of fossil fuels that produce greenhouse gases has become a major concern. In addition, human activities have introduced strong greenhouse gases that are not naturally present in the atmosphere: chlorofluorocarbons (CFCs) and other chlorine and bromine compounds. These gases not only contribute to the radiative forcing[1], but also lead to the depletion of the stratospheric ozone layer.

Mainly due to the combustion of fossil fuels (three-quarters) and the deforestation (one-quarter) (since the biosphere absorbs carbon dioxide), the concentration of carbon dioxide in the atmosphere has increased by more than 30% since pre-industrial times, and is still increasing at an unprecedented rate of on average 0.4% per year [IPCC, 2001]. It is the presence of an increased concentration of CO_2 and other greenhouse gases in the atmosphere due to anthropogenic sources that causes the enhanced greenhouse effect. An increased concentration of greenhouse gases in the atmosphere improves the absorption and emission of infrared radiation. The atmosphere's opacity increases and the altitude from which the Earth's radiation is effectively emitted into space increases. At a higher altitude the temperature is lower, and thus the energy emitted into space is lowered, causing a positive radiative forcing. This is called the

[1] Radiative forcing (RF): imbalance due to either a change in solar radiation or the infrared radiation that changes the net radiation [IPCC, 2001]. A positive radiative forcing implies a warming of the Earth's surface.

enhanced greenhouse effect [IPCC, 2001]. One of the consequences of this positive radiative forcing is an increased average temperature at the surface of the Earth.

Owing to a number of uncertainties related to various feedback mechanisms of an increased greenhouse effect, the temperature increase due to a specified additional amount of, for instance, CO_2 in the atmosphere cannot be predicted without including a wide uncertainty margin. A significant part of this uncertainty range arises from our limited knowledge of clouds, which play an important role in the Earth's energy balance, and their interactions with radiation. It is believed that the temperature rise will be higher than that caused by the additional CO_2 by itself. The most important feedback mechanism responsible for the amplification of the temperature increase is the so-called water vapour feedback, caused by an increase in atmospheric water due to a temperature increase [IPCC, 2001]. The response of the climate to human-induced forcings is complicated not only by the feedback mechanisms discussed above, but also by the strong non-linearity of many processes and by the fact that the various coupled components of the climate system have very different response times to perturbations.

Since the late 19th century a mean global warming of 0.4 to 0.8 °C of the atmosphere at the surface has been observed, see Figure 1-2.

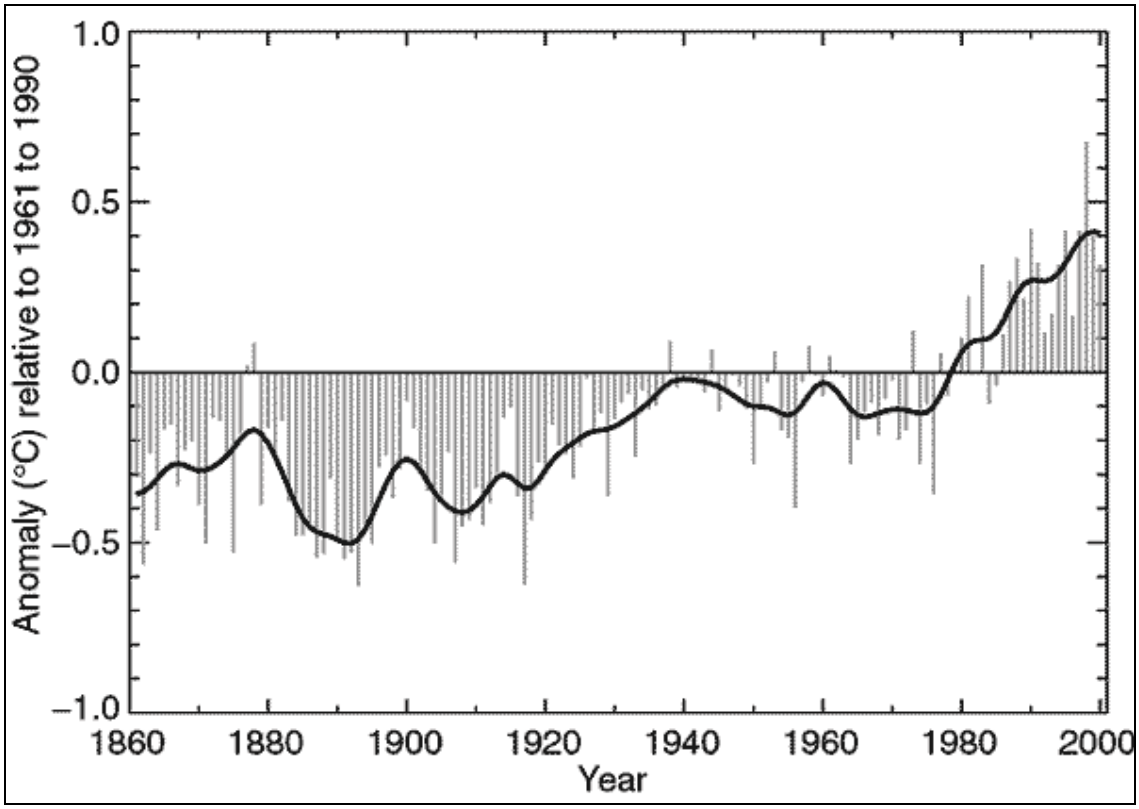

Figure 1-2. Annual anomalies of global average surface air temperature for the period 1861 to 2000 relative to 1961 to 1990 values [IPCC, 2001].

The increase in temperature took place in two distinct phases: the first one between 1910 and 1945, and recently since 1976. Surface temperature records indicate the 1990s are likely to have been the warmest decade of the millennium in the Northern

hemisphere [IPCC, 2001]. Possibly related, amongst other factors, to an increase in cloud cover, recent years have been exceptionally warm, with a larger increase in minimum than in maximum temperatures. During the twentieth century the sea level has risen by 10 to 20 cm and glaciers worldwide, except in a few maritime regions, e.g. Norway and New Zeeland, have retreated.

It is justified to question whether these observed climate changes are a consequence of increased greenhouse gas concentrations or simply an effect of natural variations. Employing detection and attribution studies, model simulations imposing different assumptions can be compared with measured data. In Figure 1-3 three different cases of model simulations are compared with observed data: (a) only natural forcing (solar variation and volcanic activity), (b) only anthropogenic forcing (greenhouse gases and an estimate of aerosols) and (c) both natural and anthropogenic forcings. As indicated in Figure 1-3 (a) natural forcings may have contributed to the observed warming during the first half of the twentieth century. On the contrary, simulations of the response to natural forcing alone do not explain the warming during the second half of the twentieth century. In IPCC (2001) it is claimed: “In the light of new evidence and taking into account the remaining uncertainties, most of the observed warming over the last 50 years is likely to have been due to the increase in greenhouse gas concentrations.”

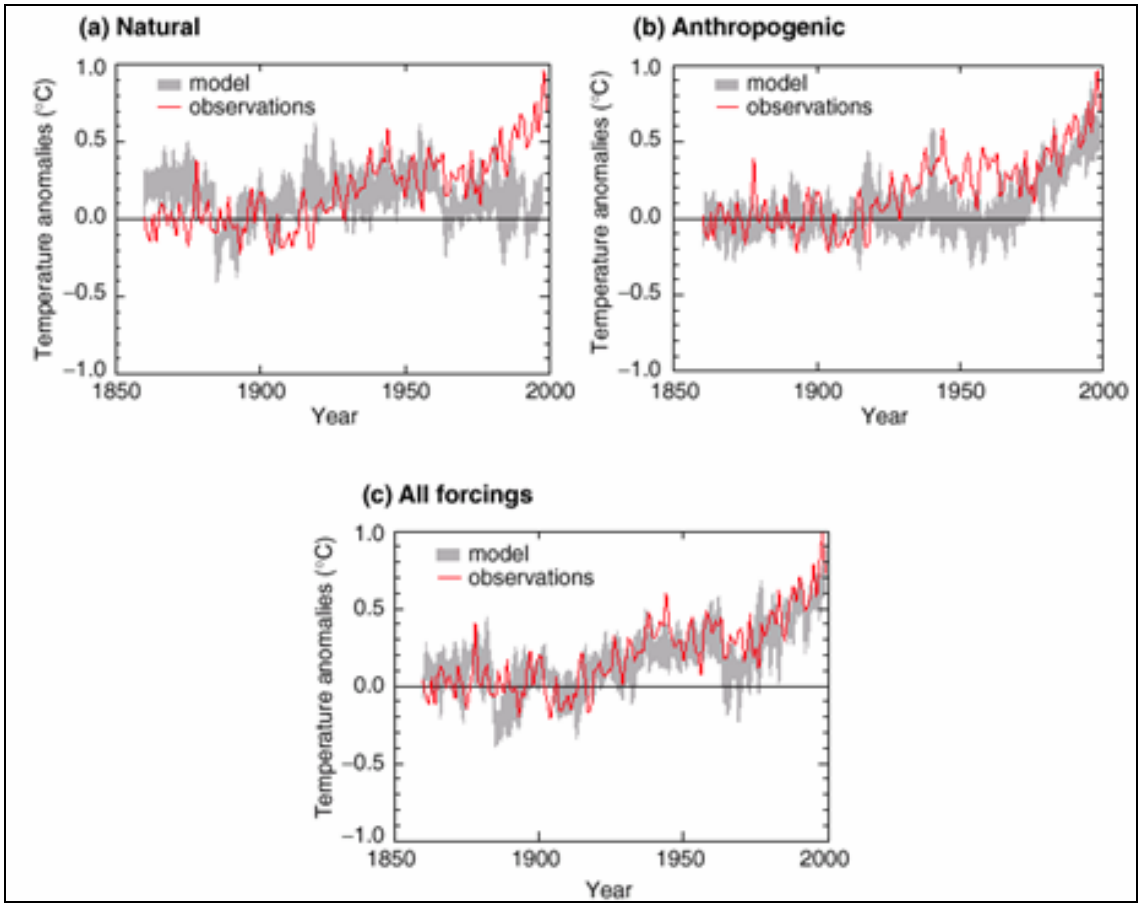

Figure 1-3. Simulation of annual global mean surface temperature variations, which are compared with measured changes [IPCC, 2001].

Having concluded that there are reasonable reasons to believe that emission from anthropogenic sources affect the climate already, it is worthwhile to take a look what might happen in the future. Using model simulations and applying various scenarios of the future, IPCC (2001) project that the global average temperature will increase by 1.4 to 5.8 °C over the period 1990 to 2100. During this period global average water vapour concentrations and precipitation are projected to increase, and extreme weather and climate events, e.g. higher maximum temperatures, more intense precipitation events and increased summer continental drying, are expected to be more frequently occurring. Owing primarily to thermal expansion and loss of mass from icecaps, global mean sea level is projected to rise by 0.09 to 0.88 meters. There is also a concern that the ocean thermohaline circulation could weaken, which would lead to a reduction of the heat transport into high latitudes of the Northern Hemisphere. If the change in radiative forcing is large enough and applied long enough, the thermohaline circulation could completely shut-down in either hemisphere beyond 2100, with major consequences on the Earth's climate system [IPCC, 2001].

From the preceding discussion it can be concluded that global warming due to anthropogenic sources is a serious concern that needs to be dealt with in order to mitigate the consequences. Taking the concern of global warming seriously and moving away from technologies based on fossil fuels is of particular interest since greenhouse gases, such as, CO_2 and N_2O, are very long-lived, and hence will continue to affect the climate system hundreds of years after they have been discharged into the atmosphere.

1.2.2 Aircraft Exhaust Emissions

Provided that a conventional fuel containing both carbon and hydrogen is burnt, the gas turbine exhaust emissions comprise the primary combustion products: carbon dioxide (CO_2) and water vapour (H_2O), and the secondary combustion products: oxides of nitrogen (NO_x), unburned hydrocarbons (UHC), carbon monoxide (CO), oxides of sulphur (SO_x) (if the fuel contains sulphur) and particulate matter. In general, NO_x, CO, UHC and particles are relevant to local air quality issues, while CO_2, H_2O, NO_x, SO_x and particles are of most concern with respect to climate perturbations [Rogers et al., 2002].

The emissions of CO_2 and H_2O are unavoidable end products of the combustion process, and their quantities are directly proportional to the fuel consumption. In order to alter any of these, either the fuel consumption or the fuel composition needs to be changed. The fuel consumption can be reduced by improving the overall efficiency of the engine and/or reducing the aircraft weight. Another option is to improve the aerodynamic efficiency of the aircraft. Both CO_2 and H_2O emissions contribute to global warming via the greenhouse effect (section 1.2.1). Carbon dioxide is a long-lived gas with a residence time in the atmosphere of 100 years or more. An increased concentration of CO_2 alters the radiative balance of the Earth, and thereby contributes to global warming. Although the present CO_2 emissions from aircraft are only about 2% of that from the total anthropogenic emissions, and thereby contribute a smaller fraction of the total CO_2 radiative forcing, this fraction is expected to increase over the next 100 years [Rogers et al., 2002].

Water vapour causes partly a direct radiative impact on the climate system, and partly an indirect effect by the formation of line-shaped ice clouds, so-called contrails. Contrails are formed in combination with particles (present in the exhaust) and they may alter the cirrus cloud coverage, which in turn may affect the climate system. In the troposphere the direct impact on the climate of water vapour is small. Studying conventional aircraft, IPCC (1999) and Morris et al. (2003) suggest that the direct impact of water vapour emissions from subsonic aviation on the radiative balance is negligibly small. Currently research is going on to assess the potential impact on the atmosphere of water vapour emitted by aviation [e.g. Morris et al., 2003; and Gauss et al., 2003]. At this point it cannot be excluded that water vapour from aircraft, including its secondary effects, plays a major role in the climate impact of air traffic.

Most of the nitrogen oxides formed during combustion are in the form of NO; however, subsequently the NO oxidizes to NO_2. Usually these are lumped together, and the result is expressed in terms of oxides of nitrogen (NO_x). The formation processes of NO in combustion are complex and generally comprise different mechanisms, see section 2.3.1. Except for very fuel lean combustion systems, thermal NO, which is produced from the nitrogen and oxygen present in the air in the high-temperature regions of the flame and in the postflame gases, is the most contributing mechanism to the total NO formation. In order to reduce the NO_x emissions there are a number of different combustor concepts suggested aimed at reducing primarily the combustion temperature, but also the residence time in the hot combustion zone. As for possibilities for low NO_x emissions when using hydrogen, this is discussed in detail in section 2.3, whereas mitigation options for conventional engines are beyond the scope of this thesis. For information on the latter the reader is directed to, for instance, Lefebvre (1998).

At ground level the presence of NO_x results in an increase in ozone concentration, which during prolonged exposure may cause respiratory illness, impaired vision, headaches and allergies [Lefebvre, 1998]. The influence of NO_x emissions on the climate is indirect through its chemical impact on the atmospheric ozone and methane concentration: at altitudes below about 15 km, NO_x emissions cause an increase of the upper tropospheric ozone, thus contributing to the greenhouse effect, while at the same time increasing the atmospheric OH concentration, which decreases the CH_4 (and CO) lifetime [e.g. Isaksen et al., 2001]. The latter lowers the atmospheric CH_4 concentration, and thereby reduces the greenhouse effect. Moreover, NO_x emissions cause damage to plant life as well as add to the problem of acid rain. At high altitudes (above about 15 km) NO_x emissions cause ozone depletion, and hence increased ground-level ultra-violet radiation, which might cause skin cancer and eye diseases [Singh, 2001].

Emissions of UHC and CO form due to incomplete combustion in regions of low temperature and/or short residence of the combustion chamber. These are circumstances that in most cases occur at low power conditions. The UHC and CO emissions are reduced by redistribution of the air flow to bring the primary zone equivalence ratio closer to the optimum value (about 0.8), and by an increase in the primary zone volume and/or residence time [Lefebvre, 1998]. Moreover, these are lowered by a reduction in liner wall-cooling air and by improved fuel atomization. Emissions of UHC and CO are both toxic. Carbon monoxide reduces the capacity of the blood to absorb oxygen and in high concentrations it can cause asphyxiation and even death [Lefebvre, 1998]. In

addition to the human health concerns of these emissions, UHC combine with oxides of nitrogen to form photochemical smog.

All of the sulphur in the fuel is oxidised to oxides of sulphur, the main part becoming sulphur dioxide (SO_2). Oxides of sulphur are toxic and corrosive, and lead to the formation of sulphuric acid in the atmosphere [Lefebvre, 1998], which contributes to the acidification. The only viable limitation strategy is to remove the sulphur from the fuel prior to the combustion.

Particulate matter is a common notation for various particles with varying chemical composition in many different sizes that can originate from a range of natural and man-made sources. With respect to particles from aviation, these can be divided into two different types: soot and volatile particles [Rogers et al., 2002]. The volatile particles are thought to form from condensed sulphuric acid and possibly condensable organic species. Soot consists mostly of carbon (96%) and a mixture of hydrogen, oxygen and other elements [Lefebvre, 1998]. It is formed in local fuel-rich regions within the engine's combustion chamber. The propensity to produce carbon is most severe at high pressures. In order to lower the soot emissions, attention should be paid to the fuel injector design and measures to enhance the mixing process of fuel and air.

Soot is not toxic in small quantities (though there are human health concerns) but the larger particles give rise to visible smoke that soils the atmosphere. However, some smoke suppressants contain heavy metals, such as barium, and whilst they may eliminate or reduce the smoke production, the resulting emissions now contain highly toxic metals [Singh, 2001]. Particles play an important role in contrail formation by acting as condensation nuclei for water vapour and other condensable species.

Considering the total climate impact of subsonic aviation in terms of radiative forcing, the best estimate for 1992 is 0.05 W/m^2 or 3.5% of the total radiative forcing by all anthropogenic activities [IPCC, 1999]. This assessment combines the effects from changes in concentrations of carbon dioxide, ozone, methane, water vapour, line-shaped contrails, and aerosols, but does not include possible changes in cirrus cloud coverage. In Figure 1-4 the contributions to radiative forcing from the different emissions are shown. The bars indicate the best estimate, while the line associated with each bar indicates the uncertainty range. Using the best knowledge and tools available at the time for publishing this graph, it is claimed that there is a 67% probability that the true value falls within the uncertainty range [IPCC, 1999]. The level of scientific understanding for each emission is indicated at the bottom of the figure. It is anticipated that aviation's contribution to global climate change is approximately in proportion to its contribution to global warming. Evidently from the figure, the magnitude of the climate impact from aviation, similarly as from other sources, is highly uncertain.

Based on recent results obtained within the EC-sponsored project TRADEOFF and other studies, the figures on the radiative forcing contribution from air traffic (Figure 1-4) have been revised [Schumann, 2003]. The main changes originate from a reduced optical thickness of line-shaped contrails and a first estimate of aviation-induced cirrus cloud cover changes. The effect of CO_2 is expected to be larger and the contrail effect smaller, while the level of scientific understanding has not changed significantly.

Recent studies suggest that the global mean radiative forcing effect (including the cirrus cloud effects) of aviation is higher than assessed in IPCC (1999), though the impact of supersonic transport is expected to be lower than assessed in IPCC (1999).

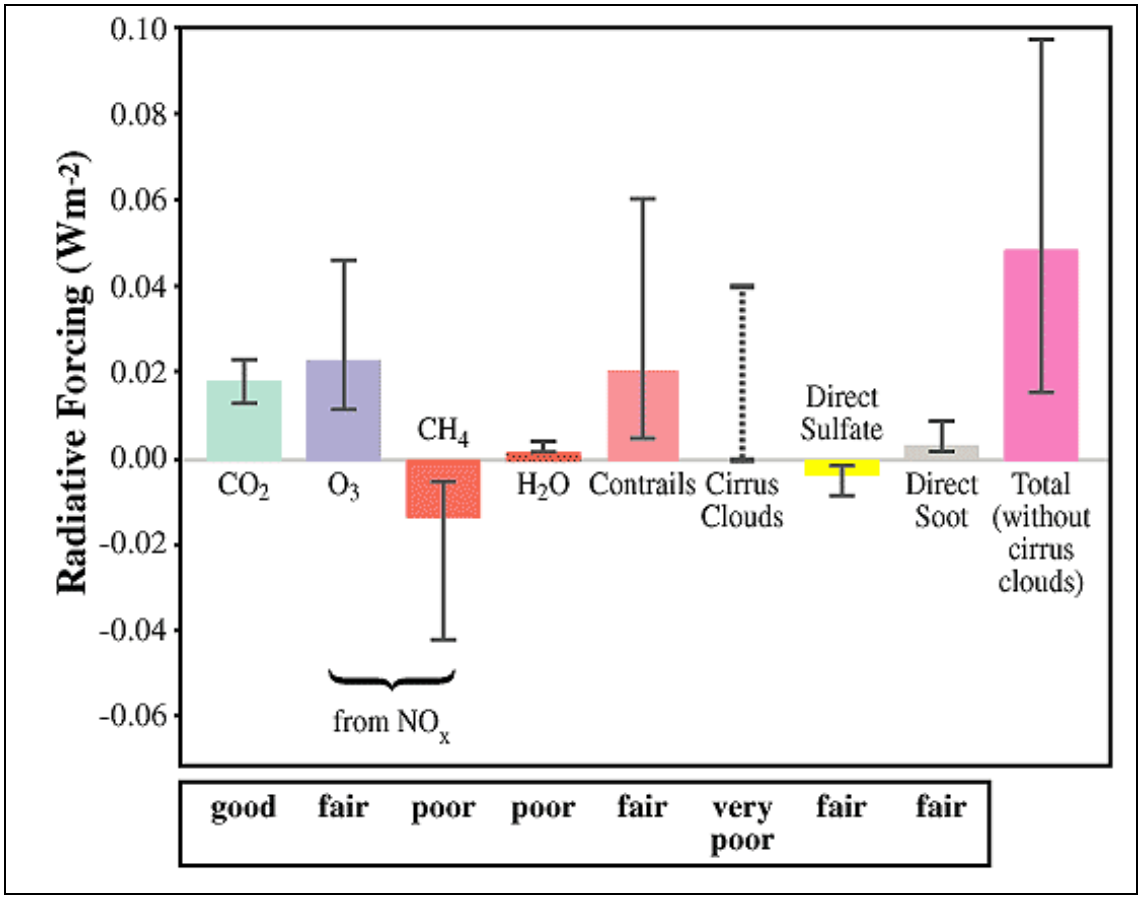

Figure 1-4. Estimates of the globally averaged radiative forcing from subsonic aircraft emissions in 1992 [IPCC, 1999].

In the future, aviation's share of the radiative forcing is expected to increase, mainly as an effect of a significant air traffic growth. By 2050, aviation's contribution to radiative forcing is expected to increase to between 3.4 and 14.7% of the total radiative forcing by all anthropogenic activities [IPCC, 1999]. The figure in 2050 depends on which scenario of the air traffic development is applied and assumptions on the development of non-aviation emissions.

1.3 Availability of Fuel Resources and Effects on Fuel Costs

Today the oil resources are concentrated in a few regions, with the Middle East holding over 40% of the total and over 65% of current conventional oil reserves [Schnieder and McKay, 2001]. When the oil resources will be completely depleted is very difficult to assess and estimations have varied over time and among different experts. In June 2000 the United States Geological Survey (USGS) published new estimates of ultimately recoverable oil resources [Schnieder and McKay, 2001]. They estimate that slightly more than 3000 billion barrels of conventional oil could ultimately be recovered with

known and expected technology (see Figure 1-5). In addition to this, they believe that another 350 billion barrels of natural gas liquids (NGLs)[2] could be recovered, and over 850 billion barrels of unconventional oil (heavy oil and bitumen) could be produced. It is worth mentioning that producing oil from unconventional sources requires substantially more energy than recovering conventional oil reserves, which will have a detrimental effect on the fuel price. According to USGS, up until 2001 about 900 billion barrels had been consumed, implying that about 21% of the ultimately recoverable oil of 4200 billion barrels was consumed by 2001. Other experts believe that significantly less oil can be ultimately recovered. For instance, Colin Campbell[3] believes that only 1800 billion barrels can ultimately be recovered.

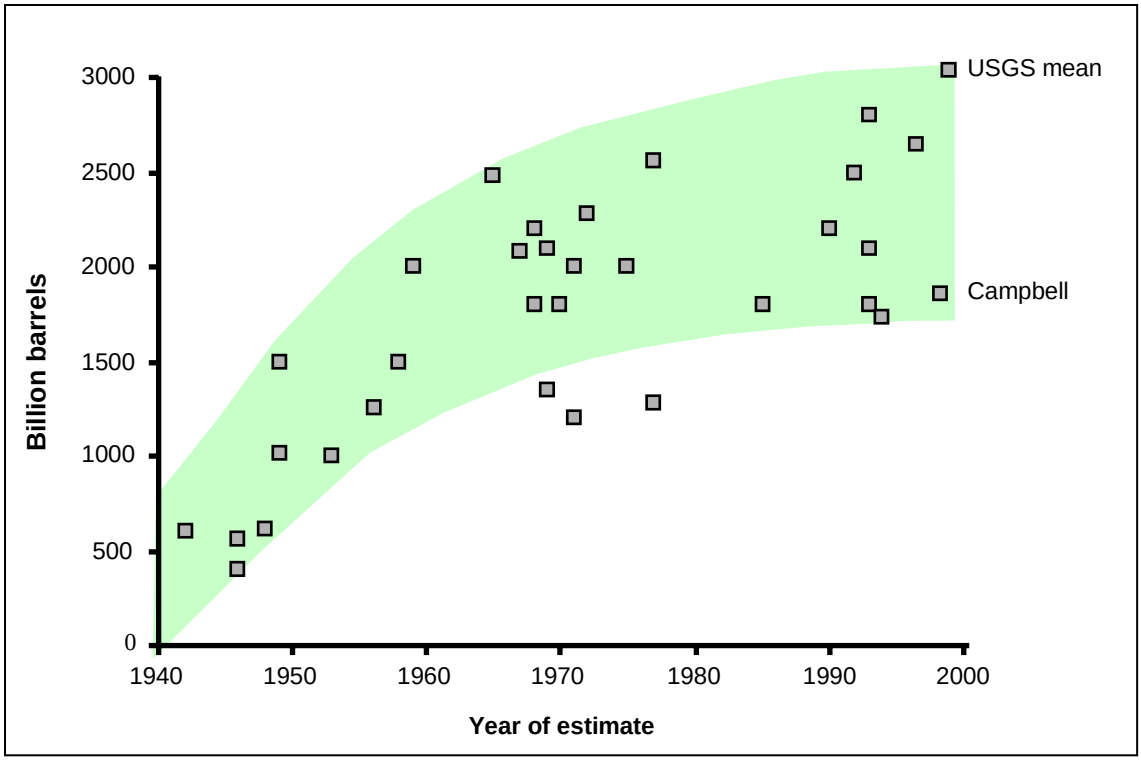

Figure 1-5. Ultimately recoverable oil of conventional resources [Schnieder and McKay, 2001].

The large deviation between these assessments is explained mainly by two reasons: different assumptions made for potential new discoveries and different expectations of the ultimate recovery factors (the percentage of oil in place that can be extracted economically) in conventional resources. Based on the declining discovery rates over the past two decades, Campbell believes that only 160 billion barrels of additional discoveries will be made, whereas USGS assesses that another 460 billion barrels could

[2] NGLs (Natural Gas Liquids): petroleum that occurs naturally as a gas in the reservoir, but as a liquid under surface conditions.

[3] Colin Campbell is a Trustee of the Oil Depletion Analysis Centre ("ODAC"), a charitable organisation in London that is dedicated to researching the date and impact of the peak and decline of world oil production due to resource constraints, and raising awareness of the serious consequences of oil depletion (see http://www.hubbertpeak.com/campbell/).

be found. According to USGS, the average recovery factor could be increased from the current 35% to over 40% during the next three decades, which would result in an additional 700 billion barrels of recoverable oil. Campbell, on the other hand, does not expect an increase in the recovery factor.

USGS estimates that the ultimate recoverable world oil resources would supply an expansion of 2% per annum through 2025, reaching around 125 million barrels per day (Figure 1-6). Thereafter a plateau could occur for around two decades before depletion would lead to a permanent decline in production. Other specialists believe that the plateau will be reached earlier. Campbell believes that a plateau of conventional oil production will be reached before 2010, with significant price rises thereafter [Schnieder and McKay, 2001]. There are a number of factors that influence whether the actual oil supply will reach these levels. Competing fuel prices and environmental concerns may cause the supply to decline earlier. Conversely, if efficiency measures are adopted over the next two decades, Schnieder and McKay (2001) suggest that the oil supply could continue to expand at a slower growth rate well beyond 2025.

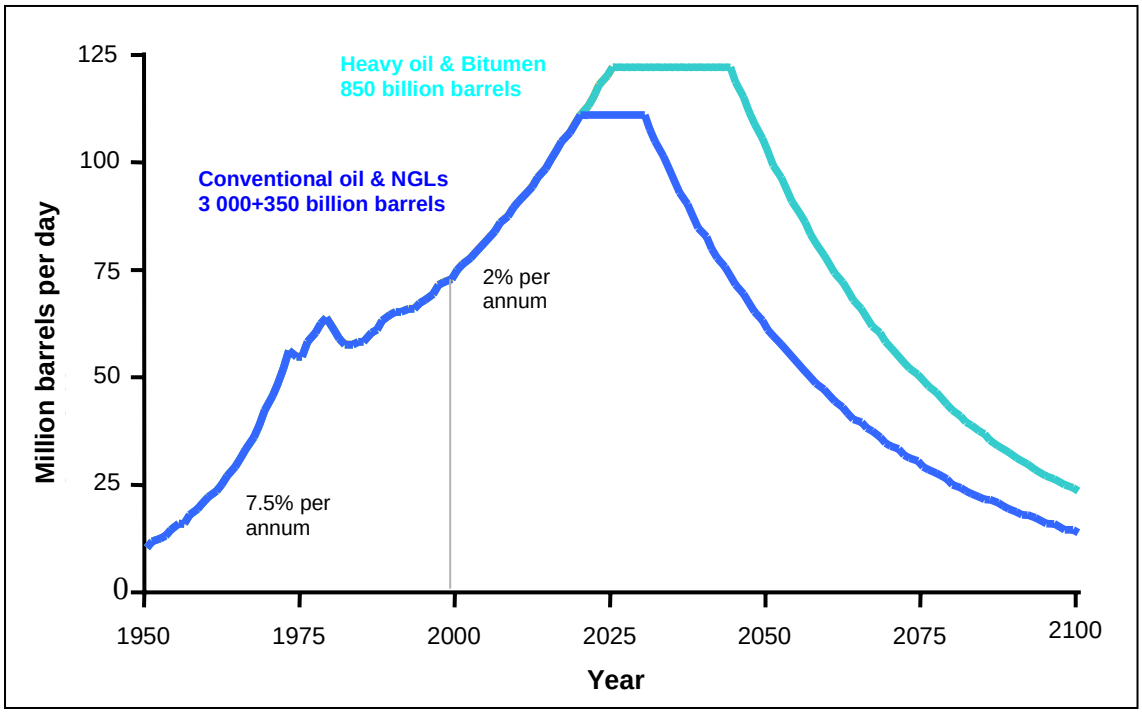

Figure 1-6. Potential of liquids (oil) production [Schnieder and McKay, 2001].

The future fuel price is difficult to predict and its magnitude is dependent on various factors. In the longer run the oil supply, which obviously is highly uncertain, probably will have the largest influence on the fuel price. Expressed in the currency of 2000, Schnieder and McKay (2001) do expect that most of the resource base could be produced for less than $20 per barrel. The production cost of unconventional resources has seen dramatic cost reductions over the past two decades, and is now estimated to be below $15 per barrel for significant proportions of the resources. Furthermore, gas to liquids technology is now competitive at below $15 per barrel of oil equivalent. The marginal cost of non-OPEC oil production has decreased from over $30 per barrel in the

early 1980s to about $16 in 2000. Then, during the first decade of the twenty-first century, Schnieder and McKay (2001) believe that available technologies lead to even lower costs until the depletion starts to outweigh technology advances and leads to cost increases.

Other forecasts predict the oil production cost to be much higher. For instance, the IEA 2000 outlook expects crude oil prices to reach $28 (2000 prices) per barrel by 2020, based on a demand of 115 million barrels per day [Schnieder and McKay, 2001]. Assuming a crude oil price of $24 per barrel, the US DOE 2000 energy outlook forecasts jet kerosene reaching around $6 (2000 prices) per GJ by 2020 [Schnieder and McKay, 2001]. There is now reason to expect kerosene prices to break out of the traditional relation to crude oil prices. It is worth mentioning that by the time of writing up this thesis (October 2004) the crude oil price has exceeded $50 per barrel, i.e. a level significantly higher than Schnieder and McKay (2001) expect for 2050; the main reason being that demand for oil is higher than the supply.

The overall efficiency of producing hydrogen is obviously dependent on the production method, and since it is unknown which methods will be available in the longer run it is hard to tell what efficiency figures may be expected. Based on the production methods of 2001, Schnieder and McKay (2001) estimate the overall efficiency of liquid hydrogen production and delivery to be around 40% for biomass and just over 50% for fossil fuels, with gas having the highest efficiency of 53%. Based on these figures and on price forecasts outlined in this section, a rough outlook for the delivery of liquid hydrogen based on the use of sustainable renewable energy and fossil fuels including CO_2 extraction and sequestration is made [Schnieder and McKay, 2001].

Schnieder and McKay (2001) claim that biomass-based hydrogen could be competitive with gas-based hydrogen by 2020. If a $100 per tonne carbon cost penalty for extracting CO_2 from a gas stream, compressing and piping it up to 500 km for sequestration in a spent oil or gas reservoir is included, this date could be advanced by about five years. Solar- and wind-based hydrogen production using electrolysis of water is unlikely to be economically competitive with biomass or fossil fuels for many decades. Moreover, Schnieder and McKay (2001) believe that kerosene, based on the $30 per barrel crude oil with a $100 per tonne carbon penalty, would still be the lowest cost per unit of energy through 2050 at around $10 per GJ (2000 prices).

Another prediction suggests that the fuel prices for kerosene and liquid hydrogen will be the same in 2037, and after that, liquid hydrogen will be cheaper than kerosene [Oelkers and Prenzel, 2001]. Based on this prediction, the direct operating cost of two medium-range equivalent aircraft – one conventional and one cryoplane – is expected to be the same in 2040. After 2040 the direct operating cost for a conventional aircraft is expected to rise due to increased fuel costs, whereas it is expected to decrease for the cryoplane as the technology has matured and as more efficient hydrogen production methods are available.

Owing to a number of uncertainties briefly discussed here, it is not possible to say when hydrogen as an aviation fuel will become economically competitive with kerosene. Sooner or later it will happen, that is for sure. However, depending on various factors,

e.g. climate effects of global warming and environmental awareness among those who consume the most energy, it might be desirable to introduce a novel fuel before the point in time when it can compete economically with kerosene.

1.4 Introduction of an Alternative Fuel in Civil Aviation

The challenge is to develop an environmentally sustainable transportation system for aviation, in the long term based on renewable energy sources, capable of coping with the increasing traffic demand and at the same time limiting the emissions of greenhouse gases. In order to achieve this, several changes need to be applied. Incentives to change people's travelling habits and introduction of external means of control will probably play an important role. However, these are issues far beyond the scope of this thesis. Instead, this thesis will focus on possible changes of a technical nature that may be applied to civil aviation. Technical improvements applied to conventional aircraft technology, such as changes of the airframe, which will increase the aerodynamic efficiency, lower structure weight and lower engine specific fuel consumption (SFC), thus reducing the total fuel burn, will help in limiting the increase in greenhouse emissions, and are important to consider. However, these improvements will never make the aviation industry independent of a fossil energy source. Furthermore, as saving fuel to minimize costs and maximize payload always has been a prime target for the manufacturers, it may be expected that further progress will be costly and slow.

Taking a completely new approach for civil aviation by fuelling with liquid hydrogen, in the longer term produced from renewable energy sources, would enable compatibility with the environment. This would reduce the unhealthy emissions in the airport vicinity, and, even more importantly, allow a significant reduction of civil aviation's contribution to global warming. Given that liquid hydrogen is produced from renewable energy sources, the emissions are reduced to water vapour (H_2O) and small quantities of oxides of nitrogen (NO_x). All emissions containing carbon and sulphur are eliminated. In addition, the civil aviation would be powered by an energy carrier (in contrast to an energy source, which kerosene is) that may be produced from any energy source, by electrolysis of water.

A fundamental difference between kerosene and liquid hydrogen concerns the fuel energy density. In order to carry the same amount of energy, which is the most relevant parameter when comparing two aircraft for the same mission, the mass of the fuel is 2.8 times less for liquid hydrogen, whereas the volume is four times larger (Figure 1-7).

The high energy content per mass of liquid hydrogen will lower the total fuel weight for a certain mission, i.e. the fuel weight will be 2.8 times lower, and thus potentially allow for a higher payload or longer range compared with an equivalent kerosene-fuelled aircraft. This effect is, however, counteracted by increased structure weight of the cryoplanes, owing to a somewhat larger aircraft needed to carry the bulky fuel and additional facilities required to handle the fuel, e.g. isolation of fuel tanks and a heat exchanger required to evaporate the fuel prior to the combustor. The low energy content per volume of liquid hydrogen will require a new aircraft design, provided with roughly four times larger fuel tanks compared with conventional airplanes. Engines must be re-designed for the new fuel, particularly with respect to minimization of NO_x emissions.

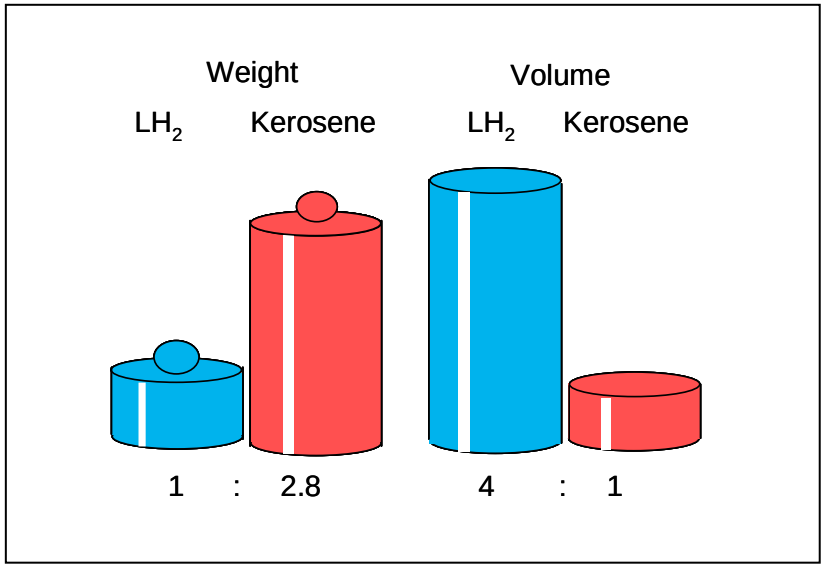

Figure 1-7. The weight and volume of kerosene and liquid hydrogen, respectively, containing the same energy content. (Illustration idea from Heinz-Günter Klug, retired from Airbus Germany.)

Moreover, the fuel system will be completely new, and its components will need dedicated technology development. Usage of hydrogen will make the fuel delivery system much more complex. Owing to heat transfer, phase change from liquid to gas, 2-phase flow and compressibility of the medium, a hydrogen system may exhibit unexpected system dynamics and critical failure modes. In the CRYOPLANE project (see section 1.5) it was found that the "Fuel System Control" especially turned out to be more complex, due to more operational functions need to be handled by the system (e.g. purging, chill-down, fuel storage on ground and warming up for maintenance), more components need to be controlled, more information needs to be gathered and evaluated (fuel system pressures and temperatures), and more possible failure cases need to be analysed [Klug, 2002].

With respect to availability of components, or at least applicability of known design principles, no major obstacles are expected. Despite the extreme performance requirement, e.g. for fuel pumps in the fuel system, it is believed that principles applied to space technology components can be utilised by scaling. A preliminary feasibility study of the aircraft fuel supply system did not disclose any technical infeasibilities [Allidiers, 2002]. However, several problems were identified, such as cavitation in the fuel pump during idle operation and icing on the heat exchanger surface employed to vaporise the fuel prior to its entry into the combustion chamber.

Hence, while offering great prospects, use of liquid hydrogen as an aviation fuel poses formidable challenges regarding technical development, energy requirement for producing hydrogen, handling, aircraft design and making liquid hydrogen (LH_2) economically compatible with kerosene.

Looking at the prospect of alternative fuels, there are a few more candidates in addition to hydrogen worth mentioning. These include alcohols, such as, ethanol and methanol, liquid methane and synthetic kerosene. Alcohols offer environmental benefits as they are renewable energy sources, and since they are liquid fuels, they do not impose any major infrastructure changes at airports. Moreover, an experimental study of ethanol blended Jet-A fuels indicates marked reductions in carbon dioxide, oxides of nitrogen and soot formation with increasing blend rates [Eiff et al., 1992]. However, as an aviation fuel their usage carries a number of drawbacks. At low power condition the combustion of alcohols produces organic acids and aldehydes, with attendant health hazards to ground support personnel [Eiff et al., 1992]. Introducing it in aviation on a large scale would require an extensive supply of hydrocarbons from renewable energy sources; a supply which is questionable whether if is available or even possible to obtain. The overall disadvantage, however, with alcohols, which makes them a less attractive substitute to kerosene, is their very low heat contents, both in terms of mass and volume (these are about half the corresponding values for kerosene), thus imposing significant penalties in aircraft range and/or payload capacity.

Another candidate, which is cryogenic just like hydrogen, is liquid methane. Since it is a cryogenic fuel, it does impose similar challenges with respect to fuel handling and aircraft design as hydrogen. In terms of energy content methane shows similar trends as hydrogen, although the differences are smaller compared with kerosene, i.e. both the penalty in energy density and the gain in specific energy are smaller. The main advantage with methane is that it is an energy source that does not need to be produced. However, since it is a fossil fuel, it might be difficult to find reasonable justification to introduce this novel fuel, taking into account its major consequences on the aircraft and airports with only a small environmental benefit, originated in its higher hydrogen/carbon ratio compared with kerosene. Methane could also be produced from renewable energy sources by digesting processes, but it is questionable if these are feasible methods for large-scale production. It is true that gas resources will be available for another few decades after the oil is depleted, but as the climate change due to anthropogenic sources is anticipated to raise the environmental concerns in the future, it seems unlikely that cryogenic methane will become an attractive option for civil aviation, at least not for large-scale applications.

The third and last alternative fuel discussed here is synthetic kerosene, which may be renewable if produced from renewable energy sources. The efficiency for producing the fuel is about the same as for producing hydrogen. It is a liquid fuel with about the same energy content as kerosene, and would therefore impose the smallest required changes at aircraft and fuel systems compared with the other alternative fuels discussed here. Owing to a small content of aromatic hydrocarbons in synthetic kerosene, it is less unhealthy to handle and produces less toxic unburned hydrocarbons emissions when burnt than conventional kerosene. Furthermore, the low content of aromatic hydrocarbons is likely to reduce the NO_x and soot emissions, where the former is an effect of lowered combustion temperature. More details on the prospects of using synthetic kerosene for aviation can be found in Eklund and Hedemalm (2002).

Blending conventional and synthetic kerosene based on biomass with up to $50\%_{vol}$ synthetic fuel, i.e. the maximum amount which is allowed according to the “Standard

Specification for Aviation Turbine Fuels" [Eklund and Hedemalm, 2002], would be a pleasing and efficient way to immediately reduce aviation's contribution to global warming. In the very long run, however, synthetic kerosene seems to be a less attractive alternative to kerosene than hydrogen, as its production requires large quantities of one single energy source, namely, biomass. In order to mitigate the climate impacts of the greenhouse effect it would be reasonable to increase CO_2 absorbing sources, of which the biosphere is one of the most important, rather than decrease them. Which alternative candidate will be the most attractive in the future is highly dependent on available future fuel production methods, implying that that fuel, for which viable, efficient and renewable production methods for large-scale applications are available, is likely to be the more attractive candidate.

1.5 Previous Work on the Concept of Using Hydrogen for Aviation

The history of hydrogen as an aircraft turbojet fuel started in 1937, when a Heinkel He-S-2 experimental turbojet engine was rig tested running on hydrogen [Dahl and Suttrop, 2001a]. At that time, the reason for choosing hydrogen was actually that the gasoline-fuelled combustor turned out to require lengthy development efforts, whereas gaseous hydrogen combustion proved to be applicable in spite of the restricted combustor volume conditions, and hence could be used immediately for an early demonstration of the feasibility of the jet engine principle.

About 20 years later in 1956, Pratt & Whitney Aircraft was commissioned by the United States Air Force to conduct a program to investigate the feasibility of using LH_2 as a fuel for aircraft engines. These efforts comprised amongst other things the testing of the J57 engine modified for hydrogen operation, and the development of a hydrogen-fuelled demonstration engine to be used for supersonic reconnaissance [Dahl and Suttrop, 2001a].

Stimulated by military needs of longer range and higher altitude, testing with hydrogen was performed at the NASA Lewis Research Centre from the mid 1950's [Dahl and Suttrop, 2001a; and Conrad, 1979]. Three different turbojet engines were evaluated in altitude test chambers (J-47, J-65-B-3 and J-71-A-11). The combustor test showed that the combustion efficiencies attained with hydrogen were superior to those achieved by the production JP-combustor at altitudes above 22-24 kilometres. The hydrogen was extremely stable and an essentially extended relight capability could be demonstrated. Somewhat surprisingly regarding the hydrogen combustion system was that exhaust gas temperature non-uniformities were observed. This drawback was, however, considered to be correctable by careful attention to the hydrogen and air injection and mixing process.

After testing in an altitude chamber, the J-65 engine and hydrogen supply system components were installed on the B-57 airplane. With one of the engines operated on hydrogen the aircraft was successfully flown in February 1957 (Figure 1-8). The left engine which was configured for hydrogen was able to run on JP-4 fuel for take-off and initial cruise. At high altitudes the transition to hydrogen operation was performed in two steps: purging of hydrogen lines and dual fuel operation for two minutes before switching to hydrogen alone. Over 40 transitions were performed in the program. The

helium in the right wing tip mounted tank was used to pressurise the ullage above the LH_2 in the left wing tip mounted tank, thus forcing it through the heat exchanger.
Having accomplished the tests, it was concluded that various technology advances were required and some technical problems needed to be solved before application to civil aviation would be feasible. Engine re-designs to better capitalise on the hydrogen characteristics to improve performance needed to be studied further. One problem that occurred was that the transition to hydrogen was accompanied by significant fluctuations in engine speed, which was believed to be a consequence of unsteady boiling in the heat exchanger and thus causing rapid changing of hydrogen flow to the engine. The activities were closed in 1958 because military studies indicated that the costs of providing hydrogen to all strategic aircraft bases would be excessive.

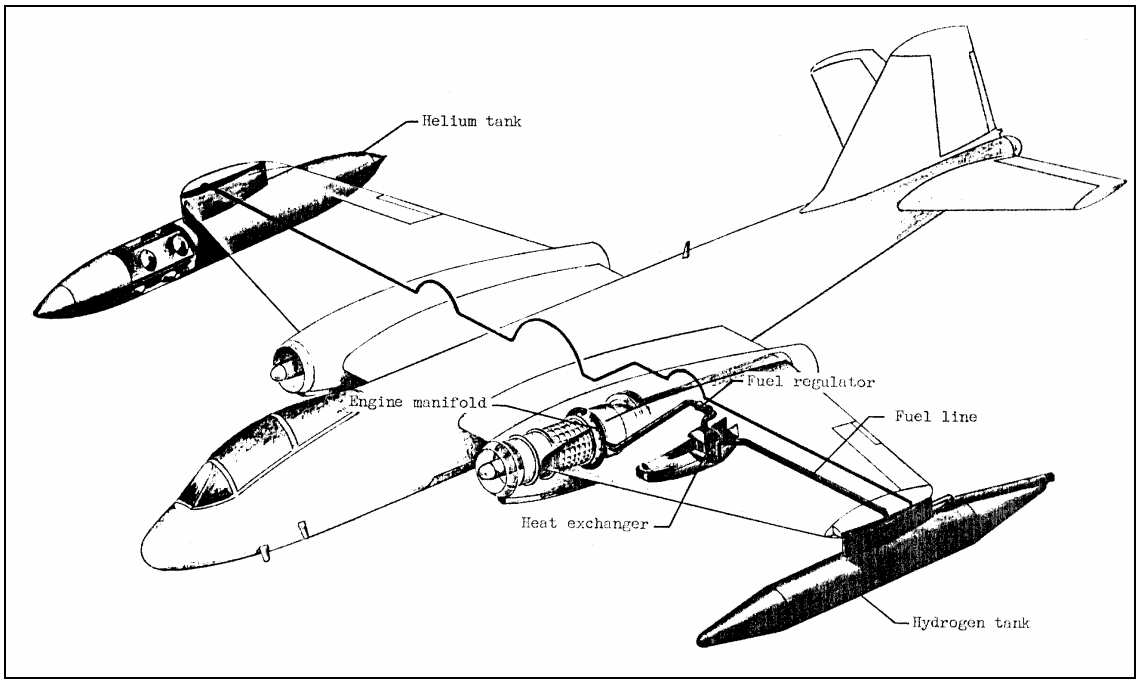

Figure 1-8. B-57 Airplane equipped with hydrogen system [Conrad, 1979].

In the 1970's, the General Electric Company participated in design studies and research and development programs concerning using hydrogen for aircraft propulsion systems [Payzer and Renninger, 1979]. These efforts were mainly a consequence of the OPEC oil price dictation which caused the world to become conscious of the possibility that the availability of fossil fuels may be restricted. Performance of various unconventional cycle configurations were evaluated and compared with a basic cycle. The predicted aircraft mission performance was also assessed. Some results and conclusions are presented in section 2.2.4.

During this period also various other studies supported by the NASA Langley Research Center were accomplished [Brewer, 1981; and Brewer, 1979]. These studies comprised investigations of both subsonic and supersonic aircraft designed to use synthetic aviation grade kerosene (synjet), liquid hydrogen and liquid methane. The results showed that LH_2 was an outstanding fuel for use in future transport aircraft. Various engine designs employed in this study were evaluated in a study performed by

AiResearch-Arizona Division [Baerst and Riple, 1979]. More of this study is outlined in section 2.2.4. Another study initiated due to the energy crisis is Pratt et al. (1974), looking at the technical, economical and environmental impact of using hydrogen as a turbojet engine fuel.

Further tests with aircraft using hydrogen were performed in the 1980's by the Russian TRUD[4] who jointly developed an experimental Tu-155 aircraft. On this aircraft one of the three production engines was converted to the dual fuel engine, NK-88, burning either kerosene and LH_2 or liquid natural gas (LNG) and kerosene [Sosounov and Orlov, 1990]. This experimental aircraft, which is based on the Tu-154 passenger aircraft, is provided with a hydrogen tank of 18 m^3 in the rear fuselage (Figure 1-9). For safety reasons the aircraft fuel section is either filled with nitrogen or constantly purged with air from the aircraft conditioning system. The aircraft is also provided with a helium system used for pipeline purging as well as control of the hydrogen fuel system valves. The first flight was accomplished in April 1998 and it lasted for 21 minutes. As opposed to earlier flight tests with aircraft using hydrogen, the whole flight mission was performed with the NK-88 running on hydrogen. This experimental aircraft conducted several flights with the NK-88 engine and all its systems running well without any shut-downs, using both LH_2 and LNG.

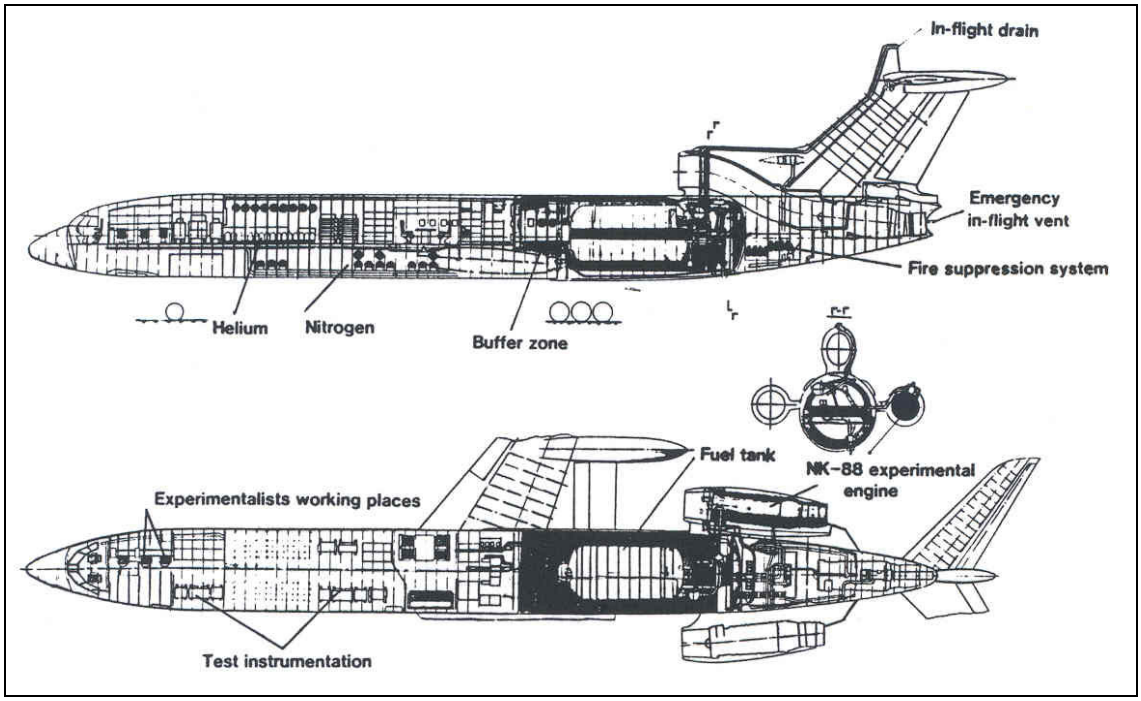

Figure 1-9. The Tu-155 aircraft layout [Sosounov and Orlov, 1990].

More recently, environmental concerns, as well as the expected depletion of fossil fuel resources, have become the driving forces for research and development towards the introduction of hydrogen energy into air traffic. During the 1990s Airbus Germany and the Russian aircraft manufacturer Tupolev put much effort on resolving these issues

[4] TRUD: Kuibyshev scientific-production association (KSPA) and Central Institute of Aviation Motors (CIAM).

[Klug, 1997; Klug et al., 1996; and Klug and Grassl, 1993]. These studies looked at hydrogen from a systems perspective including various fields which are affected by introducing hydrogen as an aviation fuel. In January 1992 a 58-month program, named Euro-Québec Hydro-Hydrogen Pilot Project (EQHHPP), involving industry and research establishments was initiated. This program was aimed at establishing the NO_x reduction potential when burning hydrogen and providing design guidelines for later development of real aero engine combustors [Shum et al., 1996]. In the third phase of EQHHPP, analytical modelling and experimental tests of low-NO_x combustors for aero engines were performed [Ziemann et al., 1998a; Ziemann et al., 1998b; and Dahl and Suttrop, 1998]. As a result of the project, combustor configurations burning hydrogen which offered very low NO_x emissions were suggested (see section 2.3.3).

In 2000 the EC-sponsored project CRYOPLANE was initiated. The project covered a period of two years (from 2000 to 2002) and involved 36 partners from industry, research institutes and universities. It was a system analysis of using liquid hydrogen for civil subsonic aviation, covering a range of subjects from hydrogen production methods to the environmental compatibility. An overview of the results is given in the project final technical report [Westenberger, 2003b]. As for the engine and combustor design when burning hydrogen, a number of papers and theses which condense results obtained within or after the CRYOPLANE project are published: Svensson and Singh (2005), Svensson and Singh (2004), Corchero and Montañes (2003), Boggia and Jackson (2002), Boggia et al. (2001), and Boggia (2001). Examples of studies covering the environmental effects of introducing hydrogen for aviation are Ponater et al. (2004), Svensson et al. (2004), and Marquart et al. (2001).

1.6 Objectives and Scope

The overall objective of this thesis is to evaluate the potential of reducing the environmental impact of civil subsonic aviation by changing the source of energy from kerosene to the energy carrier hydrogen. In addition, the practical and technical feasibility of introducing hydrogen as fuel is investigated. In order to address these issues a number of selected fields are covered. The areas to study are selected on the basis of their relevance for cryoplanes with respect to the environmental impact. When burning hydrogen the only pollutant emissions are water vapour and oxides of nitrogen. The NO_x issue is raised by studying the engine and combustion chamber design in detail, including the potential to achieve low NO_x emissions, when using hydrogen and kerosene. As the atmospheric effects of water vapour are highly dependent on the altitude of discharge, the subject of optimum cruise altitude for minimum environmental impact is addressed. In order to put the topics of the environmental impact of cryoplanes into context, the practical viability of this fuel change is assessed by investigating the implications on airports and by briefly discussing available and envisioned methods for hydrogen production.

The subject of aircraft design when using hydrogen, on the other hand, is not covered other than in general terms in the thesis. Since the thesis is focused on the environmental issues, which in this context mainly considers the pollutant emissions, it seemed natural to limit the scope of the thesis this way. In those studies where an aircraft is involved, data are taken from the final reports of the work package dealing

with the aircraft configurations within the CRYOPLANE project (see section 1.5) which suggested a number of liquid hydrogen-fuelled aircraft configurations covering a range of aircraft classes. Cost implications of introducing hydrogen fuel in civil aviation are not embodied in this thesis.

As for the aero engine, the cycle and combustion chamber design need careful attention to secure a safe and reliable operation, as well as to exploit fully the favourable properties offered by using hydrogen for aero gas turbines. The engine could be designed either with a minimum number of hardware changes or by employing unconventional cycles, which exploit the cryogenic properties of hydrogen, in order to improve the performance. In this thesis the main effects on aero gas turbines when changing to hydrogen fuel, with emphasis on environmental issues, is covered. The objective is to answer the question whether there are any significant gains, in terms of engine performance and pollutant emissions, as well as to assess the technical feasibility of changing to hydrogen fuel. For reasons discussed in the thesis, there might be the potential for lowering the NO_x emissions compared with conventional kerosene combustors. Using simulation tools, the potential of achieving low NO_x emissions is illustrated for a conventional as well as for a hydrogen-fuelled engine by calculating the flame temperature for relevant operating conditions. Different engine cycle layouts are evaluated and the consequences on design point performance are quantified. Design and operational matters of particular interest when using hydrogen are discussed.

In general, the primary contributor to global warming is carbon dioxide (CO_2). In addition, essentially depending on the cruise altitude, H_2O and NO_x can play an important role. In order to reduce the environmental burden from an aircraft, one may either perform technical design improvements, for instance, on the airframe or on the engine, or one may apply operational measures. The way of operating the aircraft may be changed in several ways. In the thesis the influence of lowering the cruise altitude, as a means of reducing the environmental impact, is investigated. The objective is to identify the optimum cruise altitude for two equivalent medium-range aircraft, one kerosene-fuelled and one LH_2-fuelled, from an environmental point of view. For this purpose both aircraft are re-optimised and compared for a number of different reduced cruise altitudes. By carrying out detailed flight simulations, differences, in terms of required changes in configuration and optimum cruise altitude for minimum environmental burden, are identified for both aircraft types. In order to allow a simple assessment of the global impact, in terms of global warming, from the emissions discharged on a certain mission, a simple parametric model is derived.

The reason for choosing a medium-range aircraft for this study is that, from an environmental point of view, flying medium ranges is preferable. For short ranges the take-off and climb phases make up a large part of the total fuel consumption, and the fuel consumption per person kilometre becomes high. For long ranges large quantities of fuel need to be carried, resulting in a high average flight weight in relation to the number of passengers, hence also giving large fuel consumption per person kilometre. Thus, independently of which fuel type used, from a fuel consumption point of view, it is preferable to fly medium ranges. Since the main driver towards this fuel change is environmental concerns, it makes sense also to suggest that the most efficient aircraft class should be used to the largest possible extent when switching to hydrogen. Another

reason for choosing a medium-range aircraft is that it is the most frequently used aircraft size in commercial aviation worldwide.

Having defined and quantified the consequences on the engine of going to hydrogen, the subject of designing an aero gas turbine using hydrogen for low environmental impact is raised. In this context, the fuel consumption and emissions (water vapour and NO_x) are regarded to be of primary interest in order to address the environmental impact. Rather than addressing a number of specific operating points, complete flight missions are evaluated. The cryoplane under consideration for this study is also a medium-range configuration.

The water vapour is proportional to the fuel consumption, whereas the NO_x emissions are dependent on the combustor inlet conditions and a number of combustion chamber characteristics. In addition, reducing fuel burn and NO_x might be in opposition to each other, implying that an engine design measure to reduce NO_x might give rise to the fuel burn and vice versa. Whilst the wish to lower the fuel consumption mainly is driven by the objective of delivering products that promise low direct operating cost, the H_2O and NO_x emissions are important to reduce due to environmental concerns of the impact on the atmosphere and climate (see section 1.2).

Whether engines should be designed for low mission fuel consumption or for low mission NO_x emissions in order to minimise the environmental impact is not obvious. Therefore, both these options are covered. In order to study the potential of lowering either fuel burn and mission H_2O, or mission NO_x emissions, a number of alternative engine cycles are selected, i.e. cycles featuring different combinations of COT (combustor outlet temperature), OPR (overall pressure ratio) and BPR (by-pass ratio). The amount of H_2O emissions is known directly from the fuel consumption (since the H_2O emissions are proportional to the fuel burn), while the NO_x emissions are calculated using a semi-empirical correlation. Rather than finding the optimum engine cycle for a specific objective, the aim is to investigate a number of promising cycles, in order to provide some guidance on how to design hydrogen-fuelled aero engines for medium-range aircraft either for minimum mission fuel consumption or mission NO_x emissions.

Introduction of cryoplanes in civil aviation has several advantages, both on a regional and on a global scale. However, it poses formidable challenges regarding infrastructure build-up at airports and obtaining efficient and viable methods for hydrogen production. In addition, there is a need for the evaluation of practical feasibility by compilation of a number of transition scenarios, which imply changing from a conventional fleet of aircraft to a LH_2-fuelled fleet over a certain time period.

The objectives of this thesis are to explore the feasibility, potential and consequences of introducing a LH_2-fuelled aircraft fleet on a regional scale. The chosen air traffic segment is Scandinavian Airline’s (SAS’s) share (major airline in the region) of the Swedish domestic air traffic. The main reason for choosing this air traffic segment is that the feasibility for introducing cryoplanes in this region is expected to be high. Traffic growth curves are compiled by means of forecasts performed by the aviation authority in Sweden, namely, the Swedish Civil Aviation Administration (SCAA).

According to these traffic growth curves and through consideration of the airline's approach to fleet development, two different conventional fleet developments are set up. Next, four realistic transition scenarios are compiled, and the fuel requirement and emissions related to these scenarios are estimated, and presented in relation to figures of the conventional fleet. The infrastructure changes needed at Stockholm/Arlanda airport and for distribution of the LH_2 are identified and assessed. Possible methods available today and in the future for producing hydrogen are briefly discussed.

1.7 Thesis Structure

This thesis consists of six chapters, references and a number of appendices. After this introductory chapter, the fundamental effects on aero engine pollutant emissions, performance and design of changing to hydrogen fuel is covered (chapter 2). In this chapter it is discussed how the engine cycle and combustion chamber should be designed to exploit fully the favourable properties, in terms of performance and pollutant emissions, offered by hydrogen usage.

In chapter 3 reducing the cruise altitude as a means to reduce the environmental impact for a conventional and an equivalent cryoplane is investigated. The environmental impact, in terms of global warming potential (GWP), of a certain mission is assessed using a simple parametric model. A derivation of the model is outlined in Appendix B.

Having looked at the fundamental effects on the engine of changing to hydrogen and the optimum cruise altitude, the subject of designing an aero gas turbine using hydrogen for low environmental impact is raised in chapter 4. The environmental impact is addressed in terms of the mission fuel consumption and emissions (water vapour and NO_x). A derivation and evaluation of a semi-empirical NO_x emission correlation is included. The flight mission fuel consumption and emissions are estimated using a computer program developed by the author for the purpose of this task.

In chapter 5 the feasibility of introducing cryoplanes on a regional level is explored by considering SAS's share of the Swedish domestic air traffic. The air traffic growth scenarios are described. Based on these growth figures, transition scenarios, i.e. scenarios in which cryoplanes are gradually introduced, are compiled. The infrastructure changes and possible hydrogen production methods at Stockholm/Arlanda airport are discussed.

To give a background to aero gas turbine performance, which this thesis discusses to a large extent, a description of the fundamental aero engine theory and a discussion of engine performance in general are given in the first appendix, i.e. Appendix A. Performance simulation softwares are described with particular emphasis on the TurboMatch (Cranfield University's own software) scheme, which is the code used for the main part of the engine performance calculations conducted in this thesis. Improvements and developments of the TurboMatch code performed by the author for the purposes of this thesis are also described.

2 EFFECTS OF USING HYDROGEN ON AERO GAS TURBINE POLLUTANT EMISSIONS, PERFORMANCE AND DESIGN

2.1 Introduction

As for the aero engine, the cycle and combustion chamber design need careful attention to secure a safe and reliable operation, as well as to exploit fully the favourable properties offered by using hydrogen for aero gas turbines. The engine could be designed either with a minimum number of hardware changes or by employing unconventional cycles, which exploit the cryogenic properties of hydrogen, in order to improve the performance.

This section covers the main effects on aero gas turbines when changing to hydrogen fuel, with emphasis on environmental issues. The objective is to answer the question whether there are any significant gains, in terms of engine performance and pollutant emissions, as well as to assess the technical feasibility of changing to hydrogen fuel. The effects on the performance are outlined in section 2.2, while the emissions are discussed in section 2.3. For reasons discussed below, there might be the potential for lowering the NO_x emissions compared with conventional kerosene combustors. Using simulation tools, the potential of achieving low NO_x emissions is illustrated for a conventional as well as for a hydrogen-fuelled engine by calculating the flame temperature for relevant operating conditions (section 2.3.4). In section 2.4 design and operational matters of particular interest when using hydrogen are discussed. The chapter is concluded by a brief overview of the conclusions (section 2.5).

2.2 Engine Performance

When burning hydrogen in an aero gas turbine there are several issues that need to be regarded. In addition to re-designing the combustion chamber, the minimum change that needs to be adopted with the engine cycle is the implementation of facilities to evaporate the hydrogen (which is stored in the tanks in a liquid state at 24 K) prior to its entry into the combustion chamber. The fuel heating can be accomplished either by an external heat source or a heat exchanger (HE) located at a suitable engine location. Placing the HE outside the engine does not affect the engine performance; however, it might cause practical problems when the fuel system is integrated with the other aircraft systems. Available external heat sources are, for instance, cooling systems of hydraulic fluids, pumps, electric equipment and the cabin area [Boggia et al., 2001].

Looking at the option of employing a HE, there are various possible engine locations which have been studied within the CRYOPLANE project [Corchero and Montañes, 2003; Boggia and Jackson, 2002; Boggia et al., 2001; and Boggia, 2001]. When deciding where to place the HE, possible benefits in performance need to be weighed against increased engine complexity and safety issues. Aiming at minimising the number of hardware changes and prioritising safety issues, a HE located at the LPT

(low-pressure turbine) exit is employed here. Other possible engine configurations are discussed in section 2.2.4.

In section 2.2.1 the engine used in the simulations is described. The heat exchanger is analysed in section 2.2.2, including an approximate assessment of the heat transferring area that would be required if the struts in the exhaust are to be employed to heat up the hydrogen. A detailed design of a heat exchanger is beyond the scope of this thesis. Effects on performance are illustrated in section 2.2.3 by carrying out engine simulations. In addition, a number of suggested unconventional engine cycle configurations are described and discussed (section 2.2.4).

2.2.1 Choice of Engine for Simulations

In order to investigate the consequences on performance when changing to hydrogen, a particular engine, namely the V2527-A5 engine manufactured by IAE[5], is simulated. This is a two-shaft boosted turbofan engine suitable for short- and medium-range aircraft. The jets from the by-pass and core are unmixed. It features a single-stage fan, a four-stage LP (low-pressure) compressor and a ten-stage HP (high-pressure) compressor. The inlet guide vane and the first three stages are variable. The HP and LP turbines feature two and five stages, respectively. The reason for choosing this engine is that it is a typical, reasonably modern, medium-thrust turbofan engine, and that there are sufficient public data on it to create a sufficiently detailed model of its performance. Furthermore, this engine is suitable for the main study aircraft within the Cryoplane project, namely the A320, which this work is based on.

With small modifications (lower HPC isentropic[6] efficiency and inclusion of losses in the exhaust duct) the model is based on the one proposed within the CRYOPLANE project [Boggia and Jackson, 2002; Boggia et al., 2001; and Boggia, 2001]. Also, as opposed to their model, a thrust coefficient, which is calculated depending on the expansion ratio of the nozzle and hence varies with the operating condition, is applied here. Using this methodology, a thrust coefficient equal to about 0.98 is applied. In total, therefore, a slightly decreased performance in terms of SFC (specific fuel consumption) and SPT (specific thrust) is obtained here than presented in the CRYOPLANE project. The main design parameters at the design point are as follows:

- Design point: take-off, static sea-level, ISA+10 K
- BPR: 4.8
- OPR: 28.5 (1.5 x 2.0 x 9.5)
- Thrust: 117.9 kN

The component efficiencies and pressure ratios assumed are given in Table 2-1, while the assumed pressure losses taken account for are displayed in Table 2-2. Neither overboard bleeds nor power extraction is included. The outer fan pressure ratio chosen here is lower than the optimum, i.e. the value that minimises SFC and maximises specific thrust for a given engine core and BPR. A fan pressure ratio lower than the

[5] International Aero-engines AG: international consortium comprising UTC (Pratt & Whitney), JAEC (Japanese Aero Engines Corporation, comprising IHI, KHI and MHI) and MTU DaimlerChrystler Aerospace).

[6] An isentropic process is a process that is both adiabatic (no heat transfer) and reversible.

optimum is often applied to reduce design and handling problems, at the expense of a very small penalty in SFC [Pilidis, 2001]. In Appendix A.3, section A.3.2 the design point performance behaviour including prerequisites for a proper choice of fan pressure ratio of a turbofan engine is outlined.

Table 2-1. Assumed component data for the V2527-A5 engine.

Component	Pressure ratio	Isentropic efficiency
Outer fan	1.7	0.88
Inner fan	1.5	0.89
Booster	2.0	0.88
High-pressure compressor	9.5	0.87
High-pressure turbine	-	0.91
Low-pressure turbine	-	0.91

Table 2-2. Losses taken account for to model the V2527-A5 engine.

Component	Pressure loss [%]
Intake	0.2
By-pass duct	1.5
Combustor	3.0
Exhaust duct	1.0

To enable higher turbine entry temperatures than the maximum allowable metal temperature, cooling of hot parts is required. This is accomplished by bleeding off a part of the compressed air which then passes through cooling passages inside the blades. Generally the NGV (nozzle guide vane) and HP turbine rotor need to be cooled. Also air needs to be taken off for sealing, aiming to stop expanding gases from penetrating the disk system. In order to simulate these effects, the same numbers as applied by Boggia et al. (2001) are applied. It is assumed that 15% of the core air is bled off after the HP compressor. Depending on where expansion work takes place, this air is mixed with the hot gases at different points along the expansion. To simulate NGV cooling, 12.5% of the bleed is injected immediately before the HP turbine, and the remaining 2.5% is injected immediately before the LP turbine to be used for HP rotor cooling and seals.

2.2.2 Evaluation of Heat Exchangers

Practically, the heat exchanging might be accomplished by employing the struts, which are the mechanical structures in the exhaust which hold the rotors in place and are connecting the bearings' outer structure. These are already-existing structures that do not add any pressure loss and do not cause any significant changes in engine complexity or engine weight. The idea is to pass the hydrogen through the hollow struts which are heated on the outside by the exhaust gases. Due to the potential detrimental consequences of a fuel leakage, there are, however, safety issues associated with this design. In order to employ this idea, the design would have to meet the airworthiness requirement. Alternatively, the HE could feature a simple coil tube placed over the inside face of the jet pipe casing, avoiding major engine changes and giving a relatively aerodynamically clean jet pipe [Corchero and Montañes, 2003].

In order to obtain a stable combustion and to avoid the critical temperature where density and viscosity of the hydrogen varies essentially with temperature, which is about 60 K, the hydrogen needs to be heated up prior to its entry into the combustion chamber. Furthermore, hydrogen re-liquefaction across the fuel nozzle due to the pressure drop is prevented by the fuel pre-heating. For these reasons it was suggested within the CRYOPLANE project that the temperature of the hydrogen prior to the combustion chamber should exceed 150 K [Corchero and Montañes, 2003]. In the subsequent calculations a fuel injection temperature of 250 K is used.

The energy necessary to raise the fuel temperature to the required value is taken into account by decreasing the exhaust gases total temperature before the nozzle expansion, which in turn decreases the thrust output slightly. The temperature drop is calculated by employing the conservation of energy equation for a steady-flow system [Cengel and Boles, 1996], with the notations given in Figure 2-1:

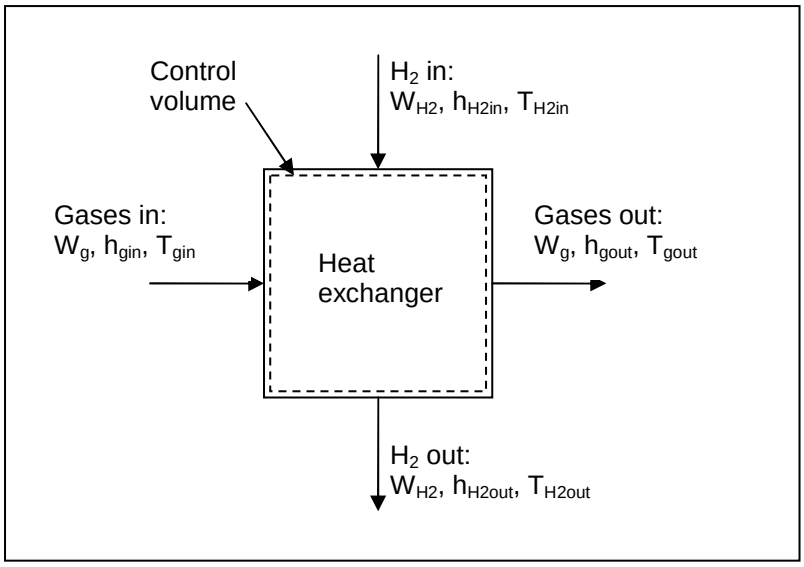

Figure 2-1. Notations for a heat exchanger to evaporate the hydrogen.

$$Q - E = \sum W_{out} \cdot h_{out} - \sum W_{in} \cdot h_{in} \tag{2-1}$$

where Q denotes heat transfer, E denotes work input (or output), W denotes mass flow and h denotes enthalpy. The left-hand side of the equation is equal to the total energy crossing the control volume boundary as heat and work per unit time. The right-hand side is equal to the change in total energy of the control volume per unit of time (potential and kinetic energy is neglected). Neglecting any heat losses of the heat exchanger (Q=0), the left-hand side is equal to zero, thus:

$$W_g \cdot \left(h_{gin} - h_{gout}\right) = W_{H2} \cdot \left(h_{H2out} - h_{H2in}\right) \tag{2-2}$$

Knowing the mass flows, inlet condition for the combustion gases (subscript g) as well as the inlet and the required outlet condition for the hydrogen for a certain operating point, the enthalpy of the gases at the outlet may be calculated, and thereby also the

temperature drop of the gas flow. The hydrogen inlet temperature is assumed to be 24 K. In accordance with the methodology for recuperators, a thermal effectiveness, ε, of the HE may be defined as the ratio of hydrogen temperature rise to the ideal value, the latter being the difference between the gas and hydrogen inlet air temperatures [Walsh and Fletcher, 1998]:

$$\varepsilon = \frac{T_{H2out} - T_{H2in}}{T_{gin} - T_{H2in}} \tag{2-3}$$

In the calculations the effectiveness is computed for the design point using equation (2-3), and for off-design conditions the temperature drop prior to the exhaust nozzle is calculated by assuming that the effectiveness is preserved. In practice, during part load conditions the effectiveness increases, as physical mass flow reduces while the volume or area remains fixed [Walsh and Fletcher, 1998]. However, as the temperature drop in the exhaust has a small influence on the thrust output, the exclusion of increased effectiveness for decreased power settings will have a negligible effect on the off-design performance.

Knowing the required heat transfer, Q, to heat up the hydrogen as desired and the temperatures of the gas and hydrogen in and out of the heat exchanger, the area, A, required to accomplish the heat exchange can be estimated. Note that this Q is different from the Q used in equation (2-1), which concerned heat fluxes across the boundaries of the control volume. The objective here is to estimate approximately the area requirement if using the struts to evaporate the hydrogen. From the definition of the overall heat transfer coefficient, U, the heat transfer for a heat exchanger can be written as [Incropera and DeWitt, 1996]:

$$Q = UA \cdot \Delta T_m \tag{2-4}$$

where ΔT_m is the overall mean temperature difference for the heat exchanger. If effects of fouling are neglected and the overall surface efficiency is assumed equal to one, the total thermal resistance to heat transfer between two fluids can be expressed as the sum of the thermal resistance for convection on the hot and the cold side, respectively, and the thermal resistance for conduction [Incropera and DeWitt, 1996]:

$$\frac{1}{UA} = \frac{1}{(\alpha \cdot A)_h} + \frac{b}{\lambda \cdot A_{HE}} + \frac{1}{(\alpha \cdot A)_c} \tag{2-5}$$

where α is the convection heat transfer coefficient, b is the wall thickness (between the hot and cold fluids), λ is the thermal conductivity of the heat exchanger material, and h and c refer to the hot and cold sides of the heat exchanger (HE), respectively. The expression for ΔT_m is dependent on the directions of the flow streams within the heat exchanger, i.e. whether it is a parallel- or counter-flow heat exchanger. In addition, it could be a mix of these types. As for the case discussed here to warm up the hydrogen, the heat exchanger appears to be more like a counter-flow type. Following Incropera and DeWitt (1996), the appropriate mean temperature difference for a heat exchanger is

a log mean temperature difference. For a counter-flow heat exchanger, the following expression for the log mean temperature difference is derived:

$$\Delta T_m = \Delta T_{lm} = \frac{(T_{hout} - T_{cin}) - (T_{hin} - T_{cout})}{ln\left[\frac{T_{hout} - T_{cin}}{T_{hin} - T_{cout}}\right]} \tag{2-6}$$

The heat transfer coefficient is estimated using the Nusselt number, defined as:

$$Nu \equiv \frac{\alpha \cdot L}{\lambda_f} \tag{2-7}$$

where L is a characteristic length of the heat transferring object and λ_f is the thermal conductivity of the fluid in question. Considering the option of employing the struts to evaporate the hydrogen, the heat transferring area is assumed to be a flat plate in parallel flow. According to Incropera and DeWitt (1996) the Nusselt number can be shown to be a function only of a dimensionless length parameter, Reynolds number, Re, and Prandtl number, Pr. The definitions of Re and Pr can be found in textbooks on heat and mass transfer, for instance, Incropera and DeWitt (1996). Assuming a flat plate in parallel flow and that the flow is turbulent, i.e. the Reynolds number of a strut is larger than the critical value of $5x10^5$, an average Nusselt number can be determined by [Incropera and DeWitt, 1996]:

$$\overline{Nu}_L = Pr^{1/3} \cdot \left(0.037 \cdot Re^{4/5} - 871\right) \tag{2-8}$$

This equation is valid for $0.6<Pr<60$, $5x10^5<Re<10^8$ and a critical Reynolds number equal to $5x10^5$.

In this context an approximate number on area requirement is sufficient. Therefore, a number of simplifying assumptions are made, in accordance with guidance from Professor Bengt Sundén at Lund University, Sweden [Sundén, 2004]. The thermal resistance for conduction (second term of the right-hand side of equation (2-5)) is expected to be small in comparison to the resistance terms for convection. Furthermore, the convection heat transfer coefficient on the cold side, α_c, where the fluid is a mixture of liquid and gaseous hydrogen, is expected to be essentially higher than that on the hot side at which the fluid is a warm gas of high velocity. For these reasons, therefore, the thermal resistance is assumed only to be constituted of the thermal resistance for convection on the hot side. An area assessment based on these simplifications indicates a minimum area requirement, as the thermal resistances for conduction and convection on the cold side are neglected (taking these into account might increase the area requirement).

Using TurboMatch (Cranfield University's own software for gas turbine engine design/off-design performance calculations) the required heat transfer, the temperature of the gas flow at inlet and outlet, and the exhaust velocity are calculated for the design point for the V2527-A5 engine (the operating point corresponds to the third column in

Table 2-5 in section 2.2.3). The version of TurboMatch employed here is changed to enable simulation of hydrogen-fuelled engines [Boggia, 2001]. A brief description of the code along with the changes and improvements that have been performed in the code are presented in Appendix A.3. The relevant heat exchanger conditions for the design point are listed in Table 2-3.

Table 2-3. Relevant heat exchanger conditions.

Parameter	Value
Q [kW]	1403.5
V_{gout} [m/s]	450.9
T_{gin} [K]	789.7
T_{gout} [K]	770.6
T_{H2in} [K]	24
T_{H2out} [K]	250

A schematic figure of the exhaust struts are shown in Figure 2-2 and approximate dimensions are listed in Table 2-4. The thermo physical properties of the exhaust gases are taken for air at the average gas temperature (780.1 K) at atmospheric pressure [Incropera and DeWitt, 1996]: kinematic viscosity: 81.53×10^{-6} m^2/s, heat conductivity: 56.35×10^{-3} W/m K and Prandtl number: 0,706. Taking the chord of the struts as the characteristic length, the Reynolds number (chord times gas velocity divided by kinematic viscosity) equals 9.57×10^5, i.e. larger than the critical Reynolds number (5×10^5) and hence the flow is turbulent. Using equation (2-8) the average Nusselt number becomes 1230.8, and from the definition of Nusselt number (equation (2-7)) an average convection heat transfer coefficient of 400.9 W/m^2 K is obtained. Equation (2-6) gives a log mean temperature difference, ΔT_{lm}, equal to 637.5 K. Combining equations (2-4) and (2-5), the minimum heat transferring area at the gas side is equal to 5.5 m^2.

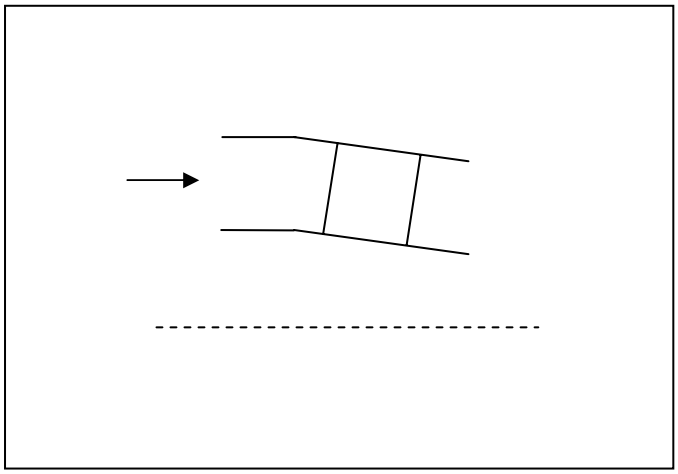

Figure 2-2. Schematic figure of the exhaust struts.

Table 2-4. Approximate dimensions of the V2500 exhaust struts [Jackson, 2004].

Parameter	Value
Chord [mm]	173
Root radius, inlet [mm]	259
Root radius, outlet [mm]	230
Tip radius, inlet [mm]	461
Tip radius, outlet [mm]	422
Thickness [mm]	35
Lean [°]	10
Number of struts	Unknown – approximately 12

Considering the approximate strut dimensions, the total area on the gas side becomes about 0.82 m^2, which is significantly less than the magnitude required to heat up the hydrogen from 24 to 250 K. Thus, in order to employ the struts as the heat exchanger, an additional heat source, such as an external system, is needed. The simplified calculations outlined here, suggest that the struts would be sufficient to heat up the hydrogen only by about 25-30 K. One option would, therefore, be to use an external heat source for the remaining temperature rise prior to the struts. An alternative is to place a heat exchanger in the exhaust, featuring a simple coil tube placed over the inside face of the jet pipe casing. Though this solution may incur additional pressure losses in the exhaust, it is, as discussed previously, believed that it would give a relatively aerodynamically clean jet pipe.

In all calculations presented in this thesis, the energy necessary to raise the fuel temperature from the storage temperature is taken into account by decreasing the exhaust gas temperature accordingly. A detailed design of a heat exchanger is beyond the scope of this thesis, and no reasonable figures on possible losses due to the inclusion of a heat exchanger are available. Therefore, no other effects of a heat exchanger than an exhaust gas temperature drop are taken into account in subsequent calculations. Looking at the design of a heat exchanger and its consequences on engine performance and weight is recommended as further work.

2.2.3 Engine Performance Estimations

The effects on the engine performance by changing to hydrogen fuel are estimated for the V2527-A5 engine using TurboMatch. Three engines with the same BPR, OPR and inlet mass flow – one using kerosene and two using hydrogen – are simulated for the design point. When changing to hydrogen, either the combustor outlet temperature or the net thrust could be retained. Performance data for these two options together with the datum engine burning kerosene are shown in Table 2-5.

Table 2-5. Performance comparison at take-off conditions.

	Ker.	H_2, eq. COT	Δ [%]	H_2, eq. F_N	Δ [%]
W_1 [kg/s]	369.3	369.3	-	369.3	-
W_F [kg/s]	1.167	0.4369	-62.6	0.4136	-64.6
F_N [kN]	117.9	121.7	3.2	117.9	-
COT [K]	1555	1555	-	1522	-2.2
TET [K]	1471	1473	0.2	1443	-1.9
SFC [g/kN s]	9.8999	3.5909	-63.7	3.5092	-64.6
ESFC [J/N s]	426.9	430.9	0.9	421.1	-1.4
SPT [m/s]	319.2	329.5	3.2	319.2	-
$A_{corenoz}$ [m^2]	0.3343	0.2862	-14.4	0.3228	-3.4
$W_{outcore}$ [kg/s]	64.839	64.109	-1.1	64.086	-1.2
$V_{outcore}$ [m/s]	387.8	450.9	16.3	391.9	1.1

Due to the considerably higher heating value of hydrogen, the fuel flow to achieve the same COT or net thrust is reduced by almost two-thirds. When the COT is preserved, the net thrust increases by 3.2% for this particular case, resulting in a corresponding increased specific thrust (SPT). The energy consumption, reflected here as energy specific fuel consumption (ESFC) (SFC times the lower heating value), increases slightly, but less than 1%. Despite the fact that the mass flow through the core nozzle decreases, the velocity increases and a smaller nozzle area is required. The other option considered is to retain the net thrust. This is obtained by lowering the COT by 33 K. In terms of energy consumption, this is slightly beneficial, since ESFC decreases by 1.4%. The values of area, nozzle mass flow and velocity of the by-pass stream are not displayed, since they do not change when changing fuel.

Following Boggia and Jackson (2002), the performance improvements could be explained by the two fundamental changes when using hydrogen: reduced mass flow and changed composition of the gases expanding through the turbine(s). Whereas the latter improves the performance, the former deteriorates the performance. Reduced mass flow through the turbine lowers the thrust output for two reasons. Decreasing the fuel flow implies that the exhaust mass flow decreases accordingly (see Table 2-5); hence, without any variation in gas composition, the thrust output decreases. For the computed cases, the mass flow through the core nozzle decreases by about 1%. In addition, a reduced mass flow through the turbine will result in a higher total temperature drop, and thereby also a total pressure drop across the turbine in order to deliver the same amount of power to the compressor. As a consequence of the lower total temperature and pressure at the turbine exit, both the pressure thrust (thrust due to different pressure at engine inlet and exit, see Appendix A.1, equation (A-1)) and the momentum thrust decrease. The latter is an effect of decreased core nozzle velocity.

However, the loss in thrust due to reduced mass flow is offset by the increased thrust owing to changed properties of the combustion products [Boggia and Jackson, 2002]. With the use of hydrogen, the combustion products contain no CO_2 and a larger portion of H_2O, which has a higher C_p (specific heat at constant pressure) value than CO_2. Having investigated a simple turbojet engine, Boggia and Jackson (2002) concluded

that the C_p value has increased by about 4% in the hot section of the engine when changing to hydrogen fuel use. Increased C_p value through the turbine will similarly, but in the opposite direction as reduced mass flow, affect the performance. For a fixed power output it will cause smaller total temperature and pressure drops across the turbine. Provided that the core nozzle is not choked, a larger nozzle expansion ratio will result in a larger exhaust velocity, which in turn will increase the momentum thrust. In total, the positive effect of increased C_p value outweighs the effect of reduced mass flow, and hence results in an increased net thrust when switching to hydrogen and retaining the COT.

Since ESFC increases slightly when changing to hydrogen and preserving the COT, slightly more fuel in terms of energy is required when burning hydrogen to attain a certain COT for the configuration investigated here. It should be pointed out that the energy consumption to attain a certain COT is highly dependent on the fuel injection temperature and the location of the heat exchanger (HE) used to evaporate the liquid hydrogen. By heating the fuel more, it is possible to achieve performance benefits (see section 2.2.4).

The effects on engine performance are quite small; but still there are some desired features that could be exploited. If the COT is kept the same, the TET is also about the same, thus requiring the same cooling technology. An increased specific thrust implies that the inlet mass flow, and thereby the physical size of the engine, may be reduced to achieve the same net thrust. The in-flight performance will in turn be beneficially affected through reduced engine drag and weight. However, to fully address the mission performance of a cryoplane compared with a conventional aircraft, the increased thrust requirement at cruise needs to be included. Mission performance estimations are addressed in chapters 3, 4 and 5.

As for the option of lowering the COT to preserve the net thrust, there are a few interesting consequences worth mentioning. The decrease in TET of more than 30 K will require less advanced cooling technology as well as having a favourable effect on turbine blade life. Due to a lower ESFC, the amount of fuel needed for a certain mission is decreased. Moreover, designing for a lower maximum cycle temperature will help to suppress the NO_x emissions (see section 2.3.1).

2.2.4 Unconventional Engine Cycles

As for the case of evaporating the hydrogen using a HE suited within the engine cycle, the cryogenic properties of hydrogen could be exploited to improve the performance through the usage of unconventional cycles. Some of these cycles are also proposed for kerosene-powered cycles; however, the main advantage when using hydrogen is the involvement of an additional fluid with favourable properties. Considering unconventional designs, there are basically four options, and various combinations of these that could be employed [Boggia and Jackson, 2002; Boggia et al., 2001; Boggia, 2001; Baerst and Riple, 1979; and Payzer and Renninger, 1979]:

- Pre-heating the hydrogen fuel with exhaust gases
- Cooling the compressor air with hydrogen fuel
- Cooling turbine cooling air with hydrogen fuel

- Hydrogen topping cycle

The design principle, objectives, advantages and drawbacks of these concepts are outlined in the following subsections.

2.2.4.1 Pre-heating the Hydrogen Fuel with Exhaust Gases

If the hydrogen was to be evaporated using a heat source within the engine cycle, a HE suited at the LPT exit is considered to be the safest solution as well as the configuration that imposes the minimum number of hardware changes. Using this configuration and heating the hydrogen to the minimum fuel temperature imposed by fuel system control needs, was considered to be the "conventional" hydrogen engine configuration within the CRYOPLANE project [Corchero and Montañes, 2003]. However, by heating the fuel more, a larger amount of energy needs to be taken out of the exhaust flow, but on the other hand, less fuel would be required to achieve a certain COT, thereby providing performance benefits. In order to extract more energy from the exhaust flow, the HE needs to be designed for a higher thermal effectiveness, which implies that the physical size of the HE needs to be increased.

By repeating the calculations for the engine discussed in section 2.2.3 (without re-optimising the outer fan pressure ratio) for a fuel temperature of 600 K instead of 250 K and preserving the COT, it was found that the ESFC decreased to 414.2 J/N s, the net thrust decreased to 120.7 kN and the HE thermal effectiveness (equation (2-1)) needs to be increased from 0.295 to 0.755. Thus, at the expense of a significantly increased HE effectiveness and a slightly decreased net thrust, the energy consumption to attain the same COT may be decreased by 3.7% as compared with the kerosene-fuelled engine. As hydrogen has a high C_p value, it is capable of capturing large amounts of energy, hence reducing the ESFC [Boggia et al., 2001]. The small thrust loss is explained by the increased temperature drop prior to the exhaust nozzle.

Although an effectiveness of 0.755 is not large compared with those of recuperators which are designed for an effectiveness of about 0.8, it might not be reasonable to exclude pressure losses in the exhaust nozzle when evaluating the engine performance. If an external heat source is not employed, a heat exchanger suited at the LPT exit to increase the fuel temperature to 600 K might give rise to non-negligible pressure losses in the exhaust nozzle.

These results are in agreement with the results of Boggia et al. (2001), who found that the SFC decreased by 3.9%, while the SPT decreased slightly, by 0.8%, when heating the fuel to 600 K instead of 250 K.

2.2.4.2 Cooling the Compressor Air with Hydrogen Fuel

As the compression work is roughly proportional to the temperature rise across the compressor (assuming constant C_p), cooling the compressor air offers performance advantages. If the compressor outlet temperature is fixed, the OPR could be increased, which mainly affects the SFC beneficially. Alternatively, the excessive work could be used to provide a higher fan pressure ratio, thus giving a higher fan thrust.

The compressor air could be cooled before the compressor (pre-cooling), between the HP and LP compressor (inter-cooling) or continuously during the compression process. The latter is accomplished through the cooling of the stator and intermediate guide vanes along the compression process. This technique offers the highest performance gains, but technically it is also the most complicated method to use [Payzer and Renninger, 1979].

Using a HE suited before the booster inlet of the V2527-A5 engine, Boggia et al. (2001) found that the SFC decreased by 5.7% and the SPT increased by 6.7% compared with their reference cycle. To obtain these benefits they increase the OPR and BPR, and even when the increased weight (due to the heat exchanger) is included, the performance is improved because the thrust to weight ratio is increased by 1.2%.

There are, however, problems with designs featuring a HE at engine inlet. In addition to the increased engine weight and complexity owing to the inclusion of a HE, the main disadvantage of this concept is the risk of foreign object damage [Corchero and Montañes, 2003]. Another problem, which is particularly pronounced for pre-cooled cycles, is the risk of icing on the air side of the HE. If the air is cooled below the equilibrium temperature at which the partial pressure of the water vapour is equal to its vapour pressure, water vapour will deposit out on the HE walls directly as an ice film [Payzer and Renninger, 1979]. Ice and frost formation initially tend to increase the heat transfer coefficient, but eventually clogging will occur and consequently the air flow will be reduced. Nevertheless, Payzer and Renninger (1979) concluded that air-to-fuel HEs that fully justify the engine fuel flow without air side freezing can be accomplished.

2.2.4.3 Cooling Turbine Cooling Air with Hydrogen Fuel

Normally the NGVs and the rotor of the HP turbine need to be cooled, as the TET exceeds the maximum allowable metal temperature. This is accomplished by bleeding off a portion of the compressed air which is passed through cooling passages inside the blades. By cooling the bleed air using the hydrogen fuel in a hydrogen-to-air HE, the blade cooling is made more effective and hence the maximum allowable TET is increased. The energy output of the core is highly dependent on the level of TET. If it is increased, more energy needs to be provided through the fuel, but the thrust output increases significantly. By employing this concept (increasing TET by 140 K) and re-designing the cycle through increased BPR and number of LPT stages, Boggia et al. (2001) attained an increased thrust to weight ratio of 8.4% and a decreased SFC of 2.1%.

One drawback associated with this technology is the complex design problems that have to be addressed when the routing of the turbine cooling air is re-designed. Another drawback is the severe thermal gradients in the blades due to the colder cooling air, which might cause low cycle fatigue damage [Baerst and Riple, 1979].

Although very advanced in terms of design features, it might in the very long run be possible to cool the relevant parts of the turbine directly using the hydrogen, without the usage of any HE. This would imply that there would be no decrease in cycle

performance as a consequence of the normal cooling air extraction [Payzer and Renninger, 1979]. Moreover, the losses associated with the heat exchanging process are eliminated, and the introduction of any significant weight penalties is avoided.

2.2.4.4 Hydrogen Topping Cycle

In order to boost the net thrust output, the main engine could be mechanically coupled to a topping loop. The topping loop could, depending on how much increased engine complexity is accepted, be more or less complex. The configuration proposed by Boggia et al. (2001) consists of a fuel pump, HE, compressor, combustor and turbine. In their design a fraction of the compressor air flow, which is fed to the topping cycle where it is pre-cooled (in a hydrogen-to-air HE) and compressed, is bled off. Hydrogen is compressed, pre-heated (in the hydrogen-to-air HE) and burnt very fuel-rich in a combustor which is provided with the bled air. The combustion products, composed of a mixture of stoichiometric products and hydrogen, are then expanded in the topping turbine and fed to the main engine burner where the hydrogen burns completely with the main air stream. Using this configuration it was found that the SPT increased by 11.1% and the SFC decreased by 1.1% compared with their reference cycle.

Looking at the practical feasibility of the additional components, Boggia et al. (2001) found that the small dimensions of the radial turbomachinery to perform the topping cycle compression do not pose any design problems. Neither is the design of the combustor of the topping loop expected to cause any problems. However, they claim that the sealing of the topping cycle, where a fuel-rich, high-pressure hot mixture must be kept separate from the air, would be technically very difficult to achieve safely. Owing to this the concept was rejected as impractical.

2.2.4.5 Conclusions on Unconventional Engine Design

According to Boggia et al. (2001) who studied and compared the four different cycles described above, the pre-cooled and high TET cycles appeared to be the most promising, offering a reduction in operational cost in the order of 3%. Furthermore, they point out that the positive aspect of these two cycles is that the innovations are technically feasible and do not involve any additional turbomachinery. The configuration with pre-heating of the fuel is the simplest solution and would require only minimum modifications to the base engine.

Payzer and Renninger (1979) conclude that there is a definite thermodynamic benefit in switching from hydrocarbon fuel to hydrogen fuel due to the difference in fuel properties. However, having evaluated eight different unconventional cycles, both in terms of uninstalled engine performance and aircraft mission performance, they state that the additional complexity associated with these cycles does not appear to be justified.

2.3 Pollutant Emissions

When burning hydrogen the emissions are reduced to water vapour (H_2O) and oxides of nitrogen (NO_x). In fact, the emission index of H_2O increases by a factor of about 2.6.

All emissions containing carbon and sulphur are eliminated. Besides, for reasons discussed in this section, there is the potential for lowering the NO_x emissions as compared with conventional combustors using kerosene. Therefore, to achieve satisfactory emission characteristics, the challenge is to minimize the NO_x emissions while preserving or reducing the SFC. Performing research focused on reducing NO_x emissions of gas turbines is highly important, since the effects of these emissions upon the environment and on human health are considerable, see section 1.2.2.

This section is introduced by a discussion of the NO_x formation processes (section 2.3.1), followed by a section dealing with the consequences on the NO_x emissions of using hydrogen (section 2.3.2). In section 2.3.3 combustion chamber design is discussed, and finally in section 2.3.4 the potential of achieving low NO_x emissions is illustrated by conducting simulations for the V2527-A5 engine.

2.3.1 NO_x Formation Processes in Combustion

Most of the nitrogen oxides formed during combustion are in the form of NO; however, subsequently the NO oxidizes to NO_2. Usually these are lumped together, and the result is expressed in terms of oxides of nitrogen (NO_x). The formation processes of NO in combustion are complex and generally comprise different mechanisms: thermal NO, prompt NO, nitrous oxide (N_2O) mechanism and fuel NO [Lefebvre, 1998]. In burning hydrogen, thermal NO formation is the most contributing mechanism to the total NO formation. Therefore this mechanism will be discussed more in detail (although still not very comprehensively), whilst the others will only be covered very briefly. As for fuel NO, this is nitrogen which is organically-bonded to the fuel that during combustion reacts with oxygen. Since neither kerosene nor hydrogen contains any nitrogen, this mechanism is not discussed any further.

Thermal NO is produced from the nitrogen and oxygen present in the air in the high-temperature regions of the flame and in the postflame gases. The process is endothermic and it proceeds at a considerable rate only at temperatures above around 1850 K [Lefebvre, 1998]. In stoichiometric and lean systems the thermal NO formation is generally considered to be predicted by the extended Zeldovich mechanism:

$$O_2 = 2O \tag{2-9}$$

$$N_2 + O = NO + N \tag{2-10}$$

$$N + O_2 = NO + O \tag{2-11}$$

$$N + OH = NO + H \tag{2-12}$$

As a consequence of the competition between the fuel and the nitrogen for the available oxygen, NO formation is found to peak on the fuel lean side of the stoichiometric fuel-air mixture [Lefebvre, 1998]. The thermal NO formation is largely controlled by flame temperature, and little NO is formed at temperatures below around 1850 K. As the flame temperature increases roughly linearly with the inlet air temperature, the thermal NO formation is expected to be highly influenced by the inlet air temperature, which also is confirmed by experimental work by Rink and Lefebvre (1989). According to Lefebvre (1998) the NO formation increases linearly with time but it does not achieve

its equilibrium value, since the time generally is too short in a conventional gas turbine combustor. For very lean premixed combustors, however, the NO formation is largely independent of residence time. In order to derive an empirical correlation to predict NO production for conventional kerosene-fuelled combustors, Lefebvre (1984) assumed that the exhaust concentrations are dependent on three terms which are selected to represent mean residence time in the combustion zone, chemical reaction rates and mixing rates.

Prompt NO is a designation for NO that under certain conditions is formed very early in the flame region. According to Nicol et al. (1992) the initiation reaction is:

$$N_2 + CH = HCN + N \tag{2-13}$$

For lean premixed combustion this formation mechanism can be a significant contributor to the NO emission produced [Correa, 1991]. Prompt NO may play a significant role for lean systems burning kerosene, whereas it does not contribute to the NO formation in combustion systems using hydrogen, since there are no carbon atoms present in the fuel.

The nitrous oxide (N_2O) mechanism is according to Nicol et al. (1992) initiated by the reaction:

$$N_2 + O = N_2O \tag{2-14}$$

and the N_2O formed is then oxidized to NO mainly by reaction with O, H or CO.

2.3.2 Effects on NO_x Emissions by Using Hydrogen

In order to address properly the issue of NO_x production of hydrogen combustion compared with kerosene combustion, several different combustion characteristics of these fuels need to be considered. The engine load in a gas turbine is controlled by varying the TET, which is determined by the overall fuel-air ratio in the combustion chamber. When a conventional kerosene-fuelled combustor is operating at full power, the primary zone operates at roughly stoichiometric fuel-air mixtures, where the flame temperature is highest and the chemical reactions are fastest [Ziemann et al., 1998a]. At low power idle conditions, the fuel-air ratio is essentially leaner and the primary zone fuel-air ratio has to be maintained above the flame-out limit with a sufficient margin. Hence, in order to minimise the NO_x emissions, it is desirable to modify the fuel-air ratio in the combustor primary zone in a way that lean combustion is achieved at all engine load conditions without suffering a flame-out [Ziemann et al., 1998a]. In Figure 2-3 the flame temperature of kerosene and hydrogen combustion versus primary zone equivalence ratio is shown.

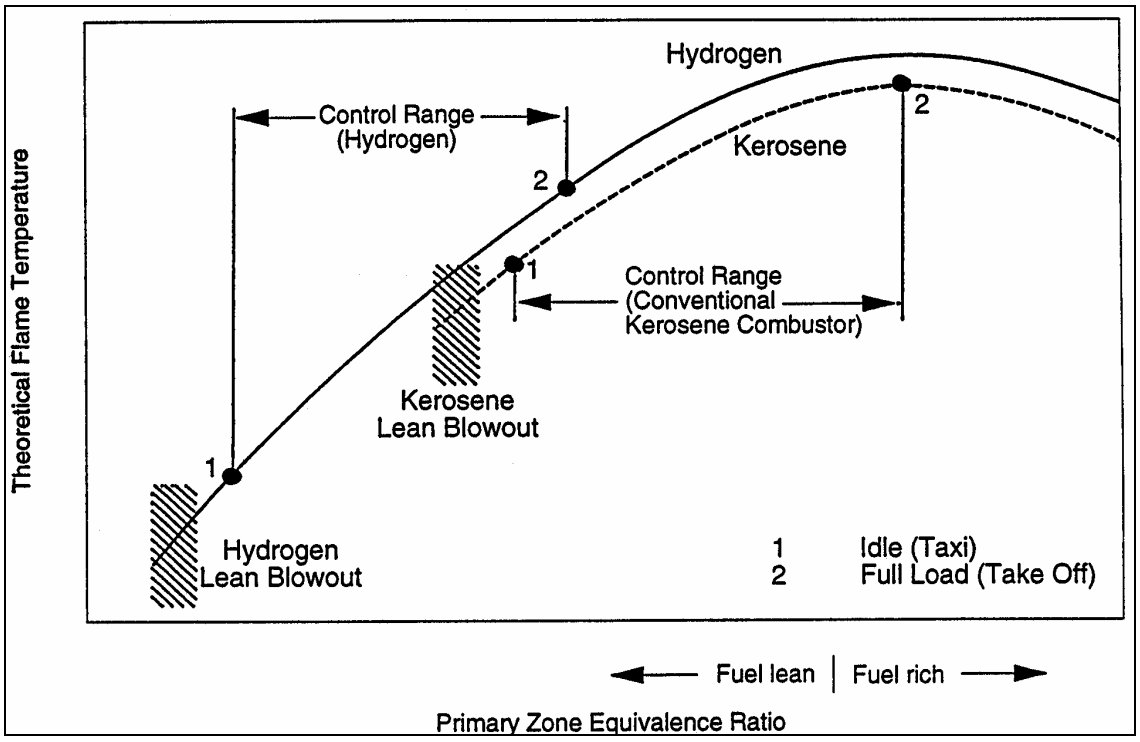

Figure 2-3. Temperature characteristics of the combustion chamber primary zone [Ziemann et al., 1998a].

The comparison illustrated in Figure 2-3 applies only to a conventional kerosene-fuelled combustor featuring a primary, intermediate and dilution zone. If the kerosene-powered combustor would employ any unconventional technology such as, for instance, a staged or an LPP (Lean Pre-mixed Pre-vaporized) combustor, the situation would change. Generally, the combustion zone of these combustors is operated at an equivalence ratio which is closer to the lean blow-out limit than the conventional, and hence it is not applicable to the situation sketched in the figure.

As illustrated in Figure 2-3, the stoichiometric flame temperature of hydrogen-air flames is in fact higher than that of kerosene-air flames (about 100 K higher), which would have a detrimental effect on the NO_x production. For a given equivalence ratio, the flame temperature is higher when burning hydrogen, which means that more NO_x would be generated. However, more importantly is that the hydrogen flame has a wider flammability range; particularly the lean limit is much lower than that encountered for kerosene flames [Ziemann et al., 1998a]. Therefore the entire operating range may be shifted further into the lean region, with reduced NO_x emissions as a consequence.

Due to the rapid reaction kinetics of hydrogen-air flames, the burning velocity increases about eight times when changing to hydrogen [Ziemann et al., 1998a]. The higher flame speed will result in a shorter combustor, hence reduced cooling requirements. Owing to this, more air will be available for the combustion, hence offering lower flame temperatures which will reduce the NO_x emissions. Another effect of the increased burning velocity is that the actual dwell time in the hot flame zone decreases, which is beneficial for hindering NO_x formation.

The fact that hydrogen is a gaseous fuel while kerosene is liquid, is also an argument in favour for hydrogen. The reason is that for liquid fuels there is always the potential of near-stoichiometric combustion temperatures in local regions adjacent to the fuel drops, and thereby high NO_x formation, even if the average equivalence ratio throughout the combustion zone may be appreciably less than stoichiometric [Lefebvre, 1998]. However, for increasing flame temperatures, the bulk flame temperature becomes closer to the stoichiometric value, and local conditions around the fuel drop have less influence on the overall combustion process and NO_x emissions. Hence, the difference in NO_x production decreases, and for equivalence ratios close to the stoichiometric value the difference becomes negligibly small. Moreover, the minimisation of the NO_x emissions of hydrogen combustion is facilitated by the fact that no other secondary combustion products (e.g. CO, UHC, soot) need to be regarded in the combustor design process.

From the preceding discussion, it may be concluded that theoretically there seems to be the potential to design a combustion system burning hydrogen that produces less NO_x emissions than a system burning kerosene. By calculation of the flame temperature at different relevant operating conditions this statement is illustrated in section 2.3.4. Before that the design of hydrogen-fuelled combustors is covered.

2.3.3 Combustor Configurations Burning Hydrogen

A brief overview of the functionality and the requirements that a conventional kerosene-powered combustor needs to satisfy is given in Appendix A.2. In order to design a reliable combustor that exploits the favourable properties offered by burning hydrogen, a range of factors needs to be regarded. In section 2.3.3.1 the design criteria for a hydrogen-fuelled combustor, and the development work that has been conducted to obtain a successful hydrogen-powered combustor are described. Next, the micromix design, which is selected for further investigation in the thesis, is described more in detail and emission results of this combustor type running on an APU GTCP 36-300 engine are outlined (section 2.3.3.2).

2.3.3.1 Design Criteria and Development Work for Obtaining a Combustor Using Hydrogen

In order to exploit the favourable characteristics of hydrogen combustion, the combustor needs to be re-designed compared with the conventional designs using regular diffusive combustion. When using conventional combustors, with their limited number of fuel injection points, the mixing of hydrogen and air tends to be incomplete. Moreover, the large-scale hydrogen diffusion flames form layers of stoichiometric mixtures of high local temperature and viscosity in which the NO formation rate remains high and acts as a barrier against the further progress of mixing [Ziemann et al., 1998a].

Generally when burning hydrogen the attempts to reduce the NO_x emissions are focused on lowering the flame temperature, eliminating hot spots from the reaction zone and reducing the duration and exposure in the flame region [Ziemann et al., 1998a].

Since the beginning of the 1990s various combustor configurations have been developed and evaluated experimentally and theoretically. In 1992 the third phase of the Euro-Québec Hydro-Hydrogen Pilot Project (EQHHPP), analytical modelling and experimental tests of low-NO_x combustors for aero engines were performed [Ziemann et al., 1998a; and Ziemann et al., 1998b]. In this program, generic tests for development of the micromix hydrogen combustion principle and others were conducted. Various burner concepts for lean hydrogen combustion were evaluated in a generic can-type combustor at Pratt and Whitney, Canada. The two most advanced burner concepts applied the principle of premixing of the fuel and air, prior to delivery to the combustor. Four of the injectors were of non-premixing devices, with the strategy of injecting gaseous hydrogen into a vigorous shear-layer mixing region of the combustor. The principle of premixing turned out to offer the highest NO_x reduction potential. However, to avoid the potential auto-ignition and flashback problems that can occur in the premixing tubes at high inlet temperatures, a major hardware design challenge is to achieve a fuel-air mixing time less than the auto-ignition time [Ziemann et al., 1998b]. Two injector concepts that seem most promising – one premixed and one non-premixed – were selected for further investigation. These were the "premixed perforated plate" and the "high shear swirl injector", representing the premixing and non-premixing concepts, respectively (see Figure 2-4).

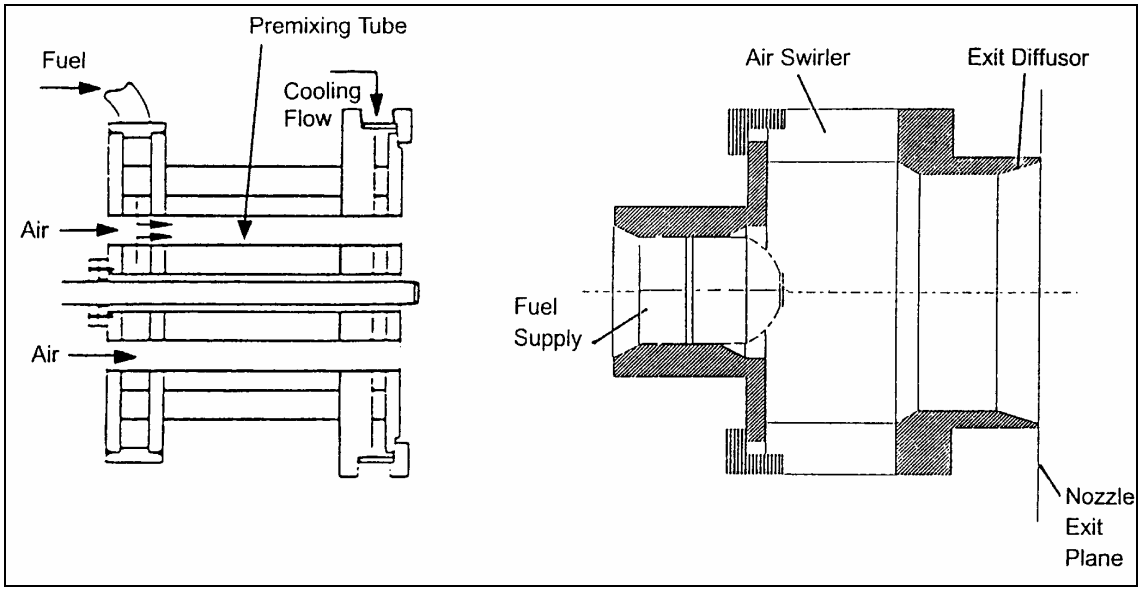

Figure 2-4. Fuel injector concepts: Premixed perforated plate (left) and High shear swirl concept (right) [Ziemann et al., 1998b].

The premixed perforated plate burner is designed so that the gaseous fuel is injected radially into the premixing tubes, where it is rapidly mixed with the turbulent axial air stream. The airflow in the tubes is kept high enough to prevent flame propagation upstream of the tubes. The aim of the high shear swirl concept is to create rapid mixing, burning and quenching of the gases. This is achieved by injection of gaseous hydrogen into a highly turbulent region created by an intense tangential shear flow.

For the two combustors, steady-state and transient sector combustor tests were performed. Trade-offs that can be encountered between emissions performance and stability margin were illustrated for the premixed perforated plate. Problems that usually occur for premixed devices, such as partial or local blowout and local flashback, were encountered. However, these problems were evident only under the most extreme conditions. The high shear swirl concept displayed excellent stability characteristics, but with higher NO_x emissions than the premixed concept [Ziemann et al., 1998b].

The above cited studies and other preceding studies show that lean premixed combustion is undoubtedly superior to any combustion scheme without premixing in terms of temperature pattern uniformity and NO production. However, premixing implies the major drawback of premature burning and flashback danger, which may cause structural damage and compromise the operational reliability [Ziemann et al., 1998b]. The risk of auto-ignition for premixed systems and the problems of large-scale hydrogen diffusion flames, have led to the lean non-premixing concept of micromix combustion, which is based on miniaturized diffusive combustion. Employing this principle, imperfections in fuel-air mixing cannot be avoided; however, the local standard deviations from the nominal equivalence ratio are kept to a minimum [Ziemann et al., 1998a].

2.3.3.2 The Micromix Combustor Configuration

The micromix combustor consists of a very large number (typically more than 1000) diffusion flames uniformly distributed across the burner's main cross section, thereby minimising the geometric size of the combustion zone [Dahl and Suttrop, 2001b; Ziemann et al., 1998a; and Dahl and Suttrop, 1998]. Theoretically, the lowest NO_x production would be achieved by an infinite number of miniaturised flames. The minimum size is, however, restricted by the manufacturing cost and the combustion stability at engine idle conditions; the latter being deteriorated with reduced flame dimensions. In addition to minimising the scale of the combustion zone, the micromix concept aims at optimally utilising the available pressure loss (providing energy for the dissipative turbulent mixing process) in the combustion system to enhance the mixing process of hydrogen and air. Simultaneously minimising the scale of combustion and maximising the intensity of mixing will minimise the number and size of local stoichiometric flame regions, where the gas phase NO formation processes are most likely to occur. Due to the high flame speed and high reactivity of hydrogen compared with other fuels, the degree of miniaturisation of hydrogen-air diffusion flames very well exceeds the possibilities of other fuels [Ziemann et al., 1998a].

The development of a gas turbine combustion system for hydrogen started in the late 1980's at the Germany University FH-Aachen. To obtain the current micromix burner configuration, which is considered in this thesis, several preceding configurations were designed and studied experimentally. The first micromix configuration was a low-cost device that could easily be manufactured. This was used to demonstrate the burner configuration by converting a FH-Aachen-owned shaft power gas turbine into hydrogen operation. This burner was called the "first generation" [Dahl and Suttrop, 2001b]. The engine was tested both using the engine's original tubular combustor with hydrogen injection nozzles instead of the original kerosene nozzles, and by using the "first

generation" of the micromix combustor. An essential NO_x reduction was measured by applying the micromix design.

Within the third phase of the EQHHPP project, generic tests of burner concepts were performed to develop the micromix hydrogen combustion principle. A considerable amount of micromix specimen burners were rig tested, including two-dimensional and matrix type designs [Ziemann et al., 1998a]. The burners may be further classified into the categories of "regular diffusion flame burners" (hydrogen injected into an air flow) and "inverted diffusion flame burners" (air jets injected into a surrounding hydrogen atmosphere). From this work one burner was selected for sector combustor demonstration tests. This burner may be called the "second generation" of the hydrogen burner development at FH-Aachen, and it is a "cone burner" with inverted diffusive hydrogen combustion. The results seemed promising with respect to low NO_x emissions (about 3 ppm at atmospheric burner entrance conditions) and uniformity of the burner exit temperature distribution [Dahl and Suttrop, 2001a].

The next step was to convert an APU GTCP 36-300 located in the Aircraft Engine Laboratory of FH-Aachen into hydrogen operation (see Figure 2-5). The engine was fitted with a micromix combustor according to the "second generation" combustion principle. As a comparison a minimum change combustor was tested, where the original combustor was provided with hydrogen injection nozzles instead of the kerosene nozzles. The NO_x emission for these two concepts was measured and compared with those of the conventional kerosene combustor (Figure 2-6). It was concluded that no NO_x reduction could be achieved by simply replacing the kerosene nozzles with gas injection nozzles for hydrogen, whereas an essential reduction in emitted NO_x fraction was observed for the micromix hydrogen combustor.

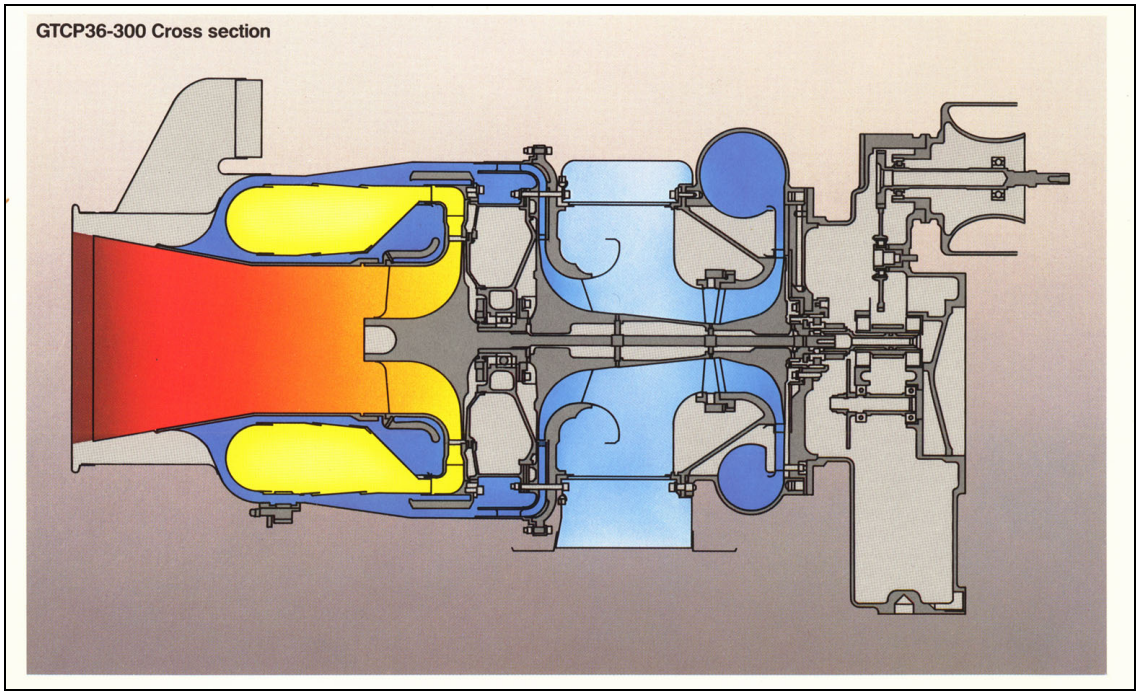

Figure 2-5. Cross section of the APU GTCP 36-300 (Honeywell) [Dahl, 2002].

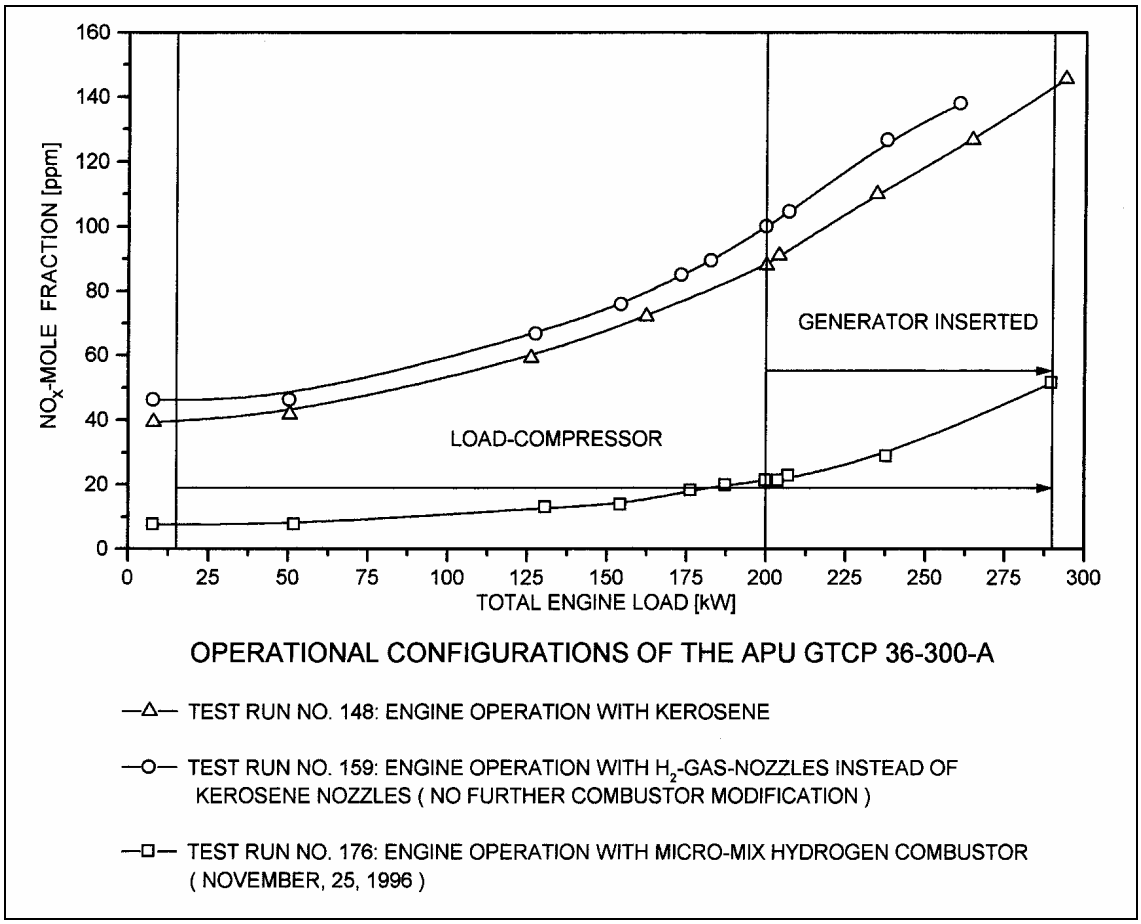

Figure 2-6. NO_x emissions for APU GTCP 36-300 operation conditions, fitted with different combustion systems, including the hydrogen micromix combustor of second generation [Dahl and Suttrop, 2001b].

In parallel with the experimental work on the "inverted diffusive hydrogen combustion" systems, the "regular diffusive hydrogen combustion" configurations were continuously developed at FH-Aachen [e.g. Bagheri, 1996; and Schweiger, 1997]. This development work resulted in a new burner that may be called the configuration of a third generation. Compared with the burners of the second generation, further NO_x reduction was achieved, and the thermal and mechanical stability were improved. A combustor based on this technology was developed, manufactured and tested in the rig as well as on the APU GTCP 36-300 engine. A drawing of the combustor, which is a ring-shaped device with 1600 flamelets spread uniformly across the burner's plate area, is shown in Figure 2-7. The fuel and air injection device is illustrated in Figure 2-8. The air stream is guided in the axial direction through individual apertures in sheets of metal to each flamelet. Aligned with these air jets, hydrogen is injected perpendicular to the main airflow direction. The degree of miniaturisation applied in this configuration is considered to be the optimum with respect to the NO_x reduction level versus expense in manufacturing costs and stability at idle engine operation conditions. The described burner of the third generation is the current solution of the micromix hydrogen combustor. This configuration is considered in this thesis.

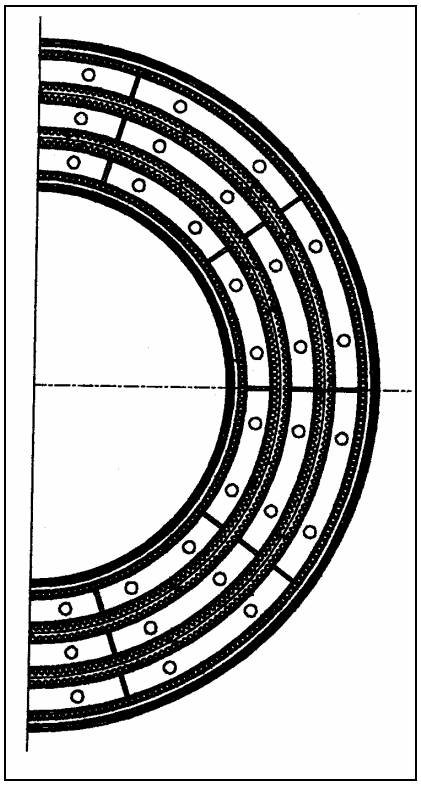

Figure 2-7. Ring-shaped structure of the micromix hydrogen combustor of third generation for the APU GTCP 36-300 engine [Dahl and Suttrop, 2001b].

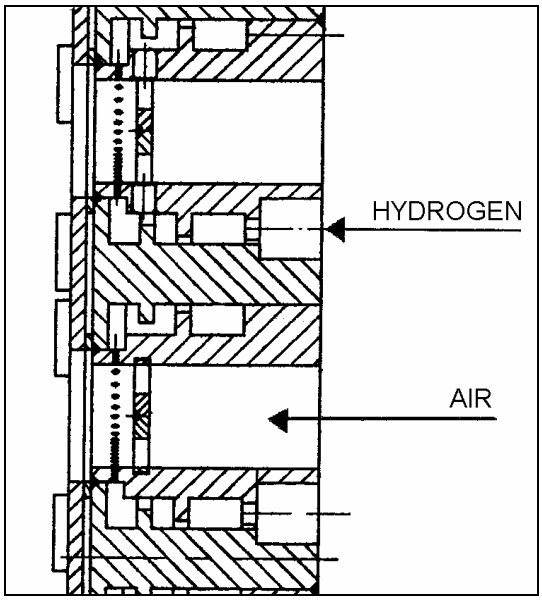

Figure 2-8. Air and hydrogen admission for diffusive combustion in the micromix hydrogen combustor of third generation for the APU GTCP 36-300 engine [Dahl and Suttrop, 2001b].

Finally, the APU GTCP 36-330 was fitted with various combustion systems and the NO_x mole fractions were measured. The combustion systems were as follows: original

combustor using kerosene, original combustor using gas nozzle hydrogen injection, micromix hydrogen combustor using inverse diffusive combustion (second generation) and present micromix combustor using regular diffusive combustion (third generation), see Figure 2-9.

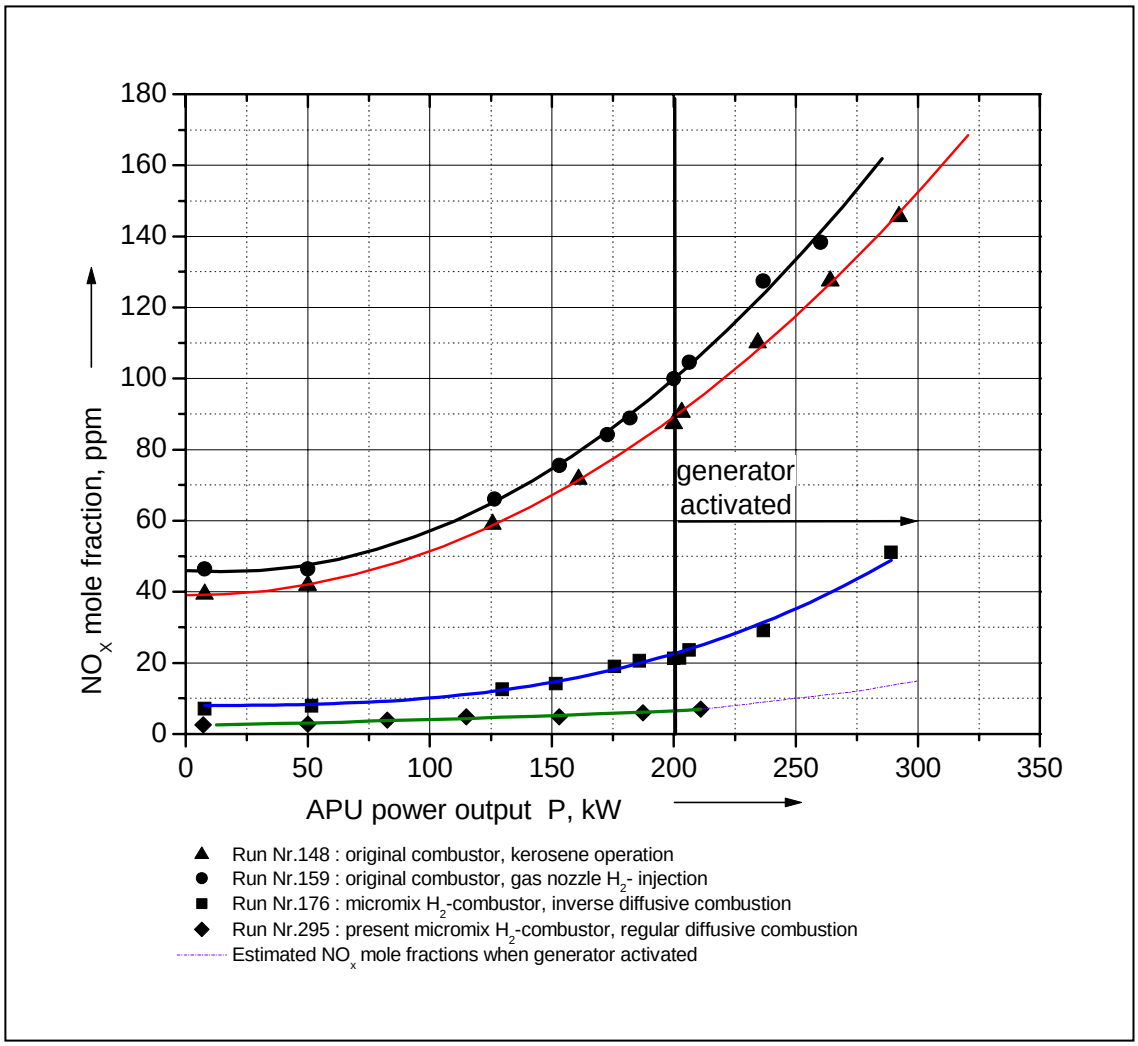

Figure 2-9. NO_x emissions of the APU GTCP 36-300 fitted with different combustion systems [Dahl and Suttrop, 2001b].

From Figure 2-9 it may be concluded that significantly lower levels of NO_x may be achieved with the micromix combustors compared with conventional combustors using kerosene. Moreover, it can be observed that the lowest level of NO_x is attained with the present configuration of a micromix combustor employing regular diffusive combustion. There is, however, no use in simply changing the injection nozzles of the original combustor to hydrogen injection nozzles; this would even increase the NO_x emissions. It is worth mentioning that by the time of the test runs, the APU output was restricted to about 210 kW because the electric generator was not available. The curve in Figure 2-9 is however extrapolated for higher power loads. A cautious estimation of the NO_x emission level for main engine start or full power operation, corresponding to an APU power output of roughly 300 kW, may yield about 20 ppm [Dahl and Suttrop,

2001b]. The figure shows that for main engine start conditions, the mole fractions of NO_x emissions are reduced by about 88% compared with the minimum change configuration (only hydrogen injection nozzles), and by roughly 85-86% when compared with the emissions of the kerosene-fuelled engine. As the output power is reduced the difference increases.

From the theoretical advantages of achieving low NO_x emissions outlined in section 2.3.2 and the experimental results presented in this section, there seems to be the potential to design a hydrogen-fuelled combustion system that produces very low NO_x emissions. In the following section the theoretical potentials of achieving low NO_x emissions for kerosene- and hydrogen-fuelled combustion systems, respectively, are assessed and compared by carrying out engine simulations.

2.3.4 Illustration of the NO_X Reduction Potential

Here, the NO_x reduction potential when using hydrogen and kerosene is illustrated by simulating the V2527-A5 engine, considered to be provided with different combustion systems. The aim of this section is to quantify and compare the leanest possible attainable levels for the operation conditions take-off and idle (assumed to be 7% power setting) at static sea level, and the flame temperatures associated with these, for kerosene and hydrogen combustion, respectively. Rather than attempting to design a combustion system, the qualitative differences in flame temperature associated with these different fuels are assessed. When designing a combustion system for an aero engine, the most challenging operating conditions, such as re-light at high altitude and low flight mach numbers, need to be addressed [Walsh and Fletcher, 1998].

The take-off condition is modelled with the performance code TurboMatch. As the compressor maps provided in TurboMatch were not sufficient to model the idle condition (resulting in that the program did not converge), GasTurb [Kurzke, 1998] is employed to simulate this operating condition. The drawbacks of using GasTurb for the off-design point, besides the fact that different codes may give slightly different results, are that there is no option of including a heat exchanger suited in the exhaust to evaporate the liquid hydrogen (unless the code is changed), as well as GasTurb assumes a slightly lower (-2.5%) heating value (LHV) than desired in this analysis. The thrust loss due to temperature drop in the exhaust is, however, negligibly small, especially for this low operating condition. For the purposes of the present study a reasonable performance estimation is sufficient, and hence it is considered acceptable to use GasTurb to model the idle condition.

The characteristics for kerosene and hydrogen used in the calculations are given in Table 2-6. The molecular weight of kerosene is taken from Goodger (1993) and of hydrogen and air from Wester (1996). The flammability limits are from Jones and Sefain (2000), the lower heating values from Jackson (2000) and the stoichiometric fuel-air ratios are calculated by setting up chemical balances and assuming stoichiometry.

Table 2-6. Characteristics of kerosene and hydrogen.

	MW [g/mol]	Flammability limits in air [$\%_{vol}$]	LHV [MJ/kg]	Stoichiometric FAR [-]
Kerosene	175	0.6-4.7	43.124	0.0683
Hydrogen	2.016	4.0-75.0	120.0	0.02916
Air	28.966	-	-	-

The flame temperatures are calculated assuming chemical equilibrium. This implies that the time dependence is cancelled, the complexity is reduced and it is possible to calculate the flame temperature without studying the flow field and chemical kinetics. Calculating the flame temperature without assuming chemical equilibrium is beyond the scope of this thesis. For the flame temperature computation, a well-established computer program developed at NASA Lewis Research Centre is employed [McBride and Gordon, 1996; and Gordon and McBride, 1994]. In the latest version of the program, which is called CEA (Chemical Equilibrium Applications), the chemical equilibrium compositions and thermodynamic properties of the equilibrium mixtures can be calculated for a variety of problems (e.g. assigned-temperature and assigned-pressure problems, assigned-enthalpy and assigned-pressure problems, and rocket problems). When a gas turbine combustor is modelled, combustion at constant pressure is assumed. For details about the mathematical analyses and physics for obtaining chemical equilibrium used in the CEA program, see Gordon and McBride (1994), and for general theory about chemical equilibrium in combustion, see, for instance, Turns (1996).

Although the flame temperature computed this way tends to be overestimated, due to the fact that the dwell time in a gas turbine combustor is slightly too short for chemical equilibrium to be achieved, it is believed to indicate qualitative differences in flame temperatures, and thereby the thermal NO levels, that may be expected from the different combustion systems. To complete the combustion a dwell time close to 5 ms is required, while the dwell time in a gas turbine typically is 3 ms [Shum et al., 1996].

Under normal operating conditions, the maximum percentage of air entering the combustor that may be introduced in the primary zone is restricted by the flame-out limit of the fuel-air mixture. Knowing the mass flows of fuel and air in the primary zone (PZ), the mass fraction of fuel, Y_F, can be calculated as:

$$Y_F = \frac{W_F}{W_F + W_A} \tag{2-15}$$

As the flammability limits shown in Table 2-6 are given in volume fractions, X_F, the calculated mass fraction needs to be transformed accordingly. This transformation can be accomplished using the molecular weights (MW) of the fuel and air with the following equation [Turns, 1996]:

$$X_F = \frac{Y_F}{MW_F \cdot \left(\frac{Y_F}{MW_F} + \frac{Y_A}{MW_A} \right)} \tag{2-16}$$

In order to avoid weak extinction at low power, Walsh and Fletcher (1998) recommend that the equivalence ratio in the primary zone for sea level static maximum rating is 1.02 for a conventional kerosene-fuelled combustor. According to the calculations performed here, this equivalence ratio is achieved by distributing about 31% of the air entering the combustor to the primary zone. An overview of the results is presented in Table 2-7. At idle condition, the overall volume fraction of fuel would become less than the lean blow-out limit of $0.6\%_{vol}$. However, since there still would be local regions of fuel-air ratios sufficiently high to sustain a flame, it would be possible to run the combustor leaner than this limit without suffering a flame-out. According to Walsh and Fletcher (1998), the weak extinction limit is around an equivalence ratio of 0.25, which is well below the equivalence ratio of 0.40 derived here for the idle condition.

At take-off condition, an equivalence ratio of 1.02 in the primary zone corresponds to a flame temperature of 2613 K, which is about 300 K higher than that given in Walsh and Fletcher (1998). Assuming chemical equilibrium, comparing the flame temperature derived here with the number given in Walsh and Fletcher (1998), it is indicated that overestimated flame temperatures by about 10-15% might be expected for stoichiometric conditions burning kerosene. This deviation is, however, not expected to change substantially the conclusions, since the main purpose of this exercise is to compare the flame temperatures (and the expected NO_x emissions production) obtained when burning two different fuels, and the difference in flame temperature between the two fuels is not expected to be affected significantly by this deviation. However, as the rate of chemical kinetics and the combustor lengths of these two fuels are different, it cannot be excluded that the difference in flame temperatures would change if the flow field and chemical kinetics were taken into account. At take-off condition with a prevailing flame temperature of 2613 K (or rather 2300 K), depending on the combustion system, it is likely that excessive amounts of thermal NO are formed.

In order to reduce the flame temperature at take-off conditions, variable geometry combustors could be employed. Practically this could be achieved by the use of variable-area swirlers to control the amount of air flowing into the combustion zone, variable air openings into the dilution zone, or a combination of these [Lefebvre, 1998]. Using this technology, a large proportion of air is admitted in the primary zone at maximum power conditions in order to lower the flame temperature and provide adequate film-cooling air, and as the power is decreased, an increasing proportion of this air is diverted to the dilution zone.

Theoretically, the utmost lowest flame temperature that may be achieved by employing variable geometry combustors at full power condition for a kerosene-fuelled combustion system, is the temperature obtained by assuming a primary zone equivalence ratio equal to the weak extinction limit including a safety margin. This is the leanest possible fuel-air mixture at which the combustion zone may be operated using any novel combustion concept. In order to achieve this condition in the

combustion zone, there might be other novel combustor concepts more appropriate than a variable geometry combustor. According to the computations conducted for idle condition when the equivalence ratio at take-off is equal to 1.02, this corresponds to an equivalence ratio of 0.40. An equivalence ratio of 0.40 is achieved at take-off by diverting up to 78% of the incoming air to the primary zone, giving a substantially reduced flame temperature of 1733 K (see Table 2-7). Combustor inlet conditions, in terms of mass flow, temperature and pressure, are also given in the table.

All forms of variable geometry systems are associated with drawbacks, like complex control and feedback mechanisms, which tend to increase cost and weight and reduce reliability [Lefebvre, 1998]. Furthermore, Lefebvre (1998) states that problems of achieving the desired temperature pattern in the combustor efflux gases could be encountered, especially if the liner pressure drop is allowed to vary too much.

Table 2-7. Comparison of combustion characteristics.

	Ker., T/O	H_2, T/O	Ker., Idle	H_2, Idle
F_N [kN]	117.9	117.9	8.3	8.3
COT [K]	1555	1522	812	807
W_3 [kg/s]	54.1	54.1	10.4	10.2
T_3 [K]	835.1	836.2	478.6	476.7
P_3 [kPa]	2882	2882	398	393
Maximum air to the primary zone during idle				
Air to PZ [%]	31	95	31	95
X_F [$\%_{vol}$]	1.14	10.36	0.45	4.43
ϕ_{pz} [-]	1.02	0.28	0.40	0.111
T_{flame} in PZ [K]	2613	1587	1438	825
Maximum air to the primary zone during T/O				
Air to PZ [%]	78	95	31	95
X_F [$\%_{vol}$]	0.46	10.36	0.45	4.43
ϕ_{pz} [-]	0.40	0.28	0.40	0.111
T_{flame} in PZ [K]	1733	1587	1438	825

As for hydrogen combustion when employing the concept of micromix combustion, there is no splitting of the combustor air into different zones, but all available air, which is the total compressor exit mass flow minus bleed air and cooling air, is used for combustion. Considering the V2500 engine, the air flow at compressor exit is divided according to the following proportions [Suttrop, 2003]: 71.9% combustion air, 13.4% liner cooling air and 14.7% bleed air. As a consequence of the high flame speed of hydrogen flames, it has been shown experimentally that the micromix combustor needs roughly one-third of the conventional combustor's liner length [Dahl and Suttrop, 2001b; and Suttrop, 2003]. Accordingly, the liner cooling air may be reduced by a factor of about one-third, as an order of magnitude. Comparing with the numbers stated for the conventional combustor of the V2500 engine, about 5% of the air entering the combustor (having subtracted the bleed air) is needed for liner cooling of the micromix combustor.

Due to the very wide flammability limits of hydrogen-air flames, it would be possible to devote all air entering the combustor for combustion. However, owing to the cooling requirement, maximally 95% could actually be used for combustion. Allowing 95% of the air to take part in the combustion, a very lean fuel-air ratio is achieved (equivalence ratio equal to 0.28) in the primary zone for take-off condition. This equivalence ratio is yielded both when maximising the amount of air to the primary zone at take-off and at idle. Despite the fact that the stoichiometric flame temperature is about 100 K higher for hydrogen-air flames, the flame temperatures corresponding to the same operating condition are essentially lower than those yielded for the kerosene case.

Looking at the take-off condition where most of the NO_x is formed, the flame temperature is 1587 K, which is about 1000 K lower than the corresponding figure for kerosene. At idle the relation is in the same order of magnitude. If the kerosene combustor would be provided with a variable geometry combustor, theoretically the difference might be reduced to about 150 K. As the hydrogen-fuelled combustor would be operated with a remarkably larger margin to the weak extinction limit than would the kerosene-fuelled combustor provided with a variable geometry combustor, the hydrogen-fuelled combustor is likely to be the more viable of these two (see section 2.4). The differences in flame temperatures will have a substantial effect on the amount of thermal NO produced by the combustion system. In addition, since the lean kerosene-powered combustor would probably also generate prompt NO, whereas the combustor burning hydrogen would not (see section 2.3.1), the difference in NO_x formation between these two fuels is likely to be even larger than assessed when looking at the primary zone flame temperatures.

Even if the flame temperatures of the hydrogen combustor are low for both take-off and idle, they are higher than the lower limit, which is the temperature required by the cycle needs to give the desired performance, namely, the combustor outlet temperature (COT). In spite of the simplicity in the approach of this study, the results of the calculations suggest that there is the potential to design a combustion system using hydrogen that produces less NO_x emissions than any system burning kerosene.

2.4 Design and Handling Issues

In order to adapt the combustion chamber for hydrogen, some changes are necessary and some others are desired in order to utilise the favourable properties of hydrogen in an optimal fashion. The minimum change that has to be done to adapt a conventional combustion chamber for hydrogen, is to replace the injection system, because when the hydrogen is injected into the combustor it is in the gaseous state, while the kerosene is liquid. In addition, there are several other changes that need to be considered to utilise optimally the changed conditions owing to burning hydrogen. The higher flame speed will result in a shorter combustor, and hence, reduced engine weight and combustor liner cooling requirements.

When burning hydrogen the thermal energy radiated to the surroundings is lower than that of kerosene, thereby beneficially affecting the liner durability and liner cooling requirements. The reason for the reduced radiation could be explained as follows. In most gas turbine combustors, a sizeable proportion of the heat from the hot gases

contained within the combustor to the liner wall is by radiation. Generally for combustion gases generated by combustion of kerosene, the total emitted radiation comprises two components [Singh, 2002]: “non-luminous” radiation which emanates from certain heteropolar gases, notably CO_2 and H_2O, and “luminous” radiation which depends on the number and size of the solid particles (mainly soot) in the flame. At high levels of pressure encountered in modern gas turbine combustors, the flame is characterised by a predominance of luminous radiation [Singh, 2002]. Since no particles at all are present in the combustion gases when burning hydrogen, there is no luminous radiation, thus essentially lowering the total heat radiation as compared with combustion gases of kerosene combustion.

As discussed, hydrogen-air flames have an essentially wider flammability range, which will allow operation of the combustion zone at an equivalence ratio which has a large margin to the lean blow-out limit. This will facilitate the handling of the engine, as well as reduce the creation of white noise (noise with lots of different frequencies) that might give rise to pulsations and vibrations in the engine, which in turn via resonance can have a detrimental effect on engine components.

2.5 Conclusions

In this chapter the effects of using hydrogen on aero gas turbine pollutant emissions, performance and design are investigated. From a technical point of view, it seems to be feasible to use hydrogen for aero gas turbines. The main changes comprise re-design of the combustion chamber and fuel control system, as well as the implementation of facilities to evaporate the hydrogen prior to its entry into the combustion chamber. The fuel heating can be accomplished either by an external heat source or a HE located at a suitable engine location. In practice, the heat exchanging might be accomplished by employing the struts, which are the mechanical structures in the exhaust which hold the rotors in place and are connecting the bearings’ outer structure. Alternatively, the HE could feature a simple coil tube placed over the inside face of the jet pipe casing, avoiding major engine changes and giving a relatively aerodynamically clean jet pipe [Corchero and Montañes, 2003]. Simplified calculations suggest that the heat transferring area available from the exhaust struts is not sufficiently large to accomplish all the desired temperature rise of the hydrogen fuel.

Small performance gains, which depend on the fuel temperature and cycle configuration, in the order of a few percent may be obtained by changing to hydrogen fuel. In order to obtain a certain performance, a lower TET could be used, thus requiring less advanced cooling technology as well as having a favourable effect on turbine blade life. By employing unconventional cycles, it would be possible to increase these performance gains. However, it appears to be questionable if these benefits justify the increased complexity imposed by unconventional cycles.

In terms of pollutant emissions, hydrogen use offers the possibility of a significantly reduced number of emission species, resulting in only H_2O and NO_x emissions. In addition, the results of the calculations suggest that there is the potential to design a combustion system using hydrogen that produces less NO_x emissions than any system burning kerosene. With respect to combustor configurations burning hydrogen, the lean

non-premixing concept of micromix combustion, which is based on miniaturized diffusive combustion, is suggested as a promising configuration.

Due to the wider flammability range of the hydrogen-air flames (compared with kerosene-air flames), which allows operation of the combustion zone at an equivalence ratio which has a large margin to the lean blow-out limit, the engine handling is facilitated and the creation of white noise is reduced. Furthermore, when burning hydrogen the thermal energy radiated to the surroundings is lower than that of kerosene, thereby beneficially affecting the liner durability and liner cooling requirements.

3 OPTIMUM CRUISING ALTITUDE FOR MINIMUM GLOBAL WARMING

3.1 Introduction

The primary contributor to global warming is carbon dioxide (CO_2). In addition, essentially depending on the cruise altitude, H_2O and NO_x can play an important role. In order to reduce the environmental burden from an aircraft, one may either perform technical design improvements, for instance, on the airframe or on the engine, or one may apply operational measures. The way of operating the aircraft may be changed in several ways.

In this thesis the influence of lowering the cruise altitude, as a means of reducing the environmental impact, is investigated. The option of changing the cruise altitude has been studied before, particularly for kerosene-powered aircraft [Grewe et al., 2002; Williams et al., 2002; Air Travel – Greener by Design, 2001; and Sausen et al., 1998], but also to a minor extent for cryoplanes [Klug et al., 1996]. At a lower altitude the air has a higher density, which causes larger loads on the airframe. The wings therefore need to be stiffer, thus increasing the structure weight [Hume, 2001]. On the other hand, the load on the fuselage would be lower due to the lower pressure difference between the cabin and outside air, which would decrease the structure weight [Hume, 2001]. Flying lower would reduce the radiation exposure, but the aircraft would be more exposed to gusts that would increase the fatigue and make the ride less comfortable.

The objective of this study is to identify the optimum cruise altitude for two equivalent medium-range aircraft, one kerosene-fuelled and one LH_2-fuelled, from an environmental point of view. For this purpose both aircraft are re-optimised and compared for a number of different reduced cruise altitudes. By carrying out detailed flight simulations, differences, in terms of required changes in configuration and optimum cruise altitude for minimum environmental burden, are identified for both aircraft types.

The methodology including modelling tools which are used are described in section 3.2. Assumptions about technology levels are outlined in section 3.3. In section 3.4 a simple parametric model is described that is used to assess the global impact, in terms of global warming, from the emissions discharged on a certain mission. The results are given in section 3.5, and the chapter is concluded by an outline and discussion of the conclusions (section 3.6).

3.2 Methodology

In order to assess the environmental improvement that is possible to be achieved by changing the aircraft configuration and flight procedures, two different simulation tools, Piano [Simos, 2000] and Hurdy-Gurdy [Hasselrot, 2000], are employed. Piano is a commercial software that may be used for performance estimations, preliminary design

studies and flight mission calculations. Hurdy-Gurdy is a software developed at FOI for off-design flight mission studies. For the purposes of this task, a module for evaluation of the Global Warming Potential (GWP) from a certain flight mission, is implemented in Hurdy-Gurdy.

The simulation procedure consists of a sequence of operations. Firstly, a datum aircraft is established in Piano by defining geometries, weights, aerodynamic performance (drag polar) and engine performance. The aircraft weights and the aerodynamic characteristics are taken from Oelkers and Prenzel (2001), while the engine performance is obtained using the gas turbine performance code TurboMatch, see Appendix A.3, section A.3.1. Then the aircraft is re-optimised for the datum as well as reduced cruise altitudes, and changes in aircraft performance, fuel burn and emissions are determined. In order to translate the changes in emissions and fuel burn into a measure of global warming, each optimised configuration is simulated in Hurdy-Gurdy to calculate the amount of emissions emitted at different altitudes. In addition, a GWP model (see section 3.4) is used. This procedure is carried out for both the kerosene- and the LH_2-fuelled aircraft. Differences between these two aircraft types due to a reduction in cruise altitude are estimated. From these results, preliminary conclusions about the optimum cruise altitude from the environmental point of view can be drawn, for both the kerosene and the hydrogen aircraft. The calculations conducted in this study using Piano and Hurdy-Gurdy are performed in collaboration with Anders Hasselrot at FOI.

The aircraft selected to be studied is a low-wing configuration based on the Airbus A321 aircraft. Since the liquid hydrogen is substantially bulkier than kerosene, storing the fuel in the wings as commonly done for conventional aircraft is not suitable. This would make the wings far too large, with a high fuel consumption penalty as a consequence. In order to minimise the tank isolation requirements and the evaporation losses, the aim is to store the hydrogen in tanks that have a high volume to area ratio. For the aircraft under consideration, an aircraft that stores its fuel on top of the fuselage and in a tank outside the pressure cabin in the tail cone of the fuselage turned out to be a viable solution that offers the lowest penalty in energy consumption [Oelkers and Prenzel, 2001]. In Table 3-1 some fundamental performance data for the two investigated aircraft are summarized, and in Figure 3-1 and Figure 3-2 the aircraft layouts for the conventional aircraft and the cryoplane are presented. Further details about the aircraft are given in Oelkers and Prenzel (2001), Westenberger (2003a) and Westenberger (2003b).

When the required aircraft fuel volume is changed due to re-optimising the aircraft, it is assumed that the fuel volume of the tail cone of the aircraft is re-sized. For simplification it is assumed that only the length of the tank in the tail cone, and hence also the aircraft length, changes when either a larger or smaller fuel volume is required. This implies that the length of the tail cone is assumed to be proportional to the change in required fuel volume.

Table 3-1. Fundamental performance data of the two investigated aircraft.

	Conventional - RK 200	Cryoplane – CMR1 200
Engine type	V2527-A5 (impr. & scaled)	V2527-A5 (impr. & scaled)
SSLT [kN]	136	136
Design range [nm]	4000	4000
No of seats (2 CL, MR)	185	185
Wing area [m^2]	170	170
MTOM [tonne]	89.3	87.6
OME (2 CL, MR) [tonne]	48.7	61.4
Payload [tonne]	16.8	16.8
Fuel capacity [tonne]	23.9	9.4
Fuel density [kg/m^3]	803	71

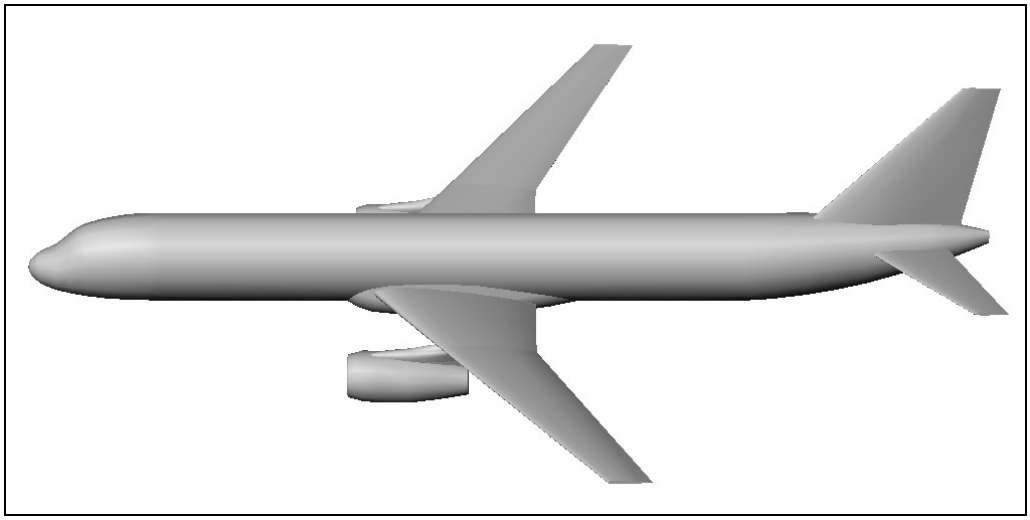

Figure 3-1. Aircraft layout for RK-200 [Oelkers and Prenzel, 2001].

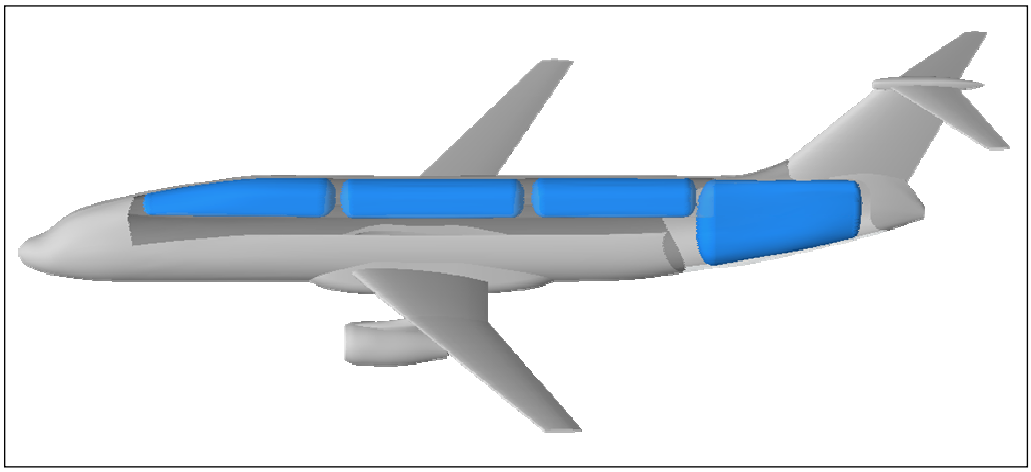

Figure 3-2. Aircraft layout for CMR1-200 [Oelkers and Prenzel, 2001].

3.2.1 Implementation of Data in Piano

Piano does include the feature of defining a new aircraft from scratch. To do so geometries, weights, fuel reserve policies and aerodynamic characteristics (drag polar), taken from Oelkers and Prenzel (2001) are specified. By applying correction factors, the aerodynamics and structure weights are adjusted to match the data published by Oelkers and Prenzel (2001), aimed at reflecting a technology level of 2010 (see section 3.3.2).

As for the engine characteristics, these data are obtained using TurboMatch. In addition, the inherent engine characteristics (fuel flow and thrust versus Mach number and altitude) provided in Piano for different engine types are employed. Having chosen a suitable engine type, the absolute performance level is adjusted using correction factors applied at different altitudes to match a desired performance. In order to estimate these correction factors, TurboMatch is used to derive installed performance for static sea-level (design point) and cruise. The emission data of the engine in question are taken from ICAO (1995) and supplied to Piano as emission indices versus fuel flow for ISA static sea-level conditions in the format that they are provided in the database. To calculate the amount of emission of a certain species, Piano uses the Boeing2 emissions method as described in ANCAT/EC (1995). The Boeing2 method is an empirical method that, based on knowledge of the fuel flow and the atmospheric conditions, corrects the emission index data from the ICAO emissions databank for other conditions than given in ICAO.

Having established the characteristics of airframe aerodynamics, engine properties and configuration structure, the range performance based on design altitude is computed. As slightly different engine data compared with Oelkers and Prenzel (2001) is chosen, the MTOM is changed slightly in order to attain the same range as reported in Oelkers and Prenzel (2001).

3.2.2 Optimisation Procedure in Piano and Hurdy-Gurdy

In order to optimize the aircraft configurations in Piano, a target function needs to be defined, i.e. what should be minimized, as well as a set of main design parameters, allowed to vary within some specified design constraints. Piano offers three basic types of target functions for optimization, namely, minimizing MTOW (maximum take-off weight), FW (fuel weight), DOC (direct operating cost) or a weighted combination of two or all of them. In this study, a function weighting the FW (fuel weight) by about two-thirds and the MTOW (maximum take-off weight) by one-third is used as the target function. The design parameters allowed to vary in the optimization procedure are wing area, wing aspect ratio and maximum take-off weight, whereas, amongst others, the engine thrust for static sea level is fixed. The given design parameters for the design range, namely, the take-off field length, landing field length and approach speed are kept within their requirements according to Oelkers and Schulz (2000).

Having optimized the datum configurations, the two aircraft are re-optimised for reduced cruise altitudes in Piano, and required changes in aircraft design are determined. It is assumed that the aircraft stays at a constant altitude during the whole cruise phase, which is slightly in contradiction to real flight procedures. The Mach number is kept constant at 0.8 for all cruise altitudes. More correct would be to keep the

total flight time constant when lowering the flight altitude, but since this complicates the assessment, the Mach number is kept constant instead. This assumption will result in the flight time decreasing to a small extent (<3%) when the cruise altitude is reduced.

3.3 Assumed Technology Level

In this section the assumptions made concerning the technology level are stated. Since future technologies are dealt with, the aircraft and engine data are meant to reflect the technology level of year 2010.

3.3.1 Performance and Emissions Data of Engines

In order to assess properly the performance and emissions data, both the effects of a future technology and the effects of switching to hydrogen need to be addressed. All engine and emission data are based on the data of the V2527-A5 engine. A description of the engine model is given in section 2.2.1. The engine performance at take-off (design point) and at cruise are calculated using the gas turbine performance code TurboMatch (a description of the code is given in Appendix A.3, section A.3.1). In addition, the inherent engine characteristics (fuel flow and thrust versus Mach number and altitude) provided in Piano for different engine types are employed. These characteristics are corrected to match the performance obtained by TurboMatch. Installed performance for the V2527-A5 engine, for burning kerosene and hydrogen, is displayed in Table 3-2.

Table 3-2. Installed performance data for an up-scaled V2527-A5 engine burning kerosene and hydrogen, respectively. The design point is take-off: static sea-level, ISA+10 K, BPR=4.8, OPR=28.5. Cruise: Ma=0.8, altitude=10 668 m, ISA. The thrust requirement at cruise is calculated for an average aircraft flight mass for a design range mission assuming a cabin factor of 65%.

	Kerosene		Hydrogen	
	Take-off	Cruise	Take-off	Cruise
Thrust requirement [kN]	136	20.9	136	22.6
TET [K]	1471	1155	1443	1174
SFC [g/kN s]	9.900	16.826	3.510	6.033
SFC_{KE} [gKE/kN s]	9.900	16.826	9.780	16.805

The only emission data of civil aircraft engines which are available in the public domain, are those reported in the ICAO Engine Exhaust Emissions Data Bank [ICAO, 1995] for certification approval. These data are measurements from engines running at static sea-level ISA conditions in a test-bed according to a specific procedure, namely, the LTO (Landing and Take-off) cycle, meant to reflect a operational cycle around airports. The regulatory data are presented in terms of a parameter that consists of the total mass in grams of a given gaseous pollutant (i.e. CO, UHC and NO_x) emitted during the LTO cycle per kilo Newton of rated thrust. The emission indices of NO_x, UHC and CO of this engine are given in Table 3-3.

Table 3-3. Selection of measured certificate data for the V2527-A5 engine [ICAO, 1995].

Mode	Power Setting [%]	EI of NO_x [g/kg fuel]	EI of UHC [g/kg fuel]	EI of CO [g/kg fuel]
Take-off	100	26.5	0.041	0.53
Climb out	85	22.3	0.041	0.62
Approach	30	8.9	0.061	2.44
Idle	7	4.7	0.105	12.43

When changing to hydrogen two fundamental differences that affect the performance occur: reduced fuel mass flow and changed composition of the gases expanding through the turbine(s) [Boggia and Jackson, 2002]. These two have opposite effects on the engine performance. While the decreased mass flow reduces the thrust, the changed gas composition causes a higher exhaust pressure; thus, if the nozzle is not choked, a higher exhaust velocity. In total these changes are slightly beneficial in terms of performance. The performance gain can be seen in Table 3-1 through lower SFC in terms of kerosene equivalent[7] (SFC_{KE}) for the hydrogen engine for equal TET. At cruise altitude this profit is eliminated due to the higher thrust requirement for the cryoplane. The effects on engine performance of changing to hydrogen fuel were covered more in detail in section 2.2.3.

The present and the future research (at least for the next few decades) concerning civil aircraft engines will focus on reducing both fuel consumption and emissions of NO_x. Since measures to reduce the SFC, such as increasing the OPR and under some circumstances the TET, tend to increase NO_x formation and vice versa, lowering both fuel consumption and NO_x emissions simultaneously is a very challenging task. Various attempts to assess the SFC and NO_x reduction potential are made, both in the context of theoretical studies and as objectives of commercial development projects [EEFAE, 2001; US NASA, 1999; and EU-BRITE/EURAM, 1999]. Depending on the time frame, the potential in SFC reduction for kerosene-fuelled engines is believed to be between 8 and 20%, while the corresponding numbers for NO_x range from 50 to 80%. The references differ slightly, but generally the reductions are compared with technology levels of the mid-1990s. In the present study a SFC improvement of 8% compared with the V2527-A5 engine performance data (Table 3-1) is assumed for both engines to reflect a technology level of 2010. Furthermore, a NO_x emission index improvement of 60% is assumed for the kerosene-fuelled engine. The emission indices of CO and UHC are assumed to be unchanged.

As for the NO_x emissions when burning hydrogen, the discussion and results outlined in section 2.3 suggest that there seem to be the potential to achieve lower NO_x emissions. Employing the concept of micromix hydrogen combustion for an APU, experimental tests have illustrated that the mole fraction of NO_x emissions can be reduced by about 85-86% compared with conventional kerosene-fuelled combustors for full power conditions (see section 2.3.3.2). By means of modelling work it was shown by Dahl and

[7] KE=Kerosene equivalent, i.e. the mass of kerosene that corresponds to the mass of hydrogen of the same energy content.

Suttrop (2001c) that to decrease the SFC by 10%, the NO_x emissions of a hydrogen-fuelled engine would increase by about 8%. Assuming that it would be possible to attain the same reduction in NO_x emission for main engines as was shown by the APU test results, taking into account the SFC improvement as well as converting to the emission index, it would be reasonable to assume a reduction potential of about 84%. This is the number that is applied for all power settings in this study.

To conclude, the emission indices used here, aimed at reflecting a technology level of 2010, are as follows. For the kerosene engine, the NO_x emission index is decreased by 60%, and the CO and UHC emission indices are unchanged compared with the emission indices of the V2527-A5 (Table 3-3). In the hydrogen case the corresponding number for the NO_x emission index is 84%, while the emission indices of UHC and CO are zero (since the fuel does not contain any carbon). Consequently, considering the 2010 technology level, the NO_x emission index for the hydrogen engine is then 60% lower than for the kerosene engine.

The produced amounts of the primary combustion products CO_2 and H_2O are proportional to the fuel consumption. In this study, the used emission indices of kerosene are 3.16 for CO_2 and 1.24 for H_2O. For LH_2 the emission index of H_2O is 3.21 (kerosene equivalent) or 8.94 (absolute, i.e. per kg LH_2).

3.3.2 Aircraft Performance

The airframe technology level of 2010 is governed by assumptions of 7.5% reduction in structure weight and 4% improvement in aerodynamic efficiency compared with the current A321 aircraft [Oelkers and Prenzel, 2001]. By having a lighter and more aerodynamically efficient aircraft to fulfil a flight mission, the total aerodynamic drag in the cruise segment becomes lower, and the net performance is remarkably improved. The reason for achieving a high improvement in performance is due to the often called “leverage effect”, which implies that several parameters combine to improve the performance. For instance, let us consider how reduced drag affects the performance. The reduced drag results in less required thrust, and thereby lower fuel consumption. Less fuel required for a certain range leads to a lighter take-off weight, due to both a lighter fuel weight and a lighter structure. The latter is a consequence of a lighter structure loading. In turn, the lighter aircraft requires even less fuel. Another effect is that a smaller engine may be used.

3.4 Global Warming Potential (GWP) Model

Each pollutant produced by aviation has a different impact on the atmosphere, depending on the quantity emitted, its chemical and light-absorption properties, and on what altitude it is discharged. In order to allow a simple assessment of the global impact, in terms of global warming, from the emissions discharged on a certain mission, a simple parametric model is derived following the methodology proposed by Klug et al. (1996) and Klug (2001a), taking into account model results and recommendations from IPCC (1999). The methodology is explained in Appendix B. This simplified treatment avoids the necessity of running a sophisticated 3-D climate model with its

formidable resources; it rather tries to comprise the influence of the numerous chemical, physical, and dynamic interactions in a parametric sense.

The model provides layer-specific values of the global warming potential (GWP), which is a measure of how pollutants contribute to the global greenhouse effect relative to the effect of CO_2 [IPCC, 1990]. The original GWP concept (which is largely adopted here) relates the effect of an instantaneous pulse emission of a given tracer to a corresponding pulse emission of CO_2, in terms of mass (see Appendix B). As the lifetime of the tested tracer is different from that of CO_2, a time horizon has to be defined to yield a unique quantitative comparison. The time horizon is somewhat arbitrary, but a value of 100 years has been established as a standard. Fuglestvedt et al. (1996) provided a critical review of the use of GWP as a climate impact measure for air pollutants that are not homogeneously mixed throughout the troposphere and that are acting indirectly through their secondary products. While there are indeed several caveats, an accepted alternative measure suited for this kind of study has not yet been proposed.

The application of the GWP concept used here is directed towards the effect of aircraft H_2O and NO_x emissions (Figure 3-3). Water vapour causes a direct radiative impact on the climate system, whereas the influence of NO_x emissions is indirect through its chemical impact on the atmospheric ozone and methane concentration: at altitudes below about 15 km, NO_x emissions cause an increase of the upper tropospheric ozone, thus contributing to the greenhouse effect, while at the same time increasing the atmospheric OH concentration, which decreases the CH_4 (and CO) lifetime [e.g. Isaksen, 2001]. The latter lowers the atmospheric CH_4 concentration, and thereby reduces the greenhouse effect. Sensitive parameters to describe these effects in the parametric model, like (ozone) production rates, chemical lifetime, atmospheric mixing times, and altitude specific radiative forcing of the species in question are chosen to represent the situation in summer atmosphere at mid-latitudes. As to be expected from such a highly parameterised model, the uncertainties are considerable, in particular with respect to the effect of NO_x emissions.

For each pollutant, the global warming potential can be estimated by multiplying the emission value in kilograms by the measure of that pollutant for each altitude. The total GWP number for a certain mission is then the sum of the individual GWPs due to CO_2, H_2O and NO_x, emitted at different altitudes over the whole mission. Total GWP calculated in this way indicates the mass of CO_2 which would produce the same effect upon the heat balance of the Earth as the various substances actually emitted do together, taking a total period of 100 years into account.

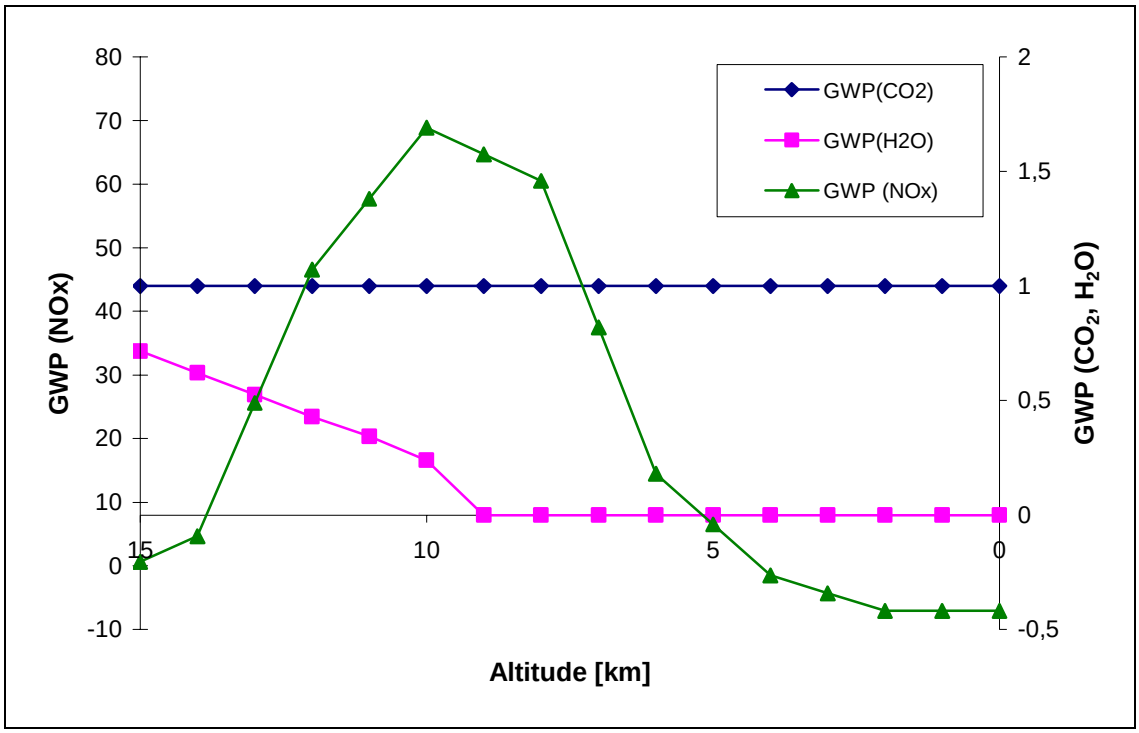

Figure 3-3. GWP numbers per kilogram pollutant versus altitude.

According to Figure 3-3, per kilogram pollutant, NO_x has the greatest impact on global warming. For altitudes below 4 km it has a negative global warming effect (cooling the Earth), and as the altitude increases its impact increases until about at 10 km in altitude, where it peaks and starts to decrease. The reason for this behaviour lies in the complex interactions among factors such as the lifetime of the NO_x, ozone (O_3) and methane in the atmosphere, ozone and methane production/destruction rates and the magnitude of the Earth's temperature changes due to a specific change in ozone or methane concentration at a certain altitude (see Appendix B).

The global warming effect of H_2O from aircraft cruising in the troposphere is negligibly small compared to that of CO_2, hence it is here assumed to be zero below 10 km. Above 10 km it has a small impact on global warming, but it increases with altitude (see Appendix B). This is in agreement with conclusions drawn in previous studies [IPCC, 1999; and Morris et al., 2003] suggesting that the impact of water vapour emissions from subsonic aviation on the radiative balance is negligibly small.

The GWP model has major drawbacks for application on aircraft emissions. The main drawback lies in its unsuitability as a means of characterising short-lived emissions, e.g. NO_x, the effects of which show strong regional and seasonal variations [Air Travel - Greener by Design, 2001; and IPCC, 1999]. Another drawback is that the model does not take into account any possible contrail formation arising from the emitted H_2O. However, it appears that partial compensation occurs between increasing contrail coverage from cryoplane traffic (due to higher H_2O emissions) and decreasing optical thickness of cryoplane contrails (due to fewer but larger ice particles, as there are less condensation nuclei present in the exhaust). The net result of contrail formation on global warming may, therefore, be in the same order of magnitude for both cryoplanes

and conventional aircraft. According to Sausen and Ponater (2002), switching from conventional aircraft to cryoplanes is likely to reduce the global average aircraft climate impact due to contrails by roughly 20%. This may imply that the conclusions of this study would not fundamentally change, if contrail effects had been included. As for many other aspects of aircraft related climate impact, all matters in this issue are not yet clarified.

In the end, in spite of its limitations and simplified approach, this model is believed to be an appropriate tool for the purposes of this study.

3.5 Results

The object of the simulations is principally to compare two similar aircraft – one conventional and one LH_2 fuelled – able to fulfil the same requirements of transportation, from a performance point of view. Moreover, both aircraft are re-optimised for reduced cruise altitudes, and differences in performance and emissions are determined. Data for the reduced cruise altitudes are compared with data for the datum cruise altitudes, and differences in changes between the two aircraft are computed.

Before the aircraft are re-designed, an important difference between the two aircraft in terms of energy consumption needs to be highlighted. If operation of both aircraft is simulated under datum conditions, i.e. a design range of 4000 nm (7408 km), assuming a cabin factor of 100% and a maximum cruise altitude of 39 000 ft (11.9 km), the fuel consumption expressed in kerosene equivalent is about 10% higher for the cryoplane than for the conventional, in spite of the fact that the MTOW is slightly less (by about 2%) for the former. The explanation for this is partly that the zero lift drag is higher for the cryoplane (3.5% penalty in drag polar compared with the equivalent conventional configuration), due to a less efficient aerodynamic design, and partly that the average flight weight is higher, owing to a higher structure weight for the cryoplane than for the conventional airplane. A higher structure weight is a consequence of increased geometric sizes and the additional facilities imposed by the handling and storing of a bulky cryogenic fuel.

All results in the following sections refer to fuel consumption and emissions of climb, cruise and descent for a range of 2500 nm with a cabin factor of 65%. For practical reasons, the fuel consumption and emissions related to operation below the take-off screen height (35 ft) are not included. This limitation is not expected to affect the qualitative results and conclusions.

3.5.1 Effect of Reduced Cruise Altitude on Aircraft Characteristics, Fuel Burn and Emissions

In order to get an understanding of how the aircraft configurations, fuel burn and emissions change due to cruising at an altitude lower than the optimum (in terms of energy consumption), both aircraft are optimised for the datum as well as for three lower cruise altitudes. In Figure 3-4 the changes in aircraft characteristics, and in Figure 3-5 the changes in fuel burn and emissions, are presented as functions of flight levels, for both the conventional airplane and the cryoplane.

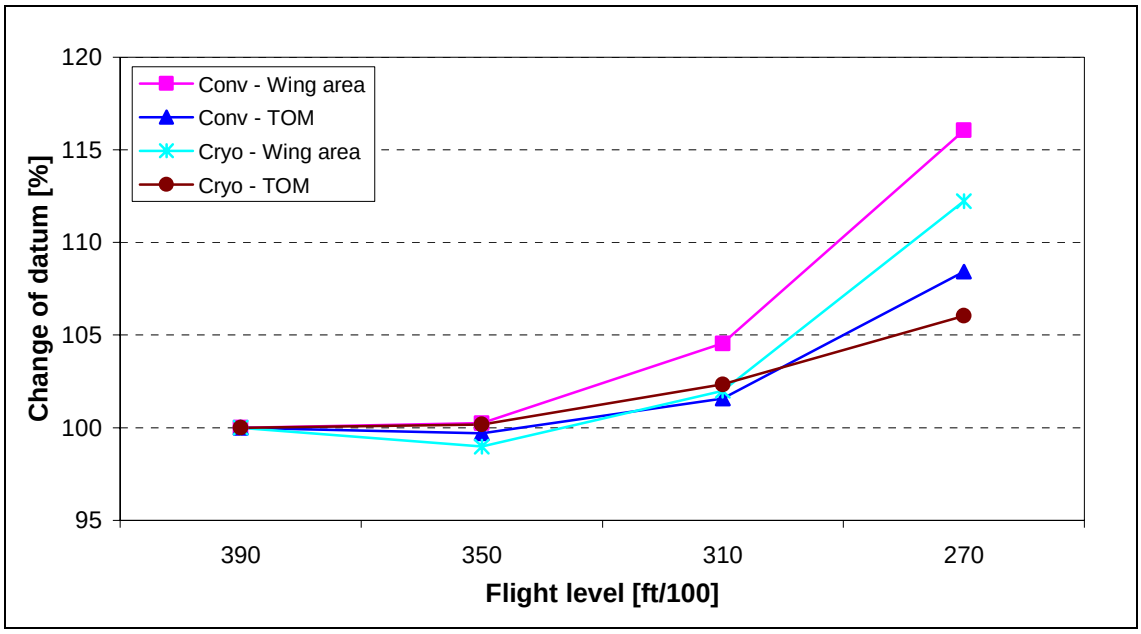

Figure 3-4. Effect of cruise altitude on aircraft characteristics.

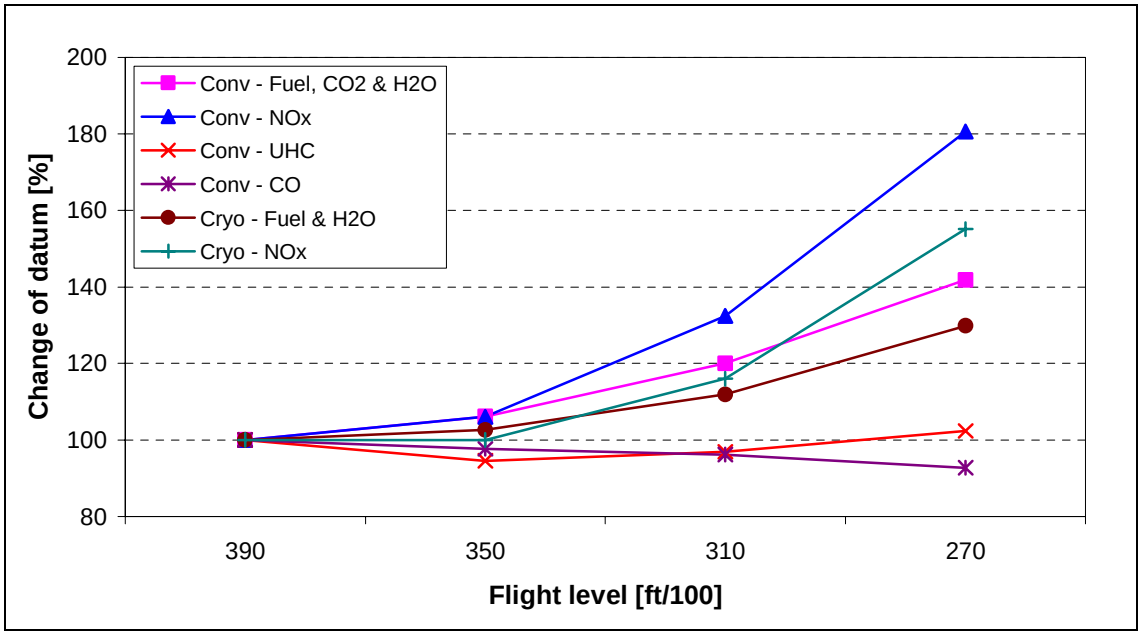

Figure 3-5. Effect of cruise altitude on fuel burn and emissions.

It may be observed in Figure 3-4 that as the cruise altitude is reduced, the wing area increases for both the airplanes, while the wing span is constant or slightly decreased. In total, the take-off mass increases to a smaller extent, which can be explained as follows. When cruising at an altitude different from the optimum, in terms of minimum energy consumption, the required fuel flow increases in order to overcome the increased drag. Increased fuel flow during the cruise phase, which represents the main share of the flight, results in an increased fuel burn for the mission (see Figure 3-5). As a consequence of the increased fuel burn, the aircraft take-off mass increases, due to both

the increased fuel weight required for the mission and the increased structural weight, including the need for bigger lifting surfaces as the take-off weight is increased. Hence, when cruising at reduced altitude, the aircraft become heavier and the wing area increases.

The effect of increased wing area, and to a smaller extent also the take-off mass, is more emphasized for the conventional aircraft than for the cryoplane. Since liquid hydrogen has a lower energy content per volume compared with kerosene (four times lower), it is thereby expected to have a greater impact on the configuration for the same amount of extra energy required, this result might at a first sight appear to be slightly surprising. When the cruise altitude is reduced and the amount of fuel required for the mission increases, larger tank volumes are demanded. As a consequence of the conventional aircraft which stores its fuel in the wings, the wing size becomes the critical point, in order to carry the additional fuel required for the mission. This implies that the wings need to be enlarged more than required for performance needs (e.g. achieving the required take-off performance).

The cryoplane, on the contrary, which stores its fuel in the fuselage, is affected through a longer fuselage when mission fuel burn is increased. Under the circumstances studied here, the results suggest that a larger performance penalty is indicated by storing the additional fuel in the wings rather than in the fuselage. It is expected that the impact on configuration and fuel burn for the conventional aircraft would be less if some of the additional fuel required when lowering the cruise altitude is stored in the fuselage, thus avoiding the wing size being the critical point. This, however, would imply that the conventional aircraft would no longer be conventional, but a novel aircraft configuration. Furthermore, preceding investigations performed by the author (of this thesis) in collaboration with colleagues, suggest that the impact on the aircraft configuration becomes larger for the cryoplane than for the conventional aircraft if part of the fuel is stored in the wings of the cryoplane. Obviously, the matter of where to store the fuel seems to make a large difference on mission performance when altering the cruise altitude.

According to Figure 3-5, the fuel consumption increases when the cruise altitude is reduced, and since the emissions of CO_2 and H_2O are proportional to the fuel consumption, they also increase by the same percentages. The UHC, CO and NO_x emissions are not, as CO_2 and H_2O, proportional to the fuel consumption, but are dependent on the specific conditions in the engine combustion chamber, such as temperature, pressure, equivalence ratio (a measure of the fuel flow related to the air flow in the combustor) and the physical design of the combustor (see section 2.3). Thermal NO is formed by the oxidation of atmospheric nitrogen in high-temperature regions of the flame and in the postflame gases, whereas UHC and CO are formed in low temperature regions, due to incomplete combustion [e.g. Lefebvre, 1998].

When the cruise altitude is reduced, the power setting during cruise must, if the cruising velocity should be kept constant, be increased to overcome the increasing drag. An increased power setting implies a higher combustion temperature, which raises the emission index of NO_x and diminishes the emission indices of UHC and CO. In addition, since the power setting is increased, the fuel flow is also increased, affecting

all emissions detrimentally. As for CO, the effect of the lowered emission index is larger than the effect of increased fuel flow (see Figure 3-5), causing reduced emissions when the cruise altitude is lowered. For UHC, the effect of increased fuel flow dominates for the lower altitudes. Generally, the emissions of NO_x increase more than the fuel consumption, and the largest increase occurs for the conventional aircraft.

3.5.2 Effect of Reduced Cruise Altitude on Global Warming Potential (GWP)

By employing the described GWP model (section 3.4), a measure of GWP due to CO_2, H_2O, NO_x and the sum of these can be estimated for an aircraft performing a flight mission. Concerning the conventional aircraft, CO_2 is the major contributor to global warming, with H_2O and NO_x being of similar magnitudes which are essentially lower than that of CO_2, see Figure 3-6. As the cruise altitude is reduced, the effect of NO_x increases slightly, whereas the effect of H_2O decreases to become zero at FL 270. The NO_x effect of altered altitude is sensitively dependent on the shape of the GWP curve (Figure 3-3), particularly the locus of the peak effect. Due to the large uncertainties associated with assessing the global warming effect using this simplified approach, it is not possible to draw any confident conclusions on the environmental effects of NO_x emissions discharged at different altitudes.

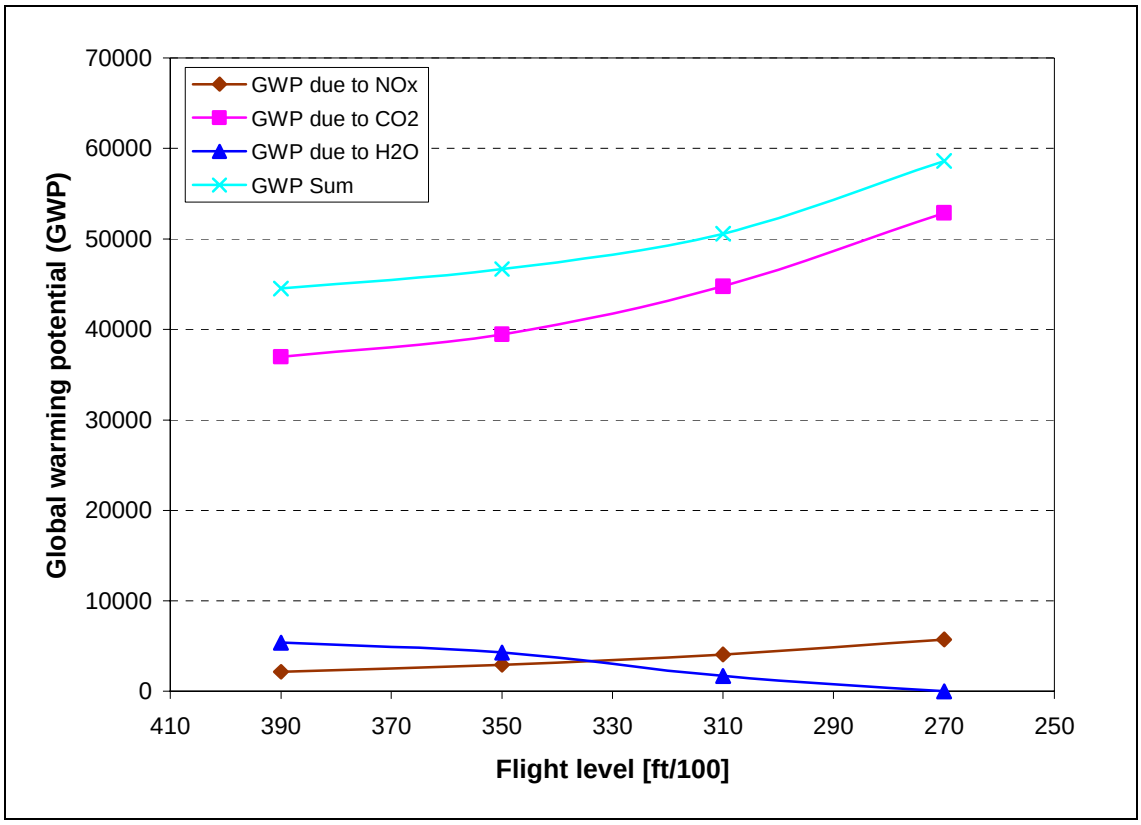

Figure 3-6. Effect of cruise altitude on GWP for the conventional aircraft.

As the effect of CO_2 on global warming is independent of the discharging altitude and since the emissions of CO_2 increase by decreasing altitude, the influence on global warming increases by decreasing cruise altitude. The net result, i.e. the sum of the

contributions from CO_2, H_2O and NO_x (upper curve in Figure 3-6), is a GWP curve mostly influenced by the effect of CO_2, which continuously increases as the cruising altitude is decreased. Hence, these results suggest that there seems to be no global warming benefit from lowering the cruise altitude for a conventional medium-range aircraft.

For the cryoplane the situation is different, see Figure 3-7. As the fuel contains no carbon, the CO_2 curve vanishes. The shape of the NO_x curve is similar to that of the conventional aircraft, but the magnitude of the GWP values is smaller, as the cryoplane is assumed to emit less NO_x. As the cryoplane discharges significantly more water vapour (2.6 times more if the same energy consumption is assumed), the H_2O effect of this aircraft is essentially greater than for the conventional aircraft. In contrast to the conventional aircraft, the H_2O effect is totally dominating for the highest flight levels, leading to a continuously decreasing contribution to global warming with decreasing cruise altitude (at least for the considered flight levels). In this case the effect of a decreasing GWP effect with decreasing flight altitude overcompensates the effect of increasing H_2O emissions.

In Figure 3-8 the "GWP sum" curves for the two aircraft are shown in the same graph. The results suggest that the global warming effect of cryoplanes is considerably less for all cruise altitudes, becoming smaller as the cruise altitude is reduced. For the datum cruise altitude (11.9 km), the contribution is slightly less than 40% of that of the conventional aircraft, and for flight level 270 (8.2 km) the contribution has decreased to a few percent compared with the conventional aircraft cruising at the datum level.

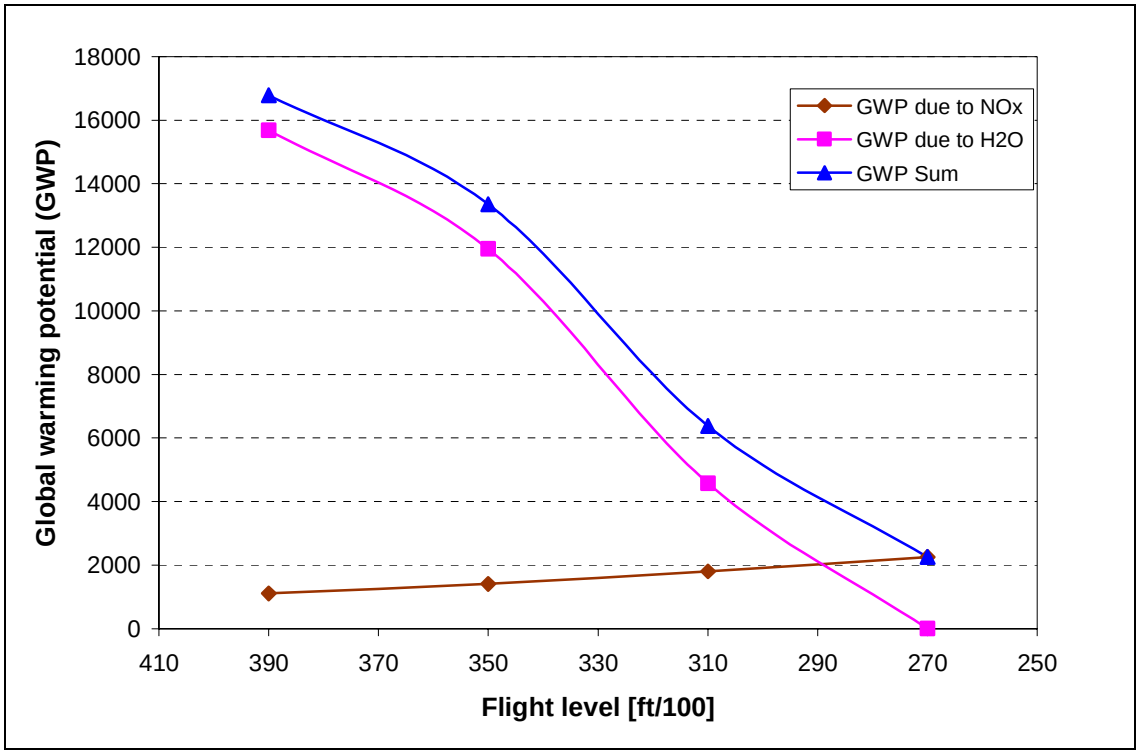

Figure 3-7. Effect on cruise altitude on GWP for the cryoplane.

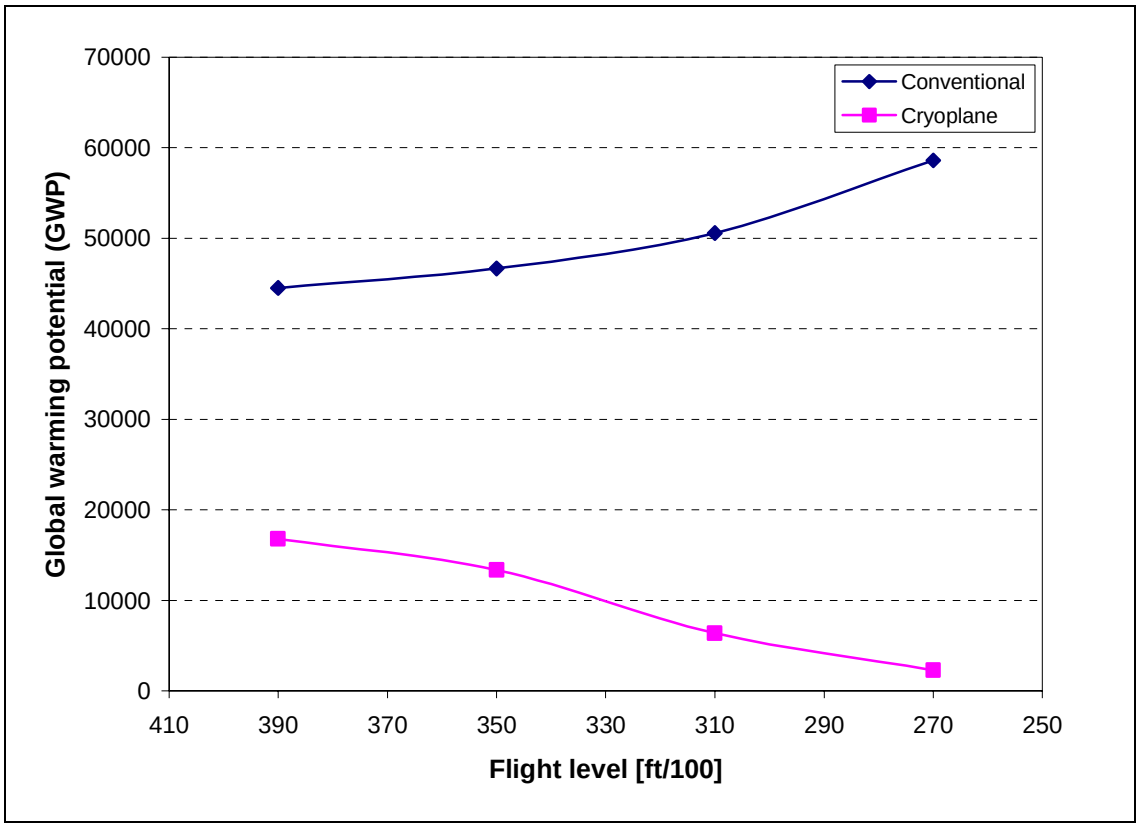

Figure 3-8. Effect of cruise altitude on GWP for both aircraft.

Finding the optimum cruise altitude from the environmental point of view for the cryoplane is in this case a trade-off between, on the one hand, reduced global warming, and on the other hand, increased operational costs due to increased fuel consumption and increased investment due to a heavier construction. Thus, cruising below the optimum cruise altitude to reduce the global warming, will always be at the expense of increased weight and fuel consumption. The important issue is to find a cruising altitude, and its corresponding configuration, that allows for a significant reduction in the GWP, with a reasonable penalty in fuel consumption and structure weight. In order to find the optimum, the change in GWP is plotted versus the change in fuel burn (Figure 3-9) and MTOM (Figure 3-10), respectively, as the cruise altitude is reduced.

As for the conventional aircraft, as far as this study is concerned, there is no obvious reason for lowering the flight altitude, since it appears that the fuel consumption and MTOW would increase for no reduction in global warming. For the cryoplane, on the other hand, the possible reduction in global warming is limited only by the amount of increase in take-off mass and fuel consumption that is accepted. If the flight level is reduced to FL 310 (9.4 km), the contribution to global warming is reduced by about 60% for a penalty of about 2% in TOM and 12% in total fuel consumption. Furthermore, there is a tendency towards higher penalty in fuel consumption the lower the reduction is applied, i.e. the penalty in fuel consumption is higher when reducing from FL 310 to 270 than from FL 390 to 350. It is thus questionable if the potential of reducing the GWP further by lowering the flight altitude below FL 310 is justified by the increased cost for manufacturing and operating the aircraft.

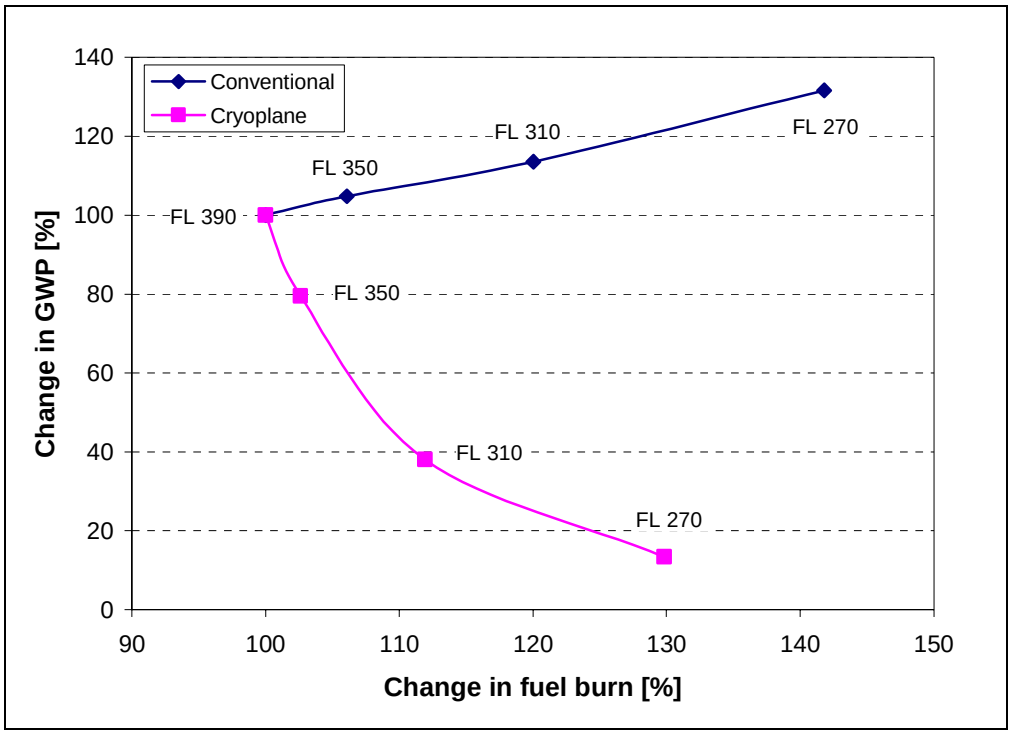

Figure 3-9. Change in GWP versus change in fuel burn for reduced cruise altitude.

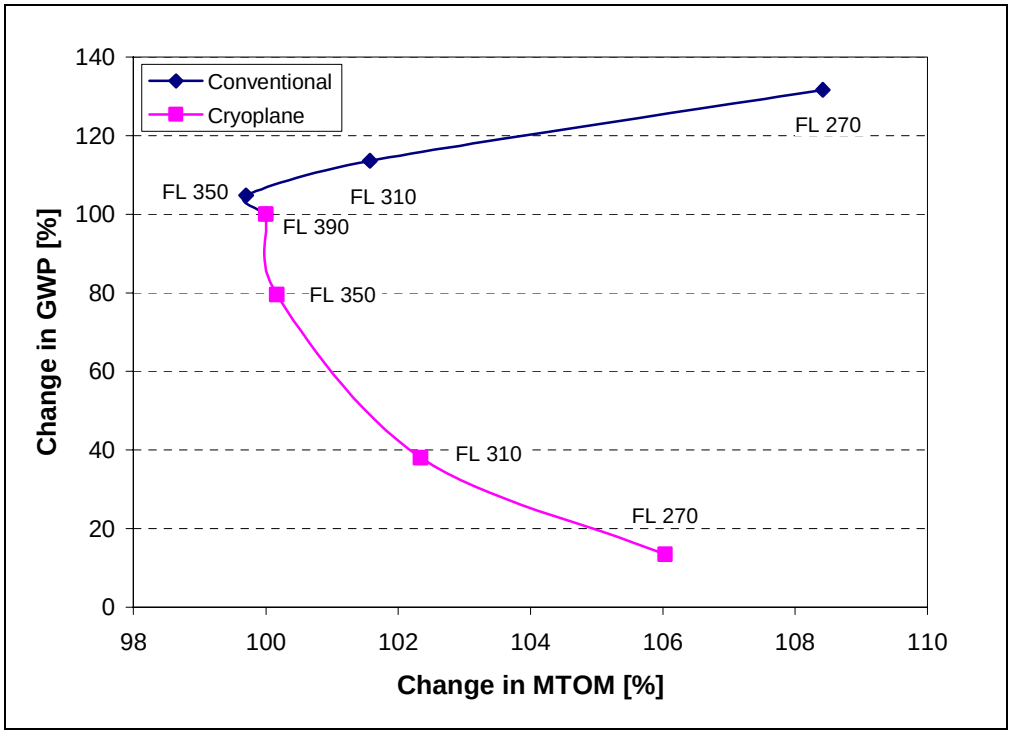

Figure 3-10. Change in GWP versus change in MTOM for reduced cruise altitude.

For comparison purposes the absolute figures of GWP and fuel burn are also plotted (Figure 3-11). The figure shows that the lower the cruise altitude, the higher the cost in fuel burn for each equivalent GWP saved, which also was indicated in previous figures.

If the flight level is, as discussed above, reduced to FL 310, 6.4 equivalent GWP is saved for every kilogram of equivalent fuel spent for the cryoplane.

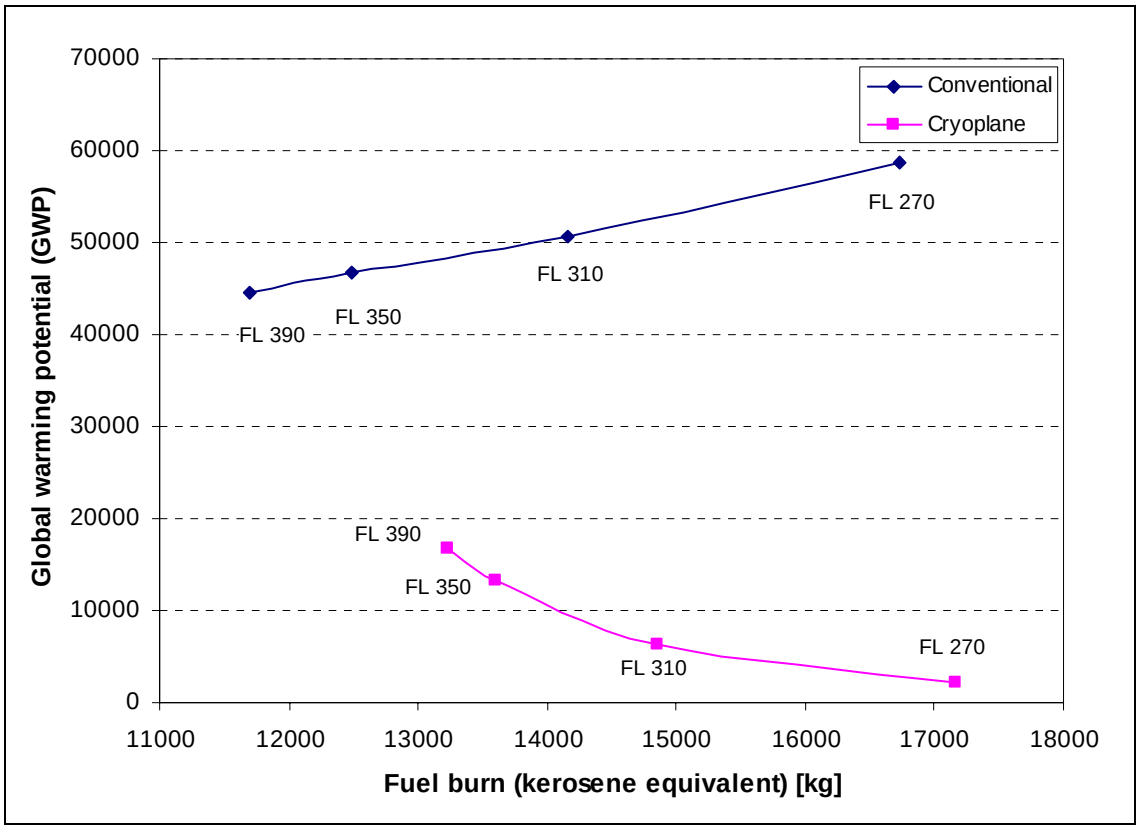

Figure 3-11. GWP versus fuel burn for reduced cruise altitude.

3.6 Conclusions and Discussion

In this section indicative results are presented, showing how changes in aircraft fuel technology and flight altitude may influence the aircraft configuration as well as the environmental impact. The study is aimed at stimulating further research work on flight altitude optimisation to reduce aircraft environmental impact. From the results obtained it is difficult to draw any confident conclusions regarding whether there are any significant gains in terms of environmental impact by lowering the cruise altitude. The main reason is that the results are highly dependent on the assumptions (e.g. the geographical location under consideration, and the type of model used to derive the figures) made in the GWP model, which is derived by comprising the influence of the numerous chemical, physical, and dynamic interactions in a parametric sense (see Appendix B). The relative influence of NO_x emissions compared with CO_2 and the altitude where the impact of NO_x emissions peaks are factors that highly influence the result. Conclusions concerning the effects on aircraft characteristics, fuel consumption and pollutant emissions when reducing the flight altitude, on the other hand, are much more reliable.

When comparing two equally performing medium-range aircraft – one powered by kerosene and one powered by LH_2 – the energy consumption is inevitably higher (in

this case by about 10%) for the cryoplane. This is due to the higher structural weight and the higher drag for the cryoplane configuration. Reduced cruise altitude has smaller impact on the cryoplane than on the corresponding conventional aircraft, in terms of physical size, fuel burn and emissions. This means that, compared with the datum case, these quantities will increase more in percentages for the conventional airplane than for the cryoplane, when the cruise altitude is lowered. The main reason for this is a different fuel storage configuration.

In spite of the uncertainty of the results concerning the change in environmental impact of lowering the cruise altitude, it might be reasonable to conclude that there seems to be a substantial qualitative difference between the conventional aircraft and the cryoplane. The results suggest that the contribution to global warming is considerably lower from the cryoplane than from conventional aircraft, particularly if the flight altitude for the cryoplane is reduced. That the effect upon the radiative balance of Earth is smaller from cryoplanes than from conventional aircraft is also suggested by Ponater et al. (2004). Ponater et al. (2004) cover the effects of changed CO_2 emissions, NO_x emissions and a change in contrail radiative impact of gradually introducing cryoplanes into the global air traffic according to different transition scenarios. According to their best estimate, a relative reduction of aircraft induced radiative forcing in 2050 by between 16% and 29% (depending on the speed of transition) could be achieved if cryoplanes were introduced. Due to inherent scientific uncertainties this range widens to between 14% and 40%.

Whereas the contribution to global warming of the conventional aircraft tends to increase, it seems to decrease essentially for the cryoplane when lowering the flight altitude. Provided that an increase in fuel consumption in the order of 10% and an increase in TOM of a few percent are accepted, the results suggest that cryoplanes should cruise at an altitude of about 2-3 km below where conventional aircraft cruise today. At this reduced flight level, the contribution to global warming from the cryoplane is slightly less than about 15% of that of the conventional aircraft cruising at the datum level. That the difference in environmental impact between the conventional aircraft and the cryoplane is, according to these results, larger than obtained by Ponater et al. (2004) is to be expected, since the results obtained here reflect only two different aircraft, whereas their results are obtained for different aircraft fleets consisting of both cryoplanes and conventional aircraft. In addition to the aspects considered here, reducing the flight altitude will help to avoid the formation of contrails [Williams et al., 2002]. Inevitably, this change in cruise altitude causes increased aircraft investments and operating costs.

In order to reduce the cruising altitude, air traffic management aspects need careful attention before such a measure may be realised. Williams et al. (2002) studied the option of limiting the cruise altitude as a means to reduce the formation of contrails. Their results indicate that this strategy could provide a net benefit to the climate, despite the associated increase in CO_2 emission. According to their analysis, the most likely operational obstacles to such a scheme are the implications for controller workload, hence a reconfiguration of the air space would be required to mitigate the impacts.

4 DESIGN OF HYDROGEN-FUELLED AERO GAS TURBINES FOR LOW ENVIRONMENTAL IMPACT

4.1 Introduction

In chapter 2 the main effects on aero gas turbines when changing to hydrogen fuel, with emphasis on environmental issues, were covered. The potential of lowering the environmental impact and the technical feasibility of changing fuel was assessed by investigating the effects on pollutant emissions, performance and design. In this section this work is extended by looking at engine design for low environmental impact. In this context, the fuel consumption and pollutant emissions (water vapour and oxides of nitrogen) for complete flight missions are considered.

The water vapour is proportional to the fuel consumption, whereas the NO_x emissions are dependent on the combustor inlet conditions and a number of combustion chamber characteristics. In addition, reducing fuel burn and NO_x emissions might be in opposition to each other, implying that an engine design measure to reduce NO_x might give rise to the fuel burn and vice versa. Whilst the wish to lower the fuel consumption is mainly driven by the objective of delivering products that promise low direct operating cost (and recently also for conforming to future environmental constraints on aviation), it is important to reduce the H_2O and NO_x emissions due to environmental concerns of their impact on the atmosphere and climate. The environmental effects of H_2O and NO_x emissions are discussed in sections 1.2.2, 3.4 and Appendix B.

Whether engines should be designed for low mission fuel consumption or for low mission NO_x emissions to minimise the environmental impact is not obvious. Therefore, both options are covered. In practice, of course, a combination of these two aims could be desired. In order to study the potential of lowering either fuel burn and mission H_2O, or mission NO_x emissions, a number of alternative engine cycles are selected, i.e. cycles featuring different combinations of COT, OPR and BPR. The amount of H_2O emissions is known directly from the fuel consumption (since the H_2O emissions are proportional to the fuel burn), while the NO_x emissions are calculated using a semi-empirical correlation. Rather than finding the optimum engine cycle for a specific objective, the aim is to investigate a number of promising cycles, to provide some guidance on how to design hydrogen-fuelled aero engines for medium-range aircraft either for minimum mission fuel consumption or mission NO_x emissions.

This chapter is introduced (section 4.2) by a derivation of a semi-empirical correlation valid for the micromix combustor concept suggested in section 2.3.3. In order to study the effects on flight mission emissions and fuel consumption of varied engine cycle parameters (COT, OPR and BPR) parametrically, a computer program is developed. In section 4.3 the methodology which the computer program is based upon is outlined. The principles for re-sizing the aircraft and the engines owing to a changed engine performance are explained. Furthermore, the physical principles and equations which

the performance estimations for the different flight phases are based upon are described. In section 4.4 the datum engine cycle is described, and a number of promising alternative engine cycle concepts, either to lower the mission fuel consumption and H_2O emissions or the mission NO_x emissions, are suggested. Evaluations of the alternative engine concepts for flight missions are described in section 4.5, and the results of the study are concluded and discussed in section 4.6.

4.2 Estimation of the NO_x Emissions for the Micromix Combustor Using a Semi-Empirical Correlation

Following the discussion in section 2.3.3, the concept of micromix combustion is suggested as a promising concept for burning hydrogen, the main reason being that this concept enables the exploitation of the favourable properties with respect to low NO_x emissions when burning hydrogen without sacrificing the safety and combustor reliability. In order to estimate the emissions of NO_x at a specific operating condition, a semi-empirical correlation valid for the micromix combustor concept is derived, following the methodology suggested by Dahl and Suttrop (2001c) (section 4.2.1). An evaluation of the correlation is given in section 4.2.2. Based on this correlation methodology, additional routines that enable the calculation of the NO_x emissions are developed and implemented in the hydrogen version of TurboMatch. A brief description of the TurboMatch code and its supplementary routines are given in Appendix A.3, section A.3.1.

4.2.1 Derivation of a NO_x Emission Correlation

Theoretical estimation of the NO_x emissions of a certain gas turbine combustor with accuracy is a very difficult task, comprising several uncertainties. As for combustion chambers using kerosene, considerable efforts have been made to predict the pollutant emissions, particularly NO_x, using 3-D models, and empirical and semi-empirical correlations [e.g. Lefebvre, 1998; Lefebvre, 1995; Rizk and Mongia, 1994; Sturgess et al., 1993; and Heywood and Mikus, 1973]. Also various experimental results are available, including measurements of the pollutant emissions [e.g. Segalman et al., 1993]. On the contrary, only a few aero gas turbines used for propulsion have been converted to hydrogen use, and none of these have been evaluated with respect to NO_x emissions (see section 1.5). Therefore, it is an even more difficult task to predict the NO_x emissions which may be expected from future hydrogen-operated aero gas turbines. The only available NO_x emissions data (at least to the author's knowledge) obtained from a hydrogen-fuelled engine are those of the Honeywell APU GTCP 36-300, as outlined in section 2.3.3. However, compared to main engines this engine is operated under relatively low temperature and pressure conditions.

To estimate the NO_x emissions of future hydrogen-powered engines in this thesis, the measured emissions data of the APU engine are extrapolated for higher combustor inlet pressures and temperatures by appropriate modelling based on similarity considerations. The methodology was proposed within the EC-sponsored project CRYOPLANE, aimed at assessing the NO_X emission level of future high-pressure ratio aircraft engines employing micromix combustors compared with those of kerosene-fuelled engines [Dahl and Suttrop, 2001c]. Using this methodology, it is assumed that the hydrogen

engine uses the same combustor configuration as the APU engine, namely, a micromix combustor of the third generation (see section 2.3.3.2). The correlation is therefore not valid for any other combustor types. The micromix combustor concept is considered to be the most promising diffusive combustion configuration, with respect to NO_x reduction, safety of operation and exit temperature pattern [Dahl and Suttrop, 2001c].

Factors that normally have an essential influence on the NO_x formation in diffusive systems, such as the structural combustor design, fuel-air mixing conditions and the uniformity of the cross sectional fuel distribution, are not taken into account since the combustor type is unchanged. In the similarity consideration the total relative pressure loss is assumed to be constant, i.e. the total relative pressure loss is the same for the APU and the main engine under consideration, and its influence on the NO_x formation is not regarded.

As for pressure losses for gas turbine combustors, there are two different dimensionless parameters that are usually regarded. These are the overall pressure loss, which is the ratio of the total pressure drop across the combustor to the inlet total pressure, and the pressure-loss factor, which is defined as the ratio of the total pressure loss across the combustor to the reference dynamic pressure, q_{ref} [Lefebvre, 1998]. The pressure-loss factor denotes the flow resistance introduced into the air stream between the compressor outlet and the turbine inlet. Whereas the overall pressure loss depends on the operation condition, the pressure-loss factor, which represents the sum of the pressure loss in the diffuser and across the liner, is a fixed property of the combustion chamber. In order to attain the same relative total pressure loss for the main engine as for the APU, the aerodynamic and mixing characteristics need to be preserved. This implies that the combustor of the main engine needs to be designed such that the pressure-loss factor, as well as the combustor dimensionless mass flow, is unchanged compared with the APU.

From NO_x emissions data obtained from a combustor rig test at an atmospheric pressure level [Ziemann et el., 1998a] and from test runs of the GTCP 36-300 under different engine load conditions [Dahl and Suttrop, 2000; Schelzig and Bleimund, 2000; and Breit, 1999], it was concluded that the NO_x formation depends on the pressure level, the equivalence ratio, ϕ, and the total relative pressure loss, $\Delta P_{t3\text{-}4}/P_3$. The equivalence ratio represents the average combustion temperature, which for a given mass flow, influences both the velocity (or residence time) and the reaction rate in the chemical reaction zone. The relative total pressure loss, which for a given combustor configuration is a function of the combustor air mass flow, represents a measure of the energy available for enhancement of the turbulent mixing rate in the diffusive reaction zone.

In this study, thermal gas phase formation of nitric oxide, only, is assumed to be representative for the total NO_x formation. All NO formation principles are described in section 2.3.1. Since neither carbon nor nitrogen is present in the fuel, both the prompt NO and the fuel NO can be disregarded. If the study is confined to high engine operating conditions, at which most of the NO is formed, the nitrous mechanism is less important and may be omitted [Dahl and Suttrop, 2001c]. For this study it is assumed that a large amount of the NO_x is formed in regions of the diffusion flames where the reactions proceed under stoichiometric or near stoichiometric conditions. Moreover, since normally almost all NO_x formed in a gas turbine combustor is made up of NO and

since NO_2 is formed by further reactions, NO is assumed to be representative of the total amount of NO_x emitted. According to Lefebvre (1998) the thermal NO formation is generally considered to be predicted by the extended Zeldovich mechanism (see section 2.3.1). The reverse reaction resulting in conversion of NO back into N_2 and O_2 is relatively slow in gas turbines; hence, the NO once produced does not decrease in concentration at an appreciable rate by cooling. The first reaction (equation (2-9)) is significantly slower than the following two reactions, thereby the NO formation is controlled by the first reaction and the NO formation rate can approximately be estimated by [Dahl and Suttrop, 2001c]:

$$\frac{d[NO]}{dt} = 2 \cdot k_1 \cdot [N_2] \cdot [O] \tag{4-1}$$

where the concentrations, [i], are given in mole/cm^3 and the rate factor, k_1, is determined by [Baulch et al., 1970]:

$$k_1 = 1.36 \cdot 10^{14} \frac{cm^3}{mole \cdot s} \cdot e^{\frac{-37700\,K}{T_{st}}} \tag{4-2}$$

where T_{st} is the prevailing stoichiometric flame temperature in the reaction zone of the diffusive flames. During the combustor tests, the mole fractions of species i, ψ_i, are measured rather than the concentrations, [i]. Converting equation (4-1) to mole fractions and inserting equation (4-2), introducing a dependence on the temperature, T_{st}, and the pressure, P, the formation rate is estimated by:

$$\frac{d\psi_{NO}}{dt} = 2.72 \cdot 10^{14} \frac{cm^3}{mole \cdot s} \cdot e^{\frac{-37700\,K}{T_{st}}} \cdot \psi_{N2} \cdot \psi_O \cdot \frac{P}{R_u \cdot T_{st}} \tag{4-3}$$

where R_u denotes the universal gas constant. By assuming that the mole fractions of N_2 and O remain approximately constant in the considered reaction zone, and combining these and all other constant quantities to one single constant, C, equation (4-3) may be integrated to obtain:

$$\psi_{NO} = C \cdot e^{\frac{-37700\,K}{T_{st}}} \cdot \frac{P}{T_{st}} \cdot t_R \tag{4-4}$$

where t_R is the available reaction time in the reaction zone of the diffusion flames. The reaction time depends on the size and dimensions of the considered diffusion flames. For the micromix diffusion hydrogen combustion principle, typically featuring a multitude of hundreds of miniaturized flamelets, the time in the reaction zone is expected to be much less than for the conventional diffusion combustion principle featuring a few large flames. The reaction time also depends on the prevailing flow velocities and all quantities that influence the molecular and turbulent mixing transport characteristics in the diffusion flame, such as the density and viscosity of the gas mixture in the reaction time (determined by the pressure and temperature), and the energy that is introduced by dissipation into the turbulent transport mechanism

(determined by the total relative pressure loss, $\Delta P_{t3\text{-}4}/P_3$). Since the pressure and temperature levels are higher in the main engine compared with the APU, the transport characteristics might differ slightly, and hence also the reaction time might differ slightly. For the preliminary NO_x assessment conducted here, these possible deviations are neglected.

Introducing the equivalence ratio (for reasons discussed earlier in this section) as a variable, considering emission the index rather than mole fractions and extending the consideration to NO_x, the NO_x production of a specific combustor design may approximately be determined by [Dahl and Suttrop, 2001c]:

$$EI_{NOx} = EI_{NOx}^{*} \cdot \left(\frac{P}{P^{*}}\right)^{n} \cdot \left(\frac{\phi}{\phi^{*}}\right)^{m} \cdot \left(\frac{T_{st}^{*}}{T_{st}}\right) \cdot \frac{e^{\frac{-37700\ K}{T_{st}^{*}}}}{e^{\frac{-37700\ K}{T_{st}}}} \qquad (4\text{-}5)$$

where P and T_{st} are the prevailing conditions of pressure and temperature in the reaction zone. The symbol "*" denotes nominal measured quantities known from experimental work [Dahl and Suttrop, 2000; Schelzig and Bleimund, 2000; and Breit, 1999]. These quantities could be selected from an arbitrary hydrogen operating condition of the APU GTCP 36-300 test engine. In the present analysis the following operation point from Dahl and Suttrop (2001c) is used: P*=6.27 bar absolute, T*=573 K, ϕ*=0.2439 (related to the total engine air flow and hydrogen fuel) and EI_{NOx}*=0.887 g/kgKE.

The equivalence ratio given for the APU engine, ϕ*, is related to the total engine airflow and hydrogen fuel; hence the corresponding equivalence ratio for the main engine should be inserted in equation (4-5). Using an equivalence ratio related to the total engine airflow and hydrogen fuel implies that differences in cooling air fractions for different combustor liners are neglected. As shown in section 2.3.4 all air could be used for combustion without getting an equivalence ratio lower than the weak extinction limit. However, due to the cooling requirement, maximally 95% of the air entering the combustor could be used for combustion. For a conventional combustor using kerosene, on the other hand, about 60-80% of the combustor inlet air takes part in the combustion, i.e. the air injected in the primary and in the intermediate zone [Lefebvre, 1998]. The remaining air is used to dilute the combustion products, aimed at reducing the temperature and creating an acceptable pattern factor (overall temperature distribution factor) into the turbine. Moreover, for the current study bleed air mass flow fractions are omitted. Omitting the bleed air and cooling air fractions is not expected to change significantly the results, since the liner cooling fraction and the bleed air mass flow fractions are considered to be the same for the different engine sizes considered.

Calculation of the stoichiometric flame temperature, T_{st}, i.e. the flame temperature obtained for equivalence ratio one, is a complex matter, involving various difficulties. It depends on the reactant pressure and temperature, and on the product species composition, which in turn depends on the time available for combustion. By assuming chemical equilibrium, which implies that the time dependence is cancelled, the complexity is reduced, and it is possible to calculate the flame temperature without

studying the flow field and chemical kinetics. However, the time is generally too short in a gas turbine combustor to attain chemical equilibrium.

According to calculations presented in section 2.3.4 it is indicated that overestimated flame temperatures by about 10-15% might be expected for stoichiometric conditions at full power when assuming chemical equilibrium. For other conditions the difference might be less. Assuming chemical equilibrium when calculating the NO_x emissions does imply that the NO_x emissions are also overestimated. Thus, the risk of obtaining a correlation that predicts lower emissions than possible to attain in a real combustor is minimised. In addition, since the objective in this study is to investigate the influence on the flight mission NO_x emissions of altered engine cycle parameters, the absolute level of the NO_x emissions is of secondary interest.

Attempting to calculate the flame temperature without assuming chemical equilibrium is beyond the scope of this thesis, and hence the stoichiometric flame temperature is calculated under the assumption of chemical equilibrium. For this purpose the NASA CEA code is used [McBride and Gordon, 1996; and Gordon and McBride, 1994]. This program was discussed in section 2.3.4.

The exponent m is estimated experimentally by comparing results calculated using equation (4-5) with experimental results of the APU GTCP 36-300 [Dahl and Suttrop, 2001c], see Figure 4-1.

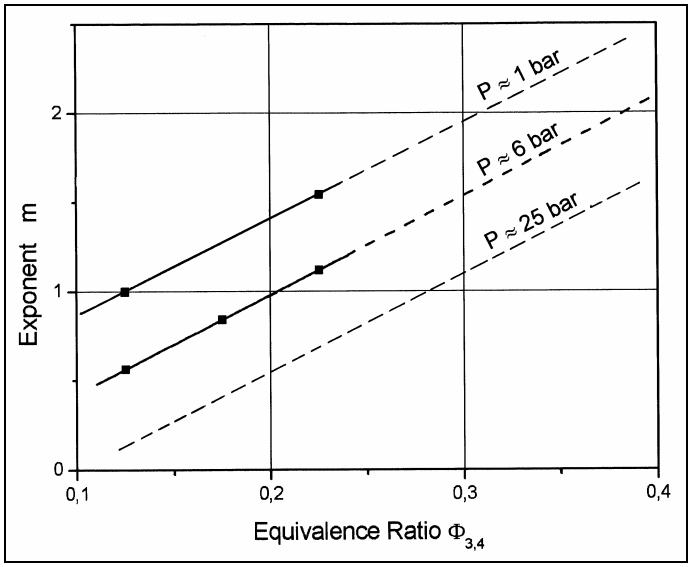

Figure 4-1. The exponent m as evaluated from experimental results [Dahl and Suttrop, 2001c].

It is found that the exponent m increases with increasing overall equivalence ratio and with lowered pressure level. In this study combustor pressures ranging from about 5 bar to about 40 bar are considered. The lowest pressures correspond to engines with a low OPR at cruise conditions, while the higher levels occur during take-off conditions. In order to take into account the pressure effect and the fact that the equivalence ratio at cruise is slightly lower than at take-off, an m value of 1.1 is used for cruise conditions

(and lower altitudes) and a slightly lower m value of about 0.9 is used for take-off conditions.

As for the exponent n, experimental results for kerosene-powered engines indicate that the NO_x formation depends on the pressure, such that n should be something between zero and about one. According to Dahl and Suttrop (2001c) independent evaluation of published ICAO data for kerosene-powered aircraft engines yields an n value of about 0.9. Since the reaction kinetics expressed in equation (4-3), which is independent of fuel type, proposes a linear dependency on pressure, it seems reasonable to assume that an n value close to one would be adequate also for the hydrogen engine. An n value equal to one is hence used in the present analysis.

4.2.2 Evaluation of the NO_x Emission Correlation

In order to evaluate the semi-empirical NO_x correlation derived above, its results are compared with other sources. The potential of reducing the NO_x emissions by replacing the combustion chamber of a full-scale conventional kerosene-powered engine by a micromix combustor is assessed by comparing the NO_x emissions results obtained using the semi-empirical correlation with known NO_x emission data of a civil kerosene-fuelled engine. For this purpose the V2527-A5 engine is chosen. By comparing the reduction potential predicted by the emission correlation for a full-scale engine with the reduction potential shown experimentally for the APU engine, it might be possible to make a first preliminary assessment of the reliability of the NO_x emission correlation.

The measured data available in the public domain [ICAO, 1995] which are interesting for the present purpose are displayed in Table 4-1. A background of the ICAO data was given in section 3.3.1. The following three cycle parameters are also given in ICAO (1995):

Bypass Ratio: 4.82
Overall Pressure Ratio: 27.2
Rated Output (F_∞) [kN]: 111.2

Table 4-1. Selection of measured certificate data of the V2527-A5 engine [ICAO, 1995].

Mode	Power Setting [%], percentage of F_∞	Fuel Flow [kg/s]	Emission Index of NO_x [g/kg Fuel]
Take-off	100	1.053	26.5
Climb out	85	0.880	22.3
Approach	30	0.319	8.9
Idle	7	0.128	4.7

In order to compare the NO_x correlation with experimental results of the APU (shown in Figure 2-9) the engine is modelled. Thermodynamic data for the engine are obtained using TurboMatch (see Appendix A.3, section A.3.1).

In addition to those three parameters given in ICAO (BPR, OPR and Rated output), figures on component efficiencies, cooling flows, the combustor outlet temperature and

losses need to be assumed. The model that is used for the present purpose is the same as the one outlined in section 2.2.1, except for a slightly different pressure ratio and efficiency of the HPC, different losses and slightly different BPR, OPR and rated output according to ICAO. The engine is designed for take-off static sea-level ISA conditions, using the component efficiencies and pressure ratios given in Table 4-2.

Table 4-2. Pressure ratios and efficiencies of the V2527-A5 engine used to equal the performance stated in ICAO (1995).

Component	Pressure ratio	Isentropic efficiency
Outer fan	1.8	0.88
Inner fan	1.5	0.89
Booster	2.0	0.88
High-pressure compressor	9.067	0.89
Combustion chamber	0.97 (3% pressure loss)	1.0 (combustion efficiency)
High-pressure turbine	-	0.91
Low-pressure turbine	-	0.91

Since the aim is to equal the performance obtained from experimental work (ICAO data), it is believed that the results have been corrected for losses in the inlet and in the nozzle. Therefore, no intake losses are taken into account and a thrust coefficient equal to one is assumed. No losses in ducts are applied.

Based on the assumptions outlined above, the SFC given in ICAO (1995) (can be calculated from the fuel flow and thrust) is fairly well emulated. For the kerosene-fuelled engine, an SFC 2.2% higher than that given in ICAO for the design point is obtained. When comparing measured results with model simulations, deviations of a few percent are fully acceptable, hence the results are considered to be satisfactory. As to the engine burning hydrogen, a slightly better performance, in terms of SFC based on energy equivalence, is achieved. The performance differences of changing to hydrogen were covered more in detail and discussed in section 2.2.3.

Since the APU results are presented in terms of mole fractions, the NO_x emission index is transformed. Using TurboMatch the flows and thermodynamic quantities (i.e. temperature and pressure) in and out of the combustor are computed. For comparison, the NO_x mole fractions are calculated at the combustor efflux. Based on the ICAO data and on the results obtained by TurboMatch, the mole fraction of NO_x for the kerosene-fuelled engine is calculated. As for the hydrogen engine, the improved version of TurboMatch which employs the above derived NO_x correlation (equation (4-5)) is employed (see Appendix A.3, section A.3.1). The results, showing the mole fraction of NO_x versus the power setting for the V2527-A5 engine using kerosene and hydrogen, are displayed in Figure 4-2. The lowest power setting, namely, 7% is not displayed since convergence problems in the engine model are encountered for the lowest thrust settings. The reason is that the standard compressor maps provided in TurboMatch are insufficient. Since the NO_x emissions are very low at this thrust setting and the comparison is mainly made for the full power condition, there is no reason to put a large effort on resolving this problem. In addition to the power settings given in ICAO (1995)

(30, 85 and 100%), another operating point of 53% power setting is included for the hydrogen-fuelled engine.

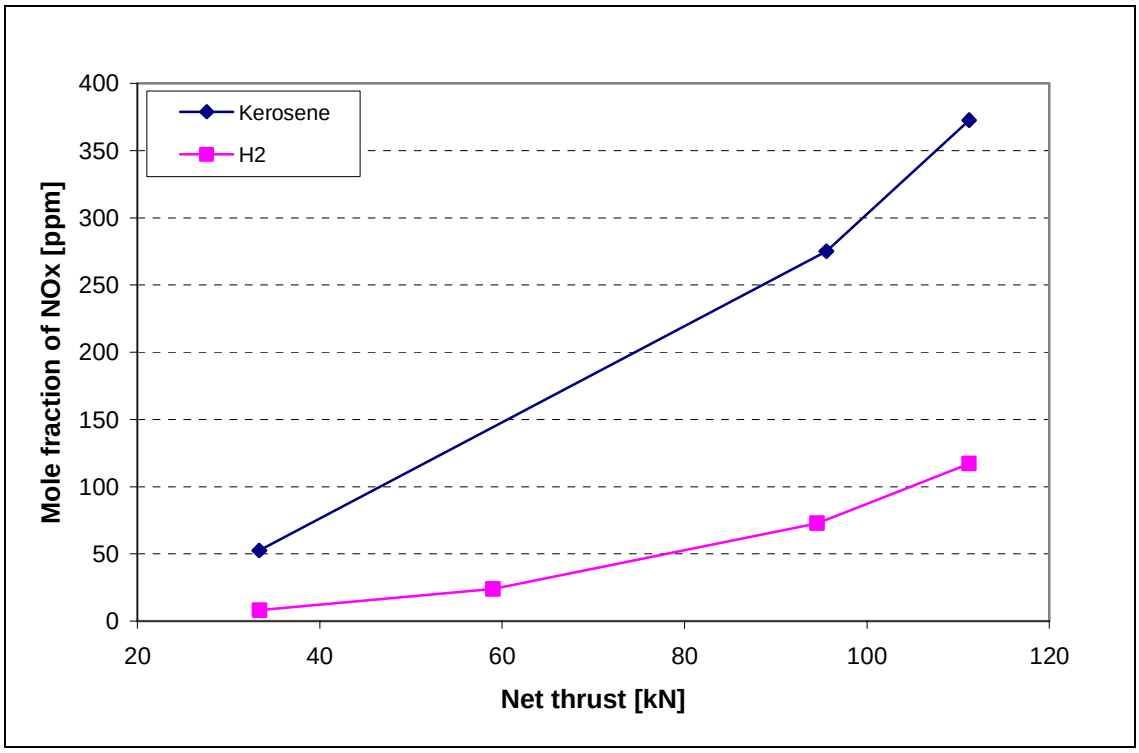

Figure 4-2. Mole fractions of NO_x at combustor efflux versus power setting for the V2527-A5 engine.

From the results in Figure 4-2 it can be concluded that the reduction in the NO_x mole fraction changing from kerosene to hydrogen is 68.6% at full power (111.2 kN), and as the load is lowered the difference increases. The reduction in NO_x emissions is about 1.6% points less when considering the emission index instead of the mole fraction. This 1.6% deviation is explained by the slightly lower molecular weight of the combustion gases when burning hydrogen (when converting from emission index to mole fraction, multiplication by the molecular weight is performed).

In qualitative terms the result is in good agreement with the measured results of the APU (Figure 2-9). However, an even larger reduction in NO_x emissions was achieved for the APU engine at full power: 85-86% in terms of mole fraction. In order to judge whether the result of the NO_x correlation is satisfactory, one needs to be aware of the simplifications involved in this methodology and several issues need to be considered.

Firstly, it might be fair to question whether it is reasonable to expect the same NO_x emission characteristics from future full-scale hydrogen-fuelled engines as demonstrated for the APU engine. In order to verify properly whether this is possible or not, it would be desirable to build and run a high-pressure combustor rig, or even better, a complete engine provided with a micromix combustor. For the time being no measurements of such tests are available. Hence, it is assumed that at least a similar NO_x reduction is to be expected for full-scale engines.

A reason why the correlation predicts too low levels of NO_x might be that the time in the combustor is too short for achieving chemical equilibrium, thus giving a too high flame temperature. If the combustion process is not completed there will be radicals such as OH, O and H present in the combustion products, which lowers the flame temperature. Unburned radicals in the combustion products can be a consequence of both insufficient time for completion of the oxidation process and dissociation.

When Dahl and Suttrop (2001c) evaluated equation (4-5), they found that the calculated NO_x levels for main engines very sensitively depend on the value of the flame temperature. When calculating the stoichiometric flame temperature assuming chemical equilibrium, they concluded that the flame temperature got too high and that the NO_x emissions become unrealistically large in comparison to the experimental results of the APU GTCP 36-300. They explained this by saying that the real combustion temperature is lower than that yielded when assuming chemical equilibrium, due to dissociation of H_2O which is beyond equilibrium. As a consequence they state that in the confined stoichiometric reaction zones of the micro-diffusion flames, it is not realistic to assume chemical equilibrium to calculate the stoichiometric flame temperature in equations (4-2) to (4-5).

In order to adjust the problem of achieving too high flame temperatures with reasonable efforts, Dahl and Suttrop (2001c) arbitrarily assumed atmospheric pressure throughout the operation range, regardless of the actual combustor pressure when estimating the stoichiometric flame temperature. Doing this adjustment, the flame temperature decreases and they got a NO_x emission reduction of about 71% in terms of emission index for the highest load for this particular engine, a reduction which they considered reasonable.

It is observed that the NO_x emissions calculated using equation (4-5) without cancelling the effect of pressure on flame temperature became lower than the level calculated by Dahl and Suttrop (2001c). The deviation is likely to be explained by a slightly different engine model (giving slightly different combustor inlet conditions) being used here, and a different computer code being used to calculate the flame temperature. A third reason, which probably is of minor importance, is that an m value of 0.9 is assumed here, while Dahl and Suttrop (2001c) assumed an m value of 1.0. Without cancelling the pressure influence on the flame temperature, a NO_x reduction of about 67% in terms of emission index is achieved. This is only 4% points less than obtained by Dahl and Suttrop (2001c) when they cancelled the pressure influence on the flame temperature.

Another issue that needs further attention in order to understand why the correlation seems to under-predict the NO_x emissions, is the choice of equivalence ratio assumed to calculate the flame temperature, and thereby to predict the NO_x formation. Considering a diffusion flame, a range of equivalence ratios are present, from infinity in the root of the flame to zero outside the flame front. The maximum flame temperature occurs at the slightly rich side of stoichiometric fuel-air ratios. In spite of that, the NO formation is found to peak on the fuel-lean side of stoichiometric fuel-air ratios [Lefebvre, 1998]. This is a consequence of the competition between fuel and nitrogen for the available oxygen. Although the flame temperature is higher for slightly fuel rich mixtures, the available oxygen is then consumed preferentially by the fuel. However, as some NO_x is

produced at both leaner and richer conditions than stoichiometric, it may be argued that an equivalence ratio different from stoichiometric, and hence a temperature lower than the stoichiometric, should be applied to predict the NO_x formation properly. Assuming, as has been done here, that it is the stoichiometric flame temperature that determines the NO_x formation might therefore over-predict the NO_x emissions.

To fully address the issues of chemical equilibrium and relevant equivalence ratio to calculate the flame temperature, more sophisticated models need to be employed. This would involve running 3-D flow calculations including heat and mass transport, and chemical kinetics. Efforts applying detailed chemical kinetic modelling of hydrogen flames in general, have shown that the rate of NO formation is dynamically controlled by numerous chemical reactions in the primary flame zone, while the thermal NO formation in the post reaction zone is mainly controlled by thermal equilibrium conditions [Shum et al., 1996]. Employing 3-D modelling tools to address the issues of flame temperature and equivalence ratio is beyond the scope of this thesis. Any attempt to investigate these issues in detail is excluded.

Being aware of the uncertainties associated with the accuracy of the correlation and with the levels of NO_x that may be expected from full-scale engines burning hydrogen, and the simplifications made when deriving the correlation, this correlation is considered to give an indication of the amount of NO_x produced at a certain operating condition. Moreover, it is believed to reflect the influence of different combustor inlet conditions on NO_x emissions good enough for the preliminary engine design studies conducted here. Equation (4-5) is therefore employed in this thesis to estimate approximately the amount of NO_x produced from various alternative turbofan engine cycles using hydrogen. Due to the large uncertainties involved and that much larger efforts would be needed to estimate the NO_x emissions more accurately, no attempts to change the equation to be more in line with the experimental results are made. The stoichiometric flame temperature, which is obtained by assuming chemical equilibrium, is assumed to predict the NO_x formation, and the pressure influence on flame temperature is included.

4.3 A Modelling Tool for Aircraft Mission Analyses (AMA)

In order to study the effects on flight mission emissions and fuel consumption of varied engine cycle parameters (COT, OPR and BPR) parametrically, a simulation tool is developed. For the investigation object, the same medium-range liquid hydrogen-fuelled aircraft as considered in chapter 3 is selected. It is a low-wing configuration based on the Airbus A321 with its fuel stored on top of the fuselage and in a tank outside the pressure cabin in the tail cone of the fuselage. The performance data in terms of range, thrust and weights are, however, slightly different; see Table 4-3. The main reason why the range differs is that the 8% improvement in SFC taken account for in chapter 3 (see section 3.3.1) not is included here. All calculations are conducted for a fully-laden aircraft, i.e. the cabin factor is assumed to be 100%. As a result of this the take-off mass is equal to the maximum take-off mass, MTOM. The aircraft was designed within the CRYOPLANE project, and more details can be found in Westenberger (2003a), Westenberger (2003b), and Oelkers and Prenzel (2001).

Table 4-3. Fundamental performance data for the datum aircraft.

Quantity	Value
Design range [km]	6614
Static sea-level thrust [kN]	134.0
MTOM [tonne]	87.6
OME [tonne]	61.2
Number of seats	185
Payload [tonne]	16.8
Fuel capacity [tonne]	9.6

When changing an engine cycle parameter, the engine and consequently also the aircraft need to be re-sized to provide still the thrust required at the most demanding flight phases. By providing a power setting (i.e. the ratio of COT at that flight phase to that of take-off) for each flight phase, the amount of engine scaling that is required is estimated. The program needs to be provided with engine data (i.e. thrust, fuel flow and emissions versus altitude, Mach number and power setting), which are obtained using the TurboMatch scheme. The NO_x emissions are calculated using the semi-empirical correlation derived in section 4.2, which is integrated into the hydrogen version of the TurboMatch program (see Appendix A, section A.3.1). Various aircraft characteristics (e.g. the aircraft drag polar and weights) are taken from the Piano software and technical reports from the CRYOPLANE project.

The main purpose of this study is to evaluate and compare different alternative engine cycles in terms of flight mission emissions and fuel consumption, rather than to perform a very accurate flight mission analysis. For this reason, the flight mission only comprises the take-off, climb and cruise phases; the descent and landing phases are excluded. Since these two neglected phases only constitute a few percent (about 2%) of the total fuel consumption, and in terms of NO_x, even less, for the medium-range flight mission of about 6600 km considered here, this simplification is not expected to affect significantly the results. Any possible variations in emissions and fuel consumption between the different engine concepts for the neglected flight phases would make a small difference, indeed, on the amounts for the complete flight missions.

In this section is outlined the methodology for assessing the effects on flight mission fuel consumption and emissions of changed engine performance. In section 4.3.1 the principles for re-sizing the aircraft and the engines owing to a changed engine performance are explained. The physical principles and equations which the performance estimations for the different flight phases are based upon are described in sections 4.3.2 to 4.3.4.

4.3.1 Re-sizing the Engines and the Aircraft

When an engine parameter is changed the performance changes, and as a consequence the engines might need to be re-sized to provide still the required thrust at the operating point that dimensions the engine. For high by-pass ratio turbofan engines considered here it is normally the thrust requirement at initial cruise that determines the engine size [Walsh and Fletcher, 1998]. This is in contrast to turbojet engines where the thrust

requirement at take-off is used to size the engine. In this study the engines are sized for the cruise point, and then checked against the required take-off field length. If the required field length turns out to be longer than permitted, the engines are up-sized to meet the maximum field length requirement.

As a consequence of both an altered engine performance and size, the engine weight changes. In order to predict accurately the engine weight for a particular engine, detailed knowledge of the engine configuration and its components is required. Knowing this, the engine weight can be calculated as the sum of the weights of the individual components, which usually are estimated using analytically-based correlations that are calibrated against historical databases. For the preliminary design studies conducted here, this detailed information is however not available. Instead, a method based on cycle parameters is employed. Methods based on cycle parameters are presently the only ones available when the aim is to estimate the weight of a non-existing engine. However, errors up to about 20% are to be expected for these types of simplified models. The accuracy of these methods, as well as other methods to estimate engine weights, is discussed in Appendix C.1.

The method used here to estimate the engine weight of different engine concepts is developed by Torenbeek (1982), and it does divide the engine into a gas generator (consisting of compressor(s), high-pressure turbine and combustor) and a propulsive device (consisting of fan, low-pressure turbine and nozzle(s)). By assuming that gas generator weight is proportional to the mass flow flowing through it and that the weight of the propulsive device is proportional to the fan thrust, the following expression for the dry engine weight including its fundamental accessories is obtained:

$$EW = F_{sto} \cdot \left[\frac{10 \cdot OPR^{0.25}}{SPT \cdot (1+BPR)} + 0.12 \cdot \left(1 - \frac{1}{\sqrt{1+0.75 \cdot BPR}} \right) \right] \tag{4-6}$$

The result is hence an equation for the dry engine weight dependent on F_{sto} (total take-off static thrust), OPR, SPT and BPR. All parameters refer to static sea-level conditions. The specific thrust (SPT) is in turn highly dependent on the turbine entry temperature (TET). Using this equation, the contribution from the fan should be 20% higher for geared fans and another 20% should be added for variable pith fans. If present, also extra weight for acoustic treatment needs to be added. Torenbeek (1982) also states that the variation of engine weight with high values of BPR cannot be predicted with certainty with this equation. A derivation of equation (4-6) is given in Appendix C.1.

In addition to the dry engine weight, the nacelle weight including its accessories is changed when the engine is re-sized. For convenience, the ratio of the diameter of the scaled engine to the diameter of the datum engine is named the linear scale factor, LSF:

$$LSF = \frac{D}{D_{dat}} \tag{4-7}$$

By assuming that the thickness of the nacelle (annulus ring) is proportional to $D^{1.5}$ and that the size changes symmetrically, i.e. that the ratio of engine length to diameter is constant, the nacelle mass of a re-scaled engine is determined by:

$$M_N = M_{Ndat} \cdot LSF^{2.5} \tag{4-8}$$

As the accessories weight is small in comparison to the nacelle weight, both these weights are scaled by the exponent for the nacelle weight. Using equation (4-6) and the information on distribution of the total engine mass from Gunston (2002), the sum of nacelle and accessories mass for the V2527-A5 engine is estimated to 1001.6 kg. A more detailed description of the background to obtain equation (4-8) is given in Appendix C.2.

Another contribution to a changed aircraft mass, i.e. MTOM, when changing the engine size, is the altered drag of the nacelles. By assuming that the engine size changes symmetrically, and that the nacelle has the form of a cylinder, it is assumed that the drag coefficient times the reference area, CDS_N, for the nacelle is proportional to the nacelle inlet diameter squared. This is in agreement with assumptions made in a similar study by Whellens (2003). More information could be found in Appendix C.2. Therefore, the change in drag coefficient times the reference area for the nacelle, ΔCDS_N, due to a re-sized engine is estimated by:

$$\Delta CDS_N = CDS_{Ndat} \cdot (LSF^2 - 1) \tag{4-9}$$

The correlations to estimate effects on nacelle and accessories mass and on CDS_N are derived assuming that the engine size changes symmetrically, i.e. the ratio of engine length to diameter is constant. This is a simplification that might overrate the effect of engine scaling on engine weight and drag. For instance, when the diameter is increased, the engine length might not increase by the same proportion. On the other hand, no interference drag that might occur due to changing the engine size is taken into account. Interference drag, which usually results from an increase in viscous separation, is the increase in drag of an aircraft component due to the change in the airflow caused by another component [Raymer, 1999]. If the engine nacelle diameter is increased, the drag of the wing might hence, owing to the interference effect, increase more than obtained by adding the contributions from the nacelle and the wing. Doing a more detailed study on the quantitative effects of overestimating the effect of altered engine diameter and the effect of excluding the interference drag is beyond the scope of this investigation. For the preliminary engine design study conducted here, the correlations as outlined above are believed to be sufficiently accurate.

When the engine size is changed, the MTOM also needs to be changed in order to preserve the range for a given payload. If the engine diameter is increased the wetted area of the nacelles is increased, and hence also the total drag. As a result the mission fuel consumption will rise. An increased engine weight will raise the need for stiffer wings, and thus a higher aircraft structure weight. Both these effects will impose the need for an aircraft with a larger MTOM. For these reasons the MTOM will increase more than the additional engine weight. If the engines are down-sized it would have the

opposite effect on the MTOM. The additional effect on MTOM, here denoted overhead mass, by altering the engine size is estimated using Piano. By changing the engine size and drag coefficient times reference area for the nacelles, CDS_N, and then finding the MTOM that gives an unchanged range, a table of changed engine sizes versus overhead mass is obtained. The change in total engine mass (dry engine mass plus the nacelle and its accessories) is denoted ΔTEM, and its contribution to the increase in the MTOM is denoted M_{OH}. The numerical values of M_{OH} versus ΔTEM are given in Appendix C.3. The effect on MTOM of a changed engine size is hence determined by:

$$MTOM = MTOM_{dat} + \Delta MTOM + \Delta TEM + M_{OH} \tag{4-10}$$

where ΔMTOM is a parameter which is used in the iteration loop in order to find the MTOM that gives a specific range. By varying ΔMTOM the number that gives the desired range could be found, and when the calculation has converged ΔMTOM becomes zero (see also section 4.3.4).

When the aircraft MTOM is changed the need for lifting surfaces also is changed. Therefore, it is reasonable also to change the wing area. In this study it is assumed that the wing area is changed in proportion to the change in MTOM (see equation (4-11)) and that the wing plan form is kept unchanged, i.e. the wing aspect ratio is unchanged. This is indeed a simplified approach. Nevertheless, it is considered to be a reasonable assumption for the type of preliminary design studies conducted here.

$$S = S_{dat} \cdot \frac{MTOM}{MTOM_{dat}} \tag{4-11}$$

Since the amount of scaling, i.e. the value on LSF, for a given power setting (here quantified by the combustor outlet temperature, COT) at cruise not only determines the thrust available, but also the aircraft weight at the initial cruise (which in turn determines the thrust required), finding the proper amount of engine scaling is an iterative process. By initially guessing the LSF, the take-off and climb phases can be modelled (see sections 4.3.2 and 4.3.3), and thus the thrust requirement at initial cruise can be calculated. Knowing the thrust requirement, a LSF to obtain this thrust can be calculated; the figure of LSF is updated and this process is continued until convergence. If it turns out that the take-off field length is shorter than permitted, the LSF that gives the maximum permitted field length is found.

Using the same approach as used in chapter 3, it is assumed that the fuel volume of the tail cone of the aircraft is re-sized when the aircraft fuel volume is changed (see section 3.2). However, for aerodynamic purposes, the minimum tail cone length is considered to be about two times the diameter of the fuselage. Below this length the tail cone is not reduced, even if it would be possible to store the required fuel volume in a smaller tank.

4.3.2 Take-off Performance

The take-off performance required here comprises the field length, the time until reaching the screen height of 35 ft, the fuel consumption and the emissions produced.

While the information on required field length is used to size the engine, the fuel consumption and emissions data are needed for the mission performance estimation. In order to estimate properly the required field length, unexpected occurrences, such as an engine failure, need to be considered. For this purpose the required field length is estimated by employing an empirical method proposed by ESDU (1985). The take-off time, the amount of fuel burnt and the emissions produced during the take-off are estimated by applying the equation of motion and integrating. The methodology for estimating the field length is outlined in section 4.3.2.1, and the principles and equations for modelling the take-off phase are described in section 4.3.2.2.

4.3.2.1 Field Length Estimation

In order to decide whether the engine size, for a given aircraft/engine combination, is sufficient for take-off, the required field length is estimated by employing an empirical method [ESDU, 1985]. This method is meant for obtaining first approximations to take-off field length of multi-engined transport aeroplanes for take-off over a 35 ft (10.7 m) screen from hard runways of zero gradient in still-air conditions. Using this methodology the take-off field length is defined as the greater of the following two:

- 1.15 times the unfactored, all-engines-operating distance to 35 ft screen height (UFL)
- The balanced field length (BFL)

The balanced field length is defined as the field length where, following an engine failure, the distance taken to abandon the take-off and to stop is equal to the distance taken to continue the take-off and to attain the safety speed, V_2, at screen height. Having calculated the parameters, TOP and $\tan(\gamma_{cseg2})$, the unfactored and balanced field lengths are obtained using diagrams provided in ESDU (1985):

$$TOP = \frac{AM^2}{C_{L2} \cdot n_{eng} \cdot F_{N07} \cdot S \cdot \sigma} \tag{4-12}$$

$$tan(\gamma_{ceng2}) = \frac{(n_{eng} - 1) \cdot F_{N2}}{AM} - \left(\frac{D}{L}\right)_2 \tag{4-13}$$

The parameters are related both to the aircraft and to the engines. The ones related to the aircraft are the aircraft mass (AM), the wing area (S), the number of engines (n_{eng}), the lift coefficient (C_{L2}) and the aerodynamic efficiency $(L/D)_2$ at the take-off safety speed (V_2), while the parameters related to the engines are the net thrust at V_2 (F_{N2}) and 0.7 times V_2 (F_{N07}). If the take-off performance is evaluated for any other than ISA condition, σ, which is the relative atmospheric density, should be given a value lower than one.

Estimating the low speed aerodynamics is inherently difficult. The aerodynamic characteristics, namely, the C_{L2} and $(L/D)_2$, used here are taken from the low speed aerodynamics provided in Piano. The lift coefficient at the take-off safety speed, C_{L2}, is equal to C_{Lmax} divided by 1.44. Piano estimates C_{Lmax} for arbitrary flap deflections on the basis of flap geometry and flap type. In addition to considering effects of flaps,

Piano includes effects of slats, adjustments for 3-D effects, for sweepback and for reduction caused by the tail download required to trim the flaps' pitching moment [Simos, 2000]. For the conditions considered in the present model flaps are extended to 15°, which corresponds to a C_{Lmax} value of 2.18.

The aerodynamic drag with high-lift devices deployed is estimated in Piano by taking into account the increase in 2-D profile drag, which is derived from empirical data matrices as a function of flap type, chord fraction and deflection, and then adjusting for 3-D effects according to the proportion of the wing covered by the flaps [Simos, 2000]. Furthermore, the effect of undercarriage is added. In the present model a $(L/D)_2$ value that equals 10.08 is used.

Physically the TOP parameter can be understood by noting that it is proportional to the distance taken to accelerate the aircraft from rest to the take-off safety speed, V_2, assuming a constant acceleration, zero retarding force and zero change of potential energy. The figures of UFL and BFL versus TOP and $\tan(\gamma_{ceng2})$ are obtained from ESDU (1985) and tabulated. The data used for the calculations are given in Appendix C.4.

4.3.2.2 Modelling the Take-Off Phase

In addition to the required field length, the time, fuel consumption and emission during the take-off phase are quantities of interest. By employing a physical model of the aircraft, these quantities are integrated during the whole take-off phase from the start until the screen height of 35 ft (10.7 m). Figure 4-3 shows a simplified picture of the forces acting on the aircraft during take-off before lift-off.

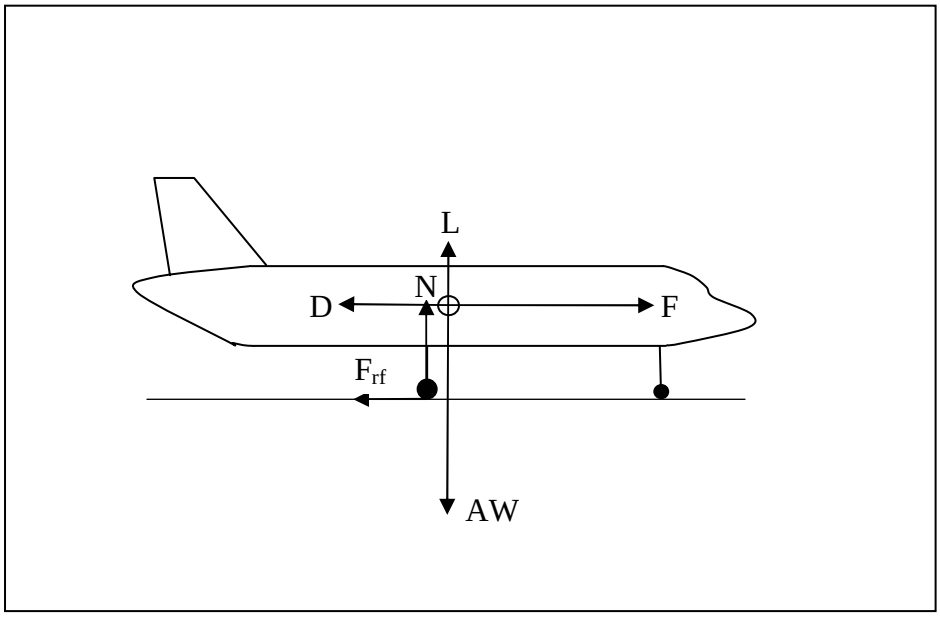

Figure 4-3. Forces acting on the aircraft during take-off before lift-off.

Summing the forces in the horizontal direction yields:

$$\sum F_h = F - D - F_{rf} = F - D - \mu \cdot (AW - L) \tag{4-14}$$

where F denotes the thrust, D the drag and F_{rf} the rolling friction of the wheels; the latter being expressed as the rolling friction coefficient, μ, times the weight on the wheels, i.e. the aircraft weight minus the lift (AW-L). A typical value for μ on a hard runway is 0.03 [Raymer, 1999]. Applying the equation of motion (Newton's second law) in the horizontal direction before lift-off yields:

$$\sum F_h = AM \cdot a_h = AM \cdot \frac{dV_h}{dt} \tag{4-15}$$

where AM denotes the aircraft mass, a the acceleration, V the velocity and t the time. The force, the acceleration and the velocity are directional quantities, which are indicated by the subscript h.

By combining equations (4-14) and (4-15) the following expression is obtained:

$$\int dV = \int \frac{F - D - \mu \cdot (AW - L)}{AM} dt \tag{4-16}$$

If the time step, Δt, is sufficiently small, the right-hand side of the equation could be assumed constant during a time step, hence:

$$V_{i+1} - V_i = \frac{F - D - \mu \cdot (AW - L)}{AM} \cdot \Delta t \tag{4-17}$$

where V_{i+1} and V_i denote velocities before and after the time step. After lift-off the flight path could be divided into several segments in each of which the aircraft steady climb gradient must equal or exceed a specified minimum value. For the second segment climb ESDU (1985) gives a minimum value on $\tan(\gamma_{cseg2})$ of 0.024, which implies a climb angle, γ, of 1.375 degrees. In the model employed here, it is assumed that the aircraft climbs with this angle from lift-off until the screen height of 35 ft (10.7 m). During this phase there is no rolling friction, but a component of the aircraft weight is acting in the flight path direction. Furthermore, the physics are simplified by neglecting the angle of attack, which implies that the thrust acts in the flight path direction (Figure 4-4 below is applicable). The velocity change during a time step is thus determined by:

$$V_{i+1} - V_i = \frac{F - D - AW \cdot \sin\gamma}{AM} \cdot \Delta t \tag{4-18}$$

The lift, L, and the drag, D, are calculated using the definitions of their coefficients:

$$L = \frac{1}{2} \cdot \rho_A \cdot V^2 \cdot S \cdot C_L \tag{4-19}$$

$$D = \frac{1}{2} \cdot \rho_A \cdot V^2 \cdot \left(C_D \cdot S + n_{eng} \cdot \Delta CDS_N \right) \quad (4\text{-}20)$$

where ρ_A denotes the density of air (other quantities are explained earlier). The change in C_D times the reference area for one nacelle (ΔCDS_N) is explained more in detail in Appendix C.2, and it applies only if the nacelle is re-sized compared with the datum engine.

From the start to the point where the rotation of the aircraft starts, C_L is approximately constant. Then it increases owing to an increased angle of attack until lift-off where it reaches its maximum value, which is the value corresponding to the velocity V_2, i.e. $C_{Lmax}/1.44$. During the remaining part of take-off until it reaches the screen height, C_L decreases as the velocity increases. For simplicity only two different C_L and their corresponding C_D are used in this model. From the start until lift-off a C_L value of 0.4 is assumed. This is a reasonable average value for a medium-range aircraft with deployed high-lift devices if applied from the start until lift-off. Using the low speed drag polar for the aircraft under consideration (provided in Piano) and assuming a flap setting of 15°, an L/D value of 5.5 is obtained for this C_L. Thus, C_D becomes 0.0727.

Assuming C_L equal to 0.4 from the start until lift-off will overestimate the drag at the beginning of the acceleration, while it will underestimate it when the aircraft approaches V_2, since the effect on C_L of rotating the aircraft is excluded. In total, the drag is probably slightly underestimated before lift-off. This is compensated by assuming a C_L equal to C_{L2} (C_L at the take-off safety speed) from lift-off until screen height. In reality, due to acceleration of the aircraft, C_L and therefore also C_D would decrease. The numerical values of C_L and C_D at V_2 used in this model are taken from Piano and equal 1.535 and 0.1496, respectively.

Data on fuel flow rate and emissions for a given thrust requirement are taken from tabulated data (i.e. thrust, fuel flow and emissions versus altitude, Mach number and power setting) that are obtained using TurboMatch. A regular take-off for a civil airliner is usually performed at full power condition or slightly reduced to increase the engine durability. The COT that should be used is given by the user during the execution of the program.

4.3.3 Climb Performance

The climb procedure is divided into three different phases: acceleration with a constant climb angle until a predefined C_L (or velocity), climb with constant IAS (indicated air speed) and climb with a constant Mach number. Here, the physics are simplified by neglecting the angle of attack, which implies that the thrust acts in the flight path direction. A simplification of the forces acting on the aircraft during climb is shown in Figure 4-4.

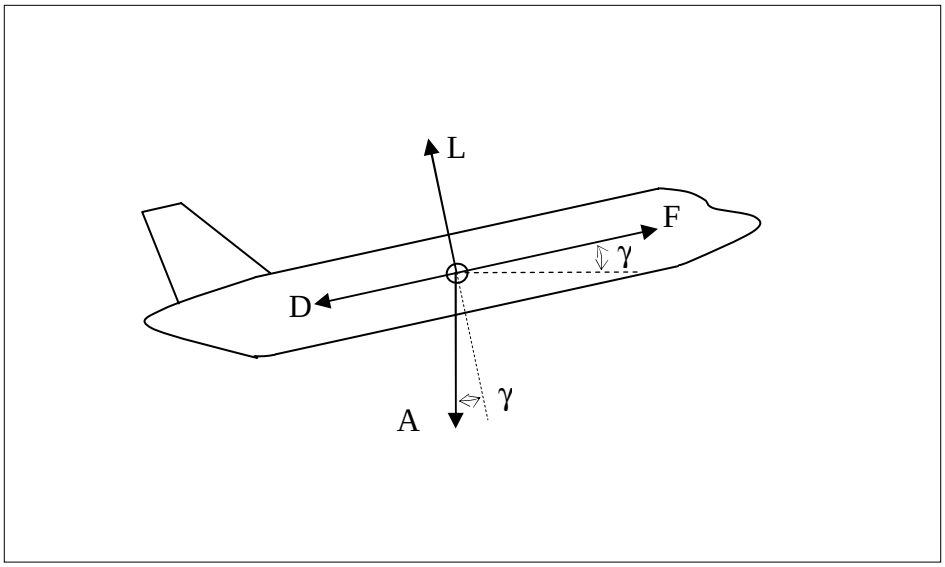

Figure 4-4. Forces acting on the aircraft during climb (angle of attack is neglected).

Following the methodology outlined in section 4.3.2.2 and applying the equation of motion in the flight path direction, the equation that describes motion for an infinitesimally small time step (or at least sufficiently small to justify that the thrust, drag and aircraft weight are constant during a time step), Δt, reads:

$$V_{i+1} - V_i = \frac{F - D - AW \cdot \sin\gamma}{AM} \cdot \Delta t \tag{4-21}$$

This is the same equation as the one that describes the motion from lift-off until the screen height. The drag is calculated using equation (4-20).

A model for calculation of the atmospheric conditions, namely, pressure, temperature and density, and the speed of sound as a function of pressure altitude and ISA deviation is described in Appendix C.5.

The drag coefficient in equation (4-20) is calculated by assuming a quadratic relationship between the drag coefficient and the lift coefficient. This is a simplified approach that tends to underestimate C_D for high C_L values; however, for the preliminary design studies conducted here it is believed to be a reasonable simplification. The drag coefficient is hence determined using the following equation:

$$C_D = C_{D0} + k \cdot C_L{}^2 \tag{4-22}$$

where C_{D0} is the drag coefficient at zero lift and k is a constant. The lift coefficient, C_L, is determined using:

$$C_L = \frac{AW \cdot \cos\gamma}{\frac{1}{2} \cdot \rho_A \cdot V^2 \cdot S} \tag{4-23}$$

Data on C_{D0} and k versus altitude and Mach number are obtained from drag polar of the aircraft under consideration [Oelkers and Prenzel, 2001] and using the aircraft characteristics provided in Piano. The characteristics in Piano are obtained by employing a variety of preliminary design-style techniques.

In the model used here it is assumed that the aircraft is clean, i.e. undercarriage and flaps are retracted, during the complete climb phase. On a real medium-range flight the undercarriage is retracted almost directly after take-off, while the flaps not are completely retracted until the aircraft has climbed about 1-2 km in altitude. Neglecting the influence of undercarriage and flaps will therefore underestimate the total drag coefficient in the beginning of the climb phase. Data on C_{D0} and k versus Mach number and altitude are supplied to the program in the form of tabulation, see Appendix C.6.

Comparing the drag coefficient results obtained using the described methodology with the complete drag polar provided in Piano for a clean aircraft, it is concluded that C_D is underestimated by 10-20% during approximately the first 400 meters (in altitude), while it is overestimated by 1-2% for the remaining of the flight mission. For low altitudes where C_L is high, a parabolic equation (equation (4-22)) is obviously not sufficient to imitate accurately the drag polar. This is the main reason why C_D becomes too low for low altitudes where C_L is high. Since the effect of undercarriage and flaps are neglected, C_D will be even more underestimated during the initial climb. However, in terms of fuel consumption and emissions this deviation might be compensated by a slightly overestimated C_D for the remaining part of the flight.

Data on the fuel flow rate and emissions for a given thrust requirement are taken from tabulated data (i.e. thrust, fuel flow and emissions versus altitude, Mach number and power setting) that are obtained using TurboMatch. The climb phase is also often performed at a constant COT, but there are minor variations for different engines in different applications. A typical value on the ratio of COT at max climb to COT at take-off for a high by-pass ratio engine at ISA condition is equal to 0.98 [Jackson, 2004]. Since the top of climb is the most difficult part, COT is usually higher at the higher altitudes than at the lower altitudes.

The vertical, S_v, and horizontal, S_h, distances for a time step are estimated by the velocity vector times the time step:

$$S_v = RoC \cdot \Delta t = V \cdot \sin\gamma \cdot \Delta t \tag{4-24}$$

$$S_h = V_h \cdot \Delta t = V \cdot \cos\gamma \cdot \Delta t \tag{4-25}$$

The velocity in the vertical direction is equal to the rate of climb (RoC), which is an essential climb performance parameter.

During the first climb phase the climb angle is kept constant, and the velocity change over the time step is determined using equation (4-21). For each time step the values on thrust, drag, aircraft weight and aircraft mass are updated. The vertical and horizontal distances are determined using equations (4-24) and (4-25), respectively. At a predefined C_L the climb mode is changed to be performed at a constant IAS. This

implies that the difference between the total and the static pressure is calculated initially, and then the velocity can be calculated, assuming that the pressure difference is unchanged. For Mach numbers larger than 0.3 the flow velocity is too large to justify the assumption of incompressible flow [Anderson, 1989]. At this flow regime, equations for subsonic compressible flow that take account for compressibility effects are used to calculate the pressure difference and the velocity, see Appendix C.7.

Knowing the velocity, the climb angle is determined using equation (4-21) and solving for γ. When the aircraft has attained the cruise Mach number (or a lower predefined value) the climb is changed to be performed at a constant Mach number for the remainder of the climb procedure. During this phase the flight velocity is calculated as the Mach number times the speed of sound at that particular altitude. Similarly as for the second climb phase, the climb angle is determined using equation (4-21) and solving for γ. Since the vertical distance, which is needed to calculate the next velocity, V_{i+1}, for a time step is initially unknown, integrating the relevant quantities over a time step is an iterative procedure for the second and third climb phases.

4.3.4 Cruise Performance

At cruise the engines need to provide exactly as much thrust as to overcome the total drag of the aircraft, i.e. the thrust of the engines equals the total drag of the aircraft. Using equations (4-20), (4-22) and (4-23) and setting the climb angle, γ, equal to zero, the total aircraft drag can be obtained. As for the cruising altitude, due to the controlled air space the most realistic choice from an operational perspective would be to cruise at a number of different discrete flight levels, measured in feet divided by 100 (this applies mainly to long-range flights). However, for simplification the cruising altitude is kept constant in this model. For short- to medium-range aircraft the benefits of step-cruising are negligibly small anyway. As fuel is consumed, the aircraft becomes lighter, C_L is decreased, and hence C_D and D are also decreased. Therefore, the power setting may be reduced with reduced fuel flow rate as a consequence along the cruise phase. Practically, in the program this is achieved by finding the COT that gives the required thrust. The cruise phase is performed at a constant Mach number.

The COT provided for cruise is used to estimate the amount of engine scaling required at the most demanding cruise condition, which is initial cruise. As fuel is consumed, the aircraft becomes lighter, the drag decreases and the power setting necessary to overcome the drag decreases. The higher the COT the larger the thrust, and the smaller the engine that is required. At a certain COT at cruise the engine becomes too small to be able to take-off within the specified maximum take-off field length, which here is defined to be 7000 ft (2133.6 m). This is the smallest possible engine size. For a high by-pass ratio engine at ISA condition, a typical value on the ratio of COT at max cruise to COT at max climb is equal to 0.965 [Jackson, 2004]. In practice, engines often are designed for significantly lower COT at cruise.

When the datum aircraft is re-scaled the question arises on how large amount of the take-off mass is fuel, which in turn determines the range. For a given MTOM, an increased engine size (which does not necessarily mean that take-off thrust is changed) would result in a decreased usable fuel mass and thus also a decreased range. Likewise,

if the MTOM is increased for a given engine size, the usable fuel mass and range would increase. In order to include properly these effects in the model, Piano is used to obtain a set of data, giving the influence on the usable fuel mass of scaled engines and MTOM for the aircraft under consideration, see Appendix C.8. Using linear interpolation these data are used to estimate the usable fuel mass for the aircraft/engine combination in question. Knowing the usable fuel mass and having subtracted the amounts used for take-off and climb, the amount left for cruise is known, which in turn determines the range. If the range turns out to be different from the desired value the MTOM is changed by adding or subtracting a minor amount, for which the value initially is unknown (ΔMTOM in equation (4-10)). Finding the desired range is hence an iterative procedure.

A comparison with flight mission fuel consumption and emissions data obtained using Piano, suggests that the flight mission modelling tool developed here gives reasonable results.

4.4 Engine Cycle Concepts

In this section the datum engine cycle is described, and a number of promising alternative engine cycle concepts either to lower the mission fuel consumption and H_2O emissions or the mission NO_x emissions are suggested. Figures for the cycle parameters for the alternative cycles are chosen so as to cover the available options to attain either of these objectives.

4.4.1 Datum Engine Cycle

The datum engine is an up-scaled version of the V2527-A5 engine, i.e. the engine described in section 2.2.1. This engine is a two-shaft boosted turbofan engine suitable for short- and medium-range aircraft. The jets from the by-pass and core are unmixed. The losses and efficiencies of various components, cooling flows and the location of the heat exchanger to evaporate the hydrogen prior to its entry into the combustion chamber are the same as assumed in chapter 2. The differences are that the datum engine considered here is designed for ISA conditions rather than ISA+10 K and that the inlet mass flow is larger to provide the thrust required by the aircraft. Furthermore, in contrast to the study outlined in chapter 2, the optimum outer fan pressure ratio is used here. As discussed in Appendix A.3 (section A.3.2), for a given core engine (i.e. specified COT and OPR) and a fixed BPR, there is an optimum value of the fan pressure ratio, that both minimises SFC and maximises the specific thrust. In practice, to reduce design and handling problems at the expense of a very small penalty in SFC, a value of the fan pressure ratio lower than the optimum is chosen [Pilidis, 2001]. Choosing a value on fan pressure ratio lower than the optimum for practical reasons seemed unnecessary for the preliminary design studies conducted here.

4.4.2 Alternative Engine Cycle Concepts

In order to study the influence on engine and flight mission performance of different values of cycle design parameters, a number of alternative cycles are selected. These engine cycles are not sufficient to define an optimum parameter combination for a

specific objective. Finding the optimum parameter combination for a specific objective requires either that performance software including an optimisation feature is used or that an extensive parameter study, indeed, is performed. The objective here is rather to investigate a number of relevant parameter combinations selected on the basis of general gas turbine performance knowledge, to provide some guidance on how to design hydrogen-fuelled aero engines for medium-range aircraft, to minimise either mission fuel consumption or mission NO_x emissions.

The options comprise employing a stronger or weaker core (higher or lower COT), a different OPR and a different BPR. During the past decades and in the future, for conventional kerosene-powered engines, there is a trend towards engines with higher COT, OPR and BPR. By increasing COT, the specific thrust is always increased, which implies that a smaller engine can be used to provide the same thrust, and SFC could be either increased or decreased depending on the values on BPR and OPR. For very high BPR engines SFC is improved with COT due to an increased core jet velocity, whereas the opposite is true for low BPR engines [Walsh and Fletcher, 1998]. If OPR is increased for fixed COT and BPR, SFC is improved due to an increased thermal efficiency for most COT and BPR combinations. The specific thrust tends to decrease with OPR for low COT, while it tends to be constant for high COTs. An increased BPR has a beneficial effect on the propulsive efficiency, and, in turn, SFC is improved and the specific thrust is lowered. As the optimum value of COT for minimum SFC increases with BPR, COT and BPR are usually increased together to achieve the best SFC [Walsh and Fletcher, 1998].

The incentive to decrease COT and OPR is to lower the emission index of NO_x and, in turn, a decrease is hoped for also in the flight mission NO_x emissions. If the BPR is unchanged this may be accomplished at the expense of deteriorated engine performance in terms of SFC and specific thrust. As the specific thrust might be decreased and SFC increased, a part of the gain in NO_x emissions expressed as emission index might be cancelled when the engine cycle is evaluated for a complete flight mission.

Similarly as for the datum engine cycle, the optimum value on fan pressure ratio is used, provided that it is not larger than 1.9, which is the highest attainable pressure ratio of a single fan stage [Walsh and Fletcher, 1998]. If the optimisation procedure would show that the optimum fan pressure ratio is larger than 1.9, the pressure ratio is set to 1.9. Here, the fan is considered to be divided into an inner and an outer fan. The inner fan pressure ratio is kept constant, while the outer fan pressure ratio is optimised for the cycle. Walsh and Fletcher (1998) suggest that the root pressure ratio should initially be assumed equal to the tip for low by-pass ratio engines, and around 80% of it for the highest by-pass ratio civil engines. The approach used here might imply that the difference between the inner and the outer fan pressure ratio becomes impractically large. From a performance point of view, however, it is expected to make very little difference.

When different engine cycles using different pressure ratios are compared, the component efficiencies (in terms of isentropic efficiencies) of the components of which the pressure ratio is altered need to be adjusted. However, for moderate changes in pressure ratios the effect of keeping the isentropic efficiency unchanged is very small.

In order to compare properly two different engine cycles that employ different pressure ratios, the polytropic efficiency[8] should be the same. When the pressure ratio is increased for a fixed polytropic efficiency, the isentropic efficiency increases for a turbine and decreases for a compressor. In this study only the pressure ratio of the high-pressure compressor (HPC) is changed when the OPR is changed. In order to make a fair comparison of the different engine cycles, the isentropic of efficiency of the HPC is changed such that the polytropic efficiency is the same as for the datum cycle. All the component efficiencies are the same for all engine cycles.

As the design point, take-off conditions, i.e. static sea-level, ISA, is chosen. Another option would be to design the engines for the cruise operation point to make sure that SFC is minimised at this operating condition, since the main share of the fuel is burnt during cruise. However, if the datum engine cycle is designed at cruise instead of take-off, SFC at cruise is reduced by less than 1%. In obtaining this figure the ratio of COT at cruise to COT take-off is equal to 0.85, which is the datum engine value. Hence, from the fuel burn point of view, there is in this case no point in letting cruise being the design point. As earlier work performed by the author and earlier work conducted within the CRYOPLANE project use take-off as the design point, the engines are also here designed for the take-off condition.

4.4.2.1 Engine A. Datum core, high BPR

In this cycle the BPR is increased without changing the core engine. This cycle is defined mainly to investigate if it would bring any gains in mission fuel consumption by only increasing the BPR.

When the by-pass ratio is increased the engine frontal area increases, and thus also do the weight and nacelle drag. Moreover, in order to keep the fan tip speed approximately constant the rotational speed needs to be decreased. The reduced rotational speed together with the fact that the turbine specific work needs to be increased, owing to the ratio of fan flow to turbine flow being increased, means that the loading of the turbine would be unacceptably high. Thus, to avoid that the high loading leads to low efficiency the number of turbine stages needs to be increased [Walsh and Fletcher, 1998].

As the by-pass ratio is increased, SFC and the specific thrust are decreased. The latter implies that the engine needs to be up-scaled, i.e. the engine weight and nacelle drag are increased, to provide the thrust required at the most demanding flight condition. A heavier engine with a larger frontal area would have a detrimental effect on mission fuel consumption. If weight and drag penalties are to be minimised, high by-pass ratio engines would therefore require shorter inlet and nozzles than conventional engines [Zimbrick and Colehour, 1988]. There is an upper limit on BPR beyond which the mission fuel consumption would increase. Le Dilosquer (1998) suggests that for kerosene-fuelled engines at about the 1995's level of technology, the optimum BPR with respect to mission fuel burn lies between six and nine depending on the installation.

[8] The polytropic efficiency is defined as the isentropic efficiency of an elemental stage in the process, such that it is constant throughout the whole process [Cohen et al., 1996].

A detailed investigation of optimum BPR for minimum mission fuel consumption for liquid hydrogen-fuelled aircraft is beyond the scope of this study. Bearing in mind the discussion above and that the equation to predict the engine weight (equation (C-5)) is not reliable for high values of BPR, a BPR equal to 6.5 is chosen for this engine cycle. This relatively modest BPR is believed to be achievable without employing a geared fan. For the datum core and with a BPR of 6.5, the optimum outer fan pressure ratio is equal to 1.6.

4.4.2.2 Engine B. Low power core, datum BPR

Aiming for reduced NO_x emissions the COT is reduced by 100 K. A reduced COT implies that there is less pressure available downstream of the turbines to produce thrust, and hence the optimum values of OPR and BPR decrease with reduced COT. In addition, a lowered OPR helps to lessen the NO_x emissions. In Figure 4-5 the effect on engine performance of varying OPR from 15 to 30 is shown for a COT equal to 1455 K and a BPR equal to the datum value of 4.8. For each parameter combination the outer fan pressure ratio is optimised.

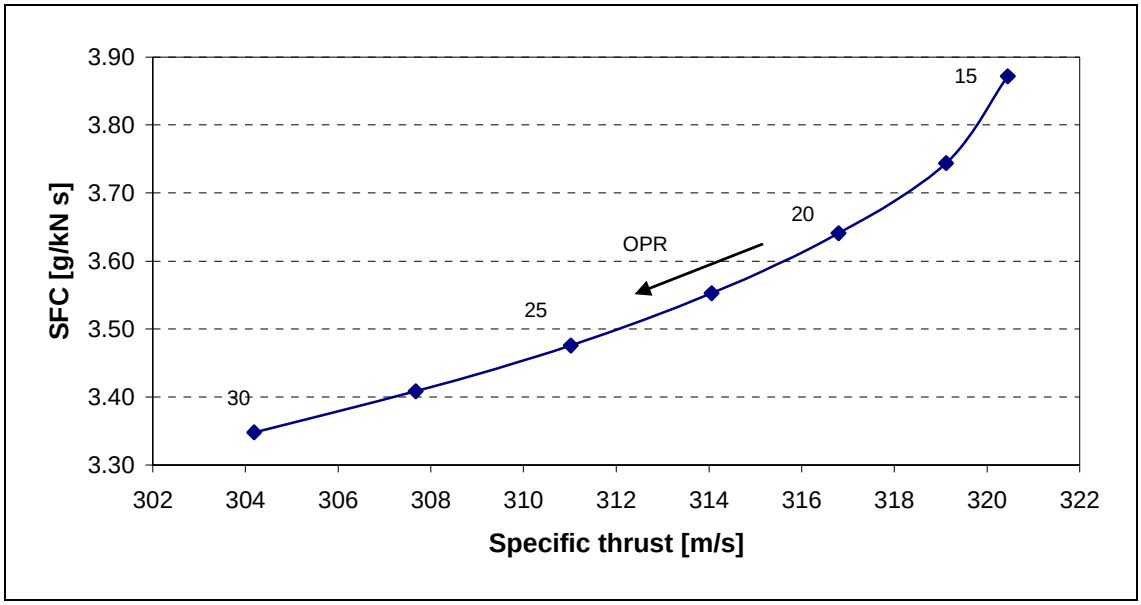

Figure 4-5. SFC versus specific thrust for varied OPR. COT is equal to 1455 K and BPR is equal to the datum value, 4.8.

For OPRs lower than 20 there seems to be a trend towards a greater penalty in SFC for a fixed gain in specific thrust. If SFC versus the NO_x emission index is plotted the trend is less emphasized; nevertheless, for OPRs lower than 20 the SFC penalty seems to rise for a given reduction in the NO_x emission index (see Figure 4-6). Therefore, an OPR equal to 20 is chosen for this cycle, which corresponds to an optimum outer fan pressure ratio of 1.71.

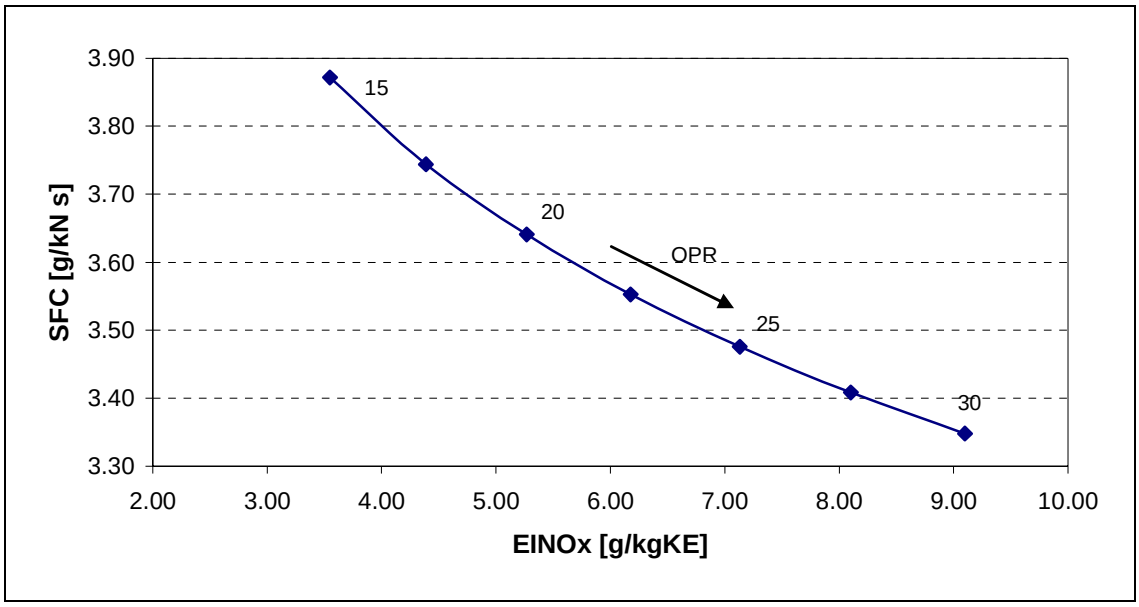

Figure 4-6. SFC versus NO_x emission index for varied OPR. COT is equal to 1455 K and BPR is equal to the datum value, 4.8.

4.4.2.3 Engine C. Low power core, low BPR

As argued for engine B, the optimum BPR decreases with reduced COT. Hence, it seems reasonable to include an option where the low power core defined for engine B is combined with a lower BPR. For this purpose a BPR of 3.8 is chosen. This figure is about 20% lower than the datum BPR, and is considered to be a reasonable value for an engine powering a medium-range aircraft. Due to the reduced BPR the optimum outer fan pressure ratio becomes larger than 1.9, and therefore the value of 1.9 is used.

4.4.2.4 Engine D. High power core, datum BPR

Instead of employing a weaker core as in engines B and C, a stronger core is employed in engines D and E. The reason for this is to study the possibility of lowering the mission fuel consumption, and thus also the mission water vapour emissions, using advanced engine technology. Being aware of the practical limitations of increasing the maximum cycle temperature of gas turbines, the COT is increased by 100 K compared with the datum value to 1655 K. Based on the same arguments as raised for the engine with reduced COT saying that the optimum values on OPR and BPR change with COT, the OPR is also increased.

In Figure 4-7 the performance, in terms of SFC versus specific thrust, is shown when OPR is varied from 27.5 to 42.5. The outer fan pressure ratio is optimised for each parameter combination. It may be concluded from the figure that the SFC is improved and that the specific thrust is deteriorated with OPR. The variation is not large, but for OPRs larger than 35 there seems to be a trend towards a larger penalty in specific thrust for a given SFC gain. Examining Figure 4-8, showing SFC versus the NO_x emission index, it may be argued that the penalty in the NO_x emission index for a given SFC improvement tends to increase for OPRs larger than 35. Based on these figures an OPR

equal to 35 is chosen for this engine cycle. Likewise, for engine C the outer fan pressure ratio becomes larger than 1.9, and thus the value of 1.9 is used.

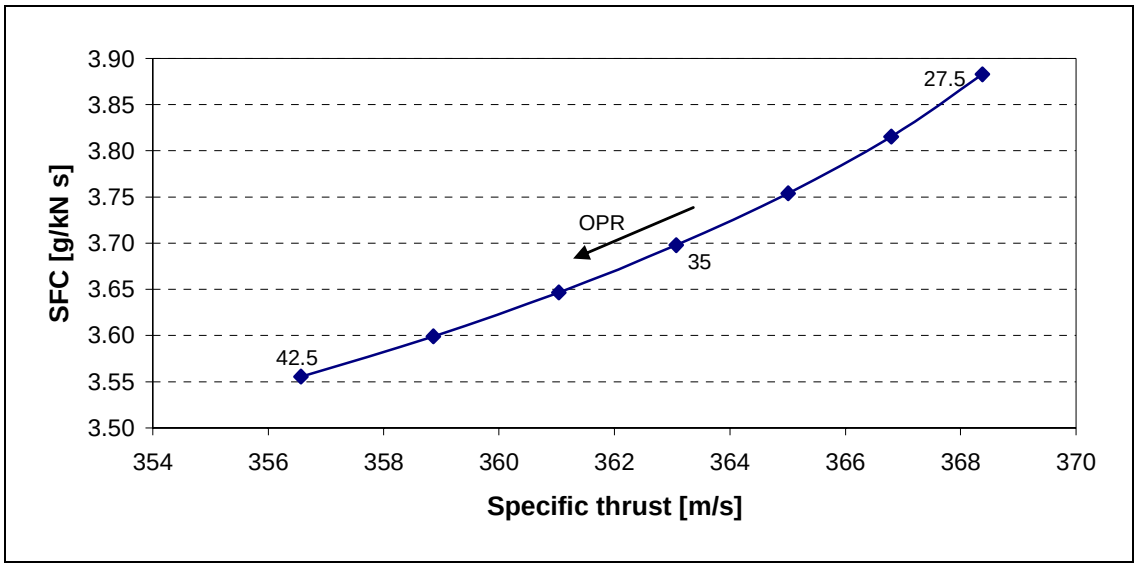

Figure 4-7. SFC versus specific thrust for varied OPR. COT is equal to 1655 K and BPR is equal to the datum value, 4.8.

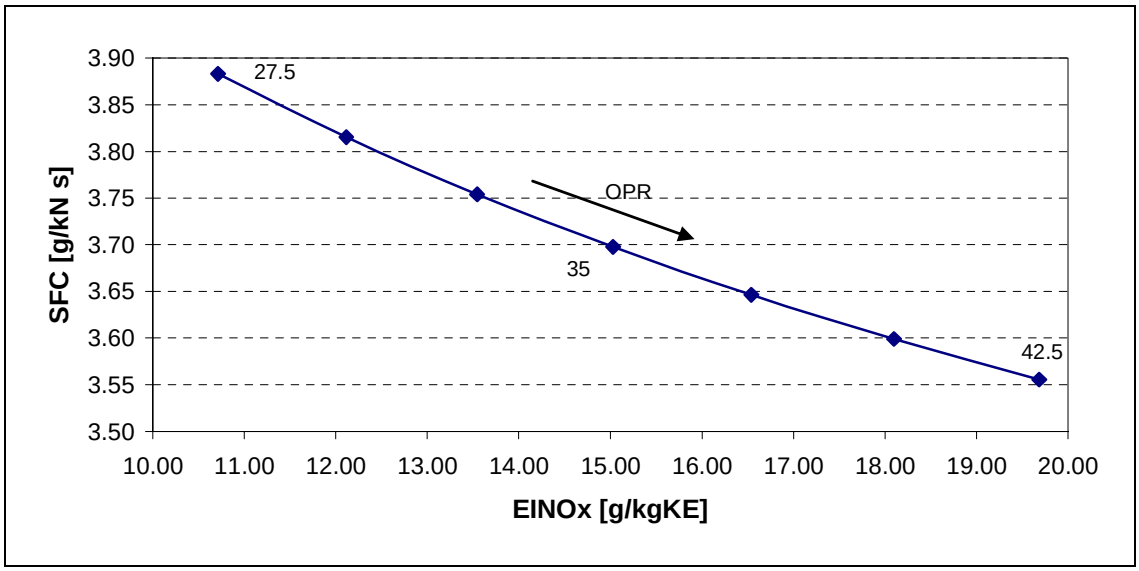

Figure 4-8. SFC versus NO_x emission index for varied OPR. COT is equal to 1655 K and BPR is equal to the datum value, 4.8.

4.4.2.5 Engine E. High power core, high BPR

Since the optimum OPR and BPR increase with COT, it seems reasonable to include an option where both OPR and BPR are increased with COT. Here the same increased BPR as chosen for engine A, namely 6.5, is chosen. The parameters for this engine are hence: COT is equal to 1655 K, OPR is equal to 35 and BPR is equal to 6.5, and the optimum outer fan pressure ratio becomes equal to 1.74.

4.4.2.6 Performance of Selected Engine Cycle Concepts

A summary of cycle parameters for the selected engine concepts is displayed in Table 4-4, and the engine performances are shown in Table 4-5. All data refer to the design point, i.e. static sea-level, ISA, and all engines have the same inlet mass flow (and hence also inlet diameter), which is equal to 395 kg/s.

Table 4-4. Engine characteristics of selected engine cycle concepts at the design point, static sea-level, ISA.

	COT [K]	OPR [-]	BPR [-]	Opt. OFPR [-]
Datum	1555	28.5	4.8	1.85
A. Datum core, high BPR	1555	28.5	6.5	1.60
B. Low power core, datum BPR	1455	20	4.8	1.71
C. Low power core, low BPR	1455	20	3.8	1.90
D. High power core, datum BPR	1655	35	4.8	1.90
E. High power core, high BPR	1655	35	6.5	1.74

Table 4-5. Performance of selected engine cycle concepts at the design point, static sea-level, ISA.

	F_N [kN]	ΔF_N [%]	SFC [g/kN s]	ΔSFC [%]	$EINO_x$ [g/kgKE]	$\Delta EINO_x$ [%]
Datum	134.0	0.0	3.6046	0.0	9.8607	0.0
A. Datum core, high BPR	116.4	-13.2	3.2099	-11.0	9.8607	0.0
B. Low power core, datum BPR	125.6	-6.3	3.6385	+0.9	5.2569	-46.7
C. Low power core, low BPR	139.3	+3.9	3.9635	+10.0	5.2569	-46.7
D. High power core, datum BPR	143.2	+6.9	3.6972	+2.6	15.0560	+52.7
E. High power core, high BPR	124.9	-6.8	3.2764	-9.1	15.0560	+52.7

Increasing the by-pass ratio and keeping the core engine unchanged for engine A has a substantial effect on the performance. The SFC is improved by 11%, while the thrust (or specific thrust) is deteriorated by 13.2%. This is the option that offers the largest SFC reduction; however, this is accomplished at the expense of the largest fall in specific thrust. As the NO_x emission index ($EINO_x$) only is dependent on the temperature and pressure at the combustor inlet as well as the fuel-air ratio, i.e. quantities that are solely dependent on the core engine, the NO_x emissions are unchanged.

By employing a core engine with lower COT and OPR (engines B and C), a reduction in $EINO_x$ by almost 47% can be achieved. If the BPR is unchanged the SFC is more or less unchanged also, but the thrust is reduced by about 6%. On the other hand, if the BPR also is lowered the thrust increases, at the expense of a 10% SFC deterioration.

Increasing COT and OPR is efficient with respect to SFC provided that the BPR also is increased; otherwise SFC actually increases. See engines D and E. In terms of specific thrust, the most beneficial option is not to increase the BPR. Inevitably a higher COT and a higher OPR imply an essential increase in $EINO_x$. For the engines considered here, the NO_x emission index is increased by more than 50%.

4.5 Flight Mission Performance

Using the computer program described in section 4.3, AMA, the mission emissions and fuel consumption are calculated for the datum engine/aircraft and the alternative engines/aircraft for a range equal to the design range of the datum engine/aircraft (6614 km). The conditions are given in section 4.5.1 and the results are given in section 4.5.2.

4.5.1 Conditions for Flight Mission Simulations

During the execution of the program the user is asked to provide the power setting in terms of COT for take-off, climb and cruise. While the values of the COT ratio, i.e. COT_i to COT_{max}, at take-off and climb are set to be the same for all engine configurations, the COT ratio at cruise is able to be varied. A regular take-off for a civil airliner is usually performed at full power condition or slightly reduced to increase the engine durability. In the calculations presented here COT is set to the maximum value at take-off. The climb phase is performed at a constant COT which is 96% of the maximum allowable value. The datum engine in this study is designed for a ratio of COT at cruise to COT at max climb equal to 0.877. The cruise phase is conducted at the Mach number of 0.8 at a constant altitude equal to 11 000 m.

4.5.2 Results

The amount of engine scaling influences the aircraft size, mission fuel consumption, mission emissions and the flight envelope (rate of climb). In Figure 4-9 the mission NO_x is plotted versus the mission fuel consumption, and in Figure 4-10 the mission NO_x is plotted versus the aircraft MTOM, for a range of COT values at initial cruise (COT_{ic}) for the datum and the selected engine cycles. Going from right to left in the figures, the maximum power setting at cruise increases, which means that the necessary engine size decreases. Smaller engines mean that the aircraft could be smaller and lighter for a given payload and range, which also implies that it consumes less fuel (see Figure 4-9). The mission NO_x emissions, on the other hand, increase, since a higher power setting during cruise, where the main share of the NO_x emissions are formed, enhances the NO_x production. In addition, the take-off distance gets longer and the rate of climb gets lower when the engine size is decreased (even if the aircraft is lighter), and hence the climb phase becomes longer and more time-consuming. All engine concepts are evaluated for

the same power settings, and the COT at initial cruise is increased until the limit where take-off becomes the operating point that sizes the engines.

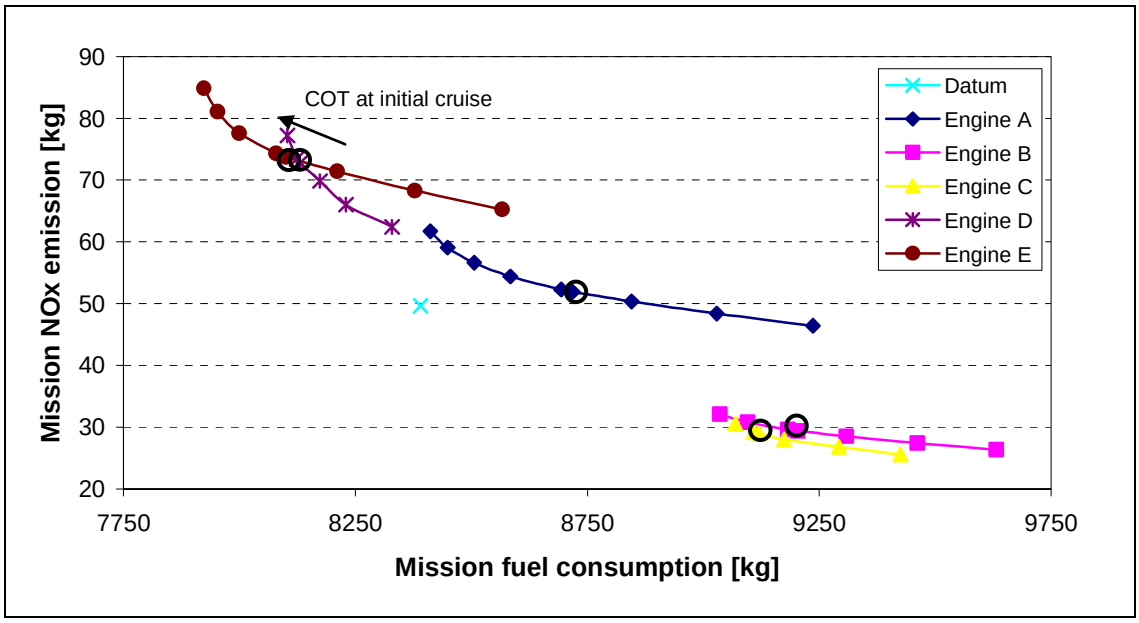

Figure 4-9. Flight mission NO_x emission versus mission fuel consumption for varied COT at initial cruise (sizes the engine) for the design range mission.

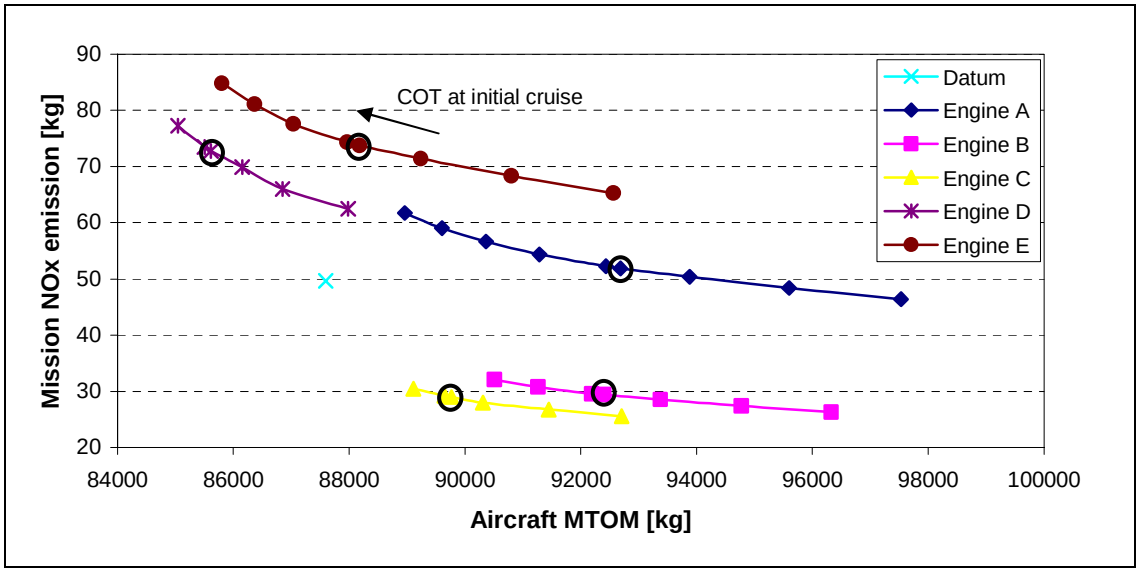

Figure 4-10. Flight mission NO_x emission versus aircraft MTOM for varied COT at initial cruise (sizes the engine) for the design range mission.

In general, the higher the by-pass ratio, the larger the ratio of thrust at take-off to thrust at cruise (for given power settings). This is because a high by-pass ratio engine, which produces its thrust by low velocity exhaust streams with high mass flows, gets a larger loss in thrust as the forward speed is increased than a low by-pass ratio engine which possesses the opposite characteristics. Therefore, the curves for engines A and E that feature a higher by-pass ratio than the other engines include more points. The encircled

points are those corresponding to the same power setting at initial cruise as the datum aircraft/engine combination. For engine C with the lowest BPR it is not possible to increase much the COT at initial cruise compared with the datum engine until the take-off thrust becomes too low. Therefore this curve features fewer points.

For values on COT_{ic} higher than the datum case the slope of the curves seems to increase, implying that the mission NO_x penalty for a given gain in mission fuel consumption or MTOM increases. Another general observation is that in relative terms the potential to reduce NO_x emissions seems to be larger than the potential to reduce fuel consumption (and the water vapour emissions) by employing alternative engine cycle concepts.

If the objective is to minimise the fuel consumption and/or the mission H_2O emissions, increasing the power of the core engine along with the BPR seems to be the most effective measure. However, if the aircraft weight plays an important role, it is questionable if the BPR should be increased. The higher BPR engine needs to be larger and hence also heavier to provide the required thrust, which has a detrimental effect on the aircraft structure weight and thus also on MTOM. For this reason engine E offers the highest fuel saving potential, while engine D seems to be the best choice if the aircraft weight also is an important factor.

According to these calculations, increasing BPR without changing the core engine does not bring any advantages in terms of mission fuel burn, mission NO_x emissions or MTOM (engine A). In order to reduce the mission NO_x emissions an engine including a low power core is to be employed, since low temperatures and pressures are effective measures to suppress the thermal NO formation (see section 2.3) (engines B and C). Furthermore, to limit the increase in MTOM the calculations suggest that the BPR should be decreased rather than increased as suggested to lower mission fuel consumption. As the BPR is decreased the specific thrust increases, and hence a smaller engine is required. The effect of decreased BPR on the NO_x emission is very small, but a smaller engine implies that the aircraft structure weight could be decreased, and due to this, both the MTOM and the mission fuel consumption are decreased compared with the case when the BPR is unchanged.

In Table 4-6 the effects on engine size, MTOM, mission fuel consumption and mission NO_x emissions of the different engine concepts are summarised. These data are obtained for ratios of COT at initial cruise to COT at max climb equal to the value for the datum engine (the encircled points in Figure 4-9 and Figure 4-10), which is 0.877. Using the datum COT ratio for engine E, the fuel consumption is reduced by 3.5%, and the MTOM is more or less unchanged at the expense of increased mission NO_x emissions by about 49%. To achieve this, the engine diameter is increased by 6.9%. By reducing the engine size to approximately the datum size, which is the smallest possible size, and allowing for a higher power setting during cruise (the ratio COT at initial cruise to COT at max climb is equal to 0.919), it would be possible to raise the fuel burn benefit to 5.6% and the MTOM benefit to 2%. However, the mission NO_x emissions would increase to being 71% higher than the datum engine.

Table 4-6. Flight mission performance for the various engine concepts for the design range of 6614 km.

	COT_{ic} [K]	LSF [-]	MTOM [kg]	Δ MTOM [%]	Mis. Fuel [kg]	ΔMis. Fuel [%]	Mis. NO_x [kg]	ΔMis. NOx [%]
Datum	1336.0	1.000	87596	0.0	8389.9	0.0	49.63	0.0
A. Datum core, high BPR	1336.0	1.157	92687	+5.8	8718.8	+3.9	51.89	+4.6
B. Low power core, datum BPR	1250.1	1.072	92400	+5.5	9203.5	+9.7	29.39	-40.8
C. Low power core, low BPR	1250.1	0.973	89767	+2.5	9120.0	+8.7	28.98	-41.6
D. High power core, datum BPR	1421.9	0.947	85613	-2.3	8130.2	-3.1	72.76	+46.6
E. High power core, high BPR	1421.9	1.069	88180	+0.7	8100.2	-3.5	73.77	+48.6

If the increased COT and OPR are combined with the datum BPR (engine D), the MTOM is reduced for a given COT_{ic}, but the potential of lowering the fuel consumption is deteriorated compared with engine E. Assuming the COT_{ic} is the same as for the datum case, the engine diameter is decreased by 5.3%, MTOM is decreased by 2.3%, the fuel burn is decreased by 3.1%, and the NO_x emissions are increased by 47%. If the engine size is decreased to the minimum size, the fuel burn becomes 3.4% lower and the MTOM becomes 2.9% lower than the figures obtained for the datum engine. In this case the mission NO_x emissions are about 56% higher than those for the datum engine.

As can be seen in Table 4-6 the mission fuel burn, mission emissions and MTOM are all detrimentally affected if the BPR is increased and the core is kept unchanged (engine A). It would be possible to keep the fuel consumption at about the same level as the datum engine/aircraft combination if the COT_{ic} is increased maximally and thereby the engine size is decreased to a minimum. However, it may be accomplished at the price of a MTOM increase of 1.6% and NO_x emission increase of 24%.

Employing engine C, the mission NO_x emissions can be reduced by 42% at the expense of increased MTOM by 2.5% and increased fuel consumption by 8.7%. Owing to an increased specific thrust, the engine diameter is actually decreased by 2.7% compared with the datum engine. If the BPR is not lowered the engine size needs to be increased (see engine B). The reduction in mission NO_x emissions is about the same, but the enlargements in MTOM and fuel consumption become larger: compared with the datum engine the MTOM increases by 5.5% and the fuel burn increases by 9.7%. Looking at engine C and employing a larger engine and thereby allowing for a lower COT during cruise (and the other phases), the reduction in the mission NO_x may be increased to

become 49% lower than that of the datum case, at the expense of an increase in MTOM by 5.8% and an increase in fuel burn by 12.3%. This is accomplished by increasing the engine diameter by 5.1% compared with the datum engine, indicating that it would be possible to increase the engine size even more to reduce NO_x emissions if desired. The extent to which the engine size may be increased is limited by how large an increase in aircraft weight and fuel consumption is considered to be acceptable, and ultimately the maximum engine size also will be limited by practical geometric constraints.

4.6 Conclusions and Discussion

In this chapter a number of alternative engine cycle concepts are selected, and their engine performance and flight mission fuel consumption and emissions are estimated and compared with a datum engine/aircraft combination. A general observation, not very unexpected, is that in relative terms, the potential to reduce NO_x emissions seems to be larger than the potential to reduce fuel consumption (and the water vapour emissions) by employing alternative engine cycle concepts.

In order to lower the mission fuel consumption and thus also the mission H_2O emissions, the results indicate that engine E, which employs increased COT, OPR and BPR, seems to be the most attractive choice. In terms of engine performance, the SFC is improved and the specific thrust and the NO_x emission index are deteriorated compared with the datum engine. Taking into account the engine scaling needed due to the loss in specific thrust, the flight mission performance is estimated. Using the same ratio of COT at initial cruise to COT at max climb as for the datum engine, the fuel consumption is reduced by 3.5% and the MTOM is more or less unchanged at the expense of increased mission NO_x emissions by about 49%.

According to these calculations, increasing BPR without changing the core engine does not bring any advantages in terms of mission fuel burn, mission NO_x emissions or aircraft MTOM (engine A).

In order to reduce the mission NO_x emissions, the results suggest that an engine including a low power core engine, i.e. reduced COT and OPR, along with a lowered BPR (engine C), should be used. Low temperatures and pressures at combustor inlet are effective measures to suppress the thermal NO formation, and a reduced BPR, which enables the use of a smaller engine, limits the increases in mission fuel consumption and MTOM. With respect to engine performance, the specific thrust is slightly increased and the SFC is deteriorated, while the NO_x emission index is substantially decreased. Employing the same ratio of COT at initial cruise to COT at max climb as for the datum engine, the mission NO_x emissions for engine C can be reduced by 42% at the expense of increased MTOM by 2.5% and increased fuel consumption by 8.7%.

Technologies involving a high power core accompanied with increased BPR are changes that are subject to improvements. Increasing the temperatures and pressures in the gas turbine cycle require advancements in high temperature materials and cooling technology. An increased by-pass ratio requires an increased number of turbine stages, shorter inlet and shorter nozzles than those of conventional engines. It is, therefore,

likely that engines based on such technologies raise the development, production and maintenance costs. Moreover, the durability of the core engine is likely to decrease.

In contrast, engines designed for lowering mission NO_x emissions employing a core engine with lowered COT and OPR along with reduced BPR, are based on reliable technology that may eliminate the development cost, reduce the production and maintenance costs and increase the durability. As for the durability, a decreased COT and OPR will have a favourable effect on turbine blade and compressor life, respectively.

5 INTRODUCTION OF CRYOPLANES INTO THE SWEDISH DOMESTIC AIR TRAFFIC

5.1 Introduction

Introduction of cryoplanes in civil aviation has several advantages, both on a regional and on a global scale. In addition to the subjects already covered in the thesis, there is a need for the evaluation of the practical feasibility by compilation of a number of transition scenarios, which imply changing from a conventional fleet of aircraft to a LH_2-fuelled fleet over a certain time period.

In doing so, one may either change over on a global or on a more specified regional level. By having a global approach, the overall consequences in terms of hydrogen fuel requirements and effects on emissions can be investigated. In order to perform a detailed study, where a realistic transition of a specific airline's fleet is changed, it is appropriate to compile regional transition scenarios, providing information on what transition rate is feasible without burdening the airline too much. Furthermore, each scenario indicates the amount of LH_2 required for a realistic transition scenario, and one may discuss different methods of hydrogen production at the airport. The required infrastructure changes of changing to hydrogen as fuel could also be investigated.

The objectives of this section are to explore the feasibility, potential and consequences of introducing a LH_2-fuelled aircraft fleet on a regional scale. The chosen air traffic segment is SAS's share (the major airline in the region) of the Swedish domestic air traffic. The main reason for choosing this air traffic segment is that the probability for introducing cryoplanes in this region is expected to be high in comparison to other regions. Traffic growth curves are compiled by means of forecasts performed by the aviation authority in Sweden, namely, the Swedish Civil Aviation Administration (SCAA). According to these traffic growth curves and through consideration of the airline's approach to fleet development, two different conventional fleet developments are set up. Next, four realistic transition scenarios are compiled, and the fuel requirements and emissions related to these scenarios are estimated, and presented in relation to figures of the conventional fleet. The infrastructure changes needed at Arlanda airport and for distribution of the LH_2 are identified and assessed. Possible methods available today and in the future of producing hydrogen are briefly discussed.

The traffic growth scenarios are outlined in section 5.2 and the transition scenarios are described in section 5.3, including projected fuel consumption and pollutant emissions of each scenario. In section 5.4 the implications on airports in general, and on Stockholm/Arlanda in particular, are discussed along with possible hydrogen production methods that may be employed to satisfy the fuel requirement as imposed by the scenarios. This chapter is completed by a section covering the conclusions and discussions (section 5.5).

5.2 Traffic Growth Scenarios

Attempting to predict the future, particularly the far future, is difficult and always associated with major uncertainties. When addressing the future there are two approaches which are slightly different that can be used: forecasting and compiling scenarios. Both these approaches imply that a synopsis of a projected course of actions or events for the future are defined. In forecasting, the not-too-distant future is predicted by making assumptions about the most likely future development. Using this method, the aim is to predict what is really going to happen as accurately as possible.

Under circumstances where it is desired to look far ahead into the future and investigate the outcome of the introduction of, for instance, a novel technology, the compilation of a number of scenarios might be a better approach. When working with scenarios it is not necessary to consider only the most likely future development; the scenarios could be used to encircle the extremes of the outcome. Then it may be claimed that the actual outcome is somewhere between the extremes. In general, for being successful in scenario and forecast compilation, the future should be predicted by knowledge of the present situation and by making reasonable assumptions about the future, rather than by merely extrapolating the past.

5.2.1 Traffic Growth Scenarios for Stockholm/Arlanda Airport

In order to perform transition scenarios, scenarios for the future development in air traffic need to be compiled. In this investigation, two different traffic growth figures – one high-growth and one low-growth – for Stockholm/Arlanda airport are compiled. These figures are assumed to be applicable for the whole Swedish domestic traffic.

In general, forecasts performed by the industry tend to assume a higher growth rate than those performed by aviation authorities. The low traffic growth scenario used in this study is, therefore, based upon forecasts for Arlanda performed by the Swedish Civil Aviation Administration. The high-growth scenario is more in line with forecasts performed by the larger aircraft manufacturing industries.

The SCAA has conducted a number of traffic growth forecasts, for different time periods and regions, which are based upon assumptions for the airport situation in Stockholm. Besides Arlanda there are two other airports with heavy air traffic in the Stockholm region, namely, Bromma airport close to the city centre and Skavsta airport, about 100 kilometres south of Stockholm. Mainly due to complaints from the inhabitants close to the airport, the Bromma airport may be closed when the airport owner's (the SCAA) contract with the local authority expires in 2011. The development at Arlanda is dependent on whether Bromma will close in 2011 or not, along with the future growth in passenger demand. Depending on those local conditions and the development of new runways at Arlanda, traffic growth figures at Arlanda for 10 and 30 years, respectively, have been performed by the SCAA [Åhlgren, 2000a; and Jonforsen, 1999]. Based on these figures and on private communication with Mats Åhlgren at the SCAA [Åhlgren, 2000b], the low-traffic growth scenario for 2001-2050 used in this study for the Swedish domestic traffic is created (Table 5-1).

One should bear in mind that as the number of passengers increases, a certain percentage increase implies a higher increase in absolute terms. The result of the low-growth curve is roughly a linear passenger growth at Arlanda (Figure 5-1). Generally the passenger growth rate is expected to decrease with time.

Table 5-1. Assumed annual growth rates for the Swedish domestic air traffic.

Low-Growth Scenario		High-Growth Scenario	
Years	Yearly Growth [%]	Years	Yearly Growth [%]
2001-2015	3.5	2001-2010	6
2016-2035	2.5	2011-2020	4
2036-2050	1.5	2021-2035	2
		2036-2050	0.5

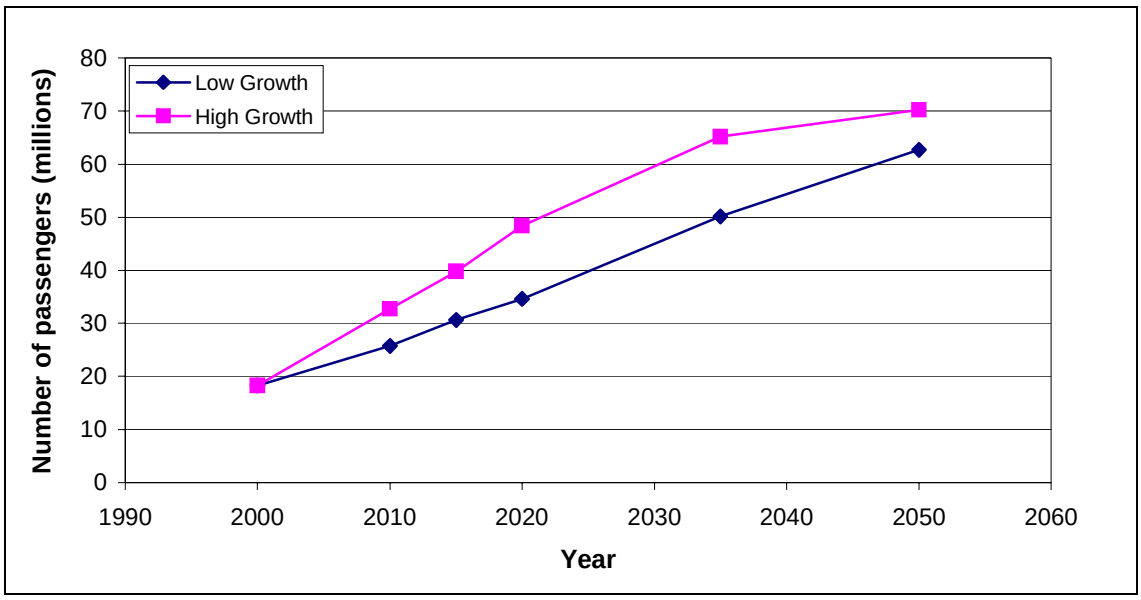

Figure 5-1. Passenger growth scenario for Stockholm/Arlanda airport 2000-2050.

Comparing these two growth rates, it is noticed that an essentially higher growth rate is expected during the first 20 years in the high-growth scenario, but then the growth rate is decreased considerably. During the first 19 years the traffic growth rate is similar to that assumed by Boeing and Airbus Industry, namely, about 5% increase per year [Kappers and Essers, 2001]. The reasons for significantly reducing the growth rate after 2020 are mainly to avoid predicting unrealistic annual passenger increases for the relatively small population of about nine million in Sweden, and to limit the number of passengers at the end of the investigated period, 2050.

In order to evaluate whether the number of passengers of about 70 million in 2050 – which is about four times the number of passengers at Arlanda in 2000 – resulting from the high-growth scenario, is reasonable, the theoretical maximum travelling that the population of about 10 million may perform is assessed. If it is assumed that each person makes one leisure trip each year, that one-fourth of the population makes one business trip once a week during 45 weeks a year and that 60% of the population travels

via Arlanda, the number of passengers at Arlanda in 2050 will be about 150 million. Since this is roughly twice the result according to the high scenario, it may be concluded that the traffic growth according to the high scenario is reasonable.

The transition scenarios presented in the next section are based on these two traffic growth figures.

5.3 Transition Scenarios

In order to compile realistic transition scenarios, a specific airline and its aircraft fleet is studied. The airline under consideration is Scandinavian Airlines (SAS), which dominates the Swedish domestic aviation market. About 70% of the Swedish domestic air traffic, in terms of passengers, is operated by SAS. Related to the total air traffic in Sweden, comprising both domestic and international flights, the corresponding number is about 35%. The following transition scenarios should be interpreted as transition scenarios, compiled to show the feasibility and gains of introducing cryoplanes into the Swedish domestic traffic, and not as SAS's future plans for their aircraft fleet.

Firstly, the aircraft fleet development based on conventional airplanes is compiled according to the two traffic growth scenarios. Secondly, four transition scenarios are compiled – two for each conventional fleet development.

Having taken a closer look at SAS's time table, showing the operation routes for individual aircraft, it may be concluded that Stockholm/Arlanda serves as a hub airport for the Swedish domestic air traffic, i.e. almost every scheduled flight within Sweden departs from or arrives at Arlanda airport. This makes Arlanda a sensible choice for the production and refuelling of liquid hydrogen. In order to restrict the complexity and costs, the implementation of production facilities for liquid hydrogen as well as infrastructure build-up is limited to Arlanda, only. As time passes this system of hydrogen production facilities may be expanded, eventually covering the whole world. Having refuelling facilities only at Arlanda will affect the fuel burn of the cryoplanes detrimentally, since these aircraft will need to carry fuel for the return trip as well. However, this drawback is relatively modest and is acceptable in this connection. When the transport capacity needs to be increased in the future, the number of individual aircraft is increased; alternatively, larger aircraft types are introduced, but it is assumed that the operation routes are unchanged.

In Table 5-2, data for a simplified current fleet, as well as for aircraft types that will be introduced when the capacity needs to be increased, are given. Data for the projected cryoplanes are also given in the table. The choices of aircraft types and their performance are explained below.

Table 5-2. Data for SAS's current and future aircraft fleet.

Aircraft type	No. of seats	Design range [nm]	Engine type[9]
Current			
B737-800	179	1000	CFM56-7B26-2p
B737-600	123	1000	CFM56-7B20-2p
Future			
A321-100	220	1000	V2530-A5
A330-200	278	1500	RR Trent 772B
Cryoplanes			
CMR1-300	220	2000	V2527-A5
CMR1-400	278	3000	V2527-A5

The design ranges of the current and future aircraft fleets are chosen according to recommendations from SAS. Since all airplanes are used for a shorter range than traditionally when they operate internationally, they are designed for a shorter range and with a higher payload. Thus, the aircraft are re-designed to suit the required demands. The basis for the liquid hydrogen-fuelled aircraft, CMR1-300, is taken from Oelkers and Prenzel (2001). A picture of the CMR1-300 showing the tank arrangement is presented in chapter 3 (Figure 3-2). The CMR1-400 is a fuselage-stretched and wing scaled-up version of the CMR1-300. The cryoplanes are designed for a range twice as large as for the corresponding conventional aircraft. The reason for this is that these aircraft need to be able to carry double the amount of fuel, since Arlanda airport is the only refuelling station for liquid hydrogen. More details of the aircraft are given in section 5.3.3.

Before the compilation of transition scenarios, SAS's expected fleet development for the next 50 years needs to be assessed.

5.3.1 Development of the Conventional Fleet

In the beginning of the considered period (2001), the SAS fleet operating as domestic in Sweden, solely, consists of eleven B737-800, seven B737-600 and two MD-87. Furthermore, a number of MD-81 operates partly within Sweden and partly within Europe. All together, the MD-80s correspond to about two aircraft operating solely domestically. In addition, there are a few regional aircraft, such as the Dash8-Q400, operating partly domestically, but due to its low passenger capacity these are neglected in the study. The MD-87s and the MD-81s will, however, be transferred to operations on the European market within the next few years, and will be replaced by the B737-600 and B737-800, respectively, in the domestic traffic. It is therefore assumed that the SAS domestic fleet in the beginning of the considered period, 2001, consists of thirteen B737-800 and nine B737-600.

The choice of future aircraft types is based on SAS's plans for the future. SAS is presently putting a number of A321 (184 seats) into international service, and in the future when more capacity is required, a domestic version of the A321 (220 seats) will

[9] The engines used in the simulations have the same performance as those stated in the table, but are scaled with respect to size according to a procedure explained in section 5.3.3.2.

also commence commercial service. The situation is similar for the A330, but as far as the author knows, no dates for introduction of this aircraft type are established yet.

When assessing the development of the conventional fleet, which means that no cryoplanes are involved, the airline's fleet development philosophy needs to be considered. An airline's transport capability can be increased either by adding individual aircraft or by replacing the current aircraft by larger types. The choice is dictated by the desire of maximising the overall profit for the airline. Figure 5-2 gives an illustration of how this might be solved. In general, one may claim that an average load factor of 50% corresponds to break even, i.e. for load factors higher than 50% the flight is profitable. The profit will increase with the average load factor until 75%. At this point it is, as shown in the figure, most favourable to change to a larger aircraft type. If the average load factor would be allowed to increase above 75%, there is a risk that the capacity is insufficient in peak hours. In general, an airline strives to have about 30-40% difference in size between their aircraft types [Näs, 2001].

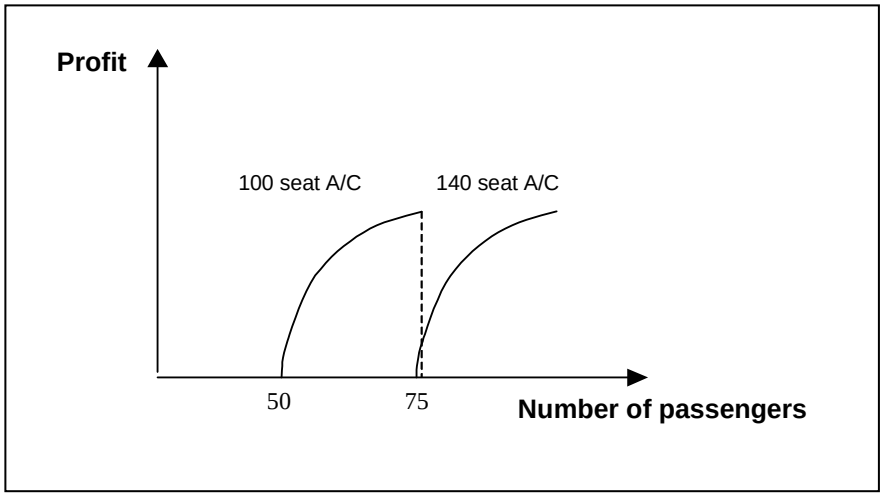

Figure 5-2. An airline's choice of aircraft size depending on load factor for maximum profit [Näs, 2001].

This is a simplified theoretical model; the reality is somewhat more complex, but still, the objective is to stick to these numbers as far as possible, with regards to types of aircraft available on the market.

Due to increased traffic demand as time passes, the average load factor will increase, and reach 75%. Then, the airline may either add aircraft types or change to a larger aircraft type. The number of airplanes that may be added is limited by the allowable increase in movements at the airport, without any rebuilding and expansion of the airport. Thus, the number of aircraft that may be added without congestion is very much dependent on the airport capacity.

In this study, the demand of increased traffic is satisfied by adding aircraft, provided that the number of movements is sufficiently low. At a certain point, depending on the assumed traffic growth, the aircraft type is replaced by a larger aircraft type. Another occasion when the aircraft are replaced by new ones, is when the retirement age of 30

years, as assumed in this study, of the aircraft is reached. In this case, the airplanes are not necessarily replaced by larger ones; they could also be replaced by aircraft of the same size. Replaced aircraft that have not reached their retirement age are assumed to be used on other routes, operated by SAS or another airline, i.e. they are no longer included in the scenarios.

In the beginning of the considered period, 2001, the average load factor is assumed to be 65%. This number is often used for the Swedish domestic traffic. In 2000, the average load factor of SAS's Swedish domestic traffic was 64% [Näs, 2001].

Figure 5-3 shows SAS's domestic fleet development for the period 2001-2050, according to the low passenger growth scenario. During this time period of 49 years, the number of aircraft increases from 22 to 39. This implies that the number of movements increases by 77%, or 1.2% on average per year. Accordingly, an essential increase in airport capacity is required. In 2045 the A321s need to be replaced by new ones, since they will have reached their retirement age. At the end of the scenario period, in 2050, the fleet operating within Sweden consists of airplanes in the size of the A321 and the A330.

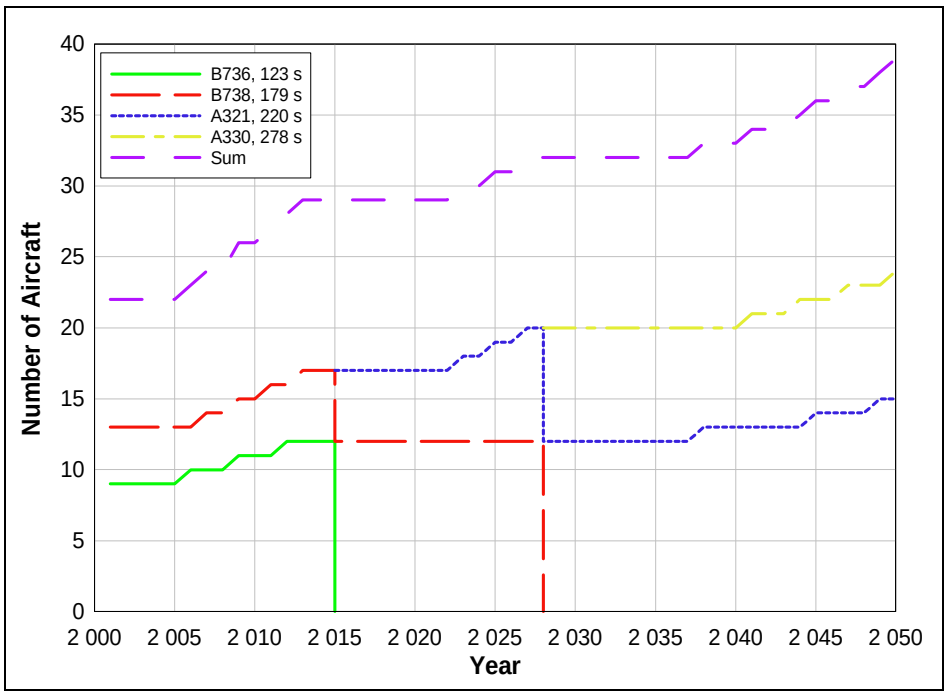

Figure 5-3. SAS's domestic fleet development, according to the low passenger growth scenario, for the period 2001-2050.

Figure 5-4 shows the corresponding graph for the high-growth passenger scenario. When a higher traffic growth is assumed, specifically notable in the first 20 years, the capacity in terms of increased number of individual aircraft needs to be increased earlier, and the change to a larger aircraft type also needs to be applied earlier. At the end of the transition period, in 2050, airplanes of the same size as for the low-growth scenario are used, but another three individuals are in service. This means that the number of movements is increased by 91%, or 1.3% on average per year, over this time

period of 49 years. Another difference is that the A321s will reach their retirement age of 30 years seven years earlier, since they are introduced earlier.

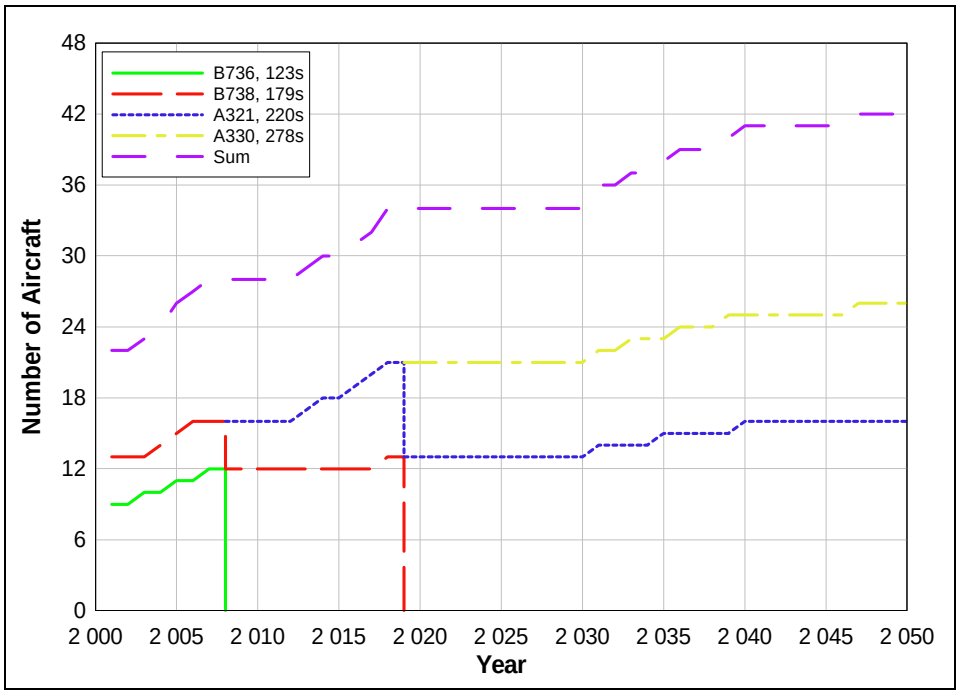

Figure 5-4. SAS's domestic fleet development, according to the high passenger growth scenario, for the period 2001-2050.

From this exercise it may be concluded that an essential increase in airport capacity, at all airports, is required in order to cope with the increasing traffic demand. So far only conventional technology has been treated, and the next step is to introduce liquid hydrogen-fuelled aircraft when the capacity needs to be enlarged.

5.3.2 Fleet development with introduction of cryoplanes

One of the main issues to consider when defining transition scenarios, is the reasonable point of time to start introducing the new unconventional aircraft types. Before any cryoplane may be put into scheduled service, much research and development is required. After the CRYOPLANE – System Analysis – which was finished in mid-2002, a phase of basic research and development, lasting about two and a half years, needs to be carried out. In addition to the research work, a demo-type aircraft may, if desirable, be developed and tested. An early introduction implies that much of the research and development work needs to be done in parallel, consequently increasing the risk of higher development costs. Later introduction of cryoplanes will allow more time for research and development, thereby minimising the risk of early cost increases. On the other hand, an extended programme may imply that the total cost of the project increases, and that interests paid on invested capital will go up [Klug, 2001b].

In this study, two different dates are assumed for the introduction of cryoplanes. In two of the scenarios, all new aircraft that are put into service in 2015 and afterwards are cryoplanes, and in the other two, all aircraft that are put into service in 2025 and

afterwards are cryoplanes. In general, reducing the environmental burden from civil aviation is probably most effectively accomplished by means of incentives, policy and legislative changes, without specifying any particular technology that should be used. It should be up to the industry to choose the proper technology in order to meet future demands.

Figure 5-5 shows scenario 1, which is a transition scenario with the introduction year 2015, where the low traffic growth scenario is applied. In practice, this is the same graph as Figure 5-3; the only difference is that cryoplanes with the same passenger capacity are introduced instead of the A321 and the A330. In this scenario, the SAS domestic fleet is operating on liquid hydrogen, solely, in 2028. In Figure 5-6, the introduction year is unchanged, but the high traffic growth figure is assumed (scenario 2). The higher traffic growth results in the changes to the larger aircraft types being required earlier, which means that the switch from the B737-800 to the A321 is needed in 2008. By this year, introduction of cryoplanes is unfeasible and not in line with the scenario. This implies that only a small number of cryoplanes in the size of the A321 may be introduced in 2015, i.e. to satisfy the capacity demand. However, when airplanes with the size of the A330 need to be introduced in 2019, cryoplanes are a feasible alternative. In this scenario, the fleet is powered by LH_2, solely, in 2038 – ten years later than when the low traffic growth scenario is assumed.

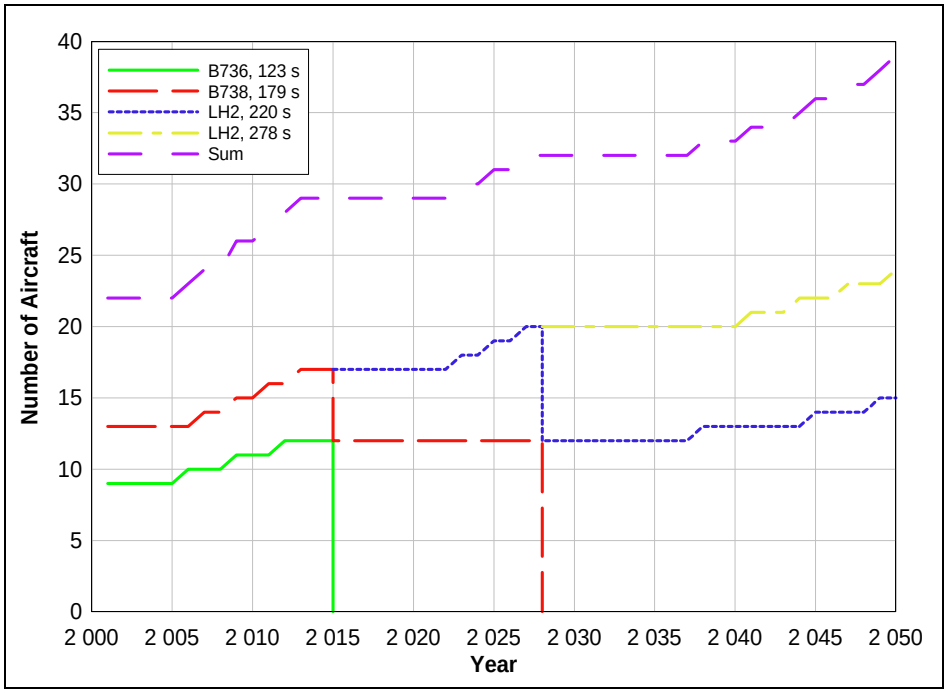

Figure 5-5. Scenario 1: all aircraft introduced in 2015 and afterwards are LH_2-fuelled; low passenger growth scenario is assumed.

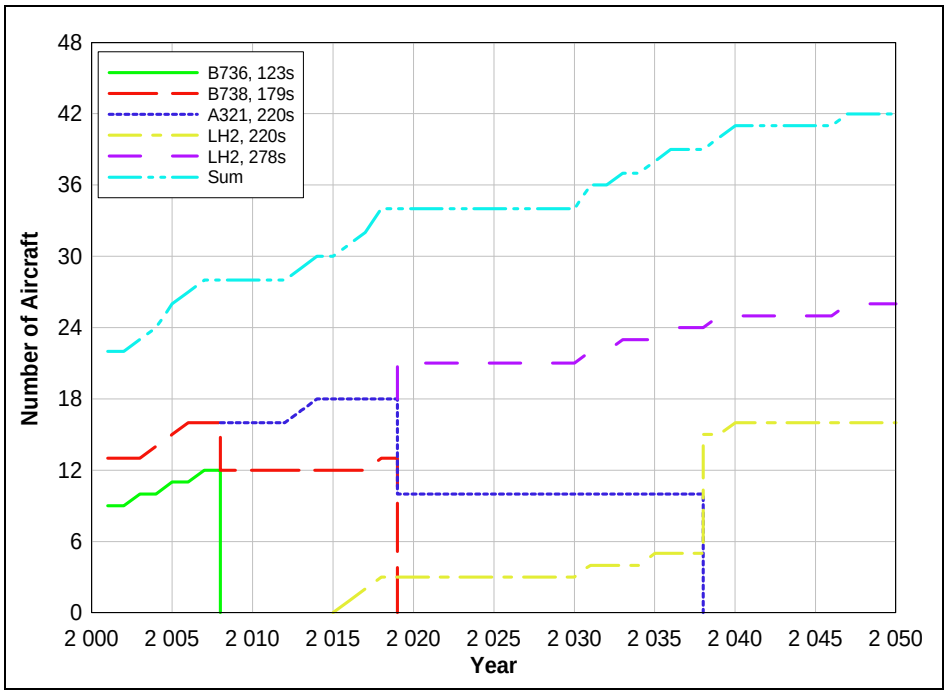

Figure 5-6. Scenario 2: all aircraft introduced in 2015 and afterwards are LH_2-fuelled; high passenger growth scenario is assumed.

In the next two scenarios it is assumed that all the aircraft that need to be introduced in 2025 and afterwards are LH_2-fuelled. In Figure 5-7 (scenario 3) the low passenger traffic growth numbers are assumed, and in Figure 5-8 (scenario 4) the high traffic growth numbers are assumed. In scenario 3 the introduction of cryoplanes starts on a small scale in 2026 with airplanes the size of the A321, followed by the introduction of larger cryoplanes, like the A330 with 278 seats, in 2028. In 2045, the major part of the conventional A321s will have reached their retirement age, and therefore are replaced by cryoplanes of the same size. In scenario 4, where the high traffic growth is assumed, the broad-scale introduction of cryoplanes is much delayed compared to the other scenarios. The introduction of both 220- and 278-seat cryoplanes starts simultaneously in 2030. In the same way as for scenario 2, the conventional A321s are replaced in 2038 by cryoplanes when the former should be phased out. When airplanes with the capacity for 278 passengers are required in 2019, it is, according to the prerequisites of the scenario, too early to introduce cryoplanes. A small number of cryoplanes of this size is required in 2030 and the next 20 years, but a broader introduction is not required until 2049, when the conventional ones will have reached their retirement age and therefore need to be replaced.

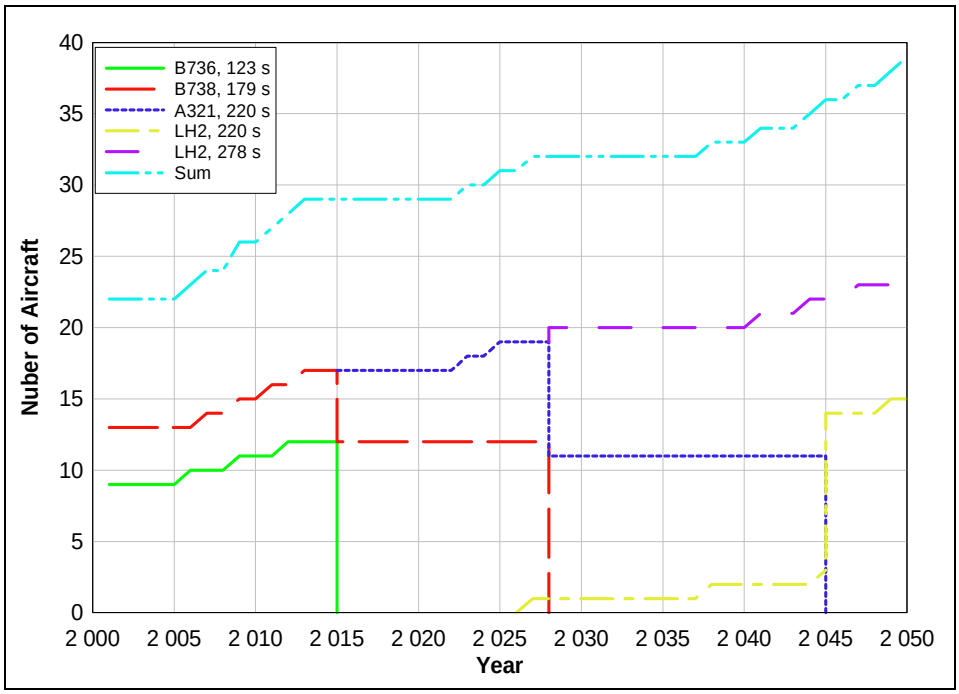

Figure 5-7. Scenario 3: all aircraft introduced in 2025 and afterwards are LH_2-fuelled; low passenger growth scenario is assumed.

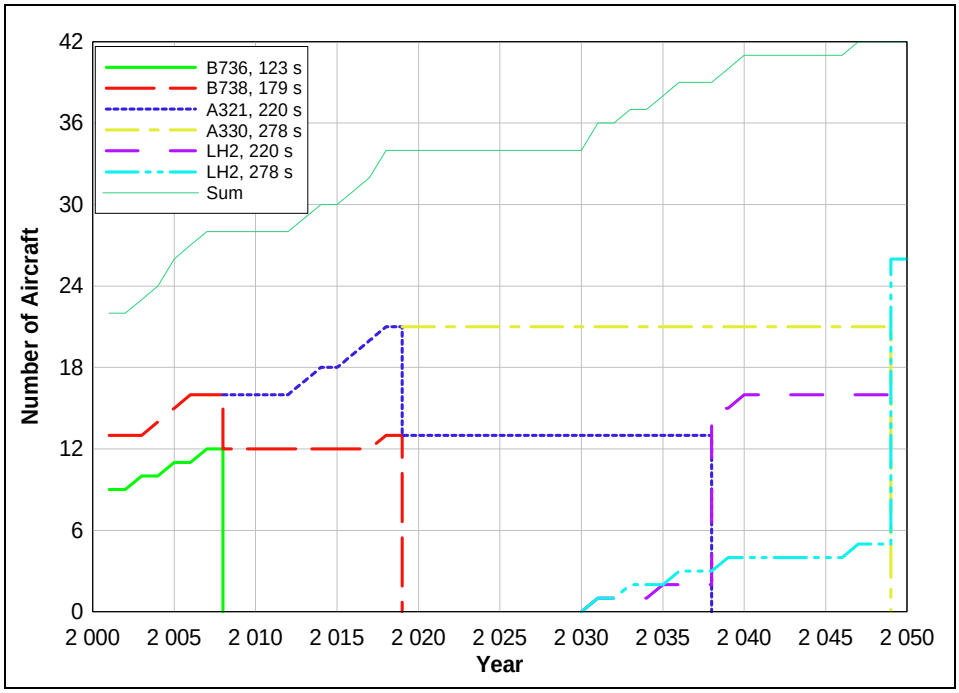

Figure 5-8. Scenario 4: all aircraft introduced in 2025 and afterwards are LH_2-fuelled; high passenger growth scenario is assumed.

All four scenarios, with respect to the percentage increase of cryoplanes by time, are summarized in Figure 5-9. After compiling these four scenarios, it may be concluded that in all scenarios it is feasible to change the fleet to be solely LH_2-fuelled over the

considered time period of 50 years. Furthermore, high traffic growth results in a delayed broad-scale introduction of cryoplanes.

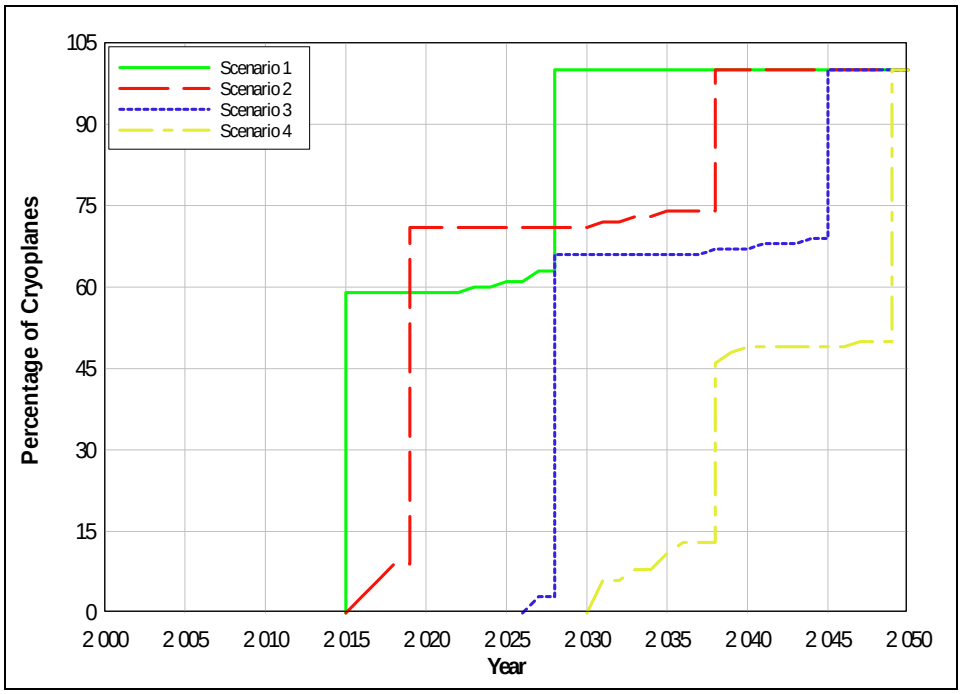

Figure 5-9. Percentage introduction of Cryoplanes, according to scenarios 1-4.

5.3.3 Emission Scenarios

Having established a number of transition scenarios, the required amount of fuel and the quantity of emissions for each of these are determined. These quantitative assessments are intended to point out differences in fuel burn and emissions among the scenarios. Furthermore, the fuel requirement is used when discussing different methods for hydrogen production. For these purposes simplified assumptions about the future technology developments (5.3.3.1) are considered to be sufficient.

In order to reflect the changes in emissions of each scenario and assumed traffic growth, the total amount of emissions on a typical day (June 6) are calculated for SAS's domestic traffic in 2001, 2010, 2020, 2030, 2040 and 2050. In order to do this, each individual aircraft's operation schedule is simulated according to SAS's timetable by means of the commercial aircraft design software Piano [Simos, 2000] and spread sheets. When the number of aircraft types and movements needs to be expanded later on, it is assumed that operation routes are unchanged and that Arlanda still serves as the hub airport.

Since the time horizon for the scenarios is as much as 50 years, technology developments need to be taken into account. In doing so the time period is divided into periods, each reflecting a certain technology level. For the conventional aircraft, the periods are 2001-2012 (today's technology level), 2013-2025, 2026-2037 and 2038-2050. Corresponding time periods for the cryoplanes are 2015-2032 and 2033-2050.

The idea is that each aircraft is at first designed for the range and the number of passengers given in Table 5-2, to obtain the performance using today's technology level. Then, fuel consumption is decreased and emissions performance is improved to reflect a technology development; the size of the improvements is predicted by the time period it is meant to reflect. With these improvements taken into account, the aircraft is re-optimised, and hence, the performance is increased, i.e. reduced fuel consumption for the same range. The technology level assigned to a certain individual aircraft is determined by the introduction year of the aircraft. The computations using Piano are conducted in collaboration with Anders Hasselrot at FOI (Swedish Defence Research Agency).

5.3.3.1 Technology Levels

When considering technology improvements for aircraft, there are three main parameters, basically independent of each other, that need to be taken into consideration: aerodynamic efficiency, structure weight and the specific fuel consumption (SFC) of the engines. In addition, the emissions, particularly oxides of nitrogen (NO_x) are of interest and subject to improvements over time.

Improved aerodynamic efficiency is equivalent to generating the aerodynamic lift at a cost of less aerodynamic drag. This may be achieved in several ways: smoother surfaces, improved aerodynamic shapes, boundary layer control, lift distribution control, etc. Based on some rough estimations, it is assumed that a reasonable improvement in aerodynamic efficiency within the next 50 years would be about 20%, i.e. the total drag may be reduced by 20% by 2050. Numbers for each time period are given in Table 5-3.

As to the structure weight, there may be an even greater potential for improvements. By introducing new lightweight materials, improving the manufacturing process of new composites, using load monitoring, etc., weight savings of about 45% may be achieved by 2050 [Ireman, 2001]. In this study a somewhat more conservative number is assumed, namely, 30% by 2050. In order to simulate this, the weights of the fuselage and the wing box mass, i.e. those parts that make up the main part of the aircraft weight, are reduced by the corresponding number depending on the technology level. Numbers for each time period are given in Table 5-3.

Finally, the engine performance in terms of SFC will improve with time. One or two decades ago most of the research on aircraft engines was focused on improving the engine efficiency, whereas most efforts during the last decade and at present are laid on reducing oxides of nitrogen (NO_x). The overall engine efficiency – the product of the thermal and the propulsion efficiency – is inversely proportional to the specific fuel consumption SFC, i.e. fuel flow for a given engine thrust (see Appendix A.1). Consequently, improved engine efficiency decreases SFC and thus decreases the total fuel burn for a specific mission. Measures for achieving reduction in fuel burn deal with improving the thermal and the propulsion efficiencies.

The propulsion efficiency is favoured by a high by-pass ratio, and the thermal efficiency may be increased through a higher overall pressure ratio (OPR) and, under some circumstances, higher turbine entry temperature (TET); two measures which are both

detrimental for the production of NO_x. Accordingly, measures to reduce SFC and NO_x emissions might be in conflict. For the scenario work conducted in this chapter, for which approximate numbers on emissions and fuel burn levels are sufficient, the reduction potential of SFC is not addressed, but the SFC level during the 50-year period is assumed constant and equal to the level of 2001.

Looking at the NO_x emissions, the reduction potential is as discussed in section 2.3 expected to be higher when burning hydrogen than kerosene. How large this reduction potential might be cannot be said without further research. Nevertheless, for the purpose of this scenario assessment some approximate numbers are applied. As shown in section 2.3.3.2, a reduction potential of about 85-86% has been illustrated for an APU engine provided with a micromix combustor using hydrogen. This number is, therefore, for this study considered to be the ultimate lowest level when using hydrogen. If LPP combustors are not considered, due to the danger of flashback and premature burning if used, and if simultaneously the CO and UHC emissions are taken into account, the NO_x reduction potential might be in the order of 50-60% when burning kerosene. These levels may be accomplished using staged or RQL combustors. The numbers on the NO_x emission levels assigned for each technology level versus time used in this study are displayed in Table 5-3. Considering recent achievements with respect to attaining low NO_x emissions, the figures applied here for the conventional aircraft might be slightly too conservative.

Table 5-3. Specifications of technology levels for the conventional aircraft and cryoplanes.

Technology level	Introduction year	Aero-dynamic drag level [%]	Structure weight level [%]	$EINO_x$ level [%]	SFC level [%]
0	2001	100	100	100	100
Conv 1	2013	92.5	90	80	100
Conv 2	2026	85	80	60	100
Conv 3	2038	80	70	50	100
Cryo 1[10]	2015	92.5	90	30	100
Cryo 2	2033	82.5	75	15	100

Measures for NO_x reduction tend to increase emissions due to incomplete combustion, namely, carbon monoxide (CO) and unburned hydrocarbons (UHC). It would, therefore, be a challenging task to reduce also the UHC and CO emissions at the same time as the NO_x emissions are lowered. Hence, in this study it is assumed that the emissions of CO and UHC are retained at the 2001 values for all technology levels.

To sum up, the assumptions for SFC reduction are very conservative, reductions for the NO_x emissions for the conventional technology might be low, and reductions for aerodynamic drag and structure weight may also be somewhat on the low side.

[10] The numbers on $EINO_x$ are given related to the NO_x emissions of kerosene in 2001, i.e. 0. This also applies to Cryo 2.

5.3.3.2 Aircraft Design Process

Before technology improvements may be applied to the different aircraft configurations, a basic version of each of these, representing the technology level of today, are created. The conventional aircraft are re-designed in the sense that the maximum take-off mass (MTOM) is adjusted to achieve payloads and ranges as recommended by SAS. This modification may involve a slight fuselage lengthening in order to accommodate the required number of passengers. The wing configuration of each aircraft is, however, kept constant regardless of the technology level.

In Oelkers and Prenzel (2001) the cryoplane configuration (CMR1-300) is designed to reflect a technology level of 2010, which implies that the total drag, aircraft weight and SFC of the engines (basically the V2527-A5) are slightly decreased compared to the general levels of 2001. Hence, these levels need to be restored to the levels of 2001. In order to find a sensible cryoplane configuration for the larger of the two studied aircraft, a new configuration is created, implying that the fuselage is stretched and the wing size is up-scaled. The larger version is denoted CMR1-400. The wing size is found by an optimisation process (using Piano) using the original technology level (2010) for a range of 4000 nautical miles, with a fixed wing shape (fixed sweep and aspect ratio). Before the scenario aircraft can be designed, the technology level is restored to the level of 2001. The wing size is kept unchanged when the aircraft are re-designed for the shorter ranges required in this study, 2000 and 3000 nm, for the CMR1-300 and the CMR1-400 aircraft, respectively.

Having found reasonable configurations for the aircraft needed in the transition scenarios, the technology improvements are applied, i.e. the total drag and the weight (of fuselage and wing box) are decreased according to the technology levels defined in Table 5-3. Reduced drag and weight either increases range or reduces fuel burn, with the latter leading to reduced MTOM. In this study, the MTOM is adapted to obtain the proper range. With a lower take-off weight, a smaller take-off thrust is required for the same take-off performance. Therefore, the aircraft is re-optimised with the engine thrust and the MTOM allowed to vary. Then a take-off thrust 20% larger than the optimum is used as a safety margin to ensure that no engine deterioration will prevent the aircraft from taking off within the allowable field performance. Finally, the proper MTOM is found with the proper engine thrust.

Table 5-4 below presents an overview of the main characteristics of all aircraft combinations that are used to quantify the fuel requirement and the emissions for each transition scenario.

Table 5-4. Main characteristics of aircraft combinations used in the transition scenarios.

Aircraft type	Technology level	Engine thrust [kN]	MTOM [kg]	Fuel for climb, cruise and descent [kg]
B737-600	0	79.2	54 200	4414
B737-800	0	96.6	66 800	5498
A321-100	0	143.1	83 200	6876
	Conv 1	132.9	78 600	6136
	Conv 2	116.9	73 800	5318
	Conv 3	104.5	69 900	4821
A330-200	(0)	212.9	143 000	14 532
	Conv 1	193.7	134 500	12 987
	Conv 2	170.3	125 500	11 521
	Conv 3	149.0	117 900	10 501
CMR1-300	(0)	169.3	98 800	2866
	Cryo 1	152.0	92 100	2492
	Cryo 2	144.0	84 000	2106
CMR1-400	(0)	203.9	118 000	4648
	Cryo 1	182.6	110 000	4039
	Cryo 2	154.9	98 900	3316

5.3.3.3 Results

In Figure 5-10 and Figure 5-11 the fuel consumption for the low- and high-growth passenger scenarios, respectively, are shown. Figure 5-12 to Figure 5-14 show emissions of CO_2, H_2O and NO_x of the low-growth scenarios. The corresponding emission figures for the high-growth scenarios are not shown, since they do not give any new information. The trends are the same; the only difference is that the changes occur earlier, owing to the high-growth rate in the beginning of the period. Fuel consumption and emissions are calculated using SAS's timetable of 6 June 2001. This day is believed to be representative of the average daily fuel consumption of SAS's domestic fleet [Näs, 2001]. There will, however, be some periods of reduced traffic on some routes; hence, the fuel consumption and emissions presented are slightly higher than the daily average. The aircraft types that are used when the emissions are calculated are presented in Appendix D.

Without introducing any cryoplanes, the daily fuel consumption is estimated to increase from about 320 000 kg in 2001 to about 950 000 kg in 2050 (Figure 5-10). This implies a threefold increase in fuel consumption during this period of 49 years. Simultaneously the number of passengers has increased 3.6 times (Figure 5-1), and the number of movements has increased 1.8 times. Thus, the fuel consumption has increased more than the movements, caused by using larger and larger aircraft types. It could also be observed that the increase in fuel use is lower than the increase in passengers, which is a consequence of technology improvements. When comparing the absolute numbers for kerosene and LH_2 use, it needs to be pointed out that the numbers for kerosene represent the total amount of fuel that needs to be supplied, divided on all Swedish airports that

are involved; whereas the numbers given for LH_2 refer to the amount that needs to be supplied at Arlanda only, since this is the only refuelling station for hydrogen.

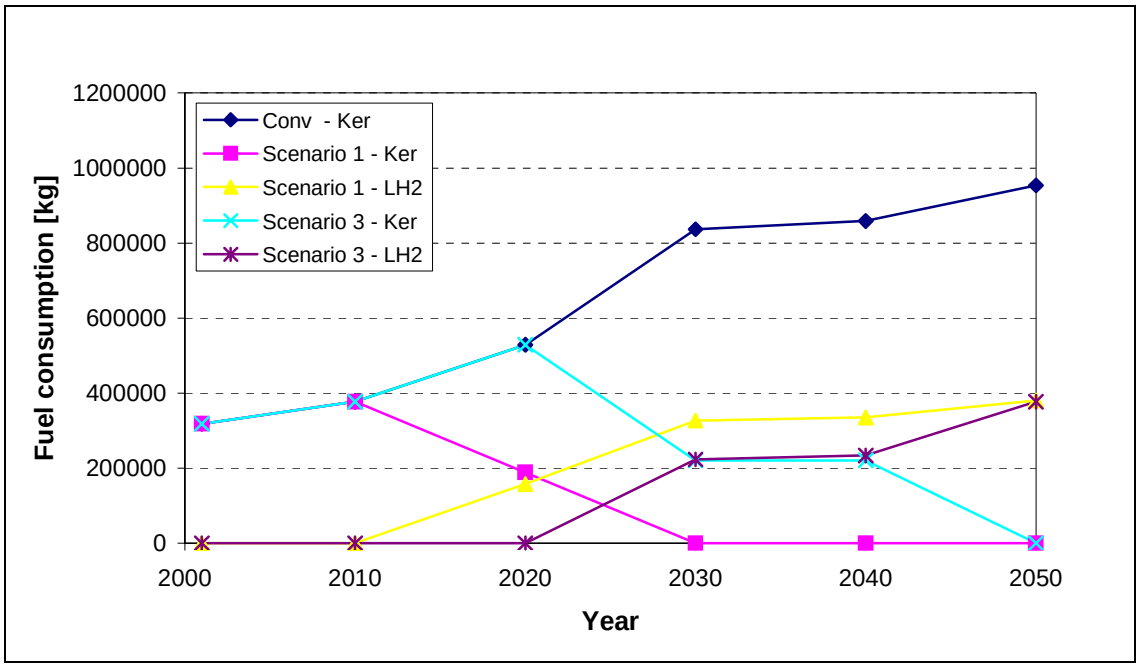

Figure 5-10. Daily consumption of kerosene and LH_2 for the low passenger growth scenario.

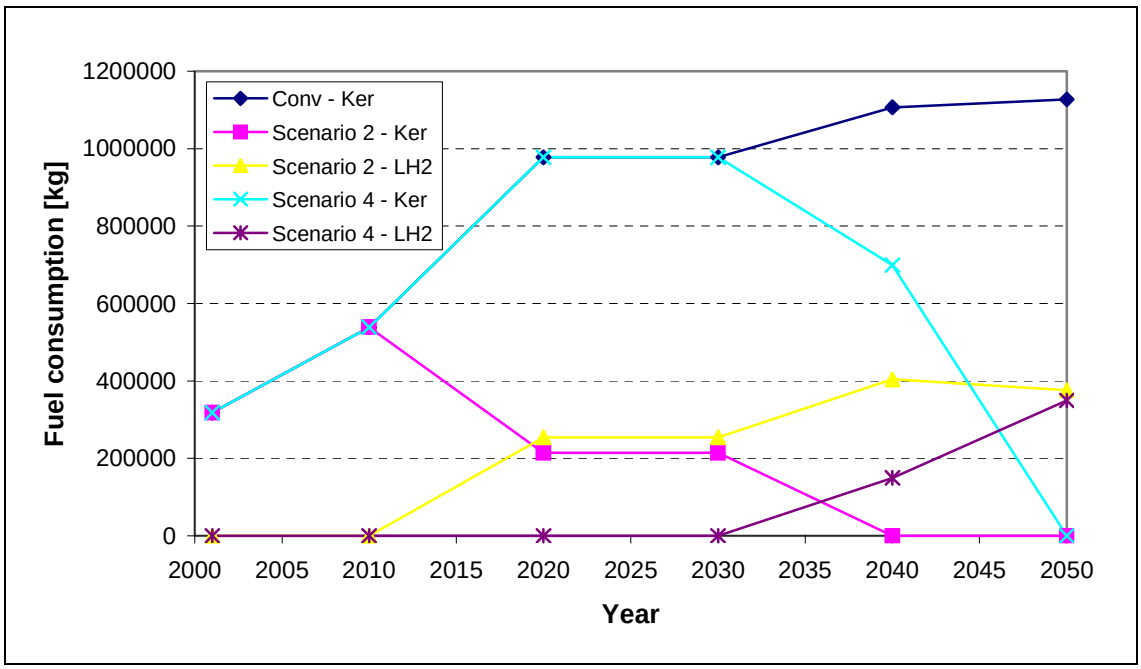

Figure 5-11. Daily consumption of kerosene and LH_2 for the high passenger growth scenario.

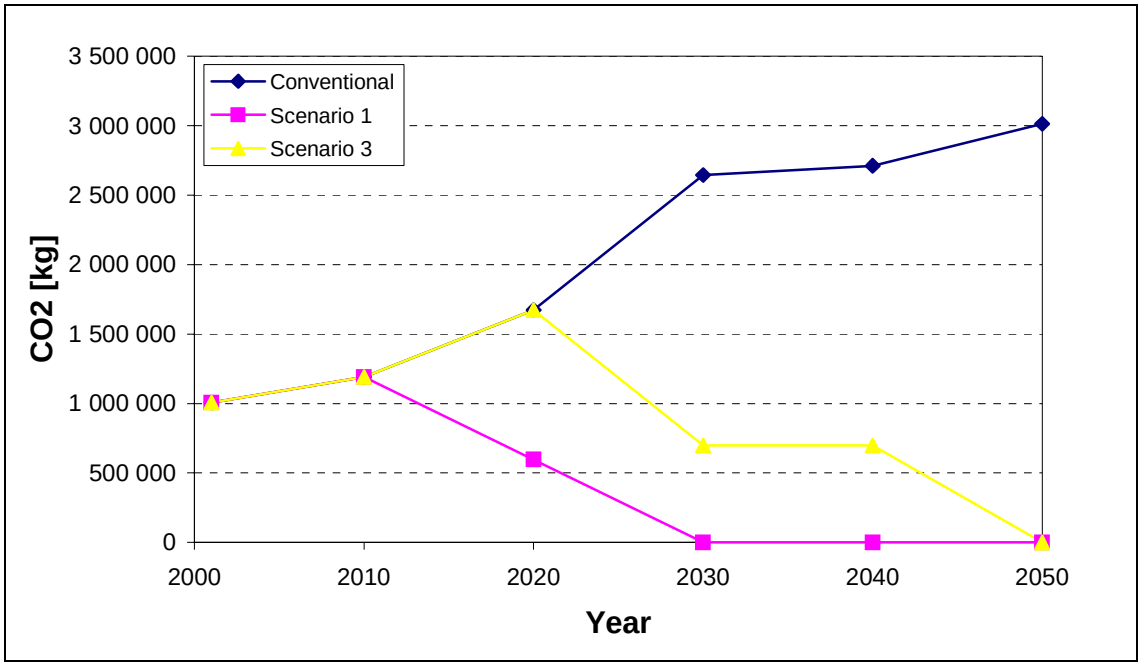

Figure 5-12. Daily emissions of CO_2 for the low passenger growth scenario.

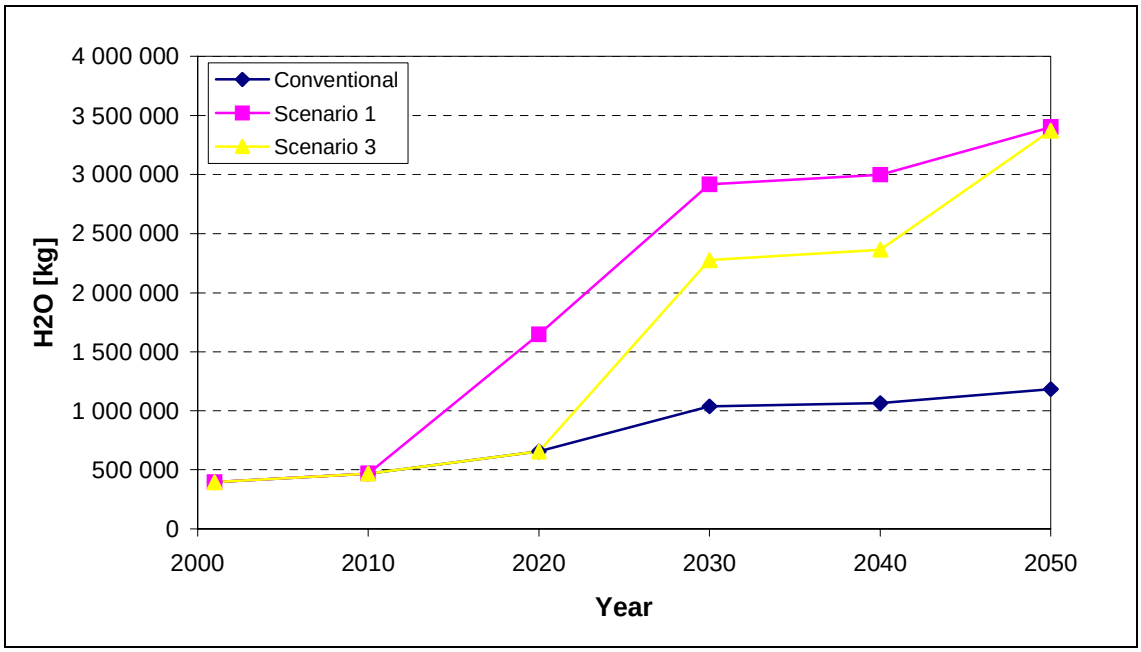

Figure 5-13. Daily emissions of H_2O for the low passenger growth scenario.

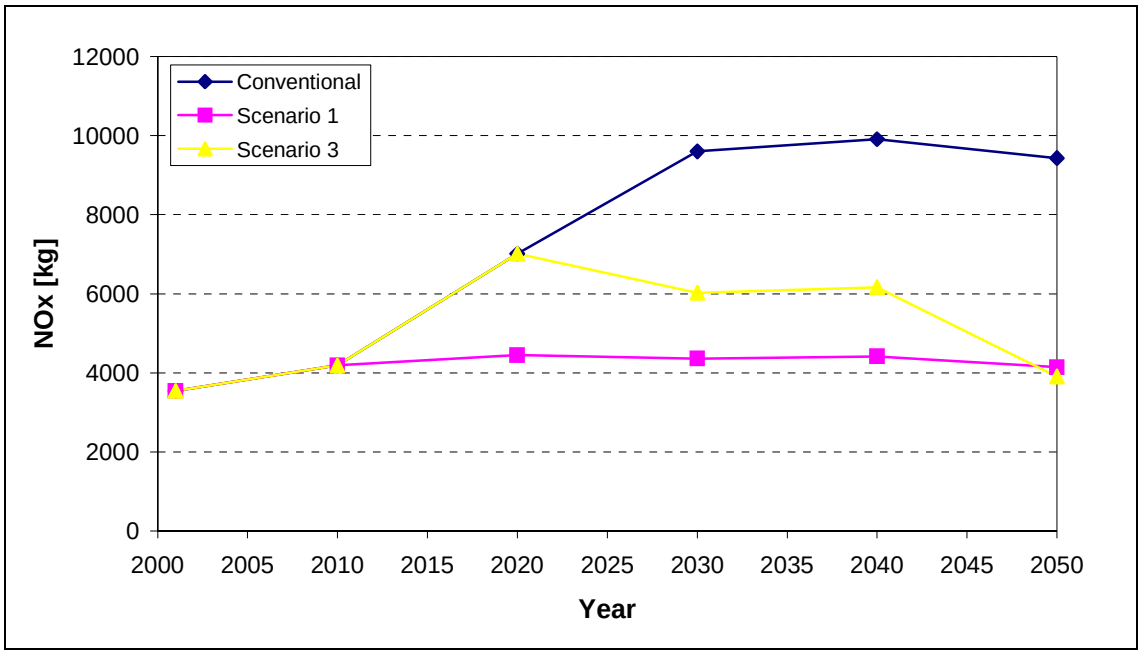

Figure 5-14. Daily emissions of NO_x for the low passenger growth scenario.

The kerosene consumption drops when the cryogenic fuel is introduced, finally falling to zero at the end of the period, 2050, for all scenarios. As to the demand for LH_2, it increases from zero in 2015 or 2025 depending on the scenario to almost 400 000 kg a day in 2050 (in Figure 5-10 and Figure 5-11 it appears that LH_2 is needed from 2010 and 2020, respectively, but this is due to the situation that only values every tenth year are used when drawing the curves). In general, the higher growth rate implies that the introduction of new aircraft types is needed earlier; hence, more generations of aircraft will be involved by 2050. A high growth rate, therefore, results in a more modern aircraft fleet at the end of the period than does the low-growth rate. This is the reason why the demand for hydrogen is roughly the same in 2050 for the low- and high-growth scenarios, even though the high traffic growth rate results in a larger aircraft fleet in 2050.

According to Figure 5-12 and Figure 5-13, the emissions of CO_2 and H_2O follow the same trends and have the same percentage changes as does the fuel consumption. This was expected, since these emissions are proportional to the fuel consumption. Note, however, that whereas the CO_2 emissions diminish when cryoplanes are introduced, the H_2O emissions increase. This is due to the fact that a cryoplane emits about 2.6 times more water than a conventional aircraft, provided that they consume the same amount of energy.

By introducing cryoplanes early, according to scenario 3, the amount of NO_x may be retained at a level not much higher than today's level (Figure 5-14). If a conventional fleet scenario is assumed, the NO_x emissions will be about 2.8 times higher in 2050 than in 2001.

Other emissions of kerosene-powered air traffic, such as CO, UHC, soot and SO_x, are not shown in any figures, but since cryoplanes emit none of these, these emissions will drop off in a manner similar to CO_2 when cryoplanes are introduced.

For the domestic traffic of SAS with the assumptions made in this study, it may be concluded from the figures that a delay in the introduction of cryoplanes would result in a lagging in emissions reduction that is larger than the delay in their introduction, i.e. starting to introduce cryoplanes in 2025 instead of 2015 would mean that it takes more than ten years for the emissions to be at the same level as those of the aircraft fleet that would be introduced in 2015.

Having defined the consequences of the different scenarios in terms of fuel consumption, the fuel sources at Stockholm/Arlanda airport are considered next.

5.4 Fuel Sources at Stockholm/Arlanda Airport

This section gives an overview of current conditions at Arlanda airport, deals with implications for the airport of using liquid hydrogen and describes different methods for hydrogen production.

5.4.1 Current Conditions

Arlanda is the largest airport in Scandinavia and Europe's sixth largest airport. During 2000 18.3 million people travelled to or from Arlanda; two out of three travelled on international flights [SCAA, 2002]. It is considered to be one of Europe's most modern airports, having, for instance, a high-speed railway to central Stockholm and a new 80-metre control tower featuring the world's most PC-based air traffic management system. Since the latter part of 2002, when a third runway was taken into operation, there are now three runways in use.

Currently, the kerosene is transported by trucks from a harbour in Stockholm (Värtahamnen) to Arlanda airport. About 40 trucks a day are normally in service. In the future, the fuel distribution system will probably be changed, such that the fuel will be transported by rail from Gävle harbour (about 200 km north of Stockholm) to Brista (about 5 km north of Stockholm). From here it will be piped to Arlanda. At Arlanda the fuel is stored in tanks located 2-4 km south of the gates and about 1 km from the closest runway, which is well beyond the 305 meters that is suggested as a safety distance in case of any aircraft accident [Sefain and Jones, 2001]. The fuel is stored in four tanks, in total giving a storage capacity of 20 000 m^3 (Figure 5-15). From the tanks the fuel is pumped in buried pipelines to the gates, i.e. hydrant system. At the gates the fuel is taken from pits (Figure 5-16) and passed via a dispenser truck (Figure 5-17) that cleans the fuel before it enters the aircraft tanks. The majority, about 85%, of the fuel is provided in this way; the other 15% is provided by tankers, which are equipped with cleaning facilities.

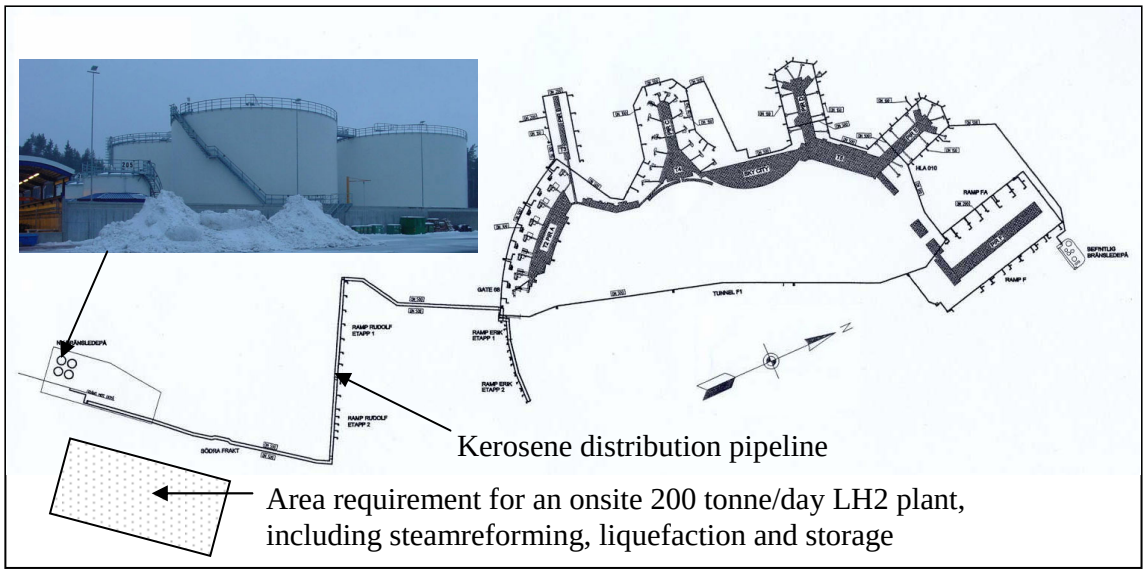

Figure 5-15. Current kerosene distribution system at Arlanda airport. For comparison the area requirement for a SMR plant producing 200 000 kg LH_2/day is shown [Bracha, 2002a] (see section 5.4.3.3). Photo by Michael Bracha, 2002, Linde Gas, Germany.

Figure 5-16. A pit where fuel is taken for refuelling. Photo by Michael Bracha, 2002, Linde Gas, Germany.

Figure 5-17. Dispenser truck in operation during refuelling. Photo by Michael Bracha, 2002, Linde Gas, Germany.

Arlanda airport covers a large area of about 32 km^2, and there are plans that another 25 km^2 will be occupied in the future. Additional buildings, such as a cargo terminal and a large post terminal, are planned to be built, but considering the large unused areas, there should still be areas left for new facilities.

The current total consumption of electrical energy, used for lighting, computers, etc., at Arlanda is about 160 GWh/year. This amount could be enlarged to 1095 GWh without any modifications of the electrical network.

5.4.2 Special Requirements and Infrastructure Changes Needed for Operation of Cryoplanes

There are a number of measures that need to be taken to ensure that the safety level at the airport is maintained when changing to hydrogen fuel use. Since hydrogen is a colourless and odourless gas, new safety detection equipment would be required. At any airport, vehicles used for the various ground support activities, such as towing aircraft, cleaning, catering and galley service, are required. In general these are powered either by diesel or spark ignition engines. In order to avoid a fire hazard, spark ignition engines should be avoided. A solution would be to provide the spark ignition engines with spark-arrestors, but better would be not to use any vehicles powered by such engines at all near cryoplanes or their fuel infrastructure. At Arlanda the majority of the vehicles in use are diesel-powered; hence, this requirement would not cause any major measures to be taken.

A pleasing and feasible solution to this constraint would be to power all airport vehicles by fuel cells powered by hydrogen. This would be very convenient, since the infrastructure and production facilities are already there and easily accessible. One obstacle for fuel cell-driven vehicles today is their limited range, but this is a limitation that does not have any relevance at an airport. Moreover, it would eliminate the pollutant emissions at and around the airport, thereby significantly improving the working environment for the personnel who are working at the ramp.

Using hydrogen for aviation would also involve the personnel who are working at the airport, such as in the training of new emergency and personnel safety procedures for all ramp personnel.

Largely, the required changes have to do with the refuelling procedures. Since hydrogen is a cryogenic fuel, what really needs to be changed is the interface between the fuel supplies and the aircraft fuel tanks, as well as most of, if not all, the fuel system components [Sefain and Jones, 2001]. A question that arises is what to do with the boil-off of hydrogen. Preferably, this could be compressed and used as fuel for H_2-buses operating at the airport. In fact, this is what is presently being done at Munich airport in Germany where a small infrastructure for hydrogen and liquid hydrogen production has been established, powering cars and busses operating at the airport [Bracha, 2002a]. This implies that H_2 recovery lines need to be established.

The intention is that the hydrogen should be distributed in a way similar and parallel to that of the kerosene. For several decades there needs to be infrastructure for handling both kerosene and hydrogen. The hydrogen should be liquefied and stored in the vicinity of the current kerosene storage, and transported to the aircraft by pipelines in a similar manner as for kerosene (see Figure 5-15). The overall airport layout and procedures do not need to be changed, and the aircraft can be refuelled at gate positions exactly like conventionally-fuelled aircraft, thus guiding and gate operating systems can remain the same.

Considering general safety aspects of handling and using hydrogen for aviation, studies have shown that the overall safety level is at least as high as when using kerosene [Sefain and Jones, 2001; and Schmidtchen and Geitmann, 2001]. According to Schmidtchen and Geitmann (2001), future hydrogen aircraft might even be safer than today's aircraft, if recommended additional precautions are realized. It will, however, involve other safety considerations. There is no reason to change the overall airport layout. Such changes would increase costs of infrastructure build-up unnecessarily. For instance, fuelling at isolated locations would probably yield excessive turn-around times, and it would require a system of taxiways.

In order to avoid that any combustible mixture of hydrogen and air occurs, tanks need to be purged prior to refuelling by an inert gas that does not liquefy upon exposure to LH_2 [Sefain and Jones, 2001]. Only a few inert gases fulfil this requirement, and amongst them, helium seems to be the most feasible one. Therefore, additional facilities handling helium, such as storage tanks and pipes, are required at the airport. The storage may be located quite close to the gates, since there are no safety risks with such storage. Connections to all aircraft refuelling places, as well as to the maintenance area, need to be established.

One important challenge of introducing cryoplanes is maintaining turn-around times as close as possible to current schedules. What undergoes the most change is the refuelling process; changes in the rest of the turn-around activities are small in comparison. Mainly owing to the higher volume of liquid hydrogen compared with kerosene, this process will be longer (in the order of twice as long). In spite of this, the refuelling time is not judged to be a critical factor (affecting the turn-around time) for cryoplanes, since it may be performed whilst other turn-around activities are being performed [Sefain and Jones, 2001]. Instead the embarking/disembarking of passengers and cleaning operations, which are the most time-consuming activities, are considered to be the critical path. These are operations that are not expected to change significantly when going to hydrogen. Neither for conventional aircraft does the refuelling process constrain the turn-around time. No significant changes on turn-around times are therefore expected with cryoplanes.

To sum up concerning the airport infrastructure, the demand for new facilities for conversion to operation of cryoplanes is evident; however, the changes required at the airport seem to be practicable and no major obstacles are expected. These conclusions are in line with conclusions drawn in other previous studies on the subject [Schmidtchen and Geitmann, 2001; and Hoyt, 1976].

5.4.3 Methods for LH_2 Production

Considering the technologies for hydrogen production that are feasible at present, there are a number of technologies, both renewable and fossil-based, that may be adopted. As time goes on, these technologies are probably made more effective, and new ones are developed. For instance, using sunlight to produce hydrogen offers large environmental benefits, especially if the efficiency of the process could be improved and the costs could be lowered. Gasification of biomass and electrolysis of water are methods that may be based on renewable energy sources. Gasification of biomass involves hydrogen being extracted from hydrocarbons, originated in a renewable energy source, by a gasification process. This process is always renewable. Electrolysis of water means that water is decomposed into hydrogen and oxygen by letting an electric current run through water. In order to state whether this method is renewable or not, one needs to know how the electric energy is produced. It could be produced from renewable energy sources, such as wind, water, solar, geothermal or biomass, but it could also be produced from fossil sources, such as oil, coal or gas.

As to the fossil-based LH_2 production methods, the feedstocks are hydrocarbons, such as gas, coal or residual oil and water. The products are hydrogen and other by-products, for instance, the greenhouse gas CO_2. Steam Methane Reforming (SMR), which uses methane from natural gas and steam as feedstocks, is the most efficient, cost-effective and widely used hydrogen production method.

Comparing the different methods for hydrogen production in terms of efficiency and costs, the fossil-based are the more favourable. In general, the fossil-based methods have the highest overall efficiency for liquid hydrogen production and delivery. It is estimated to be around 40% for biomass and just over 50% for fossil fuels, with gas having the highest of about 53% [Schnieder and McKay, 2001]. The fossil-based methods are also more cost-effective than the renewable ones to install. For a plant producing 50 000 kg/day, the investment of a SMR plant is about one-third of an electrolysis plant and about one-fifth of a biomass gasification plant [Bracha 2002a]. In terms of cost per GJ produced liquid hydrogen, Schnieder and McKay (2001) assess that solar- and wind-based hydrogen production from electrolysis is unlikely to be competitive with biomass or fossil fuels for many decades. Steam methane reforming would require the smallest amount of ground area for the plants. According to Bracha (2002b) each plant occupies about 2 000 m^2, whereas an electrolysis plant and a biomass gasification plant occupy 8 000 and 16 000 m^2, respectively.

Sarigiannis and Kronberger (2001) examined different renewable-based methods for producing hydrogen by carrying out Life Cycle Assessments (LCAs) of the technological system. All are based on producing electricity by a renewable energy source and then producing hydrogen by electrolysis of water. They concluded that wind and hydropower energy sources lead to very low emissions, even for long distance transports. Biomass also leads to low emissions of greenhouse gases, provided that the biomass is produced locally, thus avoiding transportation. Extensive transportation could lead to large amounts of emissions that contribute to acidification as well as to smog formation.

From Figure 5-10 and Figure 5-11 it was concluded that the amount of liquid hydrogen that needs to be produced varies from zero in 2015-2025 to about 400 000 kg/day in 2050. Therefore, the production capacity should be continuously increased, starting with a module capacity of 50 000 kg/day, and end up with eight modules each producing 50 000 kg/day in 2050. The minimum storage capacity for each module is two tanks, one being constantly filled and the second one being in supply operation. A storage volume corresponding to an average day of LH_2 consumption is reasonable to install as a minimum. However, as more modules will be added within a reasonable time, it is sensible to start with larger and more tanks. Furthermore, having more modules will give more flexibility. Having three tanks would imply that one may be used for filling, one for consumption and the third one for peak shaving and to cover plant failure demand [Bracha, 2002b]. With respect to the demand of SAS's domestic traffic, it would be reasonable to start with a capacity of three to four tanks of 1500 m^3 each. This would be enough for the demand in 2050.

In addition to the regular production facilities for liquid hydrogen at Arlanda, mobile refuelling facilities are required. These are required if an aircraft for some reason would land at an airport other than Arlanda without enough fuel for the return trip. The most economical and efficient mobile supply would probably be using LH_2 containers transported via rail. At airports where no railway connection is established, trucking the LH_2 is probably the most sensible way to transport the fuel.

Three different methods for the hydrogen production at Arlanda, namely, electrolysis of water, gasification of biomass and SMR (conventional method) are considered. The liquefaction process, which is needed independently of the hydrogen production, is also addressed.

5.4.3.1 Electrolysis of Water

Using electrolysis of water would have the very large benefit that the hydrogen could be produced from any energy source; preferably from renewable ones, but it could also be produced from fossil resources. The method requires large amounts of desalted water, and above all, electrical energy. Consumption data for the electrolysis plant are given in Table 5-5 and for the liquefaction plant in Table 5-6. In addition to the data given in Table 5-6, instrument air and city water are needed. The electrolyser and liquefier would need about 1.14 TWh/year per module of 50 000 kg/day. This is about seven times the consumption of electrical energy today at Arlanda and less than one percent of the total net supply of electricity in Sweden in 2000, which was about 160 TWh [SCB, 2002]. In 2050 when SAS's domestic fleet, according to the scenarios, will be operated on hydrogen, solely, eight times this amount will be required, i.e. 9.2 TWh/year.

Table 5-5. Consumption data for an electrolysis plant producing 50 000 kg/day [Kronberger, 2002].

Electric power	105 MW
Water	28 m^3/h desalted water (efficiency: 80%)

Table 5-6. Consumption data for a liquefaction plant producing 50 000 kg/day [Allidieres, 2002].

Main electrical power	25 400 kW (95% para[11] H_2)
Utilities/Control electrical power	155 kW
Cooling water (ΔT 10°C)	4000 m^3/h
N_2 (gaseous)	90 kg/h

In order to get an understanding of the amount of electrical energy that would be required to fuel the complete aircraft fleet operating at Swedish airports in 2050, the amount required for the Swedish domestic traffic of SAS's fleet are up-scaled. This is a very rough estimation, but it still gives some useful information. SAS's domestic fleet makes up about 70% of the total domestic and about 35% of the total traffic, including both the domestic and the international traffic that arrive at or depart from Swedish airports. In doing this assessment, it is assumed that the concept of using hydrogen for aviation is spread all over the world; hence, hydrogen refuelling facilities are available at the arrival/departure airports outside Sweden. Likewise, it is assumed that the average flight distance for the international routes is as long as the average flight distance for the domestic flights. In reality the average international flight is somewhat longer. This limitation will result in a slightly underestimated fuel consumption. However, this effect might be compensated for by the rather conservative technology improvements assumed for the aircraft fleet, which are to reflect new technology and more efficient aircraft with time.

Based on the traffic growth figures and technology improvements with time presented earlier, the amount of electrical energy needed to power all aircraft refuelling with liquid hydrogen in Sweden in 2050, produced by electrolysis of water, would be about 20 TWh. This is about 12% of the total net supply of electricity in Sweden in 2000 (160 TWh). In 2050 the electricity production will be considerably larger than in 2000, but still the comparison gives some indication of the magnitude of the required electrical energy in order to completely use hydrogen for aviation. In order to calculate this value, today's efficiency of producing LH_2 is used. If electrolysis of water is still the most feasible way of producing hydrogen in 2050 (which from the author's point of view seems unlikely), the efficiency of the process probably will be higher, thus reducing the requirement of electrical energy.

Next, one needs to ask whether these amounts of electricity are reasonable and from where the additional electricity will come. Today, the electricity in Sweden comes mainly from hydropower and nuclear power, and is therefore more or less free from greenhouse gas emissions. To be more specific, the total gross supply of electricity in 2000 was 163.3 TWh, based on 48.1% hydropower, 35.0% nuclear power, 5.4% conventional thermal, 0.3% wind-power and 11.2% imported power [SCB, 2002]. However, if a considerably extra amount of electrical energy would be required, the hydropower and nuclear power would not be able to deliver this without extending the facilities, since they are operating at almost full capacity already [Söder, 2002]. Instead,

[11] Para refers to the spin of the hydrogen molecule. There are two possible states: para and ortho hydrogen. At atmospheric conditions there is a mixture of 25% para and 75% ortho hydrogen. In the liquid state the equilibrium is almost 100% para hydrogen (Bracha, 2002b).

there is a risk that the additional power would be imported from sources that probably are not renewable-based. Thus, the electrical energy would be less “clean”. It is therefore important that the renewable sources, such as wind, solar and biomass are extended in Sweden parallel to the implementation of cryoplanes.

Expanding the hydropower would also be an acceptable solution from a global warming point of view. However, mostly owing to the disturbance of the local ecology and the exploitation of unspoiled countryside, no extension of hydropower is at present planned to take place in Sweden. If the airlines could assert that they only produce hydrogen from renewable energy sources, they would gain much goodwill. One possible way to obtain that would be for the aviation industry to support the development of renewable energy sources.

5.4.3.2 Gasification of Biomass

Biomass could either be used as a primary energy source for electricity production, which is utilised for hydrogen production via electrolysis, or the hydrogen could be extracted from the biomass by a gasification process. The latter technology, however, needs further development before it may enter the commercial market. Owing to the very large supply of biomass in Sweden (more than half of Sweden’s area is covered by forest), using biomass for hydrogen production seems an attractive solution.

A biomass gasification plant producing 50 000 kg/day consumes 490 000 kg biomass per day (dry basis), resulting in 179×10^6 kg biomass per year [Kronberger, 2002]. In 2015 one such plant would be enough, whereas eight would be needed in 2050. In a similar manner as the amount of electricity required to produce all hydrogen by electrolysis of water, the amount of biomass required is estimated. Taking into account the part that SAS’s domestic traffic makes up, the amount of biomass to power all traffic refuelling in Sweden in 2015 and in 2050 is estimated to be 386×10^6 and 3.087×10^9 kg (dry substance)/year, respectively. In order to compare these numbers to the biomass supply in Sweden today and in the future, the mass requirement is transformed to the energy unit TWh. If it is assumed that all the biomass is logging residuals with 40% moisture content, the heating value is about 4.9 kWh/kg (dry substance) [Lantz, 1996]. Using this value, the energy requirement in terms of biomass in 2015 and in 2050 would be 1.9 and 15.1 TWh/year, respectively.

In 1999 the total use of biomass, including biofuels, peat, etc., in Sweden was a little more than 90 TWh [Swedish Energy Agency, 2000]. Taking ecological considerations into account, the biomass supply may be expanded to about 200 TWh/year by 2020 [Svebio, 2002]. Of this amount 120-130 TWh/year would be wood fuel [Parikka, 1997 and Svebio, 2002]. Comparing the amount of energy, in terms of biomass, that would be required to power all aviation refuelling in Sweden with hydrogen, with the potential of biomass supply in Sweden, it may be concluded that the amounts that the aviation would need are not unreasonably large. However, it requires that the biomass use would be enlarged.

5.4.3.3 Steam Methane Reforming (SMR)

Steam methane reforming is based on the fossil resource natural gas and therefore is, from an environmental perspective, not preferable in the long run. At present, there is no supply of natural gas in the Stockholm region, and the closest pipeline is located in Gothenburg, about 400 km southwest of Stockholm. If there should be a pipeline established in the future this method could, if necessary, be used as an intermediate method before renewable methods have been improved, expanded and made more cost-effective. A way to avoid CO_2 emissions and still use SMR would be to extract the CO_2 in the process and sequester it in deep reservoirs or utilise it, for instance, in the chemical industry. This would make the method more expensive, but it might still be economically competitive with renewable-based production methods.

In addition to natural gas, SMR requires electrical power (Table 5-7). Having such a plant and a liquefier in operation one year would consume about 229 GWh, which would mean that the consumption would be about 2.4 times higher than currently at Arlanda. Related to the net total supply of electricity in Sweden in 2000 (160 TWh), the consumption is 0.2%. So, the requirement of extra electrical energy would not be any obstacle, not even at the end of the considered period when eight modules would be required. The electrical network at Arlanda would need to be increased in terms of capacity when several modules are taken into operation.

Table 5-7. Consumption data for a SMR plant producing 50 000 kg/day [Bracha, 2002a].

Natural gas	9800 Nm^3/h
Demin water	10 700 kg/h
Cooling water (ΔT 10°C)	520 m^3/h
Electricity	640 kW
Instrument air	Approx. 140 Nm^3/h
Export steam	12 800 kg/h

5.4.3.4 Conclusions and Discussion Concerning LH_2 Production

In the very long term, aviation, just as the energy and other transportation sectors, needs to move away from fossil-based energy sources. When introducing cryoplanes in aviation, with the primary goal of reducing emissions of greenhouse gases, it would be preferable to use renewable energy sources to the largest possible extent.

Today, steam methane reforming is the most commonly used, efficient and cost-effective method to produce hydrogen. However, since it is based on a fossil energy source it is not a preferable method in the long run. Under a transition phase it might be reasonable to employ this method to reduce production costs, particularly if the CO_2 is extracted and sequestered in reservoirs or utilised. The method does require electrical energy, but not a significant amount when compared with the total electricity production in Sweden.

Looking at possible renewable production methods viable in the near future, electrolysis of water and gasification of biomass are promising technologies. The amount of

electrical energy needed to power all aircraft refuelling in Sweden in 2050, using liquid hydrogen produced by electrolysis of water, would be about 20 TWh. This is considerably much, but not any unreasonably large number, particularly if one considers that today's technology level of LH_2 production is used when deriving this number.

In 2050, the technologies for hydrogen production will probably be considerably improved compared to today, and some will possibly be driven out of competition by other more efficient ones. However, development and extension of renewable energy sources parallel to the introduction of cryoplanes is important to make sure that no or very little fossil-based energy is used for the LH_2 production. Gasification of biomass is also a feasible alternative for hydrogen production; particularly when observing that Sweden owns a large supply of biomass. Given the estimated biomass supply in Sweden in 2020, about 8% of that would be required to power all civil aviation refuelling with hydrogen in Sweden in 2050. The most feasible renewable energy sources to extend in Sweden are probably biomass and wind-power.

In the very long run there are likely to be sustainable hydrogen production methods available which are in the early phase of research and development today. Hydrogen production in photochemical and photobiological systems using sunlight are examples that probably will offer large environmental benefits in the future if successfully developed.

It is clear that powering civil aviation with hydrogen does not necessarily imply that all emissions of greenhouse gases are eliminated, since greenhouses gases may be emitted during the hydrogen production process. However, it is a step away from the oil dependence and it offers the possibility of using renewable energy sources for aviation. This is impossible as long as kerosene is used.

5.5 Conclusions and Discussion

This chapter embodies an exploration of the feasibility, potential and consequences of introducing a liquid hydrogen-fuelled aircraft fleet on a regional scale. According to the traffic growth scenarios applied here, the number of passengers will increase three to four times by 2050. During the same time period, the number of movements will have increased, but by less than the number of passengers, due to the larger aircraft types that will have commenced on the domestic market. Depending on the scenario, the number of movements will have increased by 70-90%. Hence, it may be concluded that an essential increase in airport capacity, at all airports, is required to cope with the increasing traffic demand assumed here.

Based on the two different prerequisites, saying that all new aircraft introduced in 2015 and in 2025 and afterwards, respectively, should be cryoplanes, four different scenarios are compiled. In all scenarios, it is reasonable to change to a fleet powered solely by liquid hydrogen by 2050. A high traffic growth rate results in a delayed broad-scale introduction of cryoplanes. In general, the higher growth rate implies that the introduction of new aircraft types is needed earlier, and hence, more generations of aircraft would be involved by 2050, and a more modern fleet would be in operation at that time.

By starting to introduce cryoplanes in 2015, the amount of NO_x may be retained on a level not much higher than today's level, provided that the emission indices of NO_x for the hydrogen engine are reduced by 70-85%, depending on the technology level, compared with a conventional engine of 2001. If a conventional fleet scenario is assumed, the NO_x emissions will be about 2.8 times higher in 2050 than in 2001. The effect on the NO_x emissions for conventional aircraft is obtained by assuming a reduction potential in NO_x emission index of up to 50% (which might be slightly too conservative).

Regarding the changes needed at the airport when using hydrogen, there are a number of measures that need to be taken to ensure that the safety level at the airport is preserved. In order to avoid a fire hazard, spark ignition engines should be avoided. A pleasing and feasible solution would be to power all airport vehicles by fuel cells powered by hydrogen. The overall airport layout and procedures do not need to be changed, and the aircraft can be refuelled at gate positions exactly like conventionally fuelled aircraft. Largely, the required changes have to do with refuelling procedures. Since hydrogen is a cryogenic fuel, what really needs to be changed is the interface between the fuel supplies and the aircraft fuel tanks, as well as most of, if not all, fuel system components. However, the intention is that the hydrogen should be distributed in a way similar and parallel to that of the kerosene. Hence, ignoring the cost implications, from an infrastructure point of view, it seems feasible to change to hydrogen use. No significant changes on turn-around times are expected with cryoplanes.

Taking the local conditions into account, with respect to the availability of energy, it would be reasonable to change from kerosene to LH_2 as fuel for all civil aviation refuelling in Sweden, according to the scenarios compiled in this study. However, development and extension of renewable energy sources parallel to the introduction of cryoplanes is important to make sure that no or very little fossil-based energy is used for the LH_2 production. If electrolysis of water or gasification of biomass would be used for the LH_2 production, considerable amounts of electrical energy and biomass sources, respectively, would be required, but not unreasonably much.

It is worth mentioning that the cost penalty of changing the fleet to use LH_2 is not assessed in this study. In order to cover fully the implications with respect to costs of changing the fleet, several aspects comprising difficulties need to be addressed. As the scenarios stretch several decades ahead and as most of the technologies need further development, it is crucial to assess the costs of all new facilities. Moreover, to make a fair comparison between cryoplanes and conventional aircraft, future price trends of kerosene need to be taken into account. The price of kerosene will rise in the future, both due to dwindling oil resources and possibly due to future taxation on fossil fuels (or CO_2 emissions). As discussed in the introduction (section 1.3), prices of kerosene and hydrogen far ahead in the future are very difficult to assess. Besides, to fully understand the cost implications of introducing hydrogen in aviation, other sectors, such as the other transportation sectors and the power industry, should be considered as well. Possible co-ordination benefits could have a significant effect on the cost penalty. A study addressing these issues is beyond the scope of this thesis.

6 CONCLUSIONS, DISCUSSION AND RECOMMENDATIONS FOR FURTHER WORK

In this final chapter the major conclusions drawn in the thesis are summarised and discussed (section 6.1). In addition, a number of recommendations for further work are stated (section 6.2).

6.1 Conclusions and Discussion

As set out in the beginning (section 1.6) the overall objective of this thesis is to evaluate the potential of reducing the environmental impact of civil subsonic aviation by changing the source of energy from kerosene to the energy carrier hydrogen. In addition, the practical and technical feasibility of introducing hydrogen as fuel is investigated. In summary the objectives are the following:

- Estimate the effects of using hydrogen on aero engine pollutant emissions, performance and design.
- Identify the optimum cruise altitude for two equivalent medium-range aircraft, one kerosene-fuelled and one LH_2-fuelled, from an environmental point of view.
- Provide guidance on how to design hydrogen-fuelled aero engines for medium-range aircraft, either for minimum mission fuel consumption or mission NO_x emissions.
- Explore the feasibility, potential and consequences in terms of fuel requirements, emissions and airport implications of introducing a LH_2-fuelled aircraft fleet on a regional scale.

In those studies where an aircraft is modelled, the thesis is limited to consider only medium-range aircraft. The reasons are, as explained in the introduction section, that it is the preferable choice from an environmental point of view and that it is the most frequently used aircraft size.

The principal background of the study and conclusions regarding the effects of using hydrogen on aero engine pollutant emissions, performance and design are as follows:

The effects on the engine performance by changing to hydrogen fuel are estimated for the V2527-A5 engine using the simulation tool TurboMatch. Based on the flammability limits of hydrogen and kerosene, the NO_x emission reduction potentials are assessed by calculating the flame temperatures assuming chemical equilibrium. Various combustor configurations burning hydrogen are evaluated, and design and operational matters of particular interest when using hydrogen are discussed.

From a technical point of view, it seems to be feasible to use hydrogen for aero gas turbines. The main changes comprise re-design of the combustion chamber and fuel

control system, as well as the implementation of facilities to evaporate the hydrogen prior to its entry into the combustion chamber. The fuel heating can be accomplished either by an external heat source or a heat exchanger located at a suitable engine location. Practically, the heat exchanging might be accomplished by employing the struts, which are the mechanical structures in the exhaust which hold the rotors in place and are connecting the bearings' outer structure. Alternatively, the heat exchanger could feature a simple coil tube placed over the inside face of the jet pipe casing, avoiding major engine changes and giving a relatively aerodynamically clean jet pipe [Corchero and Montañes, 2003]. Simplified calculations suggest that the heat transferring area available from the exhaust struts is not sufficiently large to accomplish all the desired temperature rise of the hydrogen fuel.

Small performance gains, which depend on the fuel temperature and cycle configuration, in the order of a few percent may be obtained by changing to hydrogen fuel. When changing the fuel either the thrust or COT could be retained. If the thrust is kept the same the COT is decreased by more than 30 K, which would require less advanced cooling technology as well as having a favourable effect on turbine blade life. In order to produce the same amount of thrust 1.4% less energy is required (since ESFC, SFC times the fuel LHV, is reduced by 1.4%). Moreover, designing for a lower maximum cycle temperature would help to suppress the NO_x emissions. If, on the other hand, COT is retained when changing fuel the specific thrust increases slightly (3.2%), implying that the physical size of the engine may be reduced to achieve the same net thrust. The ESFC is increased by less than 1%.

Regarding unconventional engine cycles, basically four options and various combinations of these are identified from previous work: pre-heating the hydrogen fuel with exhaust gases, cooling the compressor air with hydrogen fuel, cooling turbine cooling air with hydrogen fuel and hydrogen topping cycle. By employing such cycles, it would be possible to increase the performance gains. However, it appears to be questionable if these benefits justify the increased complexity imposed by unconventional cycles.

In terms of pollutant emissions, hydrogen use offers the possibility of a significantly reduced number of emission species, resulting in only H_2O and NO_x emissions. All emissions containing carbon and sulphur are eliminated. In order to assess the NO_x emission reduction potential for combustors burning hydrogen and kerosene, respectively, the flame temperatures are calculated, assuming chemical equilibrium, and compared. The results of the calculations suggest that there is the potential to design a combustion system using hydrogen that produces less NO_x emissions than any system burning kerosene. This is a consequence mainly of the essentially leaner weak extinction limit when burning hydrogen.

As for how hydrogen-fuelled combustors should be designed, previous studies have shown that lean premixed combustion is undoubtedly superior to any combustion scheme without premixing in terms of temperature pattern uniformity and NO production. However, premixing implies the major drawback of premature burning and flashback danger, which may cause structural damage and compromise the operational reliability. Due to the risk of auto-ignition for premixed systems and the problems of

large-scale hydrogen diffusion flames, the lean non-premixing concept of micromix combustion, which is based on miniaturized diffusive combustion, is suggested as a promising hydrogen combustor configuration. The micromix combustor consists of a very large number (typically more than 1000) diffusion flames uniformly distributed across the burner's main cross section, thereby minimising the geometric size of the combustion zone. In addition to minimising the scale of the combustion zone, the micromix concept aims at optimally utilising the available pressure loss (providing energy for the dissipative turbulent mixing process) in the combustion system to enhance the mixing process of hydrogen and air. These design principles help to minimise the number and size of local stoichiometric flame regions, where the gas phase NO formation processes are most likely to occur.

Due to the wider flammability range of the hydrogen-air flames (compared with kerosene-air flames), which allows operation of the combustion zone at an equivalence ratio which has a large margin to the lean blow-out limit, the engine handling is facilitated and the creation of white noise is reduced. This combustor noise might otherwise give rise to pulsations and vibrations in the engine, which in turn via resonance can have a detrimental effect on engine components. The higher flame speed will result in a shorter combustor, and hence, reduced engine weight and combustor liner cooling requirements. Furthermore, when burning hydrogen the thermal energy radiated to the surroundings is lower than that of kerosene combustion, thereby beneficially affecting the liner durability and liner cooling requirements.

The principal background of the study and conclusions regarding the optimum cruise altitude for two equivalent medium-range aircraft, one kerosene-fuelled and one LH_2-fuelled, from an environmental point of view are as follows:

In the thesis indicative results are presented, showing how changes in aircraft fuel technology and flight altitude may influence the aircraft configuration as well as the environmental impact. This study is aimed at stimulating further research work on flight altitude optimisation to reduce aircraft environmental impact. From the results obtained it is difficult to draw any confident conclusions regarding whether there are any significant gains in terms of environmental impact by lowering the cruise altitude. The main reason is that the results are highly dependent on the assumptions (e.g. the geographical location under consideration, and the type of model used to derive the figures) made in the GWP model, which is derived by comprising the influence of the numerous chemical, physical, and dynamic interactions in a parametric sense (see appendix B). The relative influence of NO_x emissions compared with CO_2 and the altitude where the impact of NO_x emissions peaks are factors that highly influence the result. Conclusions concerning the effects on aircraft characteristics, fuel consumption and pollutant emissions when reducing the flight altitude, on the other hand, are much more reliable. The results are obtained using TurboMatch, the commercial aircraft performance simulation software Piano and HARP (in-house tool of FOI).

When comparing two equally performing medium-range aircraft – one powered by kerosene and one powered by LH_2 – the energy consumption is inevitably higher (in this case by about 10%) for the cryoplane. This is due to the higher structural weight and the higher drag for the cryoplane configuration. Reduced cruise altitude has a

smaller impact on the cryoplane than on the corresponding conventional aircraft, in terms of physical size, fuel burn and emissions. This means that, compared with the datum case, these quantities will increase more in percentages for the conventional airplane than for the cryoplane, when the cruise altitude is lowered. The main reason for this is a different fuel storage configuration.

In spite of the uncertainty of the results concerning the change in environmental impact of lowering the cruise altitude, it might be reasonable to conclude that there seems to be a substantial qualitative difference between the conventional aircraft and the cryoplane. The results suggest that the contribution to global warming is considerably lower from the cryoplane than from conventional aircraft, particularly if the flight altitude for the cryoplane is reduced. That the effect upon the radiative balance of Earth is smaller from cryoplanes than from conventional aircraft is also suggested by Ponater et al. (2004). Their study covers the effects of changed CO_2 emissions, NO_x emissions and a change in contrail radiative impact of gradually introducing cryoplanes into the global air traffic according to different transition scenarios. According to their best estimate, a relative reduction of aircraft-induced radiative forcing in 2050 by between 16% and 29% (depending on the speed of transition) could be achieved if cryoplanes were introduced. Due to inherent scientific uncertainties this range widens to between 14% and 40%.

Whereas the environmental impact of the conventional aircraft tends to increase, it seems to decrease essentially for the cryoplane when lowering the flight altitude. Provided that an increase in fuel consumption in the order of 10% and an increase in aircraft TOM of a few percent are accepted, the results suggest that cryoplanes should cruise at an altitude of about 2-3 km below where conventional aircraft cruise today. At this reduced flight level, the contribution to global warming from the cryoplane is slightly less than about 15% of that of the conventional aircraft cruising at the datum level. That the difference in environmental impact between the conventional aircraft and the cryoplane is, according to these results, larger than obtained by Ponater et al. (2004) is to be expected, since the results obtained here reflect only two different aircraft, whereas their results are obtained for different aircraft fleets consisting of both cryoplanes and conventional aircraft. In addition to the aspects considered here, reducing the flight altitude would help to avoid the formation of contrails. Inevitably a reduced cruising altitude causes increased aircraft investments and operating costs.

Furthermore, in order to reduce the cruising altitude, air traffic management aspects need careful attention before such a measure may be realised. Williams et al. (2002) studied the option of limiting the cruise altitude as a means to reduce the formation of contrails. Their results indicate that this strategy could provide a net benefit to the climate, despite the associated increase in CO_2 emission. According to their analysis, the most likely operational obstacles to such a scheme are the implications for controller workload; hence, a reconfiguration of the air space would be required to mitigate the impacts.

The principal background of the study and conclusions regarding the design of hydrogen-powered engines suited for medium-range aircraft for either minimum mission fuel consumption or mission NO_x emissions are as follows:

In this thesis a number of alternative engine cycle concepts are selected, and their engine performance and flight mission fuel consumption and emissions are estimated and compared with a datum engine/aircraft combination. For this purpose a computer program to estimate the influence on mission fuel consumption and emissions of altered engine cycle parameters, taking into account the necessary engine scaling, is developed. A general observation, not very unexpected, is that in relative terms the potential to reduce NO_x emissions seems to be larger than the potential to reduce fuel consumption (and the water vapour emissions) by employing alternative engine cycle concepts.

In order to lower the fuel consumption and thus also the mission H_2O emissions, the results indicate that an engine employing increased COT, OPR and BPR, seems to be the most attractive choice. In terms of engine performance, the SFC is improved and the specific thrust and NO_x emission index are deteriorated. Taking into account the engine scaling needed due to the loss in specific thrust, the flight mission performance is estimated. Using the same ratio of COT at initial cruise to COT at max climb as for the datum engine, the mission fuel consumption is reduced by 3.5% and the MTOM is more or less unchanged at the expense of increased mission NO_x emissions by about 49%.

According to these calculations, increasing BPR without changing the core engine does not bring any advantages in terms of mission fuel burn, mission NO_x emissions or aircraft MTOM.

In order to reduce the mission NO_x emissions, the results suggest that an engine with a low power core engine, i.e. reduced COT and OPR, along with a lowered BPR, should be used. Low temperatures and pressures at combustor inlet are effective measures to suppress the thermal NO formation, and a reduced BPR, which enables the use of a smaller engine, limits the increases in mission fuel consumption and MTOM. With respect to engine performance, the specific thrust is slightly increased and the SFC is deteriorated, while the NO_x emission index is substantially decreased. Employing the same ratio of COT at initial cruise to COT at max climb as for the datum engine, the mission NO_x emissions can be reduced by 42% at the expense of increased MTOM by 2.5% and fuel consumption by 8.7%.

Technologies involving a high power core accompanied with increased BPR are changes that are subject to improvements. Increasing the temperatures and pressures in the gas turbine cycle require advancements in high temperature materials and cooling technology. An increased by-pass ratio requires an increased number of turbine stages, a shorter inlet and shorter nozzles than conventional engines. It is therefore likely that engines based on such technologies raise the development, production and maintenance costs. Moreover, the durability of the core engine is likely to decrease.

In contrast, engines designed for lowering mission NO_x emissions employing a core engine with lowered COT and OPR along with reduced BPR, are based on reliable technology that may eliminate the development cost, reduce the production and maintenance costs and increase the durability. As for the durability, a decreased COT and OPR would have a favourable effect on turbine blade and compressor life, respectively.

The principal background of the study and conclusions regarding the feasibility, potential and consequences in terms of fuel requirements, emissions and airport implications of introducing a LH_2-fuelled aircraft fleet on a regional scale are as follows:

According to traffic growth curves and through consideration of an airline's approach to fleet development, two different conventional fleet developments are set up. Next, four realistic transition scenarios are compiled, and the fuel requirements and emissions related to these scenarios are estimated, and presented in relation to figures of the conventional fleet. The scenarios are compiled on a regional basis. The infrastructure changes needed at Stockholm/Arlanda airport and for distribution of the LH_2 are identified and assessed. Possible methods available today and in the future of producing hydrogen are briefly discussed.

According to the traffic growth scenarios applied here, the number of passengers will increase three to four times by 2050. During the same time period, the number of movements will have increased, but by less than the number of passengers, due to the larger aircraft types that will have commenced on the domestic market. Depending on the scenario, the number of movements will have increased by 70-90%. Hence, it may be concluded that an essential increase in airport capacity, at all airports, is required to cope with the increasing traffic demand assumed here.

Based on the two different prerequisites, saying that all new aircraft introduced in 2015 and in 2025 and afterwards, respectively, should be cryoplanes, four different scenarios are compiled. In all scenarios, it is reasonable to change to a fleet powered solely by liquid hydrogen by 2050. A high traffic growth rate results in a delayed broad-scale introduction of cryoplanes. In general, the higher growth rate implies that the introduction of new aircraft types is needed earlier, and hence, more generations of aircraft would be involved by 2050, and a more modern fleet would be in operation at that time.

By starting to introduce cryoplanes in 2015, the amount of NO_x may be retained on a level not much higher than today's level, provided that the emission indices of NO_x for the hydrogen engine are reduced by 70-85%, depending on the technology level, compared with a conventional engine of 2001. If a conventional fleet scenario is assumed, the NO_x emissions will be about 2.8 times higher in 2050 than in 2001. The effect on the NO_x emissions for conventional aircraft is obtained by assuming a reduction potential in NO_x emission index of up to 50% (which might be slightly too conservative).

Regarding the changes needed at the airport when using hydrogen, there are a number of measures that need to be taken to ensure that the safety level at the airport is preserved. In order to avoid a fire hazard, spark ignition engines should be avoided. A very pleasing and feasible solution would be to power all airport vehicles by fuel cells driven by hydrogen. The overall airport layout and procedures do not need to be changed, and the aircraft can be refuelled at gate positions exactly like conventionally fuelled aircraft. Largely, the required changes have to do with refuelling procedures. Since hydrogen is a cryogenic fuel, what really needs to be changed is the interface

between the fuel supplies and the aircraft fuel tanks, as well as most of, if not all, fuel system components. However, the intention is that the hydrogen should be distributed in a way similar and parallel to that of the kerosene. Hence, ignoring the cost implications, from an airport infrastructure point of view, it is certainly feasible to change to hydrogen use. No significant changes on turn-around times are expected with cryoplanes.

Taking the local conditions into account, with respect to the availability of energy, it would be reasonable to change from kerosene to LH_2 as fuel for all civil aviation refuelling in Sweden, according to the scenarios compiled in this study. However, development and extension of renewable energy sources parallel to the introduction of cryoplanes is important to make sure that no or very little fossil-based energy is used for the LH_2 production. Today, steam methane reforming is the most commonly used, efficient and cost-effective method to produce hydrogen. Since it is based on a fossil energy it is, however, not a preferable method in the long run. Under a transition phase it might be reasonable to employ this method to reduce production costs, particularly if the CO_2 is extracted and sequestered in reservoirs or utilised. The method does require electrical energy, but not significant amounts when compared with the total electricity production in Sweden.

Looking at possible renewable production methods viable in the near future, electrolysis of water and gasification of biomass are promising technologies. The amount of electrical energy needed to power all aircraft refuelling in Sweden in 2050, using liquid hydrogen produced by electrolysis of water, would be about 20 TWh. This is considerably much, but not any unreasonably large number, particularly if one considers that today's technology level of LH_2 production is used when deriving this number. In 2050, the technologies for hydrogen production will probably be considerably improved compared to today, and some will possibly be driven out of competition by other more efficient ones. Gasification of biomass is also a feasible alternative for hydrogen production; particularly when observing that Sweden has large sources of biomass. Given the estimated biomass supply in Sweden in 2020, about 8% of that would be required to power all civil aviation refuelling with hydrogen in Sweden in 2050. The most feasible renewable energy sources to extend in Sweden are probably biomass and wind-power.

In the very long run there are likely to be sustainable hydrogen production methods available which today are in the early phase of research and development. Hydrogen production in photochemical and photobiological systems using sunlight are examples that probably will offer large environmental benefits in the future if successfully developed.

It is worth mentioning that the cost penalty of changing the fleet to use LH_2 is not assessed in the thesis. In order to cover fully the implications with respect to costs of changing the fleet, several aspects comprising difficulties need to be addressed. As the scenarios stretch several decades ahead and as some technologies need further development, it is crucial to assess the costs of all new facilities. Moreover, to make a fair comparison between cryoplanes and conventional aircraft, future price trends of kerosene need to be taken into account. The price of kerosene will most certainly rise in

the future, both due to dwindling oil resources and possibly due to future taxation on fossil fuels (or CO_2 emissions). As explained in the introduction, prices of kerosene and hydrogen far ahead in the future are very difficult to assess. Besides, to fully understand the cost implications of introducing hydrogen in aviation, other sectors, such as other transportation sectors and the power industry, should be considered as well. Possible co-ordination benefits could have a significant effect on the cost penalty. A study addressing these issues is beyond the scope of this thesis.

It is clear that powering civil aviation with hydrogen does not necessarily imply that all emissions of greenhouse gases are eliminated, since greenhouse gases may be emitted during the hydrogen production process. However, it is a step away from the oil dependence and it offers the possibility of using renewable energy sources for aviation. This is impossible as long as kerosene is used.

6.2 Recommendations for Further Work

A number of recommendations for further work are identified:

Design of a hydrogen-to-gas heat exchanger

In order to obtain a stable combustion and to avoid the critical temperature where the density and viscosity of the hydrogen vary essentially with the temperature, the hydrogen needs to be heated prior to its entry into the combustion chamber. The fuel heating can be accomplished either by an external heat source or a heat exchanger located at a suitable engine location. As for employing a heat exchanger within the engine, two options are discussed: employing the exhaust struts, and employing a simple coil tube placed over the inside face of the jet pipe casing. Simplified calculations suggest that struts are not sufficient to accomplish all the desired temperature rise of the hydrogen fuel; however, no detailed heat exchanger design is conducted. Looking at the design of a heat exchanger and its consequences on engine performance and weight is hence recommended as further work. Such a study should preferably address issues such as heat exchanger type, space requirement of the heat exchanger, and weight and pressure loss implications of including a heat exchanger. In turn, consequences on engine performance and weight can be estimated.

Modelling of hydrogen-fuelled engines in TurboMatch

As discussed in section 2.2 the heat exchanger could be located at a number of different locations, each owning its merits, within the engine. In the current hydrogen-adapted version of TurboMatch, there is no “brick” (see Appendix A.3, section A.3.1) available to simulate a hydrogen-to-gas heat exchanger, but this calculation needs to be conducted externally to TurboMatch and the result, in terms of a temperature drop of the gas stream, needs to be supplied manually to the input file. The temperature drop is calculated using spreadsheets. Since the flow quantities (mass flow, temperature, pressure) which are required for the heat exchanger calculation are not known until TurboMatch is executed, this procedure needs to be performed for each operating point, making it a lengthy process if a larger number of operating points should be studied. In addition, the risk of errors increases when data are taken from and provided manually to the program.

A potential improvement to TurboMatch would be to provide it with an additional "brick" which handles a hydrogen-to-gas heat exchanger. This would enable that desired data, such as the temperature of the hydrogen in and out of the heat exchanger (concerning the design point) and heat exchanger effectiveness (concerning off-design conditions), could be supplied to the input file prior to the execution of the program. To achieve this also the routines that read data from the input file need to be changed.

Estimation of NO_x emissions

In the thesis the flame temperatures are calculated on two different occasions. In section 2.3.4 the NO_x reduction potential when burning kerosene and hydrogen, respectively, is assessed by comparing their combustor primary zone flame temperatures. The second occasion is when the NO_x emission is estimated for a hydrogen-fuelled micromix combustor using a semi-empirical correlation, in which the flame temperature is included, in section 4.2. In both cases the flame temperatures are calculated assuming chemical equilibrium. For this purpose a well-established code developed by NASA is used (see section 2.3.4). As discussed in section 2.3.4 it is a simplification to assume chemical equilibrium, since the dwell time in a gas turbine combustor in general is too short for chemical equilibrium to be attained.

As long as the deviation between the real flame temperatures and the equilibrium values for these two fuels are the same, it makes no difference on the results to assume chemical equilibrium (this concerns the study on NO_x reduction potential covered in section 2.3). However, since the rate of chemical kinetics and the combustor lengths of these two fuels are different, the deviations between the real flame temperatures and those obtained when assuming chemical equilibrium might not be exactly the same. Although this deviation due to assuming chemical equilibrium is not expected to change the overall conclusions, it could affect the qualitative difference between these fuels in terms of potential to attain low NO_x emissions. A suggestion for further work, therefore, would be to calculate the flame temperatures without excluding the influence of time, implying that the flow field and chemical kinetics are taken into account. As for the study aimed at assessing the NO_x reduction potentials, an additional substantial improvement would be not only to compare the primary zone flame temperatures, but also to calculate the amount of NO_x emission formed, taking into account all relevant formation principles.

The NO_x emission correlation derived here according to the method suggested by Dahl and Suttrop (2001c), is an initial attempt to assess the NO_x emissions of full-scale engines provided with micromix combustors. Due to a large number of simplifications and uncertainties discussed in the thesis (section 4.2), as well as the lack of experimental results of full-scale engines, the correlation's results should be interpreted as a rough assessment only. In order to improve the NO_x assessment, either or both of the following suggestions could be followed: evaluating and improving the correlation by comparing its results with results obtained when including the flow field and chemical kinetics, and comparing its results with experimental results of full-scale engines (if such results are available).

Estimation of the environmental impact of aircraft

The method adapted here to estimate the global climate impact of a specific flight, namely, using the concept of global warming potential (GWP), is as discussed in the thesis (section 3.4 and Appendix B) associated with large uncertainties. In this case the GWP model is used to estimate the influence on global warming of altered flight altitude. It is recommended that further work is done to define an optimum cruising altitude, from an environmental point of view, for both conventional aircraft and cryoplanes, using a more sophisticated climate impact model. One option is to use the concept of radiative forcing (RF) as a measure of the climate impact, which requires that a 3-D global model is employed that includes both the chemistry and radiation effects. However, these climate models require emissions from a fleet of aircraft covering the whole Earth or at least a region, e.g. northern Europe. The influence of single flights as investigated here is indiscernible in these models. It would be a challenge to develop an alternative measure to GWP, generally accepted within the atmospheric community, that can be used to study the influence on the climate impact of various technology changes, e.g. changed cruising altitude, changed engine or airframe technology.

Effects on aircraft mission performance of altered engine size and technology

In chapter 4 the influence of altered engine cycle parameters on flight mission performance is estimated. To take account for changed engine weight and drag of changed size and characteristics (BPR, OPT or COT) of the engine, highly simplified methods are used. It is recommended that correlation methods, more sophisticated than those used here, to establish the influence on nacelle drag and weight of changed engine diameter and characteristics are developed. As for the drag correlation, it should preferably, in contrast to the model employed here, take interference drag effects into account. More sophisticated models in this respect would increase the level of accuracy in the flight mission performance effects of changed engine cycle parameters.

Engine design for reduced cruising altitude

It is stated in the conclusions that provided that an increase in fuel consumption in the order of 10% and an increase in TOM of a few percent are accepted, the results suggest that cryoplanes should cruise at an altitude of about 2-3 km below where conventional aircraft cruise today. In addition, some guidance on how to design hydrogen-fuelled engines to lower either the mission fuel consumption or mission NO_x emissions is provided. However, the latter results concern an aircraft cruising at a conventional cruising altitude. A recommendation for further work would be to look at the engine design for the suggested lowered cruising altitude. Doing this, it might be possible to reduce the penalty in fuel consumption (and H_2O emissions) of cruising at an altitude different from the conventional, which is chosen to minimise the contribution to global warming. It would be worthwhile to carry out a parametric study, similar to the one outlined in chapter 4, or an optimisation study aimed at finding the optimum engine design for reduced cruising altitude.

Methods to produce and store hydrogen

Producing and storing hydrogen are areas in which extensive research are required before the commercialisation of hydrogen as an energy carrier in any field. A number of obstacles need to be solved. More efficient and cost-effective hydrogen production

methods based on renewable energy sources need to be developed. Today the renewable production methods are less efficient than those based on fossil energy. Methods to produce hydrogen are only touched upon briefly in this thesis when discussing implications on airports. Storing hydrogen is also complicated, as it is a bulky fuel in its gas state and requires insulation when liquefied. Research in these fields is recommended to enable the introduction of hydrogen as an energy carrier in aviation and other sectors.

Cost implications of using hydrogen for aviation

It is recommended that the cost implications of changing to hydrogen are investigated. Both possible additional costs of manufacturing and operating the aircraft and costs of carrying out the required infrastructure changes at airports need to be addressed. Having an idea of the cost implications, it would be reasonable to address the political and legislative changes needed to enable an introduction of liquid hydrogen-fuelled aircraft before that point in time when hydrogen can compete economically with kerosene.

REFERENCES

Air travel – Greener by Design – The Technology Challenge, 2001, Society of British Aerospace Companies Limited, London, UK.

Allidieres L., 2002, "WP3 – Systems and Components", Task Final Report 3.1, CRYOPLANE Project.

ANCAT/EC, 1995, Minutes of 17th Meeting of ANCAT/EC Emissions Inventory Database Group, Department of Trade and Industry, 20 July 1995.

Anderson J., 1989, Introduction to Flight, Third Edition, McGraw-Hill, Inc., USA.

Bagheri SH.-A., 1996, "Auslegung und Erprobung eines 2-D-Brennkammer-Segments Für Wasserstoff-Betrieb auf der Basis des Triebwerks IAE V2500. (Design and Testing of a two-dimensional combustor segment for hydrogen operation on the basis of the IAE V2500 aircraft engine.)", Diploma Thesis, FH-Aachen, Germany. Cited in: Dahl G. and Suttrop F., 2001b, "Combustion Chamber and Emissions, The Micromix Hydrogen Combustor Technology", Task Technical Report 4.4-5A, CRYOPLANE Project.

Baerst C.F. and Riple J.C., 1979, "Preliminary Studies of a Turbofan Engine and Fuel System for Use with Liquid Hydrogen". In: Hydrogen in Air Transportation, International DGLR/DFVLR-Symposium, sequence 19, Germany, 11-14 September 1979.

Baulch D.L. , Drysdale D.D. and Lloyd A.C.,1970, "Critical evaluation of rate data for homogenous, gas phase reactions, Nos. 1-5", Dept of Physical Chemistry, Leeds University, UK. Cited in: Dahl G. and Suttrop F., 2001c, "Combustion Chamber and Emissions, Estimated NO_x-Reduction Potential of Hydrogen Fuelled Aircraft Engines", Task Technical Report 4.4-5B, CRYOPLANE Project.

Beck J., Reeves C., De Leeuw F. and Penkett S., 1992, "The effect of aircraft emissions on tropospheric ozone in the Northern Hemisphere", Atmos. Env., Vol. 26A, pp. 17-29. Cited in: Klug H. G., Bakan S. and Gayler V., 1996, "CRYOPLANE - Quantitative Comparison of Contribution to Anthropogenic Greenhouse Effect of Liquid Hydrogen Aircraft versus Conventional Kerosene Aircraft", EGS XXI General Assembly, Den Haag, 6-10 May 1996.

Boggia S. and Jackson A., 2002, "Some Unconventional Aero Gas Turbines Using Hydrogen Fuel" (GT-2002-30412), Proceedings of ASME Turbo Expo 2002, Amsterdam, The Netherlands, 3-6 June 2002.

Boggia S, Jackson A. and Singh R., 2001, "Unconventional Cycles for Aero Gas Turbine Engines Burning Hydrogen", Proceedings of 13th Symposium on Air Breathing Engines, ISABE, Chattanooga, TN, USA.

Boggia S., 2001, "Four Unconventional Aero Gas Turbine Engines burning Hydrogen – Cryoplane Project", M.Sc. Thesis, Cranfield University, UK.

Bracha M., 2002a, “Infrastructure for Production, Storing and Distribution at Airports”, Task Technical Report 7.5-1, CRYOPLANE Project.

Bracha M., 2002b, Linde Gas, Germany, private communication.

Brasseur G., Müller I-F. and Granier C., 1996, “Atmospheric impact of NO_x emissions by subsonic aircraft: A three-dimensional model study”, J. Geophys. Res. Vol. 101, pp. 1423-1428. Cited in: Klug H. G., Bakan S. and Gayler V., 1996, “CRYOPLANE - Quantitative Comparison of Contribution to Anthropogenic Greenhouse Effect of Liquid Hydrogen Aircraft versus Conventional Kerosene Aircraft”, EGS XXI General Assembly, Den Haag, 6-10 May 1996.

Breit Th., 1999, “Entwicklung und Erprob einer 2-Kreis-Wasserstoff-Brennkammer für die Airbus A320 APU GTCP 36-300. (Development and testing of dual loop hydrogen combustor for the Airbus A320 APU GTCP 36-300.)”, Diploma Thesis, FH-Aachen, Germany. Cited in: Dahl G. and Suttrop F., 2001c, “Combustion Chamber and Emissions, Estimated NO_x-Reduction Potential of Hydrogen Fuelled Aircraft Engines”, Task Technical Report 4.4-5B, CRYOPLANE Project.

Brewer G.D., 1981, “The Prospects for Liquid Hydrogen Fueled Aircraft”, Int. J. Hydrogen Energy, Vol. 7, No. 1, pp. 21-41.

Brewer G.D., 1979, “Characteristics of Liquid Hydrogen-Fueled Aircraft”. In: Hydrogen in Air Transportation, Supplement of proceedings International DGLR/DFVLR-Symposium, Stuttgart, 11-14 September 1979.

Brühl C., Crutzen P., Danielsen E.F., Grassl H., Hollweg H-D. and Kley D., 1991, “Umweltverträglichkeitsstudie für das Raumtransportsystem – SÄNGER“, Max-Planck-Institut für Meteorologie, Hamburg, Germany.

Cengel Y.A. and Boles A., 1996, Thermodynamics, An Engineering Approach, McGraw-Hill, Inc. USA.

Cohen H., Rogers G. and Saravanamutto H., 1996, Gas Turbine Theory, 4th Edition, Longman Group Limited, UK.

Conrad E.W., 1979, “Turbine Engine Altitude Chamber and Flight Testing with Liquid Hydrogen”. In: Hydrogen in Air Transportation, International DGLR/DFVLR-Symposium, sequence 20, Germany, 11-14 September 1979. Cited in: Dahl G. and Suttrop F., 2001a, “Combustion Chamber and Emissions, Review of Proposed Hydrogen Combustors, Benefits and Drawbacks”, Task Technical Report 4.4-4, CRYOPLANE Project.

Corchero G. and Montañes J.L., 2003, “An Approach to the Use of Hydrogen in Actual Commercial Aircraft Engines”, Proceedings of 15th Symposium on Air Breathing Engines, ISABE, Cleveland, USA.

Correa S.M., 1991, “Lean Premixed Combustion for Gas Turbines: Review and Required Research”, Fossil Fuel Combustion, ASME PD-Vol. 33.

Dahl G., 2002, “Auxiliary Power Unit (APU)”, Task Technical Report 4.7, CRYOPLANE Project.

Dahl G. and Suttrop F., 2001a, “Combustion Chamber and Emissions, Review of Proposed Hydrogen Combustors, Benefits and Drawbacks”, Task Technical Report 4.4-4, CRYOPLANE Project.

Dahl G. and Suttrop F., 2001b, “Combustion Chamber and Emissions, The Micromix Hydrogen Combustor Technology”, Task Technical Report 4.4-5A, CRYOPLANE Project.

Dahl G. and Suttrop F., 2001c, “Combustion Chamber and Emissions, Estimated NO_x-Reduction Potential of Hydrogen Fuelled Aircraft Engines”, Task Technical Report 4.4-5B, CRYOPLANE Project.

Dahl G. and Suttrop F., 2000, “Arbeiten zur einer mit betriebenen Hilfsgasturbine vom Typ ASA GTCP 36-300. (Activities for the development of a hydrogen-operated auxiliary power unit GTCP 36-300.)”, FH-AC-TB 06-84-00-01. Cited in: Dahl G. and Suttrop F., 2001c, “Combustion Chamber and Emissions, Estimated NO_x-Reduction Potential of Hydrogen Fuelled Aircraft Engines”, Task Technical Report 4.4-5B, CRYOPLANE Project.

Dahl G. and Suttrop F., 1998, “Engine Control and Low-NO_x Combustion for Fuelled Aircraft Gas Turbines”, Int. J. Hydrogen Energy, Vol. 23, No. 8, pp. 695-705.

EEFAE – Efficient and Environmentally Friendly Aero Engine (EC-sponsored project), 2001, presented by Sjunnesson A., Volvo Aero Corporation, on Flygteknik 2001, Stockholm, 22-23 October, 2001.

Ehhalt D.H., Rohrer F. and Wahner A., 1992, “Sources and distribution of NO_x in the upper troposphere at northern mid-latitudes”, J. Geophys. Res., Vol. 97, pp. 3725-3738.

Eiff G., Putz S. and Moses C., 1992, Combustion Properties of Ethanol Blended Turbine Fuels, Proceedings of 2nd Annual FAA/AIAA Symposium on General Aviation Systems, Wichita, KS, USA, March 1992.

Eklund A. and Hedemalm P., 2002, “Bio-jet A1 – En ny typ av jetbränsle baserat på biomassa”, report of Orboros AB.

ESDU, 1986, “Equations for Calculation of International Standard Atmosphere and associated off-standard atmospheres”, Engineering Science Data Unit, Item Number 77022, Issued November 1977, Amendments A and B in February 1986.

ESDU, 1985, “First Approximation to Take-Off Field Length of Multi-Engined Transport Aeroplanes”, Engineering Science Data Unit, Item Number 76011, Issued May 1976, Amendments A in May 1985.

EU-BRITE/EURAM Projects Low NO_x 1,2,3. In: IPCC, Aviation and the Global Atmosphere, Penner J. L., Lister D. H., Griggs D. J., Dokken D. J., McFarland M. (eds.), 1999, Cambridge University Press, Cambridge, UK.

Fuglestvedt J.S., Isaksen I.S.A. and Wang W.-C., 1996, “Estimates of indirect global warming potentials for CH_4, CO and NO_x”, Climatic Change, Vol. 34, pp. 405-437.

Gauss M., Isaksen I.S.A., Wong S. and Wang W.-C., 2003, “Impact of H_2O emissions from cryoplanes and kerosene aircraft on the atmosphere”, J. of Geophys. Res., Vol. 108, No. D10, 4304, doi: 10.1029/2002JD002623.

Gerend R.P. and Roundhill J.P., 1970, “Correlation of Gas Turbine Engine Weights and Dimensions”, AIAA Paper No. 70-669.

Gleitsmann G. and Zellner R., 1998, “A modelling study of the formation of cloud condensation nuclei in the jet regime of aircraft plumes”, J. Geophys. Res., Vol. 103, pp. 19 543-19 556.

Goodger E.M., 1993, “Hydrocarbon Fuel Chemistry, With Particular Reference To Aviation”, Landfall Press, England.

Gordon S. and McBride B.J., 1994, “Computer Program for Calculation of Complex Chemical Equilibrium Compositions and Applications – I. Analysis”, NASA Reference Publication 1311 (may be obtained from http://www.grc.nasa.gov/WWW/CEAWeb/).

Grewe V., Dameris M., Fichter C. and Lee D.S., 2002, “Impact of aircraft NO_x emissions. Part 2: Effects of lowering the flight altitude”, Meteor. Z., Vol. 11, pp. 197-205.

Gunston B., 2002, “Jane’s Aero-Engines, Issue Twelve”, Jane’s Information Group Limited, Coulsdon, UK.

Hansen J., Sato M., Ruedy R., Lacis A. and Oinas V., 2000, “Global warming in the twenty-first century: An alternative scenario”, Proc. Nat. Acad. Sci. USA 97, pp. 9875-9880.

Hansen J., Ruedy R., Lacis A., Russel G., Sato M., Lerner J., Rind D. and Stone P., 1997, “Wonderland climate model”, J. Geophys. Res., Vol. 102, pp. 6823-6830.

Hasselrot A., 2000, “Database Model for Studying Emissions from Aircraft in Variable Flight Profile”, FFA TN 2000-69.

Hendricks, J., 1997, “Modellstudien zur Bedeutung heterogener Reaktioner auf und in Sulfataerosolen für die Photochemie der Tropopausregion mittlerer Breiten“, Ph.D. Thesis, Institut for Geophysics and Meteorology, University of Köln, Germany.

Hoyt J., 1976, “Design Concepts for LH_2 Airport Facilities”, International DGLR/DFVLR Symposium on Hydrogen in Air Transportation, The Ralph M. Parsons Co., Pasadena, California, USA. Cited in: Schmidtchen U. and Geitmann S., 2001, “Aircraft Specific Safety Aspects”, Task Final Report 5.3-1, CRYOPLANE Project.

Hume C., 2001, Environmental considerations in aircraft design – Emissions, Presentation at AERONET – CORSAIR Workshop, 16-17 October 2001.

Heywood J.B. and Mikus T., 1973, “Parameters controlling nitric oxide emissions from gas turbine combustion”, AGARD-CPP-125.

ICAO Engine Exhaust Emissions Data Bank, 1995, First Edition, ICAO, Doc 9646-AN/943. Also available at: http://www.qinetiq.com/aviation_emissions_databank.

Incropera F. and DeWitt D., 1996, Fundamentals of Heat and Mass Transfer, Fourth Edition, John Wiley & Sons, New York, USA.

IPCC, Climate Change 2001: The Scientific Basis, Houghton J.T., Ding Y., Griggs D.J., Noguer M., van der Linden P.J., Dai X., Maskell K., and Johnson C.A. (eds.), 2001, Cambridge University Press, Cambridge, UK and New York, USA.

IPCC, Aviation and the Global Atmosphere, Penner J. L., Lister D. H., Griggs D. J., Dokken D. J., McFarland M. (eds.), 1999, Cambridge University Press, Cambridge, UK.

IPCC, Climate Change 1995 - The science of climate change, Houghton J.T., Meira Filho L.G., Callander B.A., Harris N., Kattenberg A. and Maskell K. (eds.), 1996, IPCC, Cambridge University Press, Cambridge, UK.

IPCC, Climate Change: The Scientific Assessment, Houghton J. T. and Ephraums J. J. (eds.), 1990, Cambridge University Press, Cambridge, UK.

Ireman T., 2001, SAAB Aircraft, Sweden, Department of TKS, private communication.

Isaksen I.S.A., Berntsen T.K. and Wang W.-C., 2001, “NO_x Emissions from Aircraft: Its Impact on the Global Distribution of CH_4 and O_3 and on Radiative Forcing”, TAO, Vol. 12, No. 1, pp. 63-78.

Jackson A., 2004, Consultant at Cranfield University, UK, private communication.

Jackson A., 2000, “Engine Performance Changes”, Minutes of Meeting 4.1-2, CRYOPLANE Project.

Johnson C.E. and Derwent R.G., 1996, “Relative radiative forcing consequences of global emissions of hydrocarbons, carbon monoxide and NO_x from human activities estimated with a zonally averaged two-dimensional model”, Climatic Change, Vol. 34, pp. 439-462.

Johnson C., Strand A., Hov Ø. and Ramavoson R., “2-D simulations. Part-V, section 7.2”. In: Schumann U. (Ed.), 1995, AERONOX The impact of NO_x emissions from aircraft upon the atmosphere at flight altitudes 8-15 km. EC-DLR Publication on Research Related to Aeronautics and Environment.

Johnson C.E., Henshaw J. and McInnes G., 1992, “Impact of aircraft and surface emissions of nitrogen oxides on tropospheric ozone and global warming”, Nature, Vol. 355, pp. 69-72.

Jones R. and Sefain M., 2000, “Current Aircraft Ground Support Requirements”, Task Technical Report 7.6-1, CRYOPLANE Project.

Jonforsen H., 1999, “PROGNOSER” (Document notation: CT/HåJo 99:24), Unpublished report by the Swedish Civil Aviation Administration.

Kappers A. and Essers I., 2001, “Global Traffic and Fleet Forecast”, Task Final Report 8.2.1, CRYOPLANE Project.

Kerrebrock J., 1996, Aircraft Engines and Gas Turbines, Second Edition, The MIT Press, London, UK.

Klug H.G., 2002, “Progress Report: Hydrogen Fuelled Aircraft – System Analysis”, CRYOPLANE Project.

Klug H. G., 2001a, “Global Warming Potential Data For Simplified Sensitivity Analysis and Optimisation”, Task Technical Report 1.1-5, CRYOPLANE Project.

Klug H.G., 2001b, “Mid/Longterm Planning – Preparation for Transition”, Task Technical Report 1.1-4, CRYOPLANE Project.

Klug H. G., 1997, “CRYOPLANE – Liquid Hydrogen Propulsion for Aircraft”, Aerospace Propulsion Conference, London, UK, 8-9 December 1997.

Klug H. G., Bakan S. and Gayler V., 1996, “CRYOPLANE - Quantitative Comparison of Contribution to Anthropogenic Greenhouse Effect of Liquid Hydrogen Aircraft versus Conventional Kerosene Aircraft”, EGS XXI General Assembly, Den Haag, 6-10 May 1996.

Klug H. G. and Grassl H., 1993, “The Cryoplane Project, Aircraft Using Cryogenic Fuel and their Impact on the Atmosphere”, European Geophysical Society XVIII General Assembly, Wiesbaden, 3-7 May 1993.

Konopka, P., 1995, “Analytical Gaussian solutions for anisotropic diffusion in a linear shear flow”, J. Non-Equilib. Thermodyn., Vol. 20, pp. 78-91.

Kraabøl A.G., Flatøy F. and Stordal F., 2000, “Impact of NO_x emissions from subsonic aircraft: Inclusion of plume processes in a three-dimensional model covering Europe, North America, and the North Atlantic”, J. Geophys. Res. Vol. 105, pp. 3573-3582.

Kronberger B., 2002, “Hydrogen Production Processes Based upon Renewable Energy”, Task 7.3, CRYOPLANE Project.

Kurzke J., 1998, “User’s Manual – GasTurb 8.0 for Windows, A Program to Calculate Design and Off-Design Performance of Gas Turbines”, www.gasturb.de.

Kärcher B., Turco R.P., Yu F., Danilin M.Y., Weisenstein D.K., Miake-Lye R.C. and Busen R., 2000, “A unified model for ultrafine aircraft particle emissions”, J. Geophys. Res., Vol. 105, pp. 29 379-29 386.

Kärcher B., Hirschberg M.M. and Fabian, P., 1996, “Small-scale chemical evolution of aircraft exhaust species at cruising altitudes”, J. Geophys. Res., Vol. 101, pp. 15 169-15 190.

Lantz P., 1996, ”Framtida tillgång på trädbränslen – en sammanställning över framtida tillgång på trädbränslen”, Skogsstyrelsen, analysenheten, Sverige.

Le Dilosquer M., 1998, “Influence of Subsonic Aero Engine Design and Flight Routes on Atmospheric Pollution”, Ph.D. Thesis, Cranfield University, UK.

Lefebvre A.H., 1998, Gas Turbine Combustion, Second Edition, Edwards Brothers, Ann Arbor, MI, Philadelphia, USA.

Lefebvre A.H., 1995, “The Role of Fuel Preparation in Low-Emissions Combustion, Journal of Engineering for Gas Turbines and Power”, Vol. 117/617.

Lefebvre A.H., 1984, “Fuel Effects on Gas Turbine Combustion – Liner Temperature, Pattern Factor, and Pollutant Emissions”, Journal of Aircraft, Vol. 21, No. 11, pp. 887-898.

Marquart S., Sausen R., Ponater M. and Grewe V., 2001, “Estimate of the climate impact of cryoplanes”, Aerosp. Sci. and Techn., Vol. 5, Issue 1, pp. 73-84.

McBride B.J. and Gordon S., 1996, “Computer Program for Calculation of Complex Chemical Equilibrium Compositions and Applications – Π. Users Manual and Program Description”, NASA Reference Publication 1311 (may be obtained from http://www.grc.nasa.gov/WWW/CEAWeb/).

Morris G.A., Rosenfield J.E., Schoeberl M.R. and Jackman C.H., 2003, “Potential impact of subsonic and supersonic aircraft exhaust on water vapour in the lower

stratosphere assessed via a trajectory model", J. Geophys. Res., Vol. 108, doi: 10.1029/2002JD002614.

Nicol D., Malte P.C., Lai J., Marinov N.N. and Pratt D.T., 1992, "NO_x Sensitivities for Gas Turbine Engines Operated on Lean-Premixed Combustion and Conventional Diffusion Flames", ASME Paper 92-GT-115.

Näs A., Moldanova J., Lindskog A., Bergström R. and Langner J., 2003, "Identification and Management of Critical Environmental Impacts from Air Transportation over North Europe, EIATNE", Final report to the EU commission, LIFE99 ENV/S/000631.

Näs B.O., 2001, Director, Aircraft and Engine Analysis at Scandinavian Airlines (SAS), private communication.

Oelkers W. and Prenzel E., 2001, "Aircraft Configuration – Short/Medium Range Aircraft", Task Final Report 2.3.4, CRYOPLANE Project.

Oelkers W. and Schulz H.G., 2000, "Design Requirements for Short/Medium Range Commercial Transports", Task Technical Report 2.2-6R, CRYOPLANE project.

Parikka M., 1997, "Biosism – a method for the estimation of woody biomass for fuel in Sweden", Ph.D. Thesis, Swedish University of Agricultural Science, Sweden.

Payzer R.J. and Renninger S.W., 1979, "Hydrogen Fueled High Bypass Turbofans in Subsonic Aircraft". In: Hydrogen in Air Transportation, International DGLR/DFVLR-Symposium, Germany, 11-14 September, 1979.

Petry H., Hendricks J., Möllhoff M., Lippert E., Meier A., Ebel A. and Sausen R., 1998, "Chemical conversion of subsonic aircraft emissions in the dispersing plume: Calculation of effective emission indices", J. Geophys. Res., Vol. 103, pp. 5759-5772.

Pilidis P., 2001, "Design Point Performance", Lecture notes of course in Gas Turbine Performance, Cranfield University, UK, 11-15 June 2001.

Ponater M., Marquart S., Ström L., Gierens K., Sausen R. and Hüttig G., 2004, "On the potential of the cryoplane technology to reduce aircraft climate impact". In: European Conference on Aviation, Atmosphere and Climate (AAC) proceedings (Eds.: Sausen R., Fichter C. and Amanatidis G.), pp. 312-317.

Pradewa R., 1995, "High Bypass Ratio Turbofan Engine Design", M.Sc. Thesis, Cranfield University, UK.

Pratt D.T., Allwine K.J. and Malte C.P., 1974, "Hydrogen as a Turbojet Engine Fuel – Technological, Economical and Environmental Impact", Proceedings of 2nd Int. Symposium on Air Breathing Engines, Sheffield, UK, Royal Aeron. Soc.

Raymer D., 1999, Aircraft Design: A Conceptual Approach, Third Edition, American Institute of Aeronautics and Astronautics, Inc., Reston, Virginia, USA.

Rink K.K. and Lefebvre A.H., 1989, "The Influence of Fuel Composition and Spray Characteristics on Nitric Oxide Formation", Combustion Science and Technology, Vol. 68, pp. 1-14.

Rizk N.K. and Mongia H.C., 1994, "Emissions Predictions of Different Gas Turbine Combustors", AIAA 94-0118, Proceedings of 32nd Aerospace Sciences Meeting & Exhibit, Reno, NV, USA, 10-13 January 1994.

Rogers H. L., Lee D. S., Raper D. W., Foster P. M. de F., Wilson C. W., and Newton P. J., 2002, "The impacts of aviation on the atmosphere", The Aeronautical Journal, Vol. 106, No. 1064, pp. 521-546.

Sarigiannis D. and Kronberger B., 2001, "D22 Emissions inventory and comparative assessment of emissions from alternatives in hydrogen production from renewables", Task Technical Report 7.3-1, CRYOPLANE Project.

Sausen R. and Ponater M., 2002, "Global Effect of Gaseous Emissions and Contrails", Task Final Report 6.6-1, CRYOPLANE Project.

Sausen R., Gierens K., Ponater M. and Schumann U., 1998, "A diagnostic study of the global distribution of contrails". Theor. Appl. Climatol., Vol. 61, pp. 127-141.

SCAA, 2002, The Swedish Civil Aviation Administration web site, www.lfv.se.

SCB, 2002, Statistical Yearbook of Sweden 2002, Statistics Sweden.

Schelzig M. and Bleimund G., 2000, "Inbetriebnahme und Optimierung einer Mikro-Misch-Brennkammer in der APU GTCP 36-300, sowie deren Reglerkreisoptimierung. (Operation and Optimisation of a micromix combustor in the APU GTCP 36-300 and optimisation of the engine's control loop.)", Diploma Thesis, FH-Aachen, Germany. Cited in: Dahl G. and Suttrop F., 2001b, "Combustion Chamber and Emissions, The Micromix Hydrogen Combustor Technology", Task Technical Report 4.4-5A, CRYOPLANE Project.

Schemensky R., 1973, "Development of an Empirically Based Computer Program to Predict the Aerodynamic Characteristics of Aircraft, Volumes I and II", AFFDL-TR-73-144.

Schmidtchen U. and Geitmann S., 2001, "Aircraft Specific Safety Aspects", Task Final Report 5.3-1, CRYOPLANE Project.

Schnieder H. and McKay D., 2001, "Global Energy Resources and Hydrogen Supply Costs", Task Final Report 8.4-1, CRYOPLANE Project.

Schumann U., 2003, "Aviation, Atmosphere and Climate – What has been learned", Proceedings of the AAC-Conference, Friedrichshafen, Germany, 30 June-3 July 2003.

Schumann U., Schlager H., Arnold F., Baumann R., Haschberger P. and Klemm O., 1998, “Dilution of aircraft exhaust plumes at cruising altitudes”, Atmos. Env., Vol. 18, pp. 3097-3103.

Schumann U., Konopka P., Baumann R., Busen R., Gerz T., Schlager H., Schulte P. and Volkert H., 1995, ”Estimate of diffusion parameters of aircraft exhaust plumes near the tropopause from nitric oxide and turbulence measurements”. J. Geophys. Res., Vol. 100, pp. 14147-14162.

Schweiger M., 1997, “Optimierung einer Matrix-Konfiguration für die Mikro-Misch-Diffusionsverbrennung von Wasserstoff in der APU GTCP 36-300. (Optimisation of a matrix-configuration for the micromix diffusive hydrogen combustion in the APU GTCP 36-300.)”, Diploma Thesis, FH-Aachen, Germany. Cited in: Dahl G. and Suttrop F., 2001b, “Combustion Chamber and Emissions, The Micromix Hydrogen Combustor Technology”, Task Technical Report 4.4-5A, CRYOPLANE Project.

Sefain M. and Jones R., 2001, “Definition of facilities requiring change for LH_2 operations”, Task Final Report 7.6-2, CRYOPLANE Project.

Segalman I., McKinney R.G., Sturgess G.J. and Huang L-M., 1993, “Reduction of NO_x by Fuel-Staging in Gas Turbine Engines – a Commitment to the Future”, AGARD Meeting on Fuels and Combustion Technology for Advanced Aircraft Engines, May 1993.

Shum F., Moore M., Cohen J., Rosfjord T., Eberius H., Ziemann J., Thomaier D. and Simon B., 1996, “Potential Use of Hydrogen in Air Propulsion”, Final Report, submitted to Hydro-Québec (contract no. 16233-92-ERE-015-00) and European Union (contract no. 4541-91-11 EL ISP PC).

Simos D., 2000, Piano User’s Guide, For Piano Version 3.6, Lissys Ltd. (Information: http://www.lissys.demon.co.uk/.)

Singh R. , 2002, “Combustor Cooling and Metal Temperatures”, Lecture Notes of Course in Gas Turbine Combustion, Cranfield University, UK, 24-28 June 2002.

Singh R., 2001, “An Overview: Gas Turbine Generated Pollutants and the Emerging Technology Solutions”, Lecture Notes of course in Gas Turbine Performance, Cranfield University, UK, 11-15 June 2001.

Sosounov V. and Orlov V., 1990, “Experimental Turbofan Using Liquid Hydrogen and Liquid Natural Gas as Fuel”, AIAA 90-2421, Proceedings of AIAA/SAE/ASME/ASEE 26^{th} Joint Propulsion Conference, Orlando, USA, 16-18 July 1990.

Sturgess G.J., McKinney R.G. and Morford S.A., 1993, “Modification of Combustor Stoichiometry Distribution for Reduced NO_x Emissions From Aircraft Engines”, Transactions of the ASME, 570/Vol. 115.

Sundén B., 2004, Professor at Department of Heat and Power Engineering, Lund Institute of Technology, Lund University, Sweden, private communication.

Suttrop F., 2003, Professor at Fachhochschule Aachen, Germany, private communication.

SVEBIO, 2002, Faktablad 1/98 Bioenergi – översikt, www.svebio.se, visited April 2002.

Svensson F. and Singh R., 2005, "Design of Hydrogen-Fuelled Aero Gas Turbines for Low Environmental Impact", Proceedings of 17th Int. Symposium on Air Breathing Engines, ISABE, Munich, Germany, 4-9 September 2005.

Svensson F., Hasselrot A. and Moldanova J., 2004, "Reduced Environmental Impact by Lowered Cruise Altitude for Liquid Hydrogen-Fuelled Aircraft", Aerosp. Sci. and Techn., Vol. 8, Issue 4, pp. 307-320.

Svensson F. and Singh R., 2004, "Effects of Using Hydrogen on Aero Gas Turbine Pollutant Emissions, Performance and Design", Proceedings of ASME Turbo Expo 2004, Vienna, Austria, 14-17 June 2004.

Swedish Energy Agency, 2000, "Energiläget i siffror".

Söder L., 2002, Professor at the Department of Electrical Power Engineering, The Royal Institute of Technology, Stockholm, Sweden, private communication.

Torenbeek, 1982, Synthesis of Subsonic Airplane Design, Kluwer Academic Publishers Group, Dordrecht, Holland.

Tremmel H.G., Schlager H., Konopka P., Schulte P., Arnold F., Klemm M. and Droste-Frank B., 1998, "Observations and model calculations of jet aircraft exhaust products at cruising altitude and inferred initial OH emissions", J. Geophys. Res., Vol. 103, pp. 10 803-10 816.

TurboMatch – User's Manual: The TurboMatch Scheme, for Aero/Industrial Gas Turbine Engine Design Point/Off-Design Performance Calculation, 1999, Cranfield University, UK.

Turns R.S., 1996, An Introduction to Combustion: Concepts and Applications, McGraw-Hill, Inc., Singapore.

US NASA Advanced Subsonic Technology (AST) Program. In: IPCC, Aviation and the Global Atmosphere, Penner J. L., Lister D. H., Griggs D. J., Dokken D. J., McFarland M. (eds.), 1999, Cambridge University Press, Cambridge, UK.

Visser W. and Broomhead M., 2000, "GSP, a generic object-oriented gas turbine simulation environment", 2000-GT-0002, Proceedings of AMSE Turbo Expo 2000, Munich, Germany.

Walsh P.P. and Fletcher P., 1998, Gas Turbine Performance, Blackwell Science Ltd, UK.

Westenberger A., 2003a, “Hydrogen Fuelled Aircraft”, Proceedings of AIAA/ICAS Conference, Dayton, Ohio, USA, 14-17 July 2003.

Westenberger A., 2003b, “Liquid Hydrogen Fuelled Aircraft – System Analysis, CRYOPLANE”, Final Technical Report, GRD1-1999-10014, submitted to the European Commission.

Wester L., 1996, ”Tabeller och diagram för energitekniska beräkningar”, Västerås, Sweden.

Whellens M.W., 2003, “Multidisciplinary Optimisation of Aero-Engines Using Genetic Algorithms and Preliminary Design Tools”, Ph.D. Thesis, Cranfield University, UK.

Williams V., Noland R.B. and Toumi R., 2002, “Reducing the climate change impacts of aviation by restricting cruise altitudes”, Transportation Research, Vol. D7, pp. 451-464.

WMO, 1991, “Scientific Assessment of ozone depletion: global ozone research and monitoring project”, Rep. No 25.

Wuebles P., Luther F. and Penner J., 1983, “Effect of coupled anthropogenic perturbations on the stratospheric ozone”, J. Geophys. Res., Vol. 88, pp. 1444-1456. Cited in: Klug H. G., Bakan S. and Gayler V., 1996, “CRYOPLANE - Quantitative Comparison of Contribution to Anthropogenic Greenhouse Effect of Liquid Hydrogen Aircraft versus Conventional Kerosene Aircraft”, EGS XXI General Assembly, Den Haag, 6-10 May 1996.

Ziemann J., Mayr A., Anagnostou A., Suttrop F., Lowe M., Bagheri S. A. and Nitsche Th., 1998a, “Potential Use of Hydrogen in Air Propulsion, EQHHPP, Phase III.0-3”, Final Report, submitted to European Union (contract no. 5077-92-11 EL ISP D).

Ziemann J., Shum F., Moore M., Kluyskens D., Thomaier D., Zarzalis N. and Eberius H., 1998b, “Low-NO_x Combustors for Hydrogen Fueled Aero Engine”, Int. J. Hydrogen Energy, Vol. 23, No. 4, pp. 281-288.

Zimbrick R.A. and Colehour J.L., 1998, “An Investigation of Very High Bypass Ratio Engines for Subsonic Transports”, Proceedings of AIAA/AMSE/SAE/ASEE 24th Joint Propulsion Conference, Boston, Massachusetts, USA, 11-13 July 1998.

Åhlgren M., 2000a, “PROGNOSER”, (Document notation: Rip/MBÅ 001), Unpublished report by the Swedish Civil Aviation Administration.

Åhlgren M., 2000b, Forecast analyser at the Swedish Civil Aviation Administration, private communication.

APPENDIX A – AERO GAS TURBINE FUNDAMENTALS AND PERFORMANCE ANALYSIS

As the great majority of this thesis in one way or another deals with aero gas turbines, and in particular their performance behaviour, these subjects are raised in this first appendix. The elementary aero gas turbine theory and the most important parameters are outlined in Appendix A.1, and in Appendix A.2 a brief description of the components included in a gas turbine is given. In Appendix A.3 the performance of gas turbines, including simulation tools for estimating the performance and the general design point performance behaviours are, outlined. Particularly the performance code used for most of the computations in this thesis is described, and amendments made to the code for the purposes of the work conducted in the thesis are outlined.

Appendix A.1 – Elementary Gas Turbine Theory

In an aero gas turbine thermal energy derived from combustion of fuel with air is converted to a high-speed gas stream to propel an aircraft. A simple form of a gas turbine used for propulsion is the turbojet engine, which is shown in Figure A-1. Air enters the intake with a speed roughly equal to the speed of the aircraft, and is diffused prior to entering the compressor. In the compressor energy is added, and the temperature and pressure of the air stream increase. Thereafter, the warm compressed air stream is mixed with fuel in the combustion chamber and burnt, resulting in a large temperature rise. The hot combustion gases are then expanded in a turbine which is mounted on the same shaft as the compressor, and thus drives the compressor. The remaining energy of the gas stream leaving the turbine is expanded through a propelling nozzle, thus providing thrust.

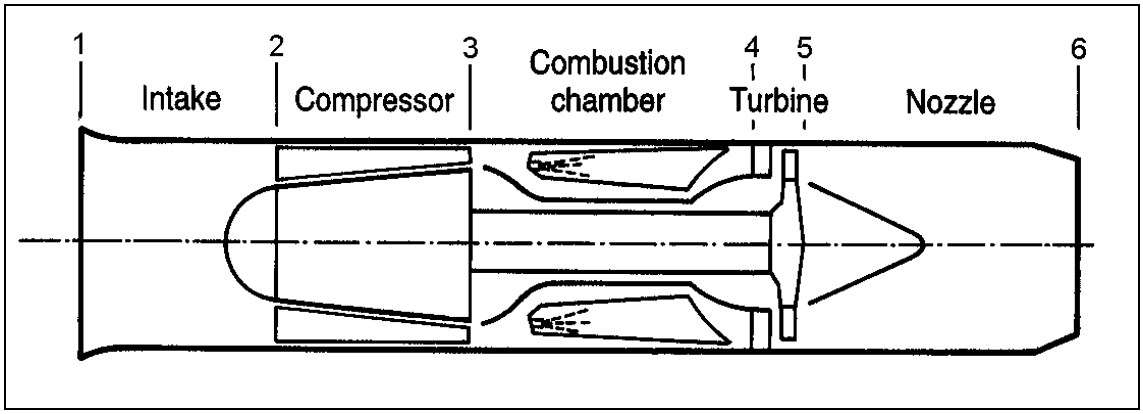

Figure A-1. Schematic description of a simple turbojet engine [adapted from Cohen et al., 1996].

Assuming that air enters the engine with the velocity V_a, leaving with the velocity V_j and neglecting any difference in mass flow, W, between the inlet and outlet streams, the thrust output of the engine is given by:

$$F = W \cdot \left(V_j - V_a\right) + A_j \cdot \left(P_j - P_a\right) \tag{A-1}$$

where the first term, W (V_j–V_a), is the momentum thrust and the second term, A_j (P_j–P_a), is the pressure thrust. The momentum thrust arises due to a change in the velocity of the air stream, while the pressure thrust arises when exhaust gases are not expanded completely to P_a in the propulsive duct, causing the exhaust pressure in the exit plane, P_j, to be greater than the pressure of the inlet, P_a, and thereby providing a pressure thrust acting over the jet exit area, A_j. For more detailed performance estimations the fuel flow should not be neglected. However, since the fuel flow is normally only a few percent of the gas flow through the turbines, neglecting it can be a reasonable assumption.

As a measure of how well an aero gas turbine performs, an overall efficiency is defined as the ratio of useful work on the aircraft to the energy of the fuel supplied:

$$\eta_o = \frac{F \cdot V_a}{W_F \cdot LHV} \tag{A-2}$$

where W_F is the fuel flow and LHV is the lower heating value of the fuel. The thermal efficiency, i.e. the conversion of thermal energy into mechanical energy, is subject to the laws of thermodynamics. Theoretically, the highest thermodynamic efficiency of a reversible heat engine operating between two thermal energy reservoirs at temperatures T_l and T_h is the Carnot efficiency, defined by [Cengel and Boles, 1994]:

$$\eta_c = 1 - \frac{T_l}{T_h} \tag{A-3}$$

where T_l and T_h are the lowest and highest temperatures within the cycle, respectively. For aircraft engines the lowest temperature is equal to the atmospheric temperature and the highest temperature is equal to the combustor outlet temperature, thus giving a Carnot efficiency of about 0.85. In practice, the thermal efficiency is lower because the Brayton cycle[12] on which aero engines operate is less efficient than a Carnot cycle for the same maximum temperature, and because of losses in the components due to viscous effects [Kerrebrock, 1996]. The thermal energy supplied in the fuel is W_F LHV, and this energy is converted into potentially useful kinetic energy for propulsion, W (V_j^2-V_a^2)/2, together with unusable enthalpy in the jet, mC_p (T_j-T_a), and hence the thermal efficiency can be defined as [Cohen et al., 1996]:

$$\eta_{th} = \frac{\frac{W \cdot \left(V_j^{\,2} - V_a^{\,2}\right)}{2}}{W_F \cdot LHV} \tag{A-4}$$

[12] The Brayton cycle is the ideal cycle for gas turbine engines [Cengel and Boles, 1996]. The cycle is made up of four internally reversible processes: isentropic compression, heat addition at constant pressure, isentropic expansion and heat rejection at constant pressure.

The effectiveness with which the propulsive duct is being used for propelling the aircraft is called the propulsive efficiency. This is defined as the ratio of used propulsive energy to the sum of that energy and the unused kinetic energy of the exhaust jet [Cohen et al., 1996]:

$$\eta_p = \frac{W \cdot V_a \cdot (V_j - V_a)}{W \cdot \left[V_a \cdot (V_j - V_a) + \frac{(V_j - V_a)^2}{2} \right]} = \frac{2}{1 + \frac{V_j}{V_a}} \tag{A-5}$$

Examining equations (A-4) and (A-5) it can be seen that the denominator of equation (A-5) is equal to the numerator of equation (A-4), and thus that:

$$\eta_o = \eta_{th} \cdot \eta_p \tag{A-6}$$

As the overall efficiency is linked to the aircraft speed, and therefore not an exclusive engine parameter, this concept is often discarded in favour of the specific fuel consumption (SFC) for propulsion engines. The specific fuel consumption is defined as the fuel consumption per unit thrust (e.g. g/kN s):

$$SFC = \frac{W_F}{F} \tag{A-7}$$

The SFC in turn is proportional to V_a/η_o [Cohen et al., 1996]. It is important to minimise SFC for applications where the mission fuel consumption is of primary interest, e.g. long-range civil aircraft applications. When comparing SFC levels for different engines, it is important to know that the heating values of the fuels are the same; otherwise they are not comparable.

Another important performance parameter is the specific thrust (SPT), which is the thrust per unit of mass flow of air at engine inlet (e.g. m/s):

$$SPT = \frac{F}{W_1} \tag{A-8}$$

Since engine size is related to the frontal area, which is determined by the air flow, the specific thrust gives an indication of the relative size of engines producing the same thrust. The engine size does not only relate to the weight of the engine, but also to the drag via the frontal area. For applications where engine weight or/and volume is crucial, or for aircraft flying at high Mach numbers where the drag per unit frontal area is high, it is particularly important to maximise specific thrust.

Looking at equation (A-1) it is clear that the required thrust can be obtained by designing the engine to produce either a high velocity jet of small mass flow or a low velocity jet of high mass flow. By doing the latter, the propulsive efficiency increases (since V_j decreases, see equation (A-5)), and hence SFC decreases at the expense of decreased SPT. In order to achieve this, the turbofan engine was conceived. The

turbofan engine features a fan, driven by an additional turbine downstream of the compressor turbine that pumps air through a secondary nozzle. The high-pressure parts of the engine, consisting of the high-pressure compressor, combustion chamber and high-pressure turbine, are commonly referred to as the core of the engine. The ratio of the cold mass flow of the by-pass to the hot mass flow passing through the core is called the by-pass ratio (BPR):

$$BPR = \frac{W_{by-pass}}{W_{core}} \tag{A-9}$$

The by-pass air could either be mixed with the hot flow from the core prior to the propelling nozzle or exhausted through a separate nozzle.

Appendix A.2 – Gas Turbine Engine Components

This appendix embodies a brief description of the components included in an aero gas turbine. The function along with the physics occurring in each component is briefly covered.

A.2.1 Inlet

The prime requirement for the aero engine intake is to diffuse the free stream air from a high Mach number, while minimising the pressure loss up to the compressor face. In addition, the flow should ideally enter the compressor with a uniform pressure and velocity at all flight conditions. If these requirements are not satisfied, the compressor might surge, which can result in either combustor flame-out or severe mechanical damage due to blade vibration induced by unsteady aerodynamic effects [Cohen et al., 1996].

By treating the inlet as an adiabatic duct it may be found that the total temperature across the inlet is constant (since there is no heat or work transfer), while a loss of stagnation pressure arises due to friction and shock waves at supersonic speeds. Under static conditions or at very low forward speeds, the intake acts as a nozzle in which the air accelerates from rest to the compressor inlet velocity. However, for normal forward speeds the air is decelerated, causing the static pressure to increase from the atmospheric pressure, P_a, to the compressor inlet pressure, P_2. It is the stagnation pressure at compressor inlet that is essential for performance calculations, and the pressure rise, P_2-P_a, is referred to as the ram pressure rise.

Engines designed for subsonic speeds usually employ a pod mounting in which the air is diffused till the engine intake leading edge, where the air is accelerated along the “nose bullet” as the flow area transitions from circular to annular before the compressor face (see Figure A-2). During static conditions the air is accelerated from behind and in front of the flight intake, and thus to avoid flow separation the leading edge needs to be rounded.

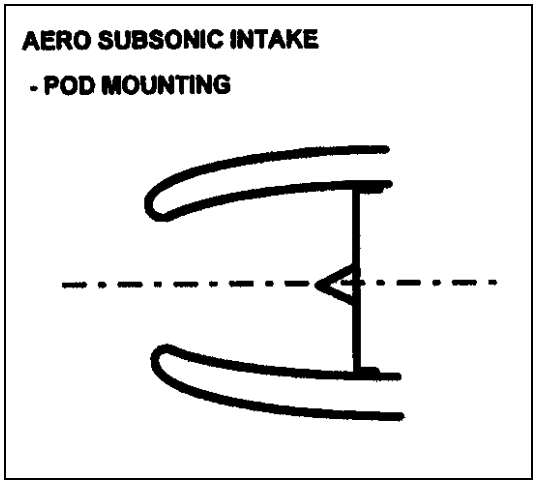

Figure A-2. Configuration of an aero subsonic intake featuring a pod mounting [Walsh and Fletcher, 1998].

At supersonic speeds the intake needs to diffuse the flow from supersonic to low subsonic speeds. A reasonable axial Mach number for the first compressor stage is in the region of 0.4-0.5 [Cohen et al., 1996]. In order to accomplish this at supersonic speeds with an acceptable level of efficiency, an intake of a convergent-divergent type often needs to be employed. Typically, such an intake is rectangular with a variable throat area.

The engine intake efficiency depends upon the location of the engine in the aircraft (in wing, pod or fuselage). The aerodynamic design also affects the intake efficiency. There are a number of ways to define the intake effectiveness: isentropic efficiency, ram efficiency and pressure (or ram) recovery factor. The isentropic and ram efficiencies are commonly used and are defined in terms of temperature rises and pressure rises, respectively, while the pressure recovery factor is defined as the total pressure ratio over the intake, P_{t2}/P_{ta}. The ram recovery factor relates to the ram pressure rises.

A.2.2 Compressor

The purpose of a compressor is to increase the total pressure of a gas stream to the pressure required by the engine cycle, while using the minimum amount of shaft power possible. There are two different types of compressors: centrifugal and axial flow compressors. As the names indicate, the difference consists of the direction of the air flow through the compressor. While the air flow in an axial compressor flows parallel to the shaft(s) of the engine, the flow is directed radially in a centrifugal impeller, followed by a radial diffuser in a centrifugal compressor. For applications where small frontal area, low weight and high efficiency are essential, the axial type is the preferable choice. The centrifugal compressors dominate for small sizes where cost is paramount. For large sizes the only possible choice is the axial flow compressor. Due to these considerations, the axial flow machine dominates the field for large power amounts and the centrifugal compressor is restricted to the lower end of the power spectrum, where the flow is too small to be handled efficiently by axial blading [Cohen et al., 1996]. An advantage of the radial compressor is that it is less sensitive to a non-uniform inlet flow.

The compressor comprises a number of stages, see Figure A-3. Each stage consists of a row of rotor blades followed by a row of stator vanes. The rotors are mounted on a common shaft. Over the rotor blades the static temperature, the flow velocity, and hence also the total temperature are increased. Assuming an adiabatic process and knowing that there is no work input, it follows that the total temperature is constant over the stator row [Cohen et al., 1996]. While all power is absorbed by the rotor row, kinetic energy is transformed to an increase in static pressure over the stator row by diffusing the flow. Moreover, the total pressure decreases slightly due to friction. As a consequence of decreasing relative velocity (velocity of the flow relative to the rotor blades and stator vanes) for both the blade row and stator row, the static pressure is increased over both these stages.

Owing to the adverse static pressure gradient through the compressor, the pressure ratio attainable in a single stage is limited to avoid flow separation and reversal flow [Walsh and Fletcher, 1998]. If the difference between the flow direction and the blade angle (angle of incidence) becomes excessive, stall arises. As opposed to the compressor, the turbine works with an advantageous pressure gradient, and as a consequence of this a single turbine stage can drive a large number of compressor stages. The adverse static pressure gradient along the compression process makes the design of the compressor a challenging task indeed.

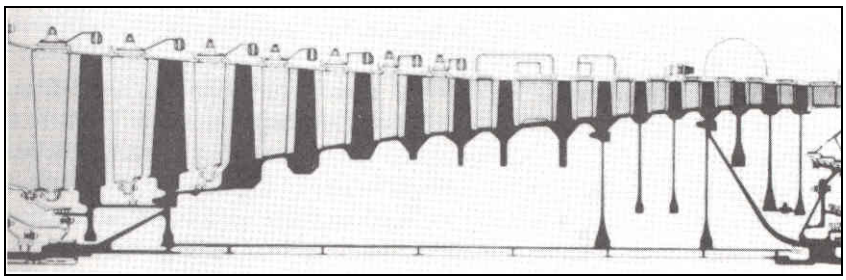

Figure A-3. Sixteen-stage high-pressure ratio compressor (by courtesy of General Electric) [Cohen et al., 1996].

Commonly the angle of the first row of stator vanes may be changed by control system action. This is called variable inlet guide vanes (VIGVs), and is used to improve the off-design operation. In addition, it might be desirable to provide more stator rows downstream with variable angles, so-called variable stator vanes (VSVs).

As a measure of the effectiveness of a compressor, an isentropic efficiency is defined as the ratio of the ideal specific work input, i.e. specific enthalpy rise for a given pressure ratio, to the actual. An alternative measure is the polytropic efficiency, which is the isentropic efficiency over an infinitesimal small step in the compression process, such that its magnitude would be constant throughout the process [Cohen et al., 1996]. For performance calculations the isentropic efficiency is the preferable measure.

In order to assess the compressor performance during part load conditions, compressor maps, i.e. plots of pressure ratio and isentropic efficiency versus quasidimensionless flow for a series of lines of constant quasidimensionless speed, are employed. Principally, a compressor map for an axial compressor is shown in Figure A-4. As seen

in the figure there are two different conditions that limit the flow, namely, the surge line and the choke condition. Surging is a complex flow phenomenon that can occur during certain operation conditions when the stall becomes severe. Describing this phenomenon is beyond the scope of this appendix. The interested reader is referred to textbooks, such as Walsh and Fletcher (1998) and Cohen et al. (1996). Choking occurs when the flow Mach number in the smallest flow passage of a stage reaches unity, making it impossible to increase the flow further.

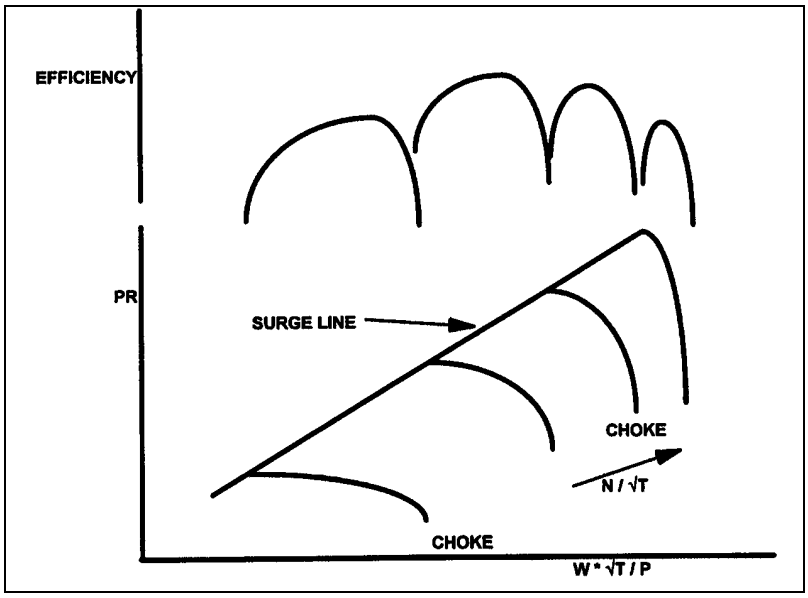

Figure A-4. Compressor map of an axial configuration [Walsh and Fletcher, 1998].

A.2.3 Combustion Chamber

Combustion in a gas turbine combustor is a continuous process in which fuel is burnt in the air supplied by the compressor. An electric spark is used to initiate the combustion process, and thereafter the flame must be self-sustaining. From an engine cycle perspective, the combustor outlet temperature is the essential parameter. There are three different possible types of combustion systems [Cohen et al., 1996]: can, cannular and annular combustors. In the can type, which was employed by the earliest aircraft engines, the air leaving the compressor is split into a number of separate streams, each supplying a separate chamber. If the flame tubes are uniformly spaced around an annular casing the concept is called cannular. This combustion system is commonly employed by industrial gas turbines. Owing to its compact dimensions, it is the annular combustor that is the preferable choice when the available space is the limiting factor. The annual combustor has no separate flame tubes, and it is this combustion system that is universally used in modern aircraft engines.

Designing a gas turbine combustion chamber is a challenging task, comprising several difficulties and trade-offs. The combustion chamber should satisfy a wide range of requirements whose relative importance varies among engine types. Amongst others the following basic requirements need to be regarded in the design process [Lefebvre, 1998]: high combustion efficiency, reliable and smooth ignition, wide stability limits,

low pressure loss, reasonable outlet temperature distribution (pattern factor), low pollutant emissions, good durability and freedom from combustion-induced instabilities. These tasks must be accomplished, requiring minimum space within the engine envelop and at the same time meeting the engine weight and cost targets [Ziemann et al., 1998a]. In Figure A-5 the main components of a conventional combustion chamber are shown.

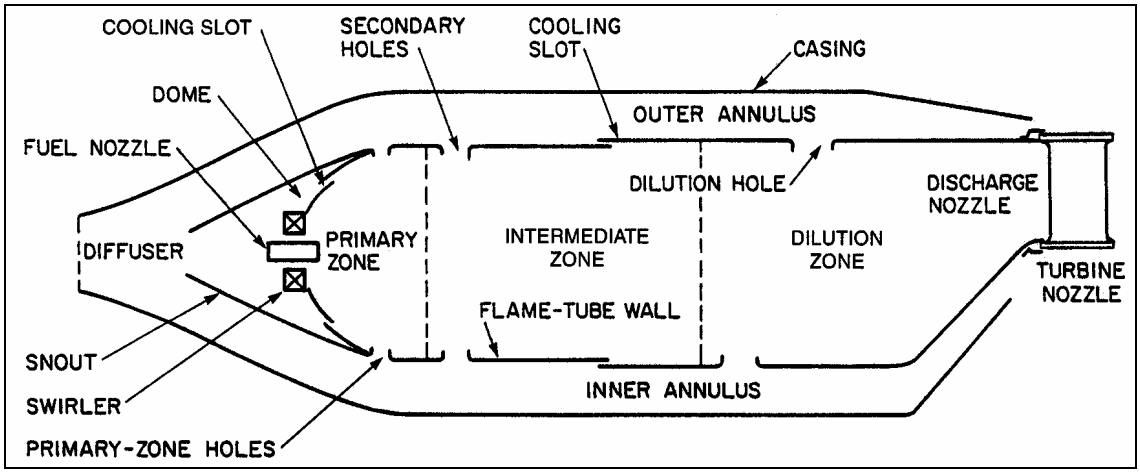

Figure A-5. Conventional combustion chamber [Lefebvre, 1998].

The main function of the primary zone is to anchor the flame and provide sufficient time, temperature and turbulence to attain essentially complete combustion of the incoming fuel-air mixture [Lefebvre, 1998]. If the temperature in the primary zone is high enough (higher than about 2000 K), dissociation reactions will result in the appearance of essential concentrations of not completely oxidized species in the efflux gases. In order to recover these dissociation losses and to continue combustion of any imperfectly mixed fuel-rich pockets, the combustion chamber features an intermediate zone. Before the combustion gases enter the turbine, the temperature needs to be reduced and a temperature distribution acceptable for the turbine needs to be created. Ideally, the temperature should be lowest where the mechanical stresses are highest, which is at the turbine blade root, and at the turbine blade tip, to protect seal materials [Lefebvre, 1998]. Reduced temperature and a reasonable temperature distribution are achieved in the dilution zone where the remaining air is admitted through holes in the annulus.

A.2.4 Turbine

The functionality of the turbine is to extract power from the gas flow leaving the combustion chamber to drive either a compressor, or in the case of a power turbine, to drive a load, such as a propeller or an electrical generator. Similarly as for compressors, these could be axial or radial. The vast majority of gas turbines employ axial turbines. Exactly the same arguments as were raised in the section discussing compressors, concerning axial versus radial flow machines, apply for turbines. The turbine stage comprises a row of nozzle guide vanes (NGVs) followed by a row of rotor blades mounted on a disc (see Figure A-6). In multi-stage turbines, the discs are mounted on a conical feature forming a drum.

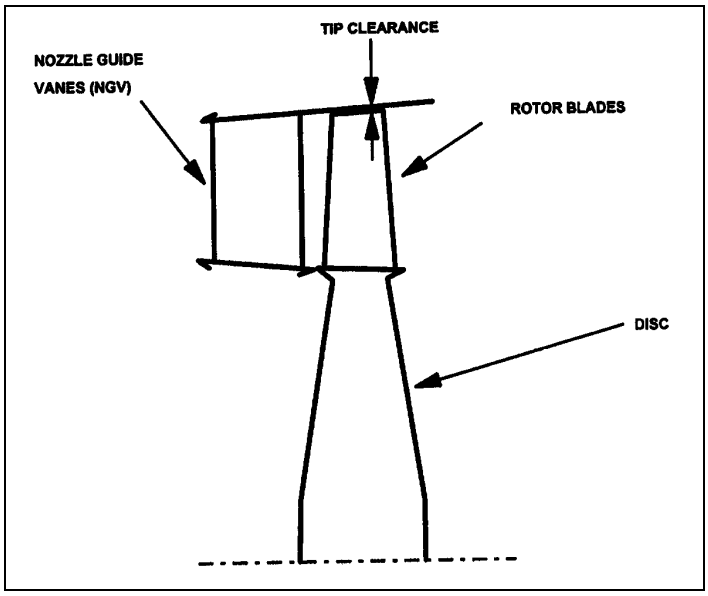

Figure A-6. Axial turbine configuration [Walsh and Fletcher, 1998].

The high temperature and pressure gas stream is accelerated and turned over the nozzle guide vanes. In this process there is no heat or work transfer, and only a small loss in total pressure owing to friction and turbulence. Furthermore, the total temperature is unchanged, and the static temperature and pressure are reduced due to increasing the flow velocity. Across the rotor, work is extracted by changing the whirl (tangential) flow velocity (which produces a torque), and the total temperature and pressure are reduced.

In order to attain a high performance of a gas turbine, there is a desire to increase the maximum allowable temperature in the cycle. One way of demonstrating that an increased combustor outlet temperature provides performance benefits, is to consider the Carnot efficiency (equation (A-3)). This efficiency says that to maximise the thermodynamic efficiency, the difference between the minimum and maximum temperature in the cycle should be maximised. The maximum cycle temperature is limited by the maximum allowable metal temperature of the nozzle guide vanes and the rotors of the high-pressure turbine, which are dependent on material properties. As discussed in this thesis, also concerns of emissions of oxides of nitrogen have become a limiting factor for the combustor outlet temperature. The effectiveness of the turbine is expressed via the isentropic efficiency defined analogously to the isentropic efficiency for a compressor.

For reasons of cooling hot parts of the turbine and providing air for several other purposes (sealing, handling bleed, customer bleed, etc.), air is extracted from a suitable engine location of the compressor. The air is transferred either internally through a series of orifices and seals, or externally via pipes outside the engine casing. The rotor blades are then cooled by forcing air from the inside of the blades through holes to remove heat and to create an effusing layer of air outside the blades, which reduces the rate of heat transfer from the hot gas stream to the blade. This principle is called internal forced convection of air and is shown in Figure A-7, together with some other methods

of blade cooling. Stator vanes are cooled in a similar manner. Extracting air and cooling hot parts this way gives rise to losses that deteriorate the performance. However, the net effect on the performance when including the effect of increasing the maximum allowable metal temperature is a substantial performance benefit [Cohen et al., 1996].

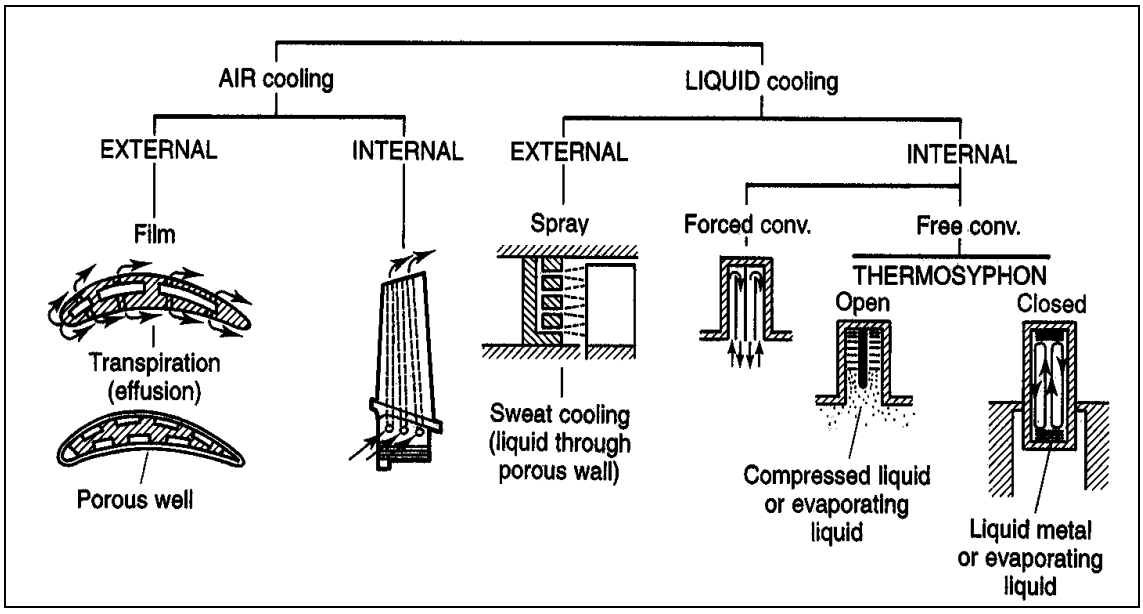

Figure A-7. Different methods of blade cooling [Cohen et al., 1996].

The performance of turbines at various operating conditions is estimated using turbine maps which are derived in a similar manner as the compressor maps. For the most common form of turbine maps, the capacity (quasidimensionless flow), efficiency and exit swirl angle are plotted for lines of constant quasidimensionless speed versus the pressure ratio. Similarly as for the compressor map, for each speed line there is a maximum flow that cannot be exceeded, i.e. the choke condition.

A.2.5 Propelling Nozzle

The function of the propelling nozzle is to convert the internal energy of the gas stream into kinetic energy, and hence provide thrust. A simple turbojet engine features a propelling nozzle downstream of the turbine, while a turbofan engine either may feature two separate nozzles for the hot and cold streams, or a single nozzle in which the two streams leave after having been mixed. Prior to the nozzle, the gas stream leaving the turbine is diffused to reduce velocity, and hence reduce friction loss, in the jet pipe. Furthermore, for military applications when thrust boosting is required, an afterburner might be included in the jet pipe.

When discussing propelling nozzles, the question arises whether to employ a simple convergent or a convergent-divergent nozzle. As the expansion ratio across the nozzle often is higher than the critical ratio (the ratio that gives sonic flow in the throat, and thus makes it impossible to increase the flow further), it appears to be desirable to use a convergent-divergent nozzle. Theoretically (i.e. assuming isentropic expansion), the maximum thrust is achieved when complete expansion to the atmospheric pressure

occurs in the nozzle. This implies that the pressure thrust (second term in equation (A-1)) due to incomplete expansion does not entirely compensate for the loss of momentum thrust due to a smaller jet velocity [Cohen et al., 1996].

However, when taking friction into account this is no longer true, since the theoretical jet velocity is not achieved. Furthermore, a convergent-divergent nozzle is heavier and larger, and thereby causes installation losses and affecting the aircraft weight detrimentally. For expansion ratios smaller than the design value, these nozzles would certainly be less efficient than the convergent, because of losses incurred by the formation of shock waves in the divergent proportion [Cohen et al., 1996]. For these reasons convergent nozzles are the most widely used. Nevertheless, the convergent-divergent are the nozzles that are used at high supersonic speeds when the large ram pressure rise in the intake results in a very high nozzle pressure ratio.

The losses of the propelling nozzle could be included either via an isentropic efficiency or via a specific thrust coefficient. The former is defined by the ratio of the actual total temperature change across the nozzle to the isentropic temperature difference. The specific thrust coefficient is expressed as the ratio of the actual specific gross thrust, namely, $[W V_j+A_j (P_j-P_a)]/W$, to that which would have resulted from isentropic flow.

Appendix A.3 – Gas Turbine Engine Performance

The subject of gas turbine performance embodies the analysis of a gas turbine-based system, involving merit parameters, such as thrust and power, and flow parameters, such as pressures, temperatures and mass flows [Whellens, 2003]. Estimating the performance is highly important during the whole engine design process, from the preliminary cycle design studies to the post-production phases.

The performance analysis can be carried out at three levels [Whellens, 2003]: design point performance, off-design performance and transient performance. At the design point the geometric quantities of the engine are defined, and the performance at this operating point affects the performance at all other operating conditions. Off-design performance refers to the performance at any other point within the operational envelope. The performance during transient modes, such as acceleration and deceleration, is referred to as transient performance. In order to assess the performance of a certain gas turbine system, a description of the engine in terms of its constituent components needs to be defined, individual engine components and the gas flowing through the system need to be modelled, and a set of compatibility laws needs to be considered.

Except for some engine components (e.g. the fan) where the flow at inlet or outlet is far from spatially uniform, the components are modelled as one-dimensional. At the design point, components are described in terms of variables that are either easily relatable to the design criteria for the engine (e.g. pressure ratio for compressors and temperature rises for combustors) or are directly obtainable from the application of the compatibility laws (e.g. the required power output for the turbines) [Whellens, 2003]. Moreover, efficiencies and pressure losses for individual components are often required. At off-design, on the contrary, performance of individual components is estimated using

"maps". Maps describe the behaviour of a certain component at part load conditions. For compressors and turbines, for instance, the maps feature the pressure ratio and efficiency versus non-dimensional flow and non-dimensional rotational speed (see also Appendix A.2). In order to model the gas flow, it is usually treated as a multi-component ideal gas.

The compatibility laws constitute the mass, energy and shaft speed compatibility [Whellens, 2003]. Mass compatibility is the same as conservation of mass within a component, while the energy compatibility implies that the energy is conserved within a component. In addition, the latter implies that the individual spools are in energetic equilibrium, usually meaning that the work required by the compressors is equal to the work provided by the turbines on the same spool. The shaft speed compatibility is only required for off-design conditions and means that all components that are mechanically linked to the same shaft rotate at the same speed.

The engine design process is initiated by selecting a certain operating point as the design point, according to which the engine thermodynamic should be designed. This operating point often corresponds to a point within the operational envelope of a high power setting, such as take-off or top of climb. Alternatively, the operating condition where an engine will spend most time is chosen as the design point. The cycle design point needs to be defined in terms of ambient conditions (altitude, Mach number and any possible temperature deviation from the ISA standard) and in terms of the components' design variables. The main output of the design point analysis is the engine geometry, including some critical flow areas, such as nozzle areas and turbine nozzle throat areas.

Once the engine geometry has been fixed, the off-design performance behaves, to a first order of accuracy, non-dimensionally [Walsh and Fletcher, 1998]. This implies that for a certain component, there is a dimensionless parameter group that is constant for all operating conditions, once the geometry is fixed. Instead of referring to full dimensionless groups, referred groups, which are groups of parameters where the constants have been removed and theta (inlet temperature/288.15 K) has been substituted for temperature and delta (inlet pressure/101.325 kPa) has been substituted for pressure, are commonly considered.

Having defined the engine geometry, the performance may be calculated at any operating point by defining the altitude, flight Mach number, any temperature variation from the ISA standard and a value defining the throttle setting, usually the combustor outlet temperature (COT). Finding the performance of a specific off-design point is an iterative procedure, involving the definition of iteration variables and seeking the set of data that both satisfies the compatibility laws and yields the same values of critical flow passage areas as determined at the design point. The required number of iteration variables is determined by the specific engine configuration and the individual component models [Whellens, 2003].

A.3.1 Simulation Tools for Modelling Performance

There are a number of simulation tools available, which have been developed by industrial or academic organisations, for modelling gas turbine performance. Some of them are commercial and others are in-house tools. In this section three of these are mentioned very briefly and one, TurboMatch, is described more in detail. In order to allow for emissions estimation, the version of TurboMatch used for hydrogen fuel has been supplemented with various routines by the author of this thesis.

One of the most well-known codes is GasTurb™ which is a Windows-based user-friendly code [Kurzke, 1998]. It allows for design, off-design as well as transient performance analysis for a number of pre-defined configurations, both stationary and airborne. Parametric, optimisation and sensitivity studies can easily be performed. One drawback of this program compared with the TurboMatch program described below is that the program does not allow for the analysis of unconventional cycles as those discussed in section 2.2.4.

Another program is the GSP (Gas turbine Simulation Program) developed by NLR (National Aerospace Laboratory) of the Netherlands which allows for both steady state and transient performance estimations [Visser and Broomhead, 2000]. It is based on a Windows platform and also has built-in facilities for emission calculations, control system design and diagnostic studies. The last program mentioned here is the NCP (National Cycle Program) program. It is the result of the combined effort of different American engine manufacturers and NASA's Lewis Research Centre. Using this tool it is possible to model an engine for both steady state and transient conditions.

TurboMatch

Below follows a brief description of the simulation tool TurboMatch, taken from the User's Manual [TurboMatch, 1999]. For more information about the simulation tool and how to use it, one is referred to the User's Manual, and for detailed information concerning the code structure and its subroutines, one is referred to Boggia (2001).

The TurboMatch scheme has been developed by the School of Mechanical Engineering at Cranfield University to conduct design and off-design calculations of gas turbines. By means of "codewords", various pre-programmed routines, known as Bricks, can be called to simulate the action of different gas turbine components, resulting in output such as engine thrust (aero gas turbine) or power (stationary gas turbine), fuel consumption, etc., together with details of individual component performance and of the gas properties at various stations along the gas turbine.

Most Bricks corresponds to particular components, e.g. intake (INTAKE), compressor (COMPRE), burner (BURNER) and turbine (TURBIN), but there are also Bricks for arithmetical operations (ARITHY) and for the final calculation of performance (PERFOR) when all component processes have been evaluated. At each station along the gas turbine, the gas state is described by a number of quantities, known collectively in TurboMatch as the Station Vector (the word vector being used in the sense of an ordered set of numbers without any directional significance). Since most Bricks simulate the thermodynamic processes that occur within a component, they can be

considered as operating upon the gas state at the component inlet so as to generate the gas state at outlet. In addition to the Station Vector, generally the Bricks require other input data items (e.g. efficiencies, pressure loss factors, pressure ratios, etc.). These items are known collectively as Brick Data, and their nature and number are different for each Brick. Furthermore, some Bricks generate output (e.g. thrust, power, etc.), known as Engine Vector Results, which are different in kind from the Station Vectors. Some Bricks also need inputs that are outputs from other Bricks employed earlier in the program (e.g. compressor work, which is generated by the COMPRE Brick and subsequently used by TURBIN Brick). Such quantities are known as Engine Vector Data. A schematic figure illustrating the described features is shown in Figure A-8.

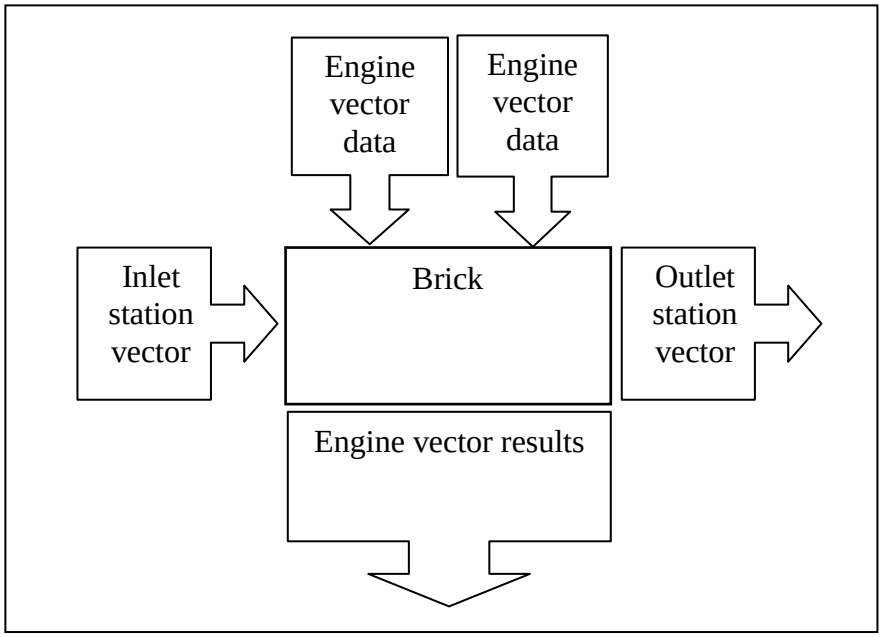

Figure A-8. Schematic description of the TurboMatch scheme structure.

In order to run a simulation an input file (*.inp) needs to be prepared. In the input file the gas turbine that is desired to be modelled is built from a series of codewords, which describe, in the order needed, the various Bricks to be used, together with information as to their Station Vector, Brick Data and Engine Vector requirements. The results of the present TurboMatch version are stored in two output files. In the ".tmr" file all results are stored in a legible fashion, while the results in the "fort.4" file are organised in a fashion that facilitates the extraction of the results to Microsoft Excel, where figures can easily be plotted.

Changes to the TurboMatch Source Code

The original version of the TurboMatch code was designed for analysis of gas turbines using kerosene only. In the EC-sponsored project CRYOPLANE, aimed at investigating the possibility of using hydrogen for aviation, performance data of aero gas turbines burning hydrogen were required, including data for design as well as off-design conditions for both conventional and unconventional cycles. Since TurboMatch is a flexible simulation tool, featuring a modular structure that makes it easy to add

additional components or input external results, it was decided that this code should be used for this purpose. However, to allow for hydrogen use, changes were needed.

Particularly, emphasis was to be given to those functions and subroutines that calculate the thermodynamic properties at various locations along the engine. These properties comprise enthalpy, entropy, C_p, R and molecular weight, and are needed by different Bricks which are called during the execution of the program. All changes made to the TurboMatch source code to enable modelling of gas turbines using hydrogen are thoroughly explained in Boggia (2001). Having performed the changes, the results have been checked and compared with results obtained by the well-established gas turbine performance simulation code GasTurb. The work with changing the code was completed successfully by Boggia (2001), and depending on fuel temperature, the changed version of TurboMatch is able to produce performance data very accurately for design as well as off-design conditions for both conventional and unconventional gas turbine cycles using hydrogen.

In addition to calculating performance data, for the purpose of the research carried out in this thesis, it was desired to calculate the amount of emission produced at certain operating points when using hydrogen. To achieve this, additional modules were developed and integrated in the TurboMatch code by the author. When burning hydrogen the only exhaust emissions are H_2O and NO_x, hence modules to estimate these emissions were required. The theory applied to estimate the emission index of NO_x is given in section 4.2, while the H_2O emissions are proportional to the fuel consumption. Moreover, a module that calculates the GWP in a certain operation point was developed. The theory about the GWP concept is explained in section 3.4 and Appendix B. The hydrogen version of TurboMatch was supplemented with the functions and subroutines listed in Table A-1, comprising the new emission features.

In addition to these files, two text files employed by the subroutines “READ-EMISSIONSDATA” and “READGWPDATA” need to be located in the same area as the other files. The file “NASA DATA.txt” contains data of flame temperature and mass fraction of H_2O at combustor exit versus temperature, pressure and equivalence ratio, obtained by the NASA CEA code [McBride and Gordon, 1996; and Gordon and McBride, 1994], while the file “GWP DATA.txt” contains GWP numbers for the species H_2O and NO_x versus altitude, from Appendix B. All subroutines are called from the main program, which is located in the file “master.for”. All changes and additional statements in the code performed by the author are preceded by remarks to facilitate for anyone who would like to work with the code in the future.

Table A-1. The new routines added to the TurboMatch code for calculation of emission indices of H_2O and NO_x, as well as GWP.

File	Routine(s)	Function
ConstAssign.for	CONSTASSIGNMENTS	All constants and parameters used in the new routines are assigned values.
Emissions.for	EMISSIONS	Calculates the emission indices of H_2O and NO_x.
GWP.for	GWP	Calculates the GWP value
Interpolation.for	INTERPOLATION	Employs interpolation routines to find the flame temperature and mass fraction of water (combustor exit) for given values of temperature, pressure and equivalence ratio.
InterpolationGWPdata.for	INTERPOLATIONGWP	Employs interpolation routines to find the GWP number for the species H_2O and NO_x for a given altitude.
IP.for	IP3,IP2, IP1, IP3F, IP2F, IP1F, DELIND, DELINDF	These routines are used for interpolation in 1-3 dimensions. Only IP1F and IP3F are used. IP1F is employed by INTERPOLATIONGWP and IP3F is employed by INTERPOLATION.
ReadData.for	READEMISSIONSDATA	Flame temperature and mass fraction of H_2O (at combustor exit) versus temperature, pressure and equivalence ratio are read from the text file “NASA DATA.txt” and stored in arrays.
ReadGWPdata.for	READGWPDATA	GWP numbers for the species H_2O and NO_x versus altitude are read from the text file “GWP DATA.txt” and stored in arrays.

A.3.2 Design Point Performance Behaviour

During the engine design process design point performance diagrams are created. These are also commonly used for comparing the performance of different engine concepts. These diagrams feature engine performance parameters, e.g. SFC or SPT, versus cycle parameters, e.g. OPR, COT or BPR, and are created by calculating the design point performance for a range of cycle parameters for which each combination represents a specific engine geometry.

For a turbojet engine there are two main design parameters: COT and OPR, while there are three for a turbofan engine: COT, OPR and BPR. In addition there is a fourth parameter, the fan pressure ratio (FPR), involved in the engine design process for a turbofan engine. However, for a given core engine (i.e. specified COT and OPR) and a fixed BPR, there is an optimum value of fan pressure ratio, which both minimises SFC and maximises SPT. Having specified the core, the amount of work provided to the low-pressure turbine is also fixed. Then the optimum fan pressure ratio is the pressure that transforms a reasonable amount of energy from the core to the by-pass stream. If a too low value of fan pressure ratio is chosen, the core jet velocity becomes excessively large, and ultimately there is no point in employing a fan. A too large fan pressure ratio, on the other hand, will result in an excessive by-pass jet velocity. By algebraic differentiation, it can be shown that the optimum value of the fan pressure ratio is the one corresponding to a ratio of by-pass jet velocity to core jet velocity equal to the energy transfer efficiency, i.e. product of low-pressure turbine and fan efficiencies [Walsh and Fletcher, 1998]:

$$\frac{V_{jby-pass}}{V_{jcore}} = \eta_{LPT} \cdot \eta_{fan} = \eta_{tf} \tag{A-10}$$

These efficiencies are about 0.9, and thus the optimum core jet velocity becomes higher by a factor of about 1.2. In practice, to reduce design and handling problems at the expense of a very small penalty in SFC, a value of fan pressure ratio lower than the optimum is chosen [Pilidis, 2001].

In Figure A-9 to Figure A-12 the design point performance for turbofan engines of different by-pass ratios for subsonic and supersonic conditions are displayed. All numbers are derived for a stator outlet temperature[13] (SOT) equal to 1500 K. More details and explanations can be found in Walsh and Fletcher (1998).

For Mach number 0.8, SFC improves significantly and SPT deteriorates essentially with increasing BPR. The main reason for the improved SFC is the increased propulsive efficiency due to the decreased core jet velocity. Owing to the increasing influence of momentum drag with speed, only by-pass ratios of 2.5 or smaller are practical at Mach number 2.2. For the reasonable small SOT shown in Figure A-11, increasing BPR

[13] SOT is a measure of the cycle temperature which is defined slightly different from COT. While COT refers to the temperature at the first turbine nozzle guide vane leading edge, SOT refers to the temperature at entry to the first turbine rotor. The difference between these is small, and depending on the design of cooling flows SOT could be slightly lower than COT.

actually makes SFC worse. However, for larger SOTs, SFC improves with increasing BPR.

Due to improved thermal efficiency, SFC improves as OPR is increased at a fixed SOT and BPR for subsonic speed. For the SOT level displayed in Figure A-10, SPT deteriorates slightly when OPR is increased. This is a consequence of the low jet velocity. At higher temperatures SFC remains constant when OPR is increased. At supersonic speed, a significant pressure increase happens due to the intake ram recovery, and hence, the optimum OPR is lower than for subsonic conditions (Figure A-11). The trend on SPT is the same, but the effect is even larger than for Mach number 0.8.

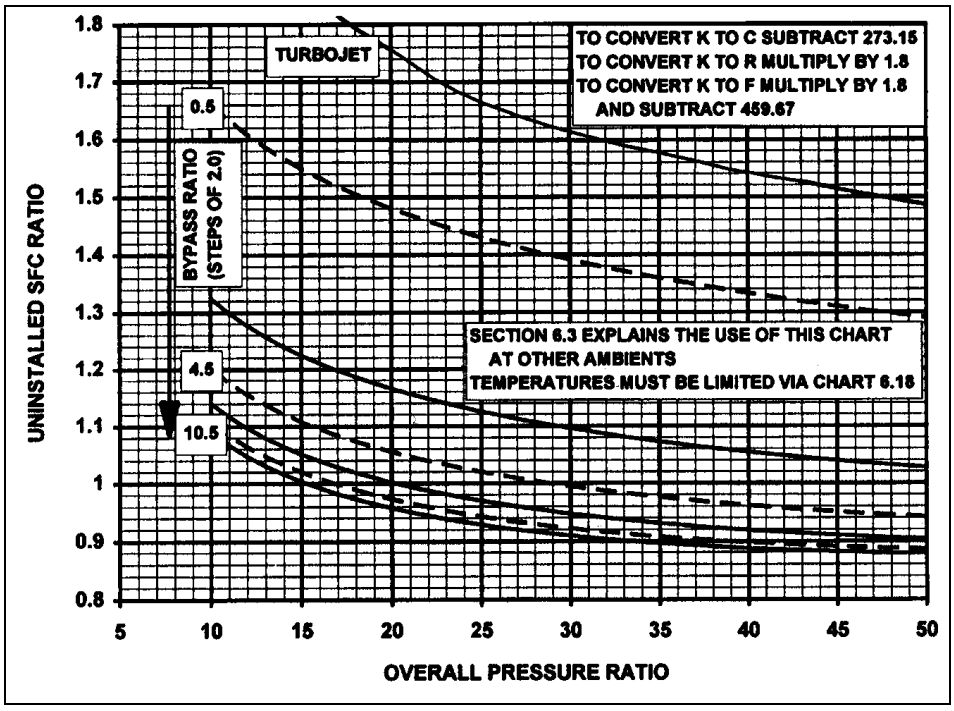

Figure A-9. Design point diagram showing SFC ratio versus OPR and BPR at optimum FPR at 11 000 m, ISA, 0.8 Mach number [Walsh and Fletcher, 1998].

Another parameter which has a large influence on the performance is the maximum cycle temperature, here defined as SOT. The figures shown here are obtained for a specified SOT, and hence its influence on the performance cannot be seen in the figures. As SOT is increased, SPT is always increased, while SFC can both decrease and increase depending on BPR. This is true for both subsonic and supersonic conditions. Increasing SOT implies that the jet velocities become larger. For a high BPR engine an increased SOT has a beneficial effect on SFC, whereas it has a detrimental effect on a low BPR engine where the jet velocities are already large. For intermediate BPR engines the optimum value on SOT for minimum SFC increases with BPR. Generally, as more power is available to the low-pressure turbine, both the optimum OPR and BPR increase as SOT is increased.

For a turbofan engine, the SFC level is lower and the SPT level is higher at Mach number 0.8 than at 2.2. The latter is a consequence of the high intake ram drag at high speeds.

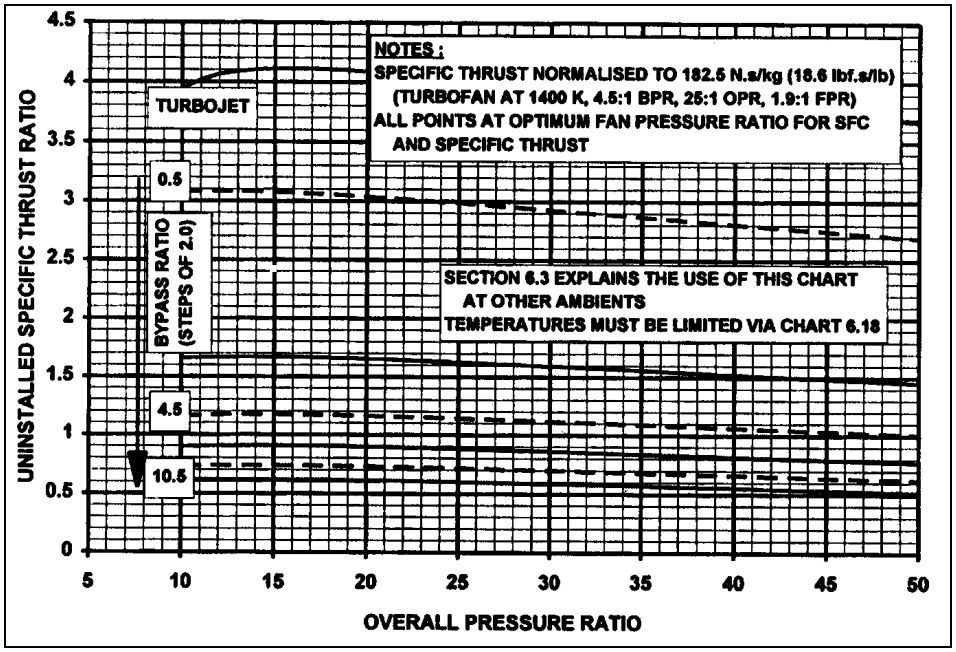

Figure A-10. Design point diagram showing SPT ratio versus OPR and BPR at optimum FPR at 11 000 m, ISA, 0.8 Mach number [Walsh and Fletcher, 1998].

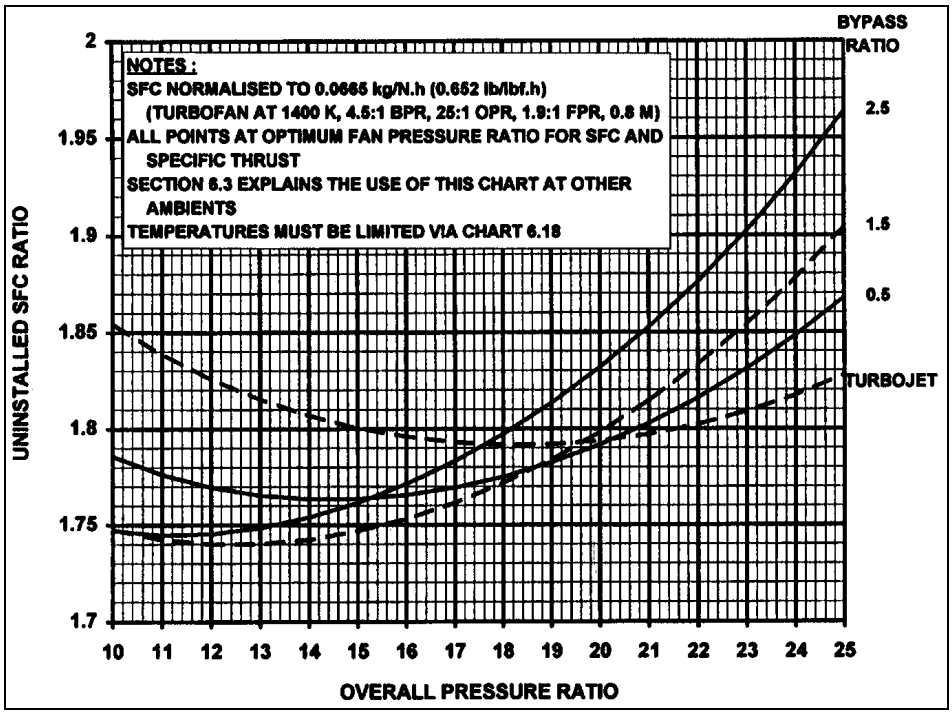

Figure A-11. Design point diagram showing SFC ratio versus OPR and BPR at optimum FPR at 11 000 m, ISA, 2.2 Mach number [Walsh and Fletcher, 1998].

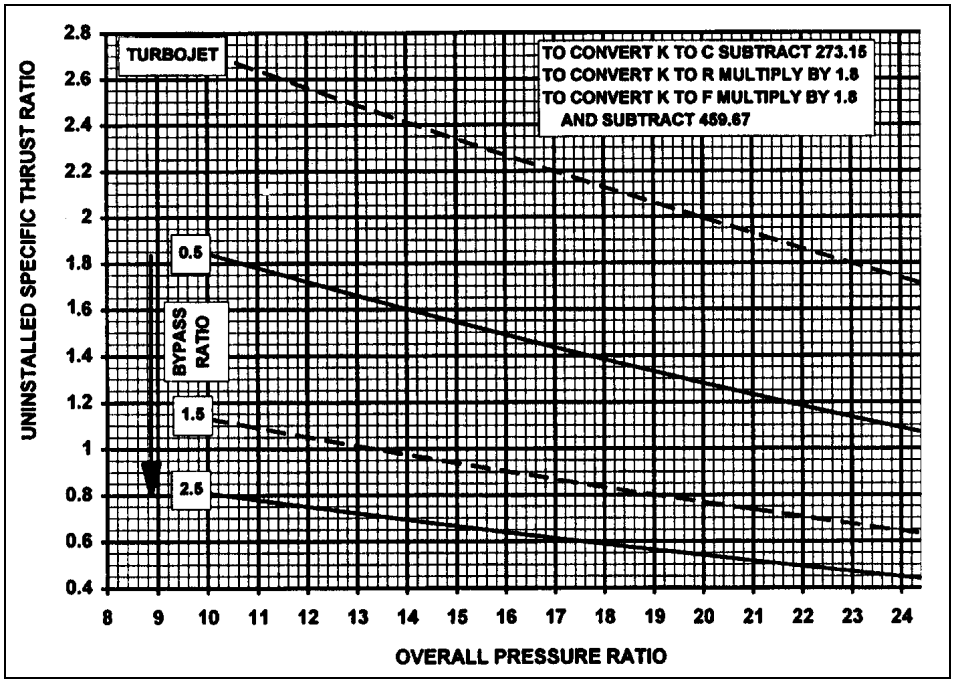

Figure A-12. Design point diagram showing SPT ratio versus OPR and BPR at optimum FPR at 11 000 m, ISA, 2.2 Mach number [Walsh and Fletcher, 1998].

A.3.3 Off-design Performance Behaviour

When the engine is designed the off-design performance may be calculated at any operation point within the operational envelope. For illustration the effects on a high by-pass turbofan engine of altered operational conditions are briefly outlined here. Investigating three different high by-pass ratio engines, Pradewa (1995) found that as the Mach number is increased the net thrust is decreased, and hence SFC is increased. For Mach numbers less than 0.3, the gain in thrust for a given reduction in Mach number is quite large, the main reason being that the momentum drag is decreased. For higher Mach numbers the ram compression becomes significant, and thus the loss in thrust decreases with Mach number. Between Mach numbers 0.6 and 0.9, the thrust is more or less unchanged.

Following Pradewa (1995) the thrust is decreased and SFC is, for high Mach numbers, decreased with altitude. For lower Mach numbers SFC is unaffected by altitude. The main reason for the decreased thrust is that the engine mass flow is decreased with altitude, because the ambient static pressure and density falls with altitude. However, the effect of lowered mass flow is partly compensated by the fact that the engine behaves non-dimensionally, which in this case implies that the engine behaves as if the rotational speed was rising. This is because the non-dimensional speed, which is defined as the ratio of the rotational speed to the square root of the ambient static temperature, is increased as the altitude is increased (in the troposphere).

Considering the non-dimensional rotational speed, it may be understood that the engine will deliver higher overall temperature and pressure ratios on a cold day than on a warm one, thus the thermal efficiency and thrust become higher.

APPENDIX B – DERIVATION OF A GLOBAL WARMING POTENTIAL (GWP) MODEL

If aircraft-produced particles and their effects upon clouds are disregarded (see sections 1.2.2 and 3.4), the aircraft emissions only affect the radiative balance of the atmosphere directly through radiative forcing of carbon dioxide and water vapour. Furthermore, emissions of oxides of nitrogen affect the radiative forcing indirectly through changes in concentrations of ozone and methane, which are both greenhouse gases. The aim of this section is to derive a method for calculating the global warming potential (GWP) of H_2O and NO_x emissions emitted by aircraft. Rather than employing a sophisticated 3-D climate model, a simple parametric method is used following the methodology proposed by Klug et al. (1996) and Klug (2001), taking into account model results and recommendations from IPCC (1999). In order to consider the nonlinearity and the large variability of the indirect effect of short-lived NO_x emissions on radiative forcing, a plume model is employed. This GWP model is derived in collaboration with Jana Moldanova at IVL, Swedish Environmental Research Institute, and published in Svensson et al. (2004). The calculations using the plume model MAP (explained below) are carried out by Jana Moldanova.

The global warming potential of a trace gas is the ratio of the global warming through emission of one kilogram of the gas to the global warming through emission of one kilogram of CO_2:

$$GWP_i(T) = \frac{E_i(T)}{E_{CO2}(T)} \tag{B-1}$$

where T is the time horizon and E_i is the warming effect of the trace gas, i. The lifetime, τ, of the trace gas usually differs from the lifetime of CO_2. Therefore, the warming effect of a trace gas is connected to a corresponding time horizon and the integrated radiative forcing, RF_i:

$$E_i(T) = \int_0^T RF_i \cdot e^{-\frac{t}{\tau}}\, dt = RF_i \cdot \tau \cdot \left(1 - e^{-\frac{T}{\tau}}\right) \tag{B-2}$$

Generally, the GWP varies with the time horizon chosen. Typically horizons of 20, 50, 100 or 500 years are used. For the GWP calculations in this study, the time horizon of 100 years is chosen. All data are intended to represent the situation in summer atmosphere at mid-latitudes if such resolution is possible.

The radiative forcing of a trace gas is related to the climate change expressed as change in surface temperature, ΔT_0, through a climate sensitivity parameter, λ:

$$\Delta T_0 = \lambda \cdot RF \tag{B-3}$$

The climate sensitivity parameter generally varies for different species and altitudes. However, for the altitudes in question (0-15 km), λ differs within a factor of 2 (a value 0.92 K per W/m^2 is recommended in IPCC (1999)). Generally, RF is seen as a parameter which is linearly related to climatic change [IPCC, 1999; and IPCC, 1990].

Increment of species, Y, at a given altitude, h, causes a change in radiative forcing. The change can be quantified using a sensitivity function, S(h), which determines the change in RF at the tropopause level with stratospheric adjustment for a unit increase of Y in the vertical column, ΔY (DU)[14]:

$$RF(h) = \Delta Y(h) \cdot S(h) \tag{B-4}$$

If Y is produced in the atmosphere from the emission of species X and the lifetime of the emission is short in relation to the time horizon, the increase in the total column of Y (DU) in the atmosphere over a certain area due to the emission, Q (kg), is:

$$\Delta Y(h) = Q \cdot \int_0^{\tau_X} (P_y(h))\, dt \cdot C \tag{B-5}$$

where $P_y(h)$ is the production rate, i.e. the number of molecules produced by one molecule X released in the atmosphere within the lifetime of X, τ_X. If Y is emitted directly, the integral expression in equation (B-5) vanishes. The constant C has the unit DU/kg and recalculates the mass of Y to a column expressed in DU for the size of the region examined, A (m^2):

$$C = \frac{10^8 \cdot V_{mol}}{MW_X \cdot A} \tag{B-6}$$

MW_X is the molar weight of X, V_{mol} = 22.414x10^{-3} is the molar volume at 273 K and 101.325x10^3 Pa (coming from the definition of DU) and the numerical value comes from the recalculation of m to 0.01mm and of kg to g. For example, taking the emission rate of NO_x in kg and considering the species being dispersed over the area between 30 and 60°N, the parameter C gets a value of 5.24x10^{-10} DU/kg.

The production rate $P_y(h)$ of secondarily-formed greenhouse gases concerns the formation of ozone and the destruction of methane through reactions with oxides of nitrogen. As argued in IPCC (1999), the GWP concept is not well suited for short-lived gases that are formed at production rates which are strongly dependent on atmospheric conditions. However, since there are no methods available that are suitable for these types of studies, the problem is approached by assuming that the species are affected by oxides of nitrogen under a rather short lifetime of NO_x, using a fairly detailed chemistry description of the dispersing plume. The ozone formation and methane destruction are evaluated under different conditions, and average values to describe the production/destruction are used. Dispersion and the radiative forcing of the ozone and methane are then estimated from the results of global models.

[14] One Dobson Unit (DU) is equal to a 0.01 mm thick column of gas at 273 K and 101.325x10^3 Pa.

In order to estimate the ozone production and methane destruction, a plume model of aircraft emissions, MAP [Näs et al., 2003], is employed. The model simulates an entire flight mission of an aircraft using aircraft emission data as described in this work. In the model, the emissions in a dispersing aircraft plume at engine outlet (approximately 10 s behind the engine) are followed for 10 days. The initial plume processes involving chemical and gas-to-particle conversion of emitted gases in the cooling plume were adopted from detailed studies by Kärcher et al. (2000), Gleitsmann and Zellner (1998), Tremmel et al. (1998) and Kärcher et al. (1996). The plume expansion in the vortex regime is described using a parameterisation of Schumann et al. (1998). After the turbulent dissipation of the vortex, i.e. after two minutes of simulation, the plume goes over to the dispersion regime when the plume expansion is induced by atmospheric diffusion. The plume is then described by the Gaussian approximation [Konopka, 1995; and Schumann et al., 1995]. The chemical reaction scheme of the expanding plume is based on work by Tremmel et al. (1998) and Hendricks (1997), which has been further developed to consider the gas phase and heterogeneous reactions possibly important for ozone cycling in the tropopause region and in the stratosphere. This chemical description considers 100 species in over 310 gas-phase and 15 heterogeneous reactions.

To consider the variability of ozone formation and the effects on methane from oxides of nitrogen, a number of simulations involving different seasons, time of the day and latitudes are studied. Effects of both conventional and hydrogen aircraft are compared. As a result of this study, it can be concluded that production of ozone relative to emitted NO_x is little sensitive to the time of the day when the emission takes place and is not sensitive at all to the aircraft type (when the cruise phase is considered). There is a large variability of $P_{O3}(h)$ with altitude over the latitudes which coincide with the position of the tropopause and with the level of NO_x pollution in this area. Table B-1 gives an overview of the results.

Table B-1. Chemical lifetime of ozone, average production/destruction of ozone $P(O_3)$ and methane $P(CH_4)$ in summer at mid-latitudes due to oxides of nitrogen emitted at different altitudes (for methane 2 different values for conventional and liquid hydrogen-fuelled aircraft are presented), and the sensitivity function, S, for 1 DU ozone change [Hansen et al., 1997] at different altitudes used in the model.

Altitude [km]	O_3 lifetime [d]	$P(O_3)$ [$g(O_3)/g(NO_X)$]	$S(O_3)$ [W/m^2 DU]	$P(CH_4)$ [$g(CH_4)/g(NO_X)$]	
				Conv.	H_2
2	16	5.3	0.009158	-0.91	-1.05
4	24	7.2	0.017400	-0.72	-0.75
6	35	12.6	0.027052	-0.70	-0.72
8	52	21.4	0.032671	-0.46	-0.55
10	79	20.2	0.025889	-0.43	-0.52
12	132	16.3	0.012964	-0.30	-0.39
14	380	1.3	0.004449	0.10	0.01
16	300	3.1	-0.002500	0.08	-0.01

The GWP is a relative number where the RF of one species is related to the RF of **carbon dioxide (CO_2)** (see equation (B-1)). It is important that the two forcings which

are compared are based on the same assumptions. The RF_{CO2} used here is based on the parameterisation of Hansen et al. (2000) which is in agreement with IPCC (1999). The RF of additional CO_2 is calculated according to:

$$RF_{CO2} = f(c) - f(c_0) \tag{B-7}$$

where

$$f(c) = 4.996 \cdot ln\left[c + 0.0005 \cdot c^2\right] \tag{B-8}$$

where c and c_0 are the CO_2 mixing ratios after and before the addition, respectively. The RF values do not increase linearly with ΔCO_2, and are dependent on the CO_2 mixing ratios into which the additional amount of CO_2 (ppm(V)) is added. However, for ΔCO_2 below 10 ppm(V), the increase in RF can be assumed to be linear, and thus S_{CO2} can be assumed to be constant. For a 370 ppm(V) CO_2 level, the dRF_{CO2}/dCO_2 has a value of 0.0156 W/m^2 ppm(V), which, assuming 1 ppm(V) throughout the whole atmosphere and the number density profile of the US standard atmosphere, corresponds to an S value of 1.947×10^{-5} W/m^2 DU. The lifetime of CO_2 is assumed to be 150 years [IPCC, 1996] and it is homogeneously mixed over the same area as the examined species but throughout the entire vertical profile. Assuming a lifetime of CO_2 of 150 years and a time horizon T of 100 years, the warming effect of CO_2, E_{CO2}, is 7.736×10^{-13} W yr/m^2 kg if the affected area is assumed to be between 30 and 60^{o}N, i.e. 9.36×10^{13} m^2. The area is a factor 5.5 smaller than the Earth's surface and is used consequently for all species. As RF is considered to increase linearly with the concentration changes considered here, the area is cancelled when the warming effects are related to each other in the GWP calculation.

Radiative forcing of the **water vapour** is coupled to large uncertainties due to a huge variability of its concentration in the troposphere where it is employed in the hydrological cycle. Furthermore, it is extremely sensitive to temperature feedbacks, such as sensitivity of cloudiness, evaporation intensity and air water vapour content on surface temperature [IPCC, 1999]. In this study RF_{H2O} values obtained from a model experiment [Brühl et al., 1991] are used. According to Brühl et al. (1991), the RF at the tropopause level (10 km) from rising H_2O concentration by 10% between 10 and 15 km altitude is 0.65 W/m^2, resulting in an S value (10-15 km) of 5.55×10^{-4} W/m^2 DU. This value does not include any stratospheric adjustment. The climate impact of water vapour is suggested to be negligibly small for subsonic aviation [IPCC, 1999; and Morris et al., 2003], hence neglected here for altitudes lower than 10 km. The residence times used in equation (B-2) are listed in Table B-2. The original lifetimes from Klug and Grassl (1993) are adjusted around the tropopause region according to Klug (2001a).

Table B-2. Lifetime and sensitivity function versus altitude of water vapour.

Altitude [km]	τ_{H2O} [yr]	S_{H2O} [W/m^2 DU]
0	0.040	0.0
1	0.041	"
2	0.042	"
3	0.044	"
4	0.046	"
5	0.050	"
6	0.054	"
7	0.058	"
8	0.068	"
9	0.110	"
10	0.250	5.55×10^{-4}
11	0.360	"
12	0.450	"
13	0.550	"
14	0.650	"
15	0.750	"

Radiative forcing of **ozone** is evaluated by combining plume modelling for ozone production calculations and estimates based on global models for radiative forcing of the ozone formed from oxides of nitrogen.

- The ozone production rate, P(h), is highly non-linear and depends on the chemical composition of the atmosphere and on the radiation intensity. Production of ozone integrated over the lifetime of NO_x emitted at altitude is calculated under a range of conditions (varying time of the day, time of the year and latitude). See Table B-1.
- The chemical lifetime of nitrogen oxides is taken from Ehhalt et al., 1992, who used a quasi-2D model. Values are varying from some hours at the ground to a few days in the lower stratosphere.
- The sensitivity function, S, is taken from Hansen et al. (1997) who performed model experiments with the Wonderland climate model where they have added 100 DU ozone to one model layer after the other and calculated the RF of the additional ozone for a period of 50-100 years after the addition. The values used at altitudes in question are displayed in Table B-1. From sensitivity tests of climate response to ozone changes at a certain altitude, Hansen et al. (1997) concluded that the response could be linearly scaled to the amount of ozone.
- The chemical lifetime of O_3 needed in equation (B-2) is longer than the chemical lifetime of NO_x. The lifetimes presented by Grewe et al. (2002) are used here (see Table B-1).

In order to consider the influence of mixing on the lifetime of ozone formed at a certain altitude, the following very simple assumptions are made [Klug et al., 1996]:

- Since the lifetime of NO_x is known to be much shorter than the lifetime of O_3, only transport of O_3 is included. The O_3 is produced exclusively within a layer of one kilometre around the emission height of NO_x.

- The produced ozone is mixed equally down to the ground and one layer upwards. Right below the tropopause no upward mixing is possible. Above the tropopause no mixing takes place at all.
- The tropopause is assumed to be located at the following altitudes with the following probabilities: 10 km: 6%, 11 km: 22%, 12 km: 44%, 13 km: 22%, 14 km: 6%.

This mixing scheme only affects the ozone lifetimes, since mixing is already included in the sensitivity function of ozone, S_{O3}, from the model simulation.

Emissions of oxides of nitrogen affect mixing ratios of **methane** through increased concentration of OH radicals and hence decreased lifetime of methane. To estimate the radiative effect of decreased methane concentrations, a method similar to that used for ozone is employed:

- The production rate, P, for methane is calculated using the MAP model. As the reduction of CH_4 is mainly driven by the increase of OH through the reaction HO_2+NO -> OH+NO_2, τ_x in equation (B-5) is equal to τ_{NOx}. The production rates are summarised in Table B-1. There is a difference in methane production/destruction between effects of emissions from conventional and hydrogen-fuelled aircraft. This difference is, however, rather small when the effect of emissions on ozone is taken into account, and hence, the GWP values of NO_x are assumed to be the same for both aircraft types.
- The chemical lifetime of NO_x is assumed to be the same as assumed for the ozone calculations.
- The differential RF to the mixing ratio of methane, dRF/dCH_4 (W/m^2 ppm(V)), is taken from Hansen et al. (2000):

$$RF = 0.0406 \cdot \left(\sqrt{m} - \sqrt{m_0}\right) - \left[g(m, n_0) - g(m_0, n_0)\right] \qquad \text{(B-9)}$$

where

$$g(m,n) = 0.5 \cdot ln\left[1 + 2 \cdot 10^{-5} (m \cdot n)^{0.75}\right] \qquad \text{(B-10)}$$

where m_0 and m are CH_4 mixing ratios before and after the CH_4 change, and n_0 and n are the N_2O mixing ratios before and after the change. The RF values differ for CH_4 and N_2O mixing ratios into which the additional amount of CH_4 (ppm(V)) is added, and do not respond linearly to the increment of the CH_4 mixing ratio. However, for a narrow range of ΔCH_4, the change in RF can be assumed to be linear. For CH_4 levels corresponding to the year 2000, i.e. 1.7 ppm(V), dRF/dCH_4 is 0.38 W/m^2 ppm(V) when 1 ppm(V) change is considered, which is in agreement with the corresponding value of 0.37 W/m^2 ppm(V) stated in IPCC (1999). For ΔCH_4 smaller than 0.1 ppb(V), the dRF/dCH_4 is equal to 0.4297 W/m^2 ppm(V), which, assuming 1 ppm(V) throughout the whole atmosphere and number density profile of the US standard atmosphere, corresponds to S equal to 5.362×10^{-4} W/m^2 DU.
- The global chemical lifetime of CH_4 (used in equation (B-2)) is assumed to be nine years [IPCC, 1999], and independent of altitude.

Using a methodology similar to that explained here and including vertical mixing, Klug et al. (1996) calculated GWP numbers due to NO_x emissions versus altitude. They compared their results with 14 different earlier model simulations of various authors, performed to estimate the change in ozone concentration due to air traffic [Brasseur et al., 1996; Johnson et al., 1995; Wuebles et al., 1993; Beck et al., 1992; WMO, 1991; and Johnson et al., 1992]. With 1 Tg NO_x emission between 10 and 12 km altitude, the model runs yielded a GWP value ranging from 120 to 400, with an average of approximately 220. Other published GWP values of NO_x cover a wide range of values between 210 [Johnson et al., 1992] and 456 [Johnson et al., 1996]. In order to obtain these values Johnson et al. (1992) assumed that the NO_x emissions are emitted at 0-12 km altitude, whereas Johnson et al. (1996) assumed an emissions height of 8-10 km. In this study, values ranging from 1.7 to 6.6 times lower are derived. The deviation is due to using a different methodology, likely to be explained mainly by the following factors:

- As opposed to the GWP model derived by Klug et al. (1996) (where it is assumed that the warming function of CO_2 is based on the area of the whole Earth), the warming function of CO_2 is based on the same area as the warming function of other species, resulting in a warming function of CO_2 about 5.5 times higher than that based on the whole Earth's surface area.
- In the large-scale models the emissions are dispersed directly over a large area which makes the ozone formation more effective, giving an overestimated value of ozone production between 30 and 150%. The deviation between plume models and global models is found using the MAP code. In addition, this deviation was found by Kraabøl et al. (2000) and Petry et al. (1998).

Having these factors in mind, the numbers obtained here are comparable to the values presented in the literature. The global warming values of NO_x and water vapour used in this paper are presented in Table B-3 and in section 3.4 (Figure 3-3).

Table B-3. GWP figures for CO_2, H_2O and NO_x versus altitude.

Altitude [km]	GWP (CO2)	GWP (H2O)	GWP (NO_x)
0	1	0.00	-7.1
1	1	0.00	-7.1
2	1	0.00	-7.1
3	1	0.00	-4.3
4	1	0.00	-1.5
5	1	0.00	6.5
6	1	0.00	14.5
7	1	0.00	37.5
8	1	0.00	60.5
9	1	0.00	64.7
10	1	0.24	68.9
11	1	0.34	57.7
12	1	0.43	46.5
13	1	0.53	25.6
14	1	0.62	4.6
15	1	0.72	0.6

APPENDIX C – ADDITIONAL DATA FOR THE AIRCRAFT MISSION PERFORMANCE MODELLING TOOL

Appendix C.1 – Prediction of the Gas Turbine Engine Weight

To enable the calculation of the engine performance at different points within the operation envelope of engines having different engine cycle parameters, the engine weight needs to be predicted. Following Whellens (2003), three categories of aero-engine weight estimation methodologies can be defined: low-accuracy methods, component-by-component methods and cycle parameter-based methods.

The low-accuracy methods rely on historical data, and the weight of the propulsion system is related to one of its main performance parameters (typically take-off thrust), or alternatively, to a simple combination of performance parameters and cycle parameters. Though these methods rely mainly on historical data, they are not suitable for estimating weights of unconventional engines which are designed for criteria other than those commonly considered in the past.

The most detailed methods are the component-by-component approaches. These methods require detailed knowledge of the engine configuration and its components. The engine weight is calculated as the sum of the weights of the individual components, which are usually estimated using analytically-based correlations that are calibrated against historical databases. These methods are necessary for very detailed studies when stage loadings, wheel speed, etc. are to be calculated. However, they are not suitable for the preliminary design studies performed in this thesis.

The method employed here falls under the category of cycle parameter-based methods. These methods rely to a smaller extent on historical data than the low-accuracy methods and do not require such a detailed engine description as the component-by-component methods do, but they principally consider the influence of main cycle parameters. Thus, they are suitable methods for assessing the aero engine weight of novel engine configurations. It is worth mentioning that in this context, novel means configurations consisting of conventional components but designed for different criteria; hence, the configurations may have unconventional combinations of engine cycle parameters.

Gerend and Roundhill (1970) proposed a cycle parameter-based method including semi-empirical correlations of engine weight and dimensions which are developed using data for over 350 engines from the time period 1940 to 1980. By splitting the total engine weight into gas generator and fan section, the weight and dimensions are, to a first order, estimated by assuming that engine weights and dimensions are a function of engine cycle and configuration parameters. Various correction factors are introduced to take account for W_1 (mass flow at engine inlet), BPR, OPR, TET, entry-into-service year, Mach cruise number and duct configuration. Furthermore, the lifetime for which the engine is designed is taken into account. Having tested and calibrated their model

against 350 turbofan engines, Gerend and Roundhill (1970) found that around 85% of the cruise engine weights are predicted within 15% of the real values.

The model developed by Gerend and Roundhill (1970) has been used recently by Whellens (2003). The original model comprised upper limits on BPR and OPR of 10 and 35, respectively, which was not considered enough by Whellens (2003). To justify this, the correction factors dealing with these parameters were extrapolated to higher values of BPR and OPR. The correction factors covering the effects of entry-into-service year and TET, were recalibrated against a pool of more recent engines spanning many major engine manufacturers. After the novel calibration Whellens (2003) concluded that errors up to 20% must be expected from the model.

In this thesis a slightly simpler model given in Torenbeek (1982) is employed. Similarly as the Gerend-Roundhill method, Torenbeek (1982) has developed a model to estimate the engine weight as a function of engine cycle parameters based on existing engine data. The main difference is that fewer factors are included in the latter model. In spite of this, the model is, as shown below, able to predict the engine weight with errors within the same orders of magnitude as Whellens (2003) illustrated for the Gerend-Roundhill model. In this method the engine is divided into a gas generator (consisting of compressor(s), high-pressure turbine and combustor) and a propulsive device (consisting of fan, low-pressure turbine and nozzle(s)). By assuming that the gas generator weight is proportional to the mass flow flowing through it and that the weight of the propulsive device is proportional to the fan thrust, the following expression for the dry engine weight including its fundamental accessories is set up:

$$EW = C_1 \cdot W_g + C_2 \cdot F_{fan} \tag{C-1}$$

Having made some simplifying assumptions, an approximate expression for the fan thrust as a fraction of total take-off static thrust is derived (for more details, see Torenbeek (1982)):

$$\frac{F_{fan}}{F_{sto}} = 1 - \frac{1}{\sqrt{1 + \eta_{tf} \cdot BPR}} \tag{C-2}$$

where η_{tf} is equal to the efficiency of the energy transformation from the low-pressure turbine to the fan (assumed to be 0.75). Elaborating equation (C-1) further and applying it to actual engine types, the constants are found to be:

$$C_1 = 10 \cdot OPR^{0.25} \tag{C-3}$$

$$C_2 = 0.12 \tag{C-4}$$

Inserting equations (C-2) to (C-4) into equation (C-1) and expressing the gas generator mass flow as a function of specific thrust (SPT) and BPR, the dry engine weight is approximated with the following equation [Torenbeek, 1982]:

$$EW = F_{sto} \cdot \left[\frac{10 \cdot OPR^{0.25}}{SPT \cdot (1 + BPR)} + 0.12 \cdot \left(1 - \frac{1}{\sqrt{1 + 0.75 \cdot BPR}} \right) \right] \quad \text{(C-5)}$$

The result is hence an equation for the dry engine weight dependent on F_{sto}, OPR, SPT and BPR. All parameters refer to static sea-level conditions. The specific thrust (SPT) is, in turn, highly dependent on the turbine entry temperature (TET). Using this equation, the contribution from the fan should be 20% higher for geared fans and another 20% should be added for variable pitch fans. If present, also the extra weight for acoustic treatment needs to be added. Torenbeek (1982) moreover states that the variation of engine weight with high values of BPR cannot be predicted with certainty with this equation.

In order to evaluate the equation, it is employed to calculate the engine weight for a number of different engines with known cycle parameters (for take-off conditions) and engine weights. A selection of engines for which sufficient data are available in the public domain [Gunston, 2002] is used. When using these data, one should be aware that the quality and scope of the data given are dependent on what the manufacturers are willing to publish. The data are from a large number of sources, and thus there is a risk that they are not always obtained for strictly the same conditions. However, Gunston (2002) is the best available source for data of civil aero engines. In Table C-1 the results of equation (C-5) are compared with the weights given in Gunston (2002) for a number of engines. Engines having BPRs between 1.7 and 6.3, and are certified between 1971 and 1998 are considered.

Amongst the selection of engines considered, the deviation in engine weight (between the results obtained using equation (C-5) and figures stated in Gunston (2002)) varies between -13.6 and 21.9%. The engine weight of the engine which is studied here (V2527-A5) is underestimated with about 8%. This deviation is acceptable, and the weight predicted by the correlation is employed in chapter 4. This limited study indicates that errors in the same order of magnitude as are expected from the Gerend-Roundhill method, i.e. up to about 20%, could be expected when using the equation proposed by Torenbeek (1982) to calculate approximately the engine weight. Any conclusions concerning prediction certainty with respect to cycle parameters or certification year are difficult to draw from these results.

Table C-1. Evaluation of the engine weight prediction model (equation (C-5)).

Engine Notation	Year of Certif.	BPR	OPR	F_{sto} [kN]	SPT [N s/kg]	EW (Gunston (2002)) [kg]	EW by eq. (C-5) [kg]	Dev. [%]
JT9D-7	1971	5.1	22.2	202.8	290.5	4014	3835	-4.5
D36	1977	5.6	20.0	63.7	250.0	1109	1255	13.2
RB211-22B	1979	4.9	25.0	186.8	298.4	4171	3604	-13.6
JT8D-217	1980	1.7	18.2	89.0	406.2	2052	2022	-1.4
CF6-80C2A1	1985	5.1	30.4	257.4	320.9	4144	4818	16.3
Tay 611	1986	3.0	15.8	616.1	331.2	1422	1255	-11.7
PW4056	1986	4.9	30.0	252.3	326.4	4273	4725	10.6
CFM56-5A4	1986	6.2	29.0	97.9	264.5	2266	1887	-16.7
V2527-A5	1992	4.8	28.5	117.9	331.6	2370	2186	-7.7
TRENT 772	1994	5.0	35.5	316.3	344.2	4785	5833	21.9
CFM56-7B26	1996	5.1	27.6	117.0	331.1	2384	2107	-11.6
PW4090	1996	6.3	38.3	408.3	330.9	7140	7112	-0.4
BR700-715C1-30	1998	4.5	37.6	102.3	354.6	2114	1952	-7.7

Appendix C.2 – Effects on Nacelle Drag and Weight of Re-Sizing the Nacelle

In order to assess easily the effects on engine drag and weights of altered engine size, approximate scaling correlations are applied. The engine consists of the engine itself, the nacelle and the accessories. The pylons are not considered, since they are considered to be part of the airframe.

In the public domain [Gunston, 2002] data, such as weights and geometries, of the considered engine, V2527-A5, may be found. Knowing the geometries and using a computer program which is aimed at predicting aerodynamic characteristics of aircraft [Schemensky, 1973], the drag coefficient times the reference area, CDS_N, for this engine is found to be 0.044 m^2. This value was derived for the cruise condition, i.e. altitude 11 000 m and Mach number 0.8, where most of the fuel is burnt. Nevertheless, it is believed to be sufficiently accurate also for other conditions. The simulation to obtain this value was performed by Anders Hasselrot at FOI (Swedish Defence Research Agency). By assuming that the engine size changes symmetrically, i.e. the ratio of diameter to length is unchanged, and that the nacelle has the form of a cylinder (see Figure C-1), CDS_N is proportional to the nacelle inlet diameter squared. This is in agreement with assumptions made in a similar study by Whellens (2003). For convenience the ratio of the diameter of the scaled engine to the diameter of the datum engine is named the linear scale factor, LSF:

$$LSF = \frac{D}{D_{dat}} \tag{C-6}$$

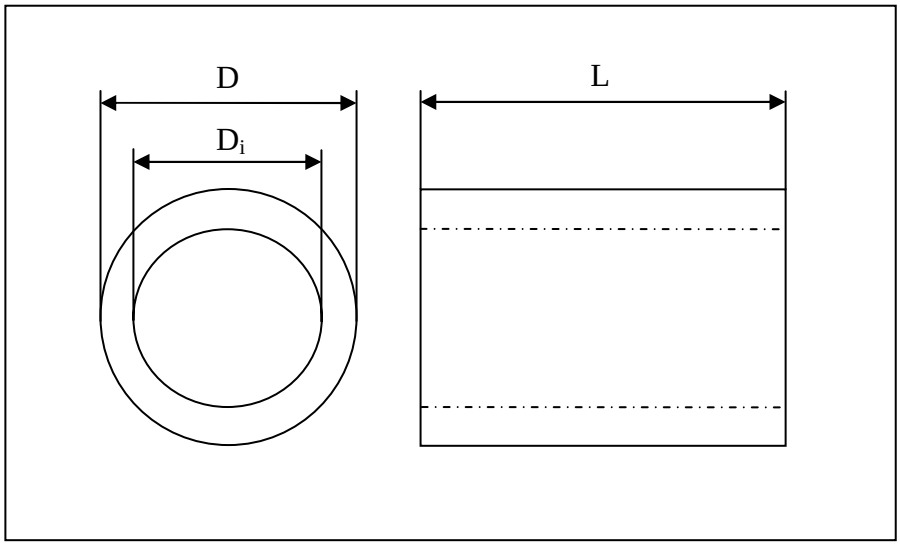

Figure C-1. Simplified nacelle geometry.

Following the definition of LSF, CDS_N for a scaled engine is:

$$CDS_N = CDS_{Ndat} \cdot LSF^2 \tag{C-7}$$

and the change in CDS_N, ΔCDS_N, is estimated by:

$$\Delta CDS_N = CDS_{Ndat} \cdot \left(LSF^2 - 1\right) \tag{C-8}$$

While the engine dry empty weight is estimated using the methodology described in Appendix C.1, the nacelle and accessories mass are scaled. By assuming that the nacelle is a symmetric cylinder, with the length, L, the outer diameter, D_o, and the inner diameter, D_i, (see Figure C-1) its mass can be estimated as:

$$M_N = \frac{1}{4} \cdot \rho_N \cdot \pi \cdot L \cdot \left(D_o^2 - D_i^2\right) = k \cdot L \cdot \left(D_o - D_i\right) \cdot \left(D_o + D_i\right) \tag{C-9}$$

where ρ_N is the density of the nacelle material and k is a constant. If it is assumed that the thickness, i.e. $(D_o-D_i)/2$, increases in proportion to the diameter, then the nacelle mass becomes proportional to the diameter squared, whereas the nacelle mass becomes proportional to the diameter if it is assumed that the thickness is independent of the diameter. In reality there probably is some relation between the thickness and the diameter, but it is probably not reasonable to assume that the thickness changes in proportion to the diameter. By assuming that the thickness is proportional to the $D^{1.5}$ and that the size changes symmetrically, the nacelle mass of a re-scaled engine is determined by:

$$M_N = M_{Ndat} \cdot LSF^{2.5} \quad \text{(C-10)}$$

Since the accessories weight is small in comparison to the nacelle weight, both these weights are scaled by the exponent derived for the nacelle weight. Using equation (C-5) and the information on distribution of the total engine mass from Gunston (2002), the sum of the nacelle and accessories mass for the V2527-A5, M_{Ndat}, engine is estimated to be 1001.6 kg.

Appendix C.3 – Data on Overhead Mass versus Changed Engine Size

When the engine size is changed, the MTOM of the aircraft also needs to be changed in order to preserve the range for a given payload. If the engine diameter is increased, the wetted area of the nacelles is increased, and hence also the total drag. As a result the mission fuel consumption rises. An increased engine weight will increase the need for stiffer wings, and thus a higher aircraft structure weight. Both these effects will impose the need for an aircraft with a larger MTOM. For these reasons the MTOM will increase more than the additional engine weight. If the engines are down-sized it would have the opposite effect on the MTOM. The additional effect on MTOM, here denoted overhead mass, M_{OH}, by altering the engine size is estimated using Piano. By changing the engine size and drag coefficient times the reference area for the nacelles, CDS_N, and finding the MTOM that gives an unchanged range, data on the overhead mass versus the changed engine sizes are obtained; see Table C-2.

The effect of scaling the engine on the dry engine weight is estimated using equation (C-5), on the nacelle including its accessories mass using equation (C-10), and on CDS_N using equation (C-8). In Table C-2 the effect on the overhead mass of scaling the engines for the medium-range aircraft in question for a range of 6 818 km is shown. Using linear interpolation this table is used to estimate the overhead mass (M_{OH} in equation (4-10)) for a given change in total engine mass.

Table C-2. Effect of scaling the engines on the aircraft MTOM.

Quantity	Value		
Linear scale factor (LSF) [-]	0.85	1.0	1.15
Difference in total engine mass, all engines [kg]	-2080.5	0	2483.3
Difference in CDS_N, all engines [m^2]	-0.05224	0	0.06071
Difference in MTOM [kg]	-4057	0	4831
Overhead mass [kg]	-1976.4	0	2347.7

Appendix C.4 – Data on Balanced and Unfactored Field Lengths

Table C-3. Unfactored field length and balanced field length versus TOP and tan(γ_{ceng2}) (see section 4.3.2.1 for definitions). The numbers are obtained from figures in ESDU (1985).

tan(γ_{ceng2})	TOP	Unfactored field length [m]	Balanced field length [m]
0.01	2500	455	790
0.03	2500	420	605
0.05	2500	390	530
0.1	2500	350	465
0.15	2500	327	465
0.01	5000	765	1120
0.03	5000	715	945
0.05	5000	675	850
0.1	5000	635	778
0.15	5000	610	775
0.01	7500	1100	1440
0.03	7500	1020	1270
0.05	7500	965	1165
0.1	7500	905	1070
0.15	7500	870	1058
0.01	10000	1420	1770
0.03	10000	1318	1592
0.05	10000	1260	1485
0.1	10000	1170	1370
0.15	10000	1105	1320
0.01	12500	1740	2105
0.03	12500	1625	1910
0.05	12500	1550	1798
0.1	12500	1420	1640
0.15	12500	1345	1583
0.01	15000	2070	2442
0.03	15000	1920	2223
0.05	15000	1835	2090
0.1	15000	1680	1910
0.15	15000	1575	1840
0.01	17500	2375	2790
0.03	17500	2203	2540
0.05	17500	2100	2385
0.1	17500	1925	2180
0.15	17500	1798	2105
0.01	20000	2655	3150
0.03	20000	2465	2865
0.05	20000	2350	2665
0.1	20000	2155	2440
0.15	20000	2010	2355
0.01	22500	2920	3540

0.03	22500	2710	3175
0.05	22500	2580	2940
0.1	22500	2355	2680
0.15	22500	2220	2600
0.01	25000	3155	3958
0.03	25000	2935	3480
0.05	25000	2775	3203
0.1	25000	2550	2930
0.15	25000	2420	2830

Appendix C.5 – Computation of Atmospheric Conditions and the Speed of Sound

The atmospheric pressure, temperature and density for International Standard Atmosphere (ISA) conditions can be determined as a function of pressure altitude and ISA deviation using the equations provided in Table C-4 [ESDU, 1986; and Le Dilosquer, 1998].

Table C-4. Equations for computation of atmospheric conditions.

Range of pressure heights, h [m]:			<11 000 m	11 000-20 000 m
Quantity	Format of numerical expressions	Constants in numerical expressions		
Temperature for ISA conditions [K]	A + Bh	A=	288.15	216.65
		B=	-6.5×10^{-3}	0
Pressure for ISA and off-ISA conditions [Pa]	$(C + Dh)^E$	C=	8.9619638	
		D=	$-0.20216125 \times 10^{-3}$	
		E=	5.2558797	
	F exp(Gh)	F=		128244.5
		G=		$-0.15768852 \times 10^{-3}$
Density for ISA conditions [kg/m^3]	$(I + Jh)^L$	I=	1.048840	
		J=	$-23.659414 \times 10^{-6}$	
		L=	4.2558797	
	M exp(Nh)	M=		2.0621400
		N=		$-0.15768852 \times 10^{-3}$
Density for off-ISA conditions	$\frac{\rho_{ISA}}{1+\frac{\Delta T}{T_{ISA}}}$			

Knowing the temperature, T, and considering air as a perfect gas, the speed of sound, a, is determined by [Anderson, 1989]:

$$a = \sqrt{\gamma \cdot R \cdot T} \tag{C-11}$$

where γ denotes the ratio of the specific heat at constant pressure, C_p, to the specific heat at constant volume, C_v, and R denotes the gas constant. For air γ equals 1.4 (approximate value) and R equals 287 J/kg K.

Appendix C.6 – Data on Drag Coefficients for Zero Lift versus Mach Number and Altitude

The drag coefficient is estimated using equation (4-22). Data on C_{D0} and k versus altitude and Mach number are obtained from the drag polar of the aircraft under consideration [Oelkers and Prenzel, 2001] and using the aircraft characteristics provided in Piano. The characteristics in Piano are obtained by employing a variety of preliminary design-style techniques. The total drag in Piano is derived by adding the zero lift, the lift dependent, the compressibility and the trim drag contributions. In the model used here it is assumed that the aircraft is clean, i.e. undercarriage and flaps are retracted, during the complete climb phase. On a real medium-range flight, the undercarriage is retracted almost directly after take-off, while the flaps not are completely retracted until the aircraft has climbed about 1-2 km in altitude. Neglecting the influence of undercarriage and flaps will therefore underestimate the total drag coefficient in the beginning of the climb phase. Data on C_{D0} and k versus Mach number and altitude are supplied to the program in the form of tabulation, see Table C-5. Using linear interpolation, C_{D0} for the specific altitude and Mach number is calculated. The parameter k equals 0.0409 and is independent of altitude and Mach number.

Comparing the drag coefficient results obtained using the described methodology with the complete drag polar provided in Piano for a clean aircraft, it is concluded that C_D is underestimated by 10-20% during approximately the first 400 meters (in altitude), while it is overestimated by 1-2% for the remaining of the flight mission. For low altitudes where C_L is high, a parabolic equation (equation (4-22)) is obviously not sufficient to imitate accurately the drag polar. This is the main reason why C_D becomes too low for low altitudes where C_L is high. Since the effect of undercarriage and flaps is neglected, C_D will be even more underestimated during the initial climb. However, in terms of fuel consumption and emissions, this deviation might be compensated by a slightly overestimated C_D for the remaining part of the flight.

Table C-5. Drag coefficient for zero lift versus altitude and Mach number.

Altitude [m]	Mach number	C_{D0}
0	0.4	0.01461
0	0.6	0.01503
0	0.8	0.01517
6000	0.4	0.01619
6000	0.6	0.01647
6000	0.8	0.01650
12000	0.4	0.01839
12000	0.6	0.01846
12000	0.8	0.01835

Appendix C.7 – Equations for Subsonic Compressible Flow

For Mach numbers larger than 0.3, the flow velocity is too large to justify the assumption of incompressible flow [Anderson, 1989]. During the second phase of the climb procedure the velocity exceeds this value but it is lower than the sonic speed. At this flow regime, equations for subsonic compressible flow that take account for compressibility effects should be used to calculate the pressure difference and the velocity that are needed in the model.

Using relations valid for isentropic flow, the following equation to estimate the difference between the total pressure, P_t, and the static pressure, P_s, can be derived [Anderson, 1989]:

$$P_t - P_s = P_s \cdot \left[\left(1 + \frac{\gamma - 1}{2} \cdot Ma^2 \right)^{\frac{\gamma}{\gamma - 1}} - 1 \right] \tag{C-12}$$

where γ denotes the ratio of the specific heat at constant pressure, C_p, to the specific heat at constant volume, C_v, and Ma denotes the flow Mach number. For preliminary design calculations, a fixed value on γ may be assumed: 1.4 for air and 1.333 for combustion gases [Cohen et al., 1996].

Knowing the pressure difference the actual air speed can be calculated as [Anderson, 1989]:

$$V = \sqrt{\frac{2 \cdot a^2}{\gamma - 1} \cdot \left[\left(\frac{P_t - P_s}{P_s} + 1 \right)^{\frac{\gamma - 1}{\gamma}} - 1 \right]} \tag{C-13}$$

where *a* denotes the speed of sound. During the second climb phase the aim is to keep the indicated air speed, IAS, constant, which is achieved by keeping the pressure difference between the total and the static pressure constant. The true air speed, TAS, is then calculated using equation (C-13).

Appendix C.8 – Data on Aircraft Usable Fuel Volume

In order to estimate the effect on the usable fuel volume for the aircraft under consideration of scaled engines and MTOM, Piano is used to obtain a set of data. These data are supplied to the program in the form of a tabulation of usable fuel mass versus changed engine size (in terms of kilograms) and MTOM. For given engine mass and MTOM, the usable fuel mass is then obtained using linear interpolation.

When the engine size is changed the wetted areas of the nacelles are increased, and hence also the total drag. This is achieved in Piano by applying a change in CDS_N (drag coefficient times the reference area) for the nacelles (equation (C-8)). As for the effect on the nacelle mass of re-sizing the engine, the effect on the dry engine mass is estimated using equation (C-5) and on the nacelle including its accessories mass using

equation (C-10). When the MTOM is changed the wing area is changed in proportion (equation (4-11)).

When the required aircraft fuel volume is changed, it is assumed that the fuel volume of the tail cone of the aircraft is re-sized. For simplification it is assumed that only the length of the tank in the tail cone, and hence also the aircraft length, changes when either a larger or smaller fuel volume is required. This implies that the length of the tail cone is assumed to be proportional to the change in required fuel volume. However, for aerodynamic purposes, the minimum tail cone length is considered to be about two times the diameter of the fuselage. Below this length the tail cone is not reduced, even if it would be possible to store the required fuel volume in a smaller tank.

Using the described methodology the usable fuel mass, i.e. total fuel mass minus fuel reserves, for three different engine sizes and maximum take-off masses are obtained; see Table C-6.

Table C-6. Effects on the usable fuel mass and range of changed engine size and MTOM.

LSF	Difference in total engine mass. all engines [kg]	MTOM [kg]	Wing area [m^2]	Fuel mass [kg]	Fuel reserve [kg]	Usable fuel mass [kg]	Range [km]
0.85	-2080.6	83000	161.1	9127	1203	7924	6707
1	0	83000	161.1	8387	1232	7155	5864
1.15	2483.3	83000	161.1	7479	1273	6206	4876
0.85	-2080.6	87594	170	10405	1220	9185	7663
1	0	87594	170	9636	1247	8389	6823
1.15	2483.3	87594	170	8700	1280	7420	5831
0.85	-2080.6	92000	178.6	11620	1240	10380	8518
1	0	92000	178.6	10858	1264	9594	7696
1.15	2483.3	92000	178.6	9935	1295	8640	6733

APPENDIX D – AIRCRAFT TYPES USED IN EMISSION SCENARIOS

Table D-1. Aircraft types used in the emission scenarios of the conventional fleet development, assuming the low passenger growth scenario.

Aircraft Type	Tech. level	2001	2010	2020	2030	2040	2050
B737-600	0	9	11	-	-	-	-
B737-800	0	13	15	12	-	-	-
A321-100	0	-	-	-	-	-	-
	Conv 1	-	-	17	12	12	-
	Conv 2	-	-	-	-	1	-
	Conv 3	-	-	-	-	-	15
A330-200	(0)	-	-	-	-	-	-
	Conv 1	-	-	-	-	-	-
	Conv 2	-	-	-	20	20	20
	Conv 3	-	-	-	-	-	4
CMR1-300	(0)	-	-	-	-	-	-
	Cryo 1	-	-	-	-	-	-
	Cryo 2	-	-	-	-	-	-
CMR1-400	(0)	-	-	-	-	-	-
	Cryo 1	-	-	-	-	-	-
	Cryo 2	-	-	-	-	-	-
Sum		22	26	29	32	33	39

Table D-2. Aircraft types used in the emission scenarios of the conventional fleet development, assuming the high passenger growth scenario.

Aircraft Type	Tech. level	2001	2010	2020	2030	2040	2050
B737-600	0	9	-	-	-	-	-
B737-800	0	13	12	-	-	-	-
A321-100	0	-	16	8	8	-	-
	Conv 1	-	-	5	5	5	-
	Conv 2	-	-	-	-	2	2
	Conv 3	-	-	-	-	9	14
A330-200	(0)	-	-	-	-	-	-
	Conv 1	-	-	21	21	21	-
	Conv 2	-	-	-	-	3	3
	Conv 3	-	-	-	-	1	23
CMR1-300	(0)	-	-	-	-	-	-
	Cryo 1	-	-	-	-	-	-
	Cryo 2	-	-	-	-	-	-
CMR1-400	(0)	-	-	-	-	-	-
	Cryo 1	-	-	-	-	-	-
	Cryo 2	-	-	-	-	-	-
Sum		22	28	34	34	41	42

Table D-3. Aircraft types used in the emission scenarios of scenario 1.

Aircraft Type	Tech. level	2001	2010	2020	2030	2040	2050
B737-600	0	9	11	-	-	-	-
B737-800	0	13	15	12	-	-	-
A321-100	0	-	-	-	-	-	-
	Conv 1	-	-	-	-	-	-
	Conv 2	-	-	-	-	-	-
	Conv 3	-	-	-	-	-	-
A330-200	(0)	-	-	-	-	-	-
	Conv 1	-	-	-	-	-	-
	Conv 2	-	-	-	-	-	-
	Conv 3	-	-	-	-	-	-
CMR1-300	(0)	-	-	17	-	-	-
	Cryo 1	-	-	-	12	12	3
	Cryo 2	-	-	-	-	1	12
CMR1-400	(0)	-	-	-	-	-	-
	Cryo 1	-	-	-	20	20	20
	Cryo 2	-	-	-	-	-	4
Sum		22	26	29	32	33	39

Table D-4. Aircraft types used in the emission scenarios of scenario 3.

Aircraft Type	Tech. level	2001	2010	2020	2030	2040	2050
B737-600	0	9	11	-	-	-	-
B737-800	0	13	15	12	-	-	-
A321-100	0	-	-	-	-	-	-
	Conv 1	-	-	17	11	11	-
	Conv 2	-	-	-	-	-	-
	Conv 3	-	-	-	-	-	-
A330-200	(0)	-	-	-	-	-	-
	Conv 1	-	-	-	-	-	-
	Conv 2	-	-	-	-	-	-
	Conv 3	-	-	-	-	-	-
CMR1-300	(0)	-	-	-	-	-	-
	Cryo 1	-	-	-	1	2	-
	Cryo 2	-	-	-	-	-	15
CMR1-400	(0)	-	-	-	-	-	-
	Cryo 1	-	-	-	20	20	20
	Cryo 2	-	-	-	-	-	4
Sum		22	26	29	32	33	39

Table D-5. Aircraft types used in the emission scenarios of scenario 2.

Aircraft Type	Tech. level	2001	2010	2020	2030	2040	2050
B737-600	0	9	-	-	-	-	-
B737-800	0	13	12	-	-	-	-
A321-100	0	-	16	8	8	-	-
	Conv 1	-	-	2	2	-	-
	Conv 2	-	-	-	-	-	-
	Conv 3	-	-	-	-	-	-
A330-200	(0)	-	-	-	-	-	-
	Conv 1	-	-	-	-	-	-
	Conv 2	-	-	-	-	-	-
	Conv 3	-	-	-	-	-	-
CMR1-300	(0)	-	-	-	-	-	-
	Cryo 1	-	-	3	3	4	1
	Cryo 2	-	-	-	-	12	15
CMR1-400	(0)	-	-	-	-	-	-
	Cryo 1	-	-	21	21	23	2
	Cryo 2	-	-	-	-	2	24
Sum		22	28	34	34	41	42

Table D-6. Aircraft types used in the emission scenarios of scenario 4.

Aircraft Type	Tech. level	2001	2010	2020	2030	2040	2050
B737-600	0	9	-	-	-	-	-
B737-800	0	13	12	-	-	-	-
A321-100	0	-	16	8	8	-	-
	Conv 1	-	-	5	5	-	-
	Conv 2	-	-	-	-	-	-
	Conv 3	-	-	-	-	-	-
A330-200	(0)	-	-	-	-	-	-
	Conv 1	-	-	21	21	21	-
	Conv 2	-	-	-	-	-	-
	Conv 3	-	-	-	-	-	-
CMR1-300	(0)	-	-	-	-	-	-
	Cryo 1	-	-	-	-	1	1
	Cryo 2	-	-	-	-	15	15
CMR1-400	(0)	-	-	-	-	-	-
	Cryo 1	-	-	-	-	2	2
	Cryo 2	-	-	-	-	2	24
Sum		22	28	34	34	41	42